POLITECNICO DI TORINO

Corso di Laurea Magistrale in Ingegneria Energetica e Nucleare

Tesi di Laurea Magistrale

Multi-scale modelling and validation of smart polymer composites

Relatore:

Dr. Matteo Fasano

Correlatore:

Dr. Rajat Srivastava

Candidato:

Fabio Ferri

A.A. 2019/20

ACKNOWLEDGEMENTS

First, I would like to thank my Professors Matteo Fasano and Rajat Srivastava for giving me the opportunity to join this project through my thesis activities. Despite the obstacles I have encountered, I have always received great support from them, in terms of tools, material, precious advices and motivation, even in not easy moments. It has been for me a great experience, in which I have had the possibility to improve a lot, by facing challenging tasks, and to be in contact with inspiring people.

In addition, I would like to thank all the members of SMaLL Research Team and ITAINNOVA Researchers for sharing their works with me, particular thanks to Carlos Sáenz, Agustyn Chiminelli and Francesco Bellussi, for precious material and advices. I am also grateful to all the partners of European H2020 Project SMARTFAN for the opportunity.

A special thank goes to my mother and my father for their encouragements and for making me feel very lucky, to my aunt for her enthusiasm and to all my family for the continuous support, without forgetting my parents' dog, Boris.

Last, but not least I want to thank all my friends for all the moments shared with me and because each of them is source of inspiration for me.

I am sure that it would have been impossible without them.

CONTENTS

LIST OF FIGURES

LIST OF TABLES

ABSTRACT

In recent times, innovative materials are playing a central role in new technologies development, for many areas of application. In a rapidly changing world, new materials are necessary to meet today and tomorrow's technological challenges.

There are many examples, like electronic components, photovoltaic cells, fuel cells, storage systems just to name a few, for which the engineering of new materials opens the doors to the creation of new devices, or allows existing ones to improve their performance or efficiency.

The development of new materials takes time and has a cost due to the effort on the research and the numerous tests that are necessary. The possibility of predicting the thermo-physical properties of a material with some precision, even if it is not yet commercially available, can be a very interesting prerogative.

The aim of this work is to develop protocols for the estimation of thermo-physical properties starting from the chemical composition alone, by means of simulations of molecular dynamics (MD). The framework is the SMARTFAN European Project, which involves several partners, companies and universities, including Politecnico di Torino, who is the leader of Work Package 5 (WP5), namely "*Modelling-Enhanced continuum mechanics approaches (from atoms to continuum mechanics)*". This work consists in the mesoscale part of a nano- to-continuum multiscale study of an epoxy-based thermosetting polymer, which is of interest for one of the project's partner company, specialized in motorsport applications. In particular, the goal is to define some procedures useful to characterize mechanical and thermal behaviour of this compound, by computing several thermo-physical property. Nanoscale atomistic simulations results are the input, from which a mesoscale coarse-grained model is carried out. Conversely, the outputs are computed thermo-physical properties, including stiffness matrix and thermal conductivity, suitable to characterize the material in future continuum simulations.

The first part provides a general overview on the family of materials and on the specific compound under investigation, including chemical, thermo-physical and mechanical properties. Two literature reviews follow. The first review is on the mesoscale MD models, including theoretical aspects, mapping, parametrization and simulation details for different methods focused on mechanical properties computation. The second review is always on the mechanical behaviour study, but by means of continuum models. In addition, some analytical models, used for computational results validation, are discussed. This introductory chapter aims to frame the problem and to provide the scientific background.

The second part focuses on the methods and on the procedures used to run the simulation and to get the results, including parameters and hypothesis for force fields adopted, mapping and cross-linking process with all the simulation protocols.

The third part shows the results obtained with comments, comparison with other computational and/or experimental results and open issues.

After the Conclusions, Appendix A contains details about the force field, while all the script implemented during the work are in Appendix B, in human-readable form, widely commented.

This thesis has been developed in the frame of SMARTFAN Project (Grant No. 760779, funded by European Union).

1. INTRODUCTION

This work focuses on the Coarse-grained molecular dynamics (CGMD) modelling of a reference carbon reinforced epoxy, with the aim to compute mechanical and thermal properties starting from parameters derived from atomistic simulations. This chapter introduces the reference material characteristics, first from a chemical point of view, then concerning possible uses. Afterwards, a literature review on the mesoscale, continuum and analytical models to predict mechanical and/or thermal properties follows, in order to investigate on methods and procedures already implemented for this kind of simulations. As per my knowledge, there are still no simulations protocols of the reference material (DGEBA/DICY/DETA) available in literature, and the focus of the review is on similar systems, e.g. thermosetting polymers with the same matrix but different hardeners. Once a proper framework is set for the problem and for the material system, an overview on thesis targets closes the introductory chapter.

1.1 Epoxy Materials and Composites

1.1.1 OVERVIEW

The term epoxy refers to a bridge containing an oxygen atom bonded to two other atoms already unite in some way, forming the epoxy ring or group (also called epoxide or oxirane).

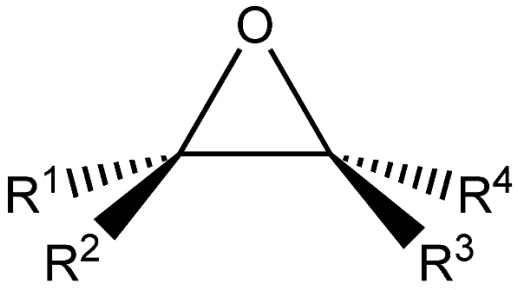

Figure 1 Generic epoxy group (1)

Such groups undergo to a big variety of addition and polymerization reactions leading to the formation of several thermosetting polymers called epoxy resins. The focus is on these resins, obtained after an irreversible curing process that improves mechanical properties, passing from a liquid pre-polymer to a solid material below the glass transition temperature.

Curing involves some chemical compounds called curing agents, which react with the epoxy in several ways. Depending on their chemical structure and on curing conditions, it is possible to manipulate several characteristics of the final product like toughness, flexibility/hardness but also chemical resistance, thermal and electrical conductivity and some others. There are three main classes in which curing agents can be divided (2):

- Active hydrogen compounds (polyamines, poly-acids, polyphenols etc.), which cure by poly-addition reaction.
- Ionic initiators, which are divided into anionic or cationic and involve polymerization with Lewis-type bases and acids.
- Cross-linkers, which couple through the hydroxyl functionality of bisphenol A-type epoxy resins.

The latter typology is the object of this study, and analysed models take into account cross-linking reaction

Cross-linked epoxies have many technologically interesting features like very high adhesion to several surfaces due to the presence of polar groups or high variety in the monomers and hardeners selection, which allows designing materials properties like stiffness, rubbery window or weight, depending on end uses.

The polymerization process is without contractions and with no emission of volatile products. For these reasons, epoxy resins have been widely used as high performance materials such as adhesives, electronic encapsulating materials or as a polymer matrix for composites (3).

1.1.2 CHEMICAL PROPERTIES

The material under investigation is composed by a thermosetting epoxy resin as neat polymer, while CNT, G, GO and rGO are the possible fillers.

More precisely, the neat polymer is a DGEBA/DICY/DETA based epoxy resin, composed by DGEBA as chief ingredient, DICY and DETA as curing agents, acting as hardener or accelerator.

- DGEBA (Diglycidyl Ether of Bisphenol A)

The reference epoxide is LY556 DGEBA, available in the market for example with the registered name Araldite® LY556 (by BASF) (4) .

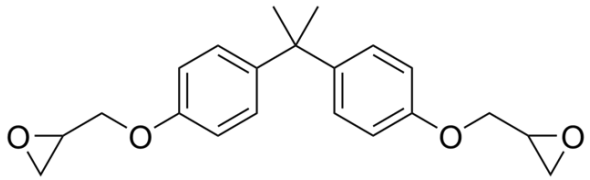

Figure 2 2D sketch of DGEBA molecule

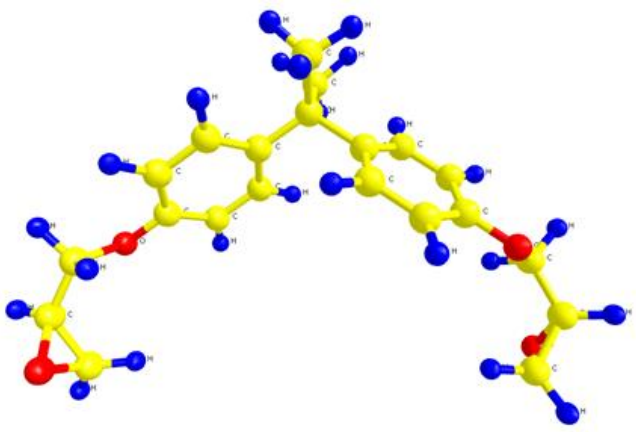

Figure 3 3D view of DGEBA molecule (own work by VEGAzz)

Araldite LY 556		
Aspect (visual)	clear, pale yellow liquid	
Colour (Gardner, ISO 4630)	≤ 2	
Epoxy content (ISO 3000)	5.30 - 5.45	[eq/kg]
Viscosity at 25 °C (ISO 9371B)	10000 - 12000	[mPa s]
Density at 25 °C (ISO 1675)	1.15 - 1.20	[g/cm^3]
Flash point (ISO 2719)	> 200	[°C]
Storage temperature (see expiry date on original container)	2 - 40 °C	[°C]

Table 1 Technical data from Ciba catalogue

- DICY (Dicyandiamide)

The first curing agent is DICY, a nitrile derived from guanidine, used also as a slow fertilizer and as a fuel for explosives.

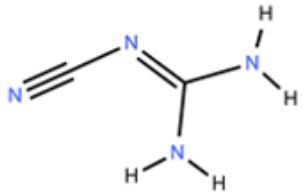

Figure 4 2D sketch of DICY molecule

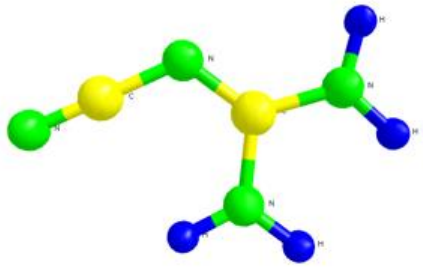

Figure 5 3D view of DICY molecule (own work by VEGAzz)

It is present in some commercial curing agents with registered name like Aradur® 1571 by Huntsman co., a dispersion of DICY in liquid epoxy resin that acts as a hardener, and Accelerator 1573 by Huntsman co. (5), similar to the other but with the aim to accelerate the crosslinking reaction.

Aradur® 1571		
Aspect (visual)	White viscous paste	
Viscosity at 25 °C	28000 - 40000	[mPa s]
Density at 25 °C (ISO 1675)	1.2	[g/cm^3]
Storage temperature	< 8	[°C]
Accelerator 1573		
Aspect (visual)	White viscous paste	
Viscosity at 25 °C	60000 - 90000	[mPa s]
Density at 25 °C (ISO 1675)	1.08	[g/cm^3]
Storage temperature	< 8	[°C]

Table 2 Technical data of DICY-based curing agents by Huntsman co. catalogue (5)

- DETA (Diethylenetriamine)

The second curing agent is DETA, a linear ethylene-amine containing two primary and one secondary nitrogen. DETA is a single-component product that is clear and colourless, with an ammonia-like odour. It has many applications in several sectors like textile, minerals, asphalt production and many others (6).

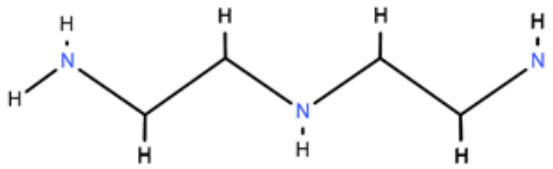

Figure 4 2D sketch of DETA molecule

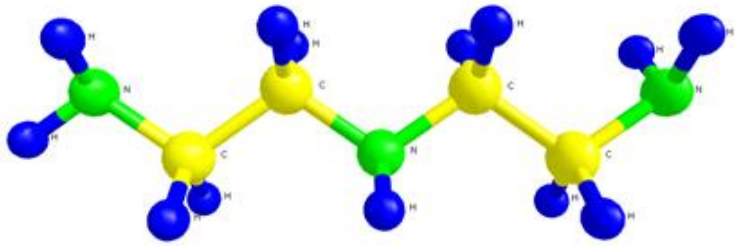

Figure 5 3D view of DETA molecule (own work by VEGAzz)

Regulatory Information	
DOT/TDG Classification	Diethylenetriamine
HMIS Code	3-1-0
WHMIS Classification	D2A, D2B, E
CAS Number	111-40-0
Chemical Control Laws	
Canada, DSL	Listed
United States, TSCA	Listed
Typical Physical Properties	
Amine value, mg KOH/g	1626
Boiling point, 760 mm Hg, °C (°F)	207 (405)
Coefficient of expansion, 1/°C, 20°C	0.00106
Density, g/ml, 20°C	0.952
Dielectric constant, 25°C and 1 kHz	12.0
Electrical conductivity, µmhos/cm, 24°C	0.32
Flash point, PMCC, °C (°F)	102 (215)
Freezing point, °C	- 39
Heat of formation, kcal/mol	- 17.3
Heat of vaporization, BTU/lb	194.8
Heat of combustion, BTU/lb	14008
Ionization constants, K_b 1	7.1E-5
Ionization constants, K_b 2, 25°C	5.2E-6
Kinematic viscosity, cSt, 25°C	5.8
Kinematic viscosity, cSt, 40°C	3.7
Molecular weight, Linear component	103.17
Molecular weight , Typical product	103.1
Nitrogen content, %	40.6
pH	12-13
Refractive index, 25°C	1.481
Specific gravity, 20/20°C	0.95
Specific heat, cal/g °C, 20°C	0.522
Surface tension, dynes/cm, 20°C	41.8
Thermal conductivity, cal/cm-sec-°C, 20°C	0.000523
Vapor pressure, mm Hg, 20°C	0.37
Viscosity, cSt, 25°C (77°F)	4
Water solubility	>10

Table 3 Technical data of DETA by Huntsman co. bulletin (6)

1.1.3 CROSSLINKING PROCESS

The neat polymer DGEBA/DICY/DETA is the result of epoxy cross-linking with curing agents. The reactive groups involved are the epoxy groups (COC rings) for the chief ingredient and primary or secondary amine groups (NH_2^-) for curing agent molecules. With lower frequency also hydroxyl groups (OH^-), already present or generated by the other reactions, can react with epoxy forming another active hydroxyl group. Epoxy groups are very reactive; their reaction enthalpy is around 96 [kJ/mol] with many chemical species, with consequent little endothermic reaction. Typically, using amine-functional curing agents, crosslinking takes place at room temperature.

The dominant reactions are the ones involving epoxy and primary or secondary amines, both forming a hydroxyl group and respectively a secondary and a tertiary amine.

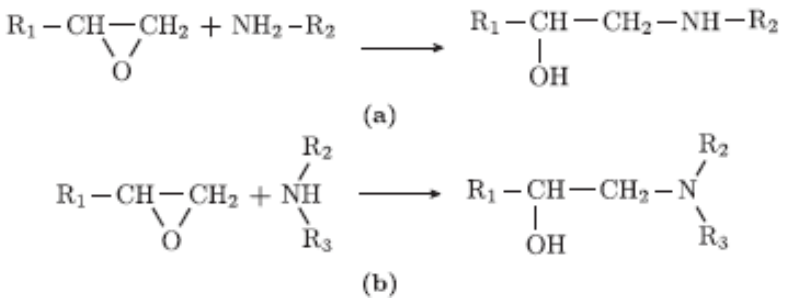

Figure 6 Main reaction between epoxy and (a) primary or (b) secondary amine (7), with permission of the publisher (License n. 4784301158452)

Beside these reactions, there is one more involving hydroxyl groups, which is the etherification reaction of the epoxy group, where OH groups may belong to one of the products of the previous reactions.

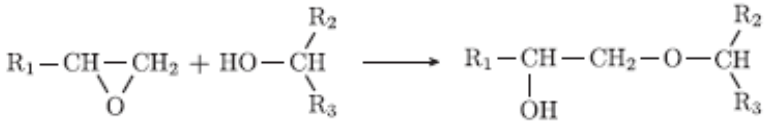

Figure 7 Etherification reaction between epoxy and hydroxyl group (7), with permission of the publisher (License n. 4784301158452)

R. Unger et al. (7) conducted Near Infrared (NIR) spectroscopic measurements, during a 5 hours isothermal curing at 80 [°C] with an additional heat up of 50 minutes as starting ramp from room temperature. Spectroscopy methods are suitable to identify chemical composition and guess the variation in concentration of each chemical species present in the compound.

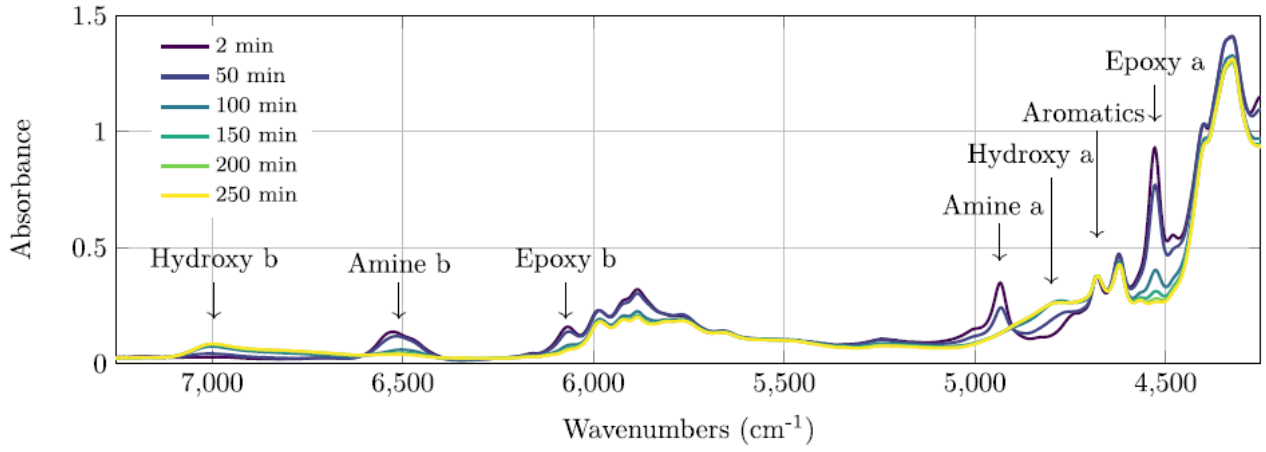

Figure 8 Results of NIR measurements during the crosslinking process (7), with permission of the publisher (License n. 4784301158452)

Looking at the signals in Figure 10: “Amine a” are primary amine groups, “Amine b” are both primary and secondary amine groups, “Epoxy a” are functional epoxy groups, “Epoxy b” are overtone signals from CH stretching, “Hydroxyl a” are functional hydroxyl groups, “Hydroxyl b” are overtone of OH stretching and “Aromatics” are combination of aromatic C-C and CH stretching.

From exemplarily spectra, is possible to observe the decrease of epoxy and amines in time and on the other hand the increase of hydroxyl groups. Aromatics signals act as invariant reference signals and do not depend on the curing process. For a standard mixture of this type (e.g. 100:30 epoxy/agents ratio), after around 50% of epoxy groups consumption, almost all primary amines are already bonded and there is a peak in secondary amines concentrations, which are the product of the first reaction, since the latter is dominant. This leads to an increase of the occurrence of the second reaction, which becomes dominant until the end of curing process, with tertiary amines as products. At the end, both primary amines and epoxides concentration converge to zero, while there is still an amount of secondary amines left, tertiary amines and hydroxyl groups. Changing the mixture composition there are no evident changes in the hydroxyl signals, which means that even

with poor amines content the possible etherification reaction between epoxy and hydroxyl is quite rare.

V. Strehmel et al. (8) found that for amine curing processes without accelerator agents, the etherification reaction involving hydroxyl groups does not take place at all. However, is noteworthy that such reaction, besides being rare, does not modify hydroxyl groups' balance, since one active hydroxyl group is present among both reactants and products. For this reason, cross-linking models usually neglect etherification reactions.

1.1.4 MECHANICAL PROPERTIES

A.A. Benzerga et al. (9) carried out the elastic and plastic behaviour of DGEBA epoxy under uniaxial tension and compression, with different mixing ratios of curing agents.

Material parameter	Units	Description	DGEBA 50:50	DGEBA 100:0
ρ	kg/m^3	Mass density	1,100	1,100
E	GPa	Young's modulus	2.6	2.9
ν	—	Poisson's ratio	0.4	0.4
s_0	MPa	Initial shear strength	40	45
s_1	MPa	Prepeak strength	75	90
s_2	MPa	Saturation strength	42	57
h_0	MPa	Slope of yield drop	1,200	1,500
$\dot{\varepsilon}_0$	$10^{15}\ s^{-1}$	Rate-sensitivity factor	200	200
A	K^{-1}	Temperature-sensitivity factor	550	550
α	—	Pressure sensitivity parameter	0.027	0.02
C^R	MPa	Rubbery modulus	7.5	15
N	—	Number of links between entanglements	3.8	4

Table 4 Mechanical properties of DGEBA LY556 with two different mixing ratios for curing agents (9)

In 50:50 configuration, the rubbery modulus is about one-half of respect to the 100:0, while the Young modulus is slightly lower. Hence, the second configuration is slightly stiffer, but for temperatures higher than the glass transition temperature, within the rubbery plateau, where elastic modulus decrease by an order of magnitude, the difference between the two increases.

Considering that Young modulus of the most common steels is around 200 [GPa] (10), is possible to state that steel is about 100 times stiffer than DGEBA.

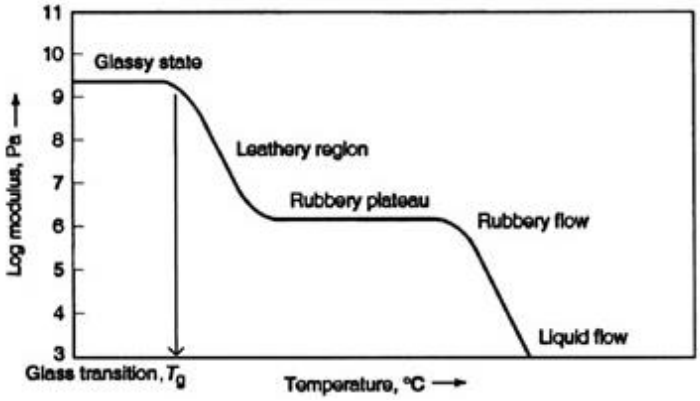

Figure 9 Elastic modulus vs temperature for polymers (11)

The stress-strain curves under tension and compression show the high non-linearity of the behaviour. Under tensile stress, the component fails for a deformation of about 0.1 and 50:50 configuration fails at a tension of a little bit more than one-half of 100:0.

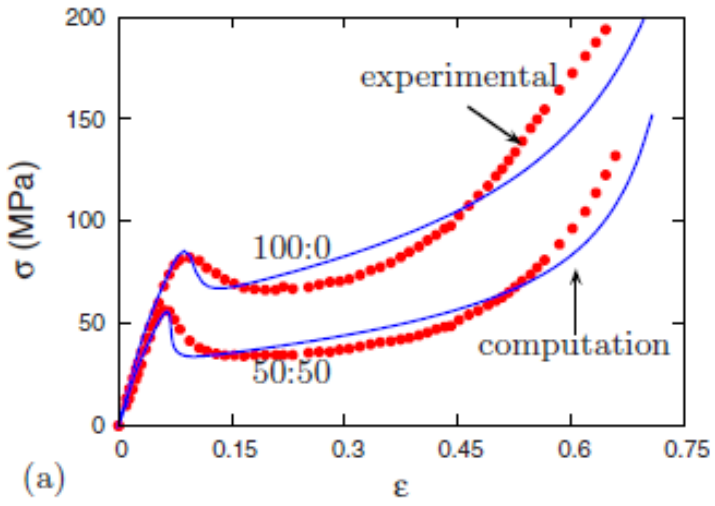

Figure 10 Uniaxial compression (experimental data from (12)) with two different mixing ratios for curing agents (9)

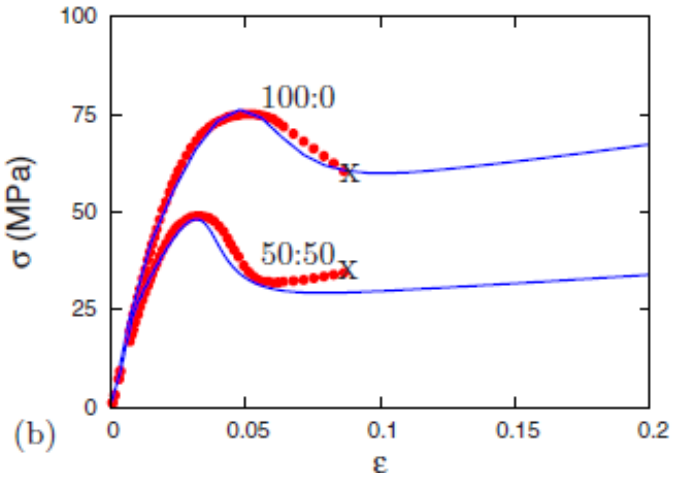

Figure 11 Uniaxial tension (experimental data (12)) with two different mixing ratios for curing agents (9)

1.2 Mesoscale Models of Epoxy in the literature

1.2.1 WHY MESOSCALE MODELS?

The focus of this literature review is on the modelling of mechanical properties like Young modulus, Shear modulus and Poisson ratio, in order to compute the stiffness matrix and carry out the strain-stress behaviour. The materials considered are carbon-reinforced polymers, a combination of polymer matrix with a large range of filler materials that have at least one dimension in the order of nanometres. Polymers are among the most interesting materials because of their low cost, reproducibility and easy processing compared to ceramics and metals, while graphene compounds (G, GO, rGO) or carbon-nanotubes (CNT) act as fillers, with many possible applications like sensors, gas storage devices, conductive glues, lightweight tough materials for aerospace or motorsport etc.

In order to investigate on mechanical properties of such a material, several models from nanoscale to meso/macro scale can be useful, as steps of a multiscale approach.

Due to the very small size is difficult to measure mechanical properties of such a material by direct methods. For this reason, various experimental techniques (SEM, TEM, AFM, Raman spectroscopy)

are adoptable, but they provide insufficient insight into molecular scale processes such as the interfacial interactions between nanotubes and matrix and the strain-stress behaviour.

Hence, several theoretical models like Molecular Dynamics (MD), Finite Elements (FE), continuum and analytical models are available in different scales, validated through the comparison with experimental results.

Atomistic MD simulations have been widely used in modelling nanocomposites, but the huge computational effort needed limits their applicability to relatively small systems and over a small time-scale.

This review does not include atomistic MD models (order of Angstrom), but is focused on mesoscale and continuum models (micro up to macroscale).

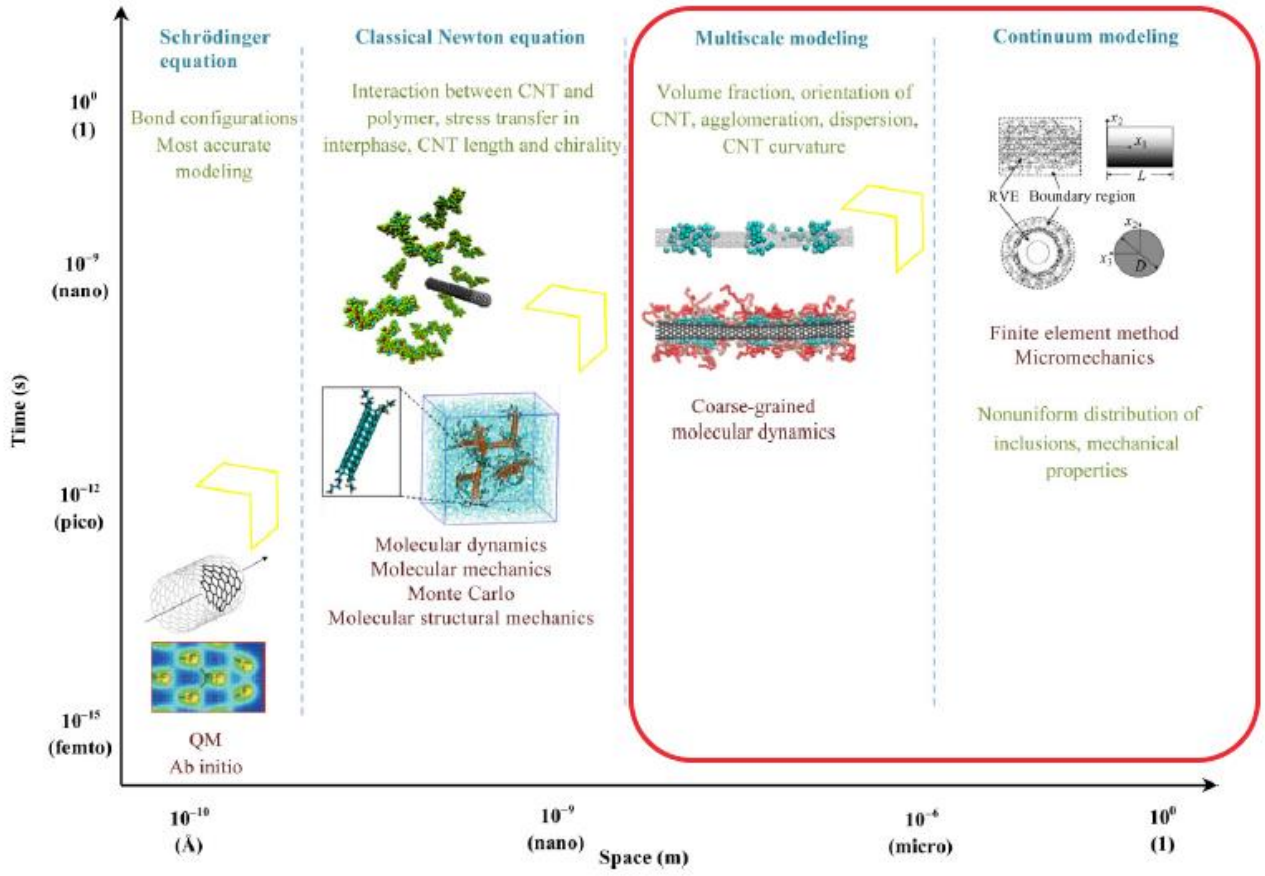

Figure 12 Time and space scales of composite modelling (13)

Atomistic simulations give a very good level of chemical details, but are prohibitively expensive concerning computational cost. Moreover, they are limited in time and length scale.

The basic idea to overcome those limits is to study systems with less particles, reducing the degree of freedom of the system (DOF). Coarse-grained molecular dynamics (CGMD) models follow this path. In CGMD models, atoms cluster into groups, called beads of super-atoms, which are the new basic particles of the system, typically spherical. Then, for each typology, dimensions and potential calculation for each bead follows.

The main reason to do this is to overcome MD limitation about time step (tens of microsecond) and length scales (tens of nm), currently not accessible with fully atomistic description.

There are several methods to cluster the atoms and to calculate the coarse-grained (CG) force field, namely Coarse-Graining Methods. Some example from literature are below.

1.2.2 COARSE-GRAINING: THEORETICAL ASPECTS

The aim of coarse-graining is to replace full atomistic representation by a model with less particles (CG beads), each one including several atoms forming a pattern which is repeated inside the simulation box. This allow to overcome time and space limits and to get lower computational cost, which can be critical for atomistic models of complex systems. For this reason, it is widely used for biological systems in which complexity of molecules can reach very high level. Recently, also CGMD for polymers is subject of study.

In mathematical terms, given an atomistic Hamiltonian function for an atomistic model AA, which describes the energy content of the system as the sum of kinetic and potential energy:

$$H^{AA} = \sum_{i=1}^{n} \frac{p_i^2}{2m_i} + U^{AA}(r_1, \dots, r_n)$$

Where p_i , m_i and r_i are respectively momentum, mass and Cartesian coordinate of i^{th} atom and U^{AA} is the potential energy resulting from the different bonded and non-bonded interactions between atoms.

In the same way is possible to define a Hamiltonian function for a coarse-grained model CG as:

$$H^{CG} = \sum_{j=1}^{N} \frac{P_j^2}{2M_j} + U^{CG}(R_1, \dots, R_N)$$

Where P_j, M_j and R_j are respectively momentum, mass and Cartesian coordinate of j^{th} bead and U^{CG} is the potential energy resulting from the different bonded and non-bonded interactions between beads.

Formally, these two configurations are linked by the application of a mapping operator $M(r^i)$, which describes how CG beads are constructed starting from the atomistic configuration

$$M(r^i) = \{M_1(r^i), \dots, M_2(r^i)\}$$

A typical mapping choice, once identified a subset of atoms establishing a pattern, is to consider the centre of mass of such a discrete systems of points as a bead, but other choices are possible depending on the case. The most challenging task for a CG model is to define a proper set of interaction potentials $U^{CG}(R_1, \dots, R_N)$ between beads.

Concerning polymers, literature shows several approaches to this problem, classifiable in[1]:

- United Atoms (UA) consisting in small functional group beads (e.g. methyl)
- Pearl-necklace, mostly used for polymer solutions (14)
- Ellipsoidal beads for long chains of most complex organic systems (15)
- Bead-spring, using standard harmonic potentials to describe interactions

[1] CG Theoretical aspects and classification from *R. Raflee* (13)

It is possible to calculate the force field by iteratively adjusting potential parameters starting from the potential of mean forces derived from Boltzmann inversion or inverse Monte Carlo method, in order to have a good match with structural aspects, such as distribution functions. The main issue here is to reproduce identical thermodynamic conditions for inter-beads potential's transferability.

For this reason, a good agreement between structural aspect and thermodynamic properties is impossible in practice, there is a trade-off between these two features concerning accuracy of the models.

Moreover, there are several ready-to-use force fields, which are available for different areas of interest. Typically, they come from by *ab initio* calculations or by tuning parameters to experimental evidences. COMPASS force field has been employed for several full atomistic MD, while MARTINI force field has been widely used for biological systems CGMD, but it has been recently extended to polymers, in particular, *G.Rossi et al.* applied it to a thermoset polyester coating (16). *C.Chen et al.* (17) have studied poly-ethylene oxide (PEO) modelling and compared Explicit Atoms (EA), in which every, UA grouping CH_2-CH_3 groups, and CG clustering six atoms in one bead. It has been observed that the performance of all three models is comparable and in agreement with neutron diffraction for static properties, so it is not relevant that one more accurate than the others.

1.2.3 ITERATIVE BOLTZMANN INVERSION (IBI)

It is a structure-based systematic coarse-graining method to determine the effective pair potential of particles in thermal equilibrium from the Radial Distribution Function (RDF) obtained in atomistic simulations. RDF is a pair correlation function describing how atoms are radially packed in a system around each other, on average:

$$g(r) = \frac{n(r)}{4\pi r^2 \rho \Delta r}$$

With $n(r)$ the mean number of atoms in a shell of width Δr at distance r.

Then, once the RDF of the corresponding DOF q (stretching, bending, torsion, non-bonded, etc.) is available, Boltzmann inversion is applied:

$$U(q) = -k_B T ln P(q)$$

Where the Boltzmann constant is $k_B = 1{,}38 \cdot 10^{-23} \left[\frac{J}{K}\right]$, T is the temperature in Kelvin and $P(q)$ is the probability of the corresponding DOF.

Inversion can be direct for bonded potentials, but not for non-bonded as Van der Waals and Coulomb one. In case of non-bonded interactions, the method can be iteratively refined:

$$U^{CG\,(i+1)} = U^{CG\,(i)} + \lambda k_B T ln\left(\frac{g_i^{CG}(r)}{g_*^{CG}(r)}\right)$$

Where i is the iteration number, $g_*^{CG}(r)$ is the target RDF and λ is a stabilization factor initialised at 0.45 and then increased up to convergence.

However the so obtained $U(q)$ do not provide necessarily the correct thermodynamic behaviour due to the pressure effect. Therefore, there is an additional correction:

$$\Delta U_p = -f \frac{p_i - p_0}{p_i} k_B T \left(1 - \frac{r}{r_{cut-off}}\right)$$

Where i is the iteration, f is a stabilization factor initialised at 10^{-5}, p is the pressure in atm, $r_{cut-off}$ is a fixed cut-off distance beyond which correction vanishes.

IBI method gives unique force field for a RDF according to Henderson Theorem which states:

"*Two potential energy functions that produce the same RDF can differ only by a constant".*

In other words, for a given RDF there may exist only a single pair interaction potential, which returns the target RDF. The main drawback of IBI is that convergence is difficult to achieve in practice (18).

1.2.4 MARTINI FORCE FIELD

It is a structure/thermodynamic based method developed by *S.J. Marrink et al.* (19), suitable for molecular dynamics simulation of biomolecular systems like lipids, sugars and proteins, but the viability recently has recently tested also for polymers and nanoparticles.

Original MARTINI for biomolecules

MARTINI approach is based on a four-to-one mapping, i.e. typically four heavy atoms and associated hydrogens are represented by a single interaction centre, except for ring-like molecules (benzene etc.), for which a higher resolution is required. The name "MARTINI" was coined in 2007 and is a nickname of Groningen in Netherlands, where the force field was developed, which is famous for the 100 meters Martini tower. The name also reflects the universality and the flexibility of the Martini cocktail, very few ingredients for and endless variety of tastes (20).

For the sake of simplicity, there are only four main types of interaction sites: polar (P), nonpolar (N), apolar (A), charged (Q). Subtypes are also defined by a letter denoting the hydrogen-bonding capabilities ("d" for donor, "a" for acceptor, "da" for both, "0" for none), or by a number between 1 and 5 indicating the degree of polarity.

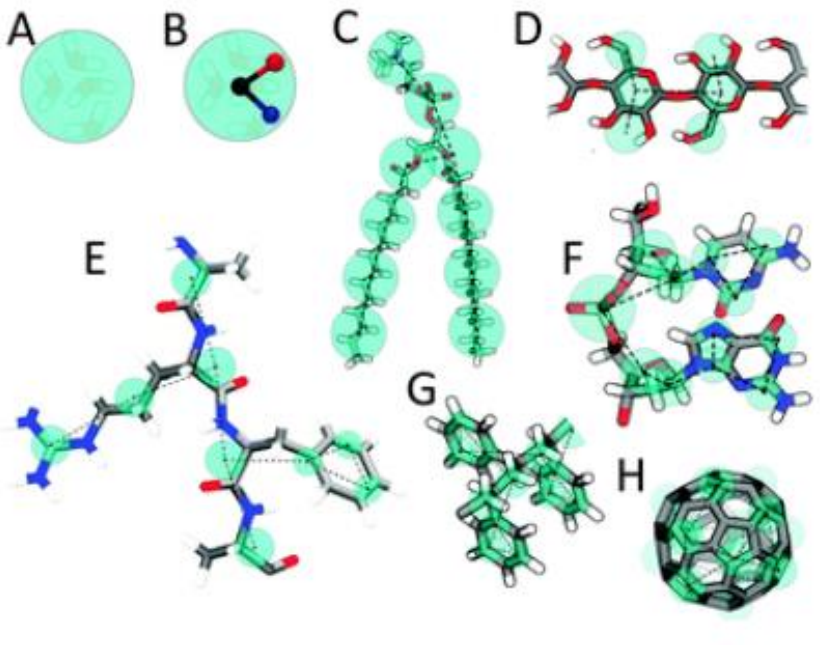

Figure 13 Martini mapping examples for: (A) Standard particle representing four H2O molecules, (B) Polarizable water molecule with embedded charges, (C) DMPC lipid, (D) Polysaccharide fragment, (E) Peptide, (F) DNA fragment, (G) Polystyrene fragment, (H) Fullerene. Reprinted with permission of (21), Copyright © 2008, American Chemical Society

For example, *L. Monticelli et al.* (22) extended the model to proteins, in particular to a peptide-bilayer system. All the different amino acids are represented in one of the four types.

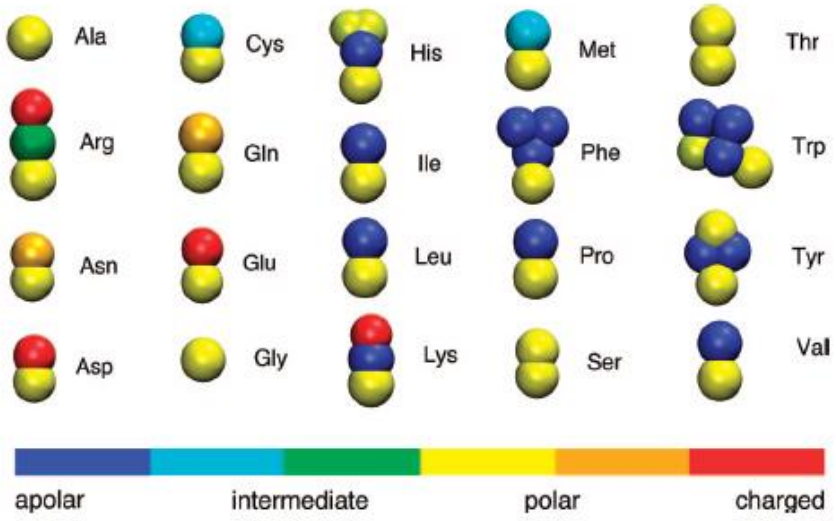

Figure 14 CG representation of all amino acids. Reprinted with permission of (22), Copyright © 2008, American Chemical Society.

A comparison between simulation results and experimental measurements of the water/oil partitioning coefficients of the amino-acid side-chain analogues leads to a proper choice of particle type's definition.

Simulation data are calculated from equilibrium densities of low concentrations of CG beads dissolved in a water/butane two-phase system. The free energy of partitioning between oil and aqueous phases $\Delta G^{oil/aq}$ was obtained from the equilibrium densities ρ of CG particles in both phases as:

$$\Delta G^{oil/aq} = kTln\left(\frac{\rho_{oil}}{\rho_{H2O}}\right)$$

Equilibrium densities are the results of MD simulation of the two-phase system in which around 0.01 molar fraction of the target compound is dissolved.

side chain	CG representation	mapping scheme[a]	free energy (kJ/mol) CG	free energy (kJ/mol) exptl.
Leu	C1[b]		22	22
Ile	C1[b]		22	22
Val	C2[b]		20	17
Pro	C2[b]		20	
Met	C5		9	10
Cys	C5		9	5
Ser	P1		−11	−14
Thr	P1		−11	−11
Asn	P5		< −25	−28
Gln	P4		−23	−25
Asp	Qa		< −25	
Asp (uncharged)	P3		−18	−19
Glu	Qa		< −25	
Glu (uncharged)	P1		−11	−11
Arg	N0−Qd	N0: Cβ−Cγ−Cδ−Nε	< −25	
Arg (uncharged)	N0−P4	Qd/P4: Cζ−Nω1−Nω2	−23	−25
Lys	C3−Qd	C3: Cβ−Cγ−Cδ	< −25	
Lys (uncharged)	C3−P1	Qd/P1: Cε−Nω	−1	−2
His	SC4−SP1−SP1	SC4: Cβ−Cγ SP1: Cδ−Nε SP1: Nδ−Cε	−19	−20
Phe	SC4−SC4−SC4	SC4: Cβ−Cγ−Cδ1 SC4: Cδ2−Cε2 SC4: Cε1−Cζ	19	17
Tyr	SC4−SC4−SP1	SC4: Cβ−Cγ−Cδ1 SC4: Cδ2−Cε2 SP1: Cε1−Cζ−OH	−1	−2
Trp	SC4−SP1−SC4−SC4	SC4: Cβ−Cγ−Cδ2 SP1: Cδ1−Nε−Cε1 SC4: Cε2−Cζ2 SC4: Cε1−Cω	12	9

Table 5 Mapping of the amino acids and free energy of partitioning water-butane. Reprinted with permission of (22), Copyright © 2008, American Chemical Society.

Thermoset polyester resin MARTINI-based model

G. Rossi et al. (16) adopted MARTINI CG model to a thermoset polyester resin, in which there is the issue of cross-linking, a condition that occurs because of chemical reaction between monomers and for example some curing agents (HMMM, DICY/DETA etc.).

Several MD simulations with mathematical post-processing in between are necessary to obtain the equilibrated cross-linked molecules, with updated partial charges, for several cross-linking degrees (CD). During these simulations, there are some bonding steps, in which some groups form new bonds (depending on $r_{cut-off}$). Therefore, there is a temporary formation of new structures. Breaking step follows, in which bonds or atoms in excess are deleted.

In this case, non-bonded interactions of beads are parametrized based on their free energy transfer between water and octanol, and polyester chains split into chemical moieties characterized by different polarity, in order to associate each of them to the correct MARTINI bead-type.

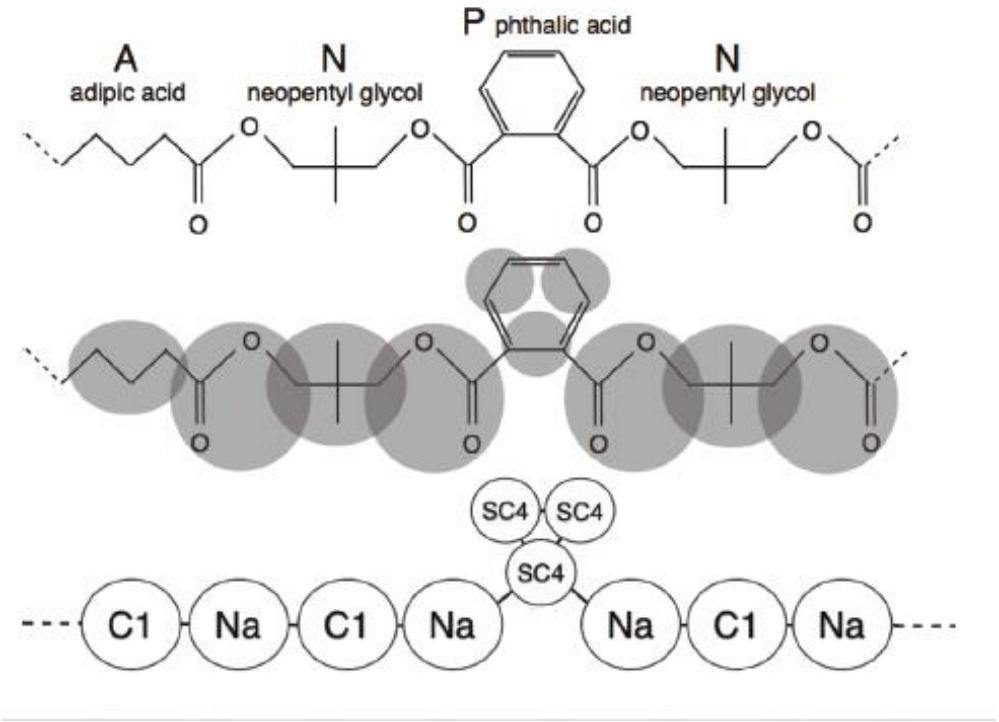

Figure 15 Atoms-to-MARTINI CG mapping schemes. Reprinted with permission of (16), Copyright © 2011, American Chemical Society.

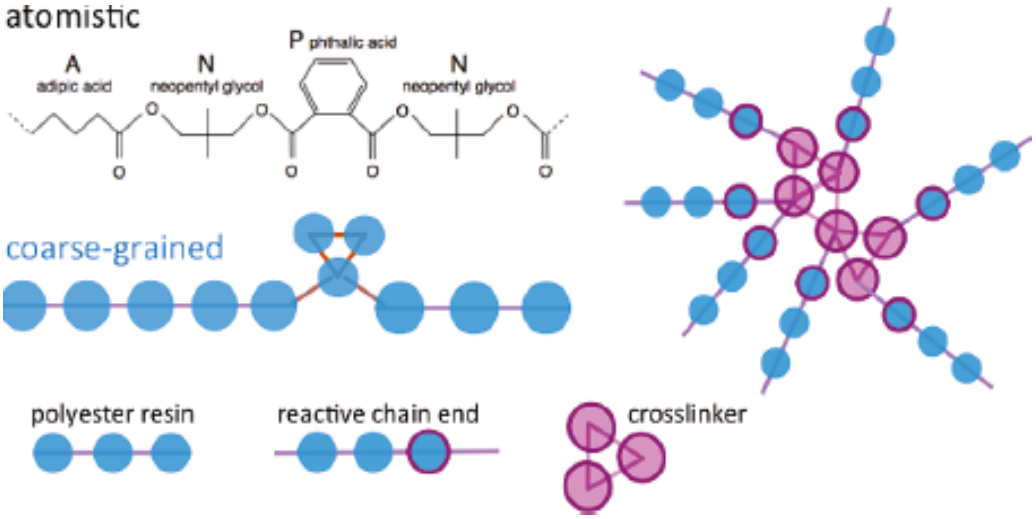

Figure 16 Cross-linking process between polyester and curing agent. Reprinted with permission of (16), Copyright © 2011, American Chemical Society.

Polyester resin parametrization

After the system mapping phase, is possible to calculate the force field by parametrizing bonded and non-bonded interactions.

According to MARTINI model, non-bonded pairs i and j at distance r_{ij} interact through a Lennard-Jones (LJ) potential, which includes attractive and repulsive Van Der Waals forces.

$$U_{LJ}(r_{ij}) = 4\varepsilon_{ij}\left[\left(\frac{\sigma_{ij}}{r_{ij}}\right)^{12} - \left(\frac{\sigma_{ij}}{r_{ij}}\right)^{6}\right]$$

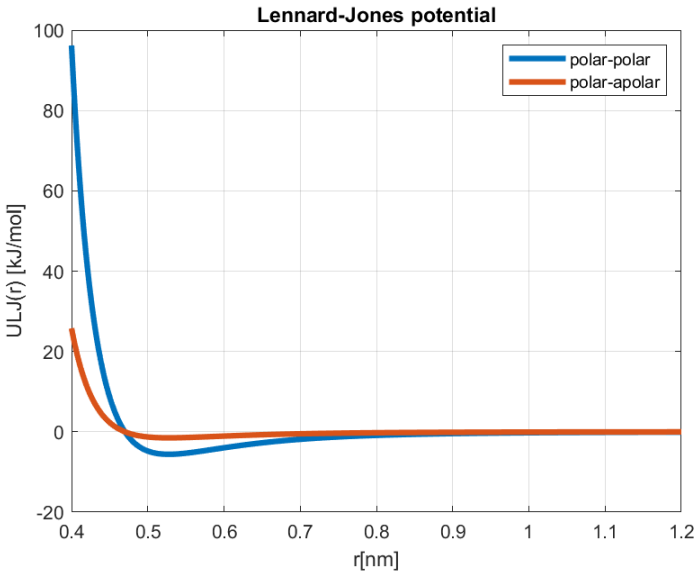

Figure 17 LJ potential vs distance for polar-polar and polar-apolar interactions (own work, MATLAB)

ε_{ij} parameter determines the strength of interaction and it ranges from 5.6 [kJ/mol] for strong polar-polar interactions, to 2.0 [kJ/mol] for polar-apolar interactions mimicking hydrophobic effect.

σ_{ij} parameter depends on the effective size of the particles, 0.47 [nm] for all normal particle types and 0.43 nm for model ring-ring interactions with ε_{ij} scaled to 75% of the standard value.

Moreover, charged groups with a charge q interact via a Coulombic potential:

$$U_{el}(r_{ij}) = \frac{q_i q_j}{4\pi\varepsilon_0\varepsilon_{rel} r_{ij}}$$

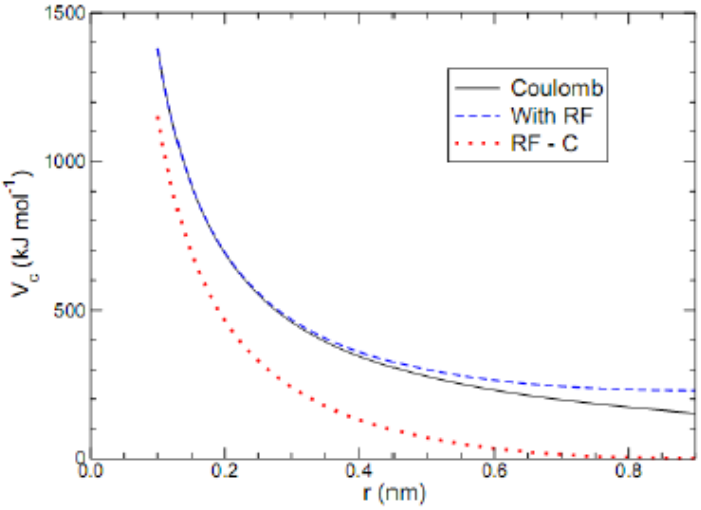

Figure 18 Coulomb potential vs distance (own work, MATLAB)

Where ε_0 and ε_{rel} are the dielectric constants respectively of vacuum and screening medium.

Cut-off and shifting distances are fixed to avoid unwanted noise, respectively at 1.2 [nm] and 0.9 [nm].

Bonded interactions are by means of simple harmonic bond and angle potentials, similar the ones of classical MD simulations. As already done in polystyrene modelling by *G. Rossi et al.* (16), it is possible to omit the torsional proper dihedral angle at the CG level.

- Bond Stretching between two covalently bonded sites i and j

$$U_b(r_{ij}) = \frac{k_d}{2}(r_{ij} - b_{ij})^2$$

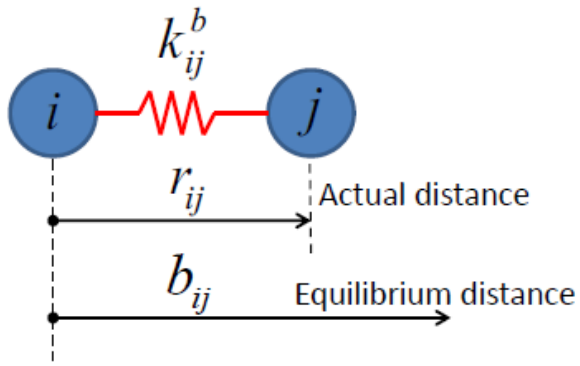

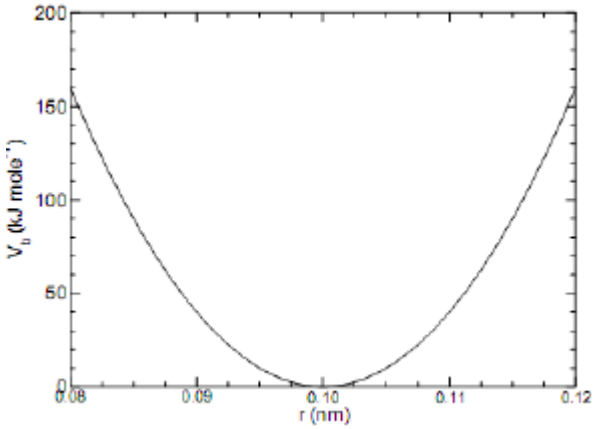

Figure 19 Stretching potential representation (42)

- Bond Angle vibration between a triplet of sites i, j and k:

$$U_a(\theta_{ijk}) = \frac{k_\theta}{2}(\theta_{ijk} - \theta_{ijk}^0)^2$$

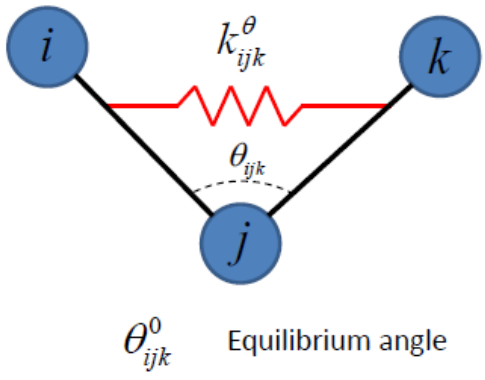

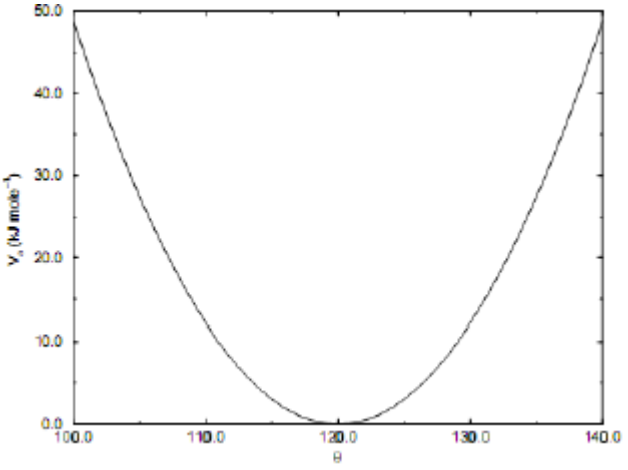

Figure 20 Bending potential representation (42)

- Improper dihedral potentials, meant to keep planar groups (e.g. aromatic rings) planar. Four sites i, j, k and l are involved. Improper dihedral angle is defined by two planes (i, j, k) and (j, k, l):

$$U_{id}(\xi_{ijkl}) = k_{\xi}(\xi_{ijkl} - \xi_0)^2$$

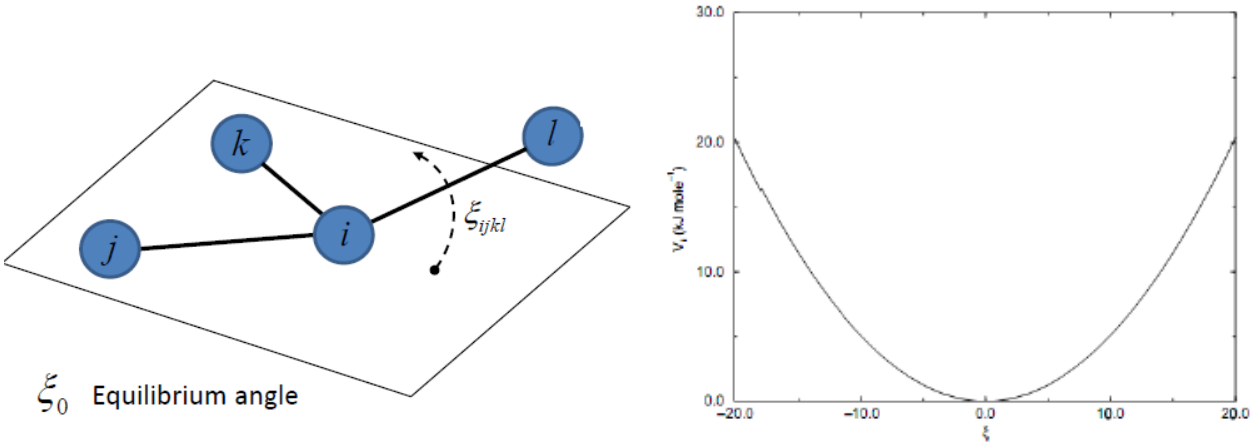

Figure 21 Improper dihedral potential representation (42)

- Proper dihedral potentials affect the torsion. Four sites i, j, k and l are involved. Proper dihedral angle is defined by two planes (j, k, i) and (k, i, l):

$$U_d(\phi_{ijkl}) = k_{\phi}[1 + \cos(n\phi_{ijkl} - \phi_s)]$$

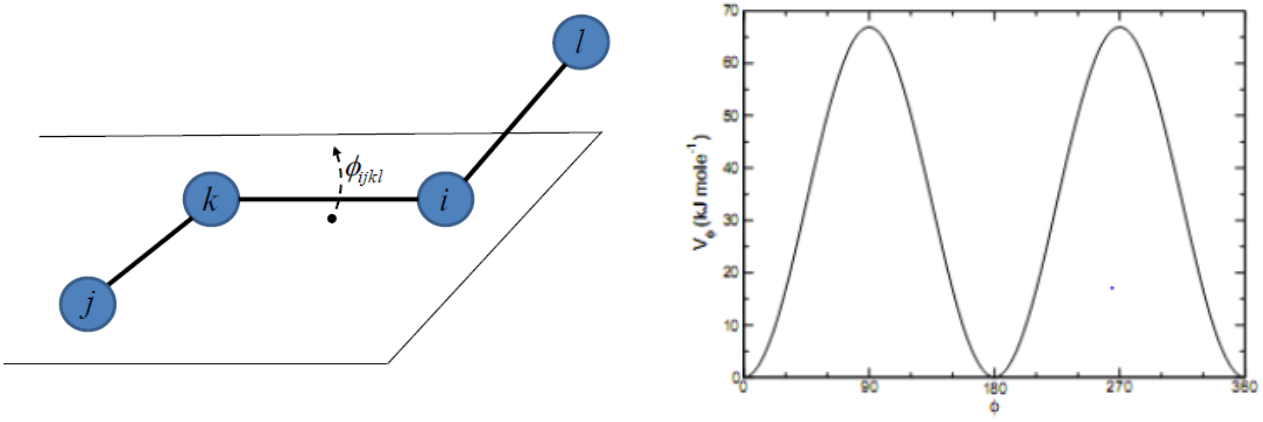

Figure 22 Torsional potential representation (42)

Equilibrium positions and elastic constant values are obtained through atomistic MD, with GROMACS 4.0.2 MD package, on NPT (isothermal-isobaric) ensemble. Nosè-Hoover thermostat and Parrinello-Rahman barostat control respectively temperature and pressure. Time step is set to 2 [fs] and the system is equilibrated at room T and atmospheric p. The distributions of bonds and angles are averaged over 200 [ns] trajectories and equilibrium values for CG bonds and angles are chosen as the average values of atomistic distribution. In CG simulation, same thermodynamic conditions are set, but the time step is 20 fs (16).

Concerning cross-linking, in this case HMMM is mapped using three beads. Each CG bead is at the centre of mass of two (CH_2) groups, an N atom, a C and two N atoms from triazine ring. Beads include two N atoms from central triazine group in common with the other two beads. Distance between beads is set at an equilibrium value of 0.4 [nm].

For non-bonded interactions, the particle type for HMMM beads depends on free energy related to the transformation of HMMM molecule between water and octanol. According to this, the most suitable representation in terms of MARTINI beads are three N0 particles:

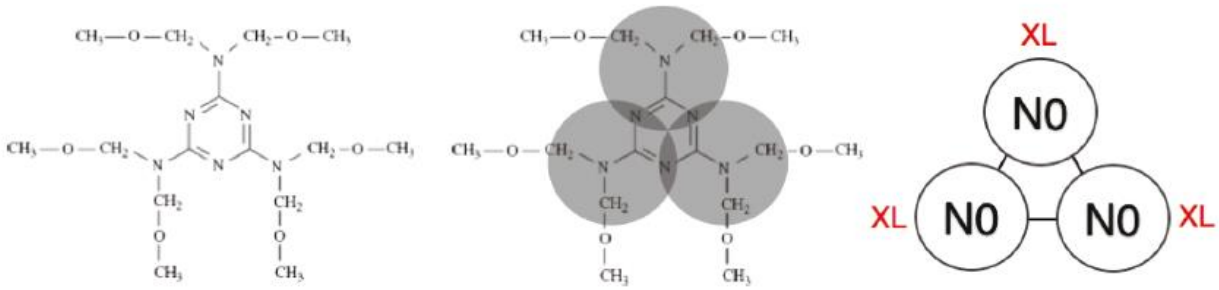

Figure 23 Atomistic-to-CG mapping of HMMM. Reprinted with permission of (16), Copyright © 2011, American Chemical Society.

We can consider cross-links as covalent bonds between the terminal hydroxyl groups of polymer chains and the HMMM methoxide groups.

Cross-linking interactions are modelled through *ad hoc* potentials between HMMM beads, called XL and some terminal beads of the chains, called CE. There are both XL-CE and XL-XL interactions to be taken into account. CD depends on XL-CE bonds number.

Such *ad hoc* potential has a harmonic part up to 0.5 [nm], with an elastic constant $K_b = 8000 \left[{}^{kJ}/_{mol}\right]$, and it smoothly goes to zero between 0.5 [nm] and 0.6 [nm] by means of a fourth order polynomial.

Polyester resin mechanical properties computation

CGMD simulations are performed on a system with several polyester chains, considering different samples: non cross-linked, partially cross-linked and fully cross-linked; all simulations are run in NPT ensemble, with a time step of 20 [fs].

1. As a first step, pure resin melt equilibration is conducted, chains are stacked close to each other in an intermediate-coiled state, and allowed to collapse at T=500 [K] for 1 [μs]. Self-diffusion coefficient of the chains of the reference system during equilibration is measured as $D = 1.2 \cdot 10^{-8} \left[{}^{cm^2}/_{s}\right]$. Starting from equilibrated snapshot, several independent equilibration runs over a time scale corresponding to the time that chains need to diffuse over a length scale comparable to their radius of gyration (0.3 [μs]).

   Equilibrium density $\rho = 1300 \left[{}^{kg}/_{m^3}\right]$ is carried out, about +17% with respect to experimental data.

2. Cross-linking takes place by inserting HMMM molecules, in random position, in each of the previously generated equilibrium configurations. Local energy minimization is useful to eliminate overlaps and a new equilibration for 0.1 [μs] at 500 [K] is conducted, not considering yet cross-linking *ad hoc* potentials, in order to allow a proper dispersion of HMMM.

   The high temperature enhances the curing agent dispersion ($D_{HMMM} = 8 \cdot 10^{-7} \left[{}^{cm^2}/_{s}\right]$), such as solvent agents that are normally added during the paint preparation which takes place at room temperature. By equilibrating at 500 [K], it is not necessary to add further molecules and complicate the simulations. XL-XL and XL-CE bonds are activated in another run of 0.1 [μs] at 500 [K] leading to the formation of more than 98% of bonds between active

chains ends and cross-linkers. A subsequent cool down at 300 [K] with a cooling rate of 1.25 [K/ns] takes place in preparation for the tensile test.

3. Tensile tests are performed in order to study the stress-strain behaviour, by applying semi-isotropic pressure coupling to the simulation box. X and y stress tensor components are set to atmospheric pressure, compressibility is set as null in z direction, and the z edge of the box is expanded at a rate of 8.3e-8 [nm/ps] up to a deformation of 1.2%.

   After averaging the stress-strain curves from the different simulations, the slope of the best linear fit of the curves in the 0÷1 % strain range is the Young modulus E.

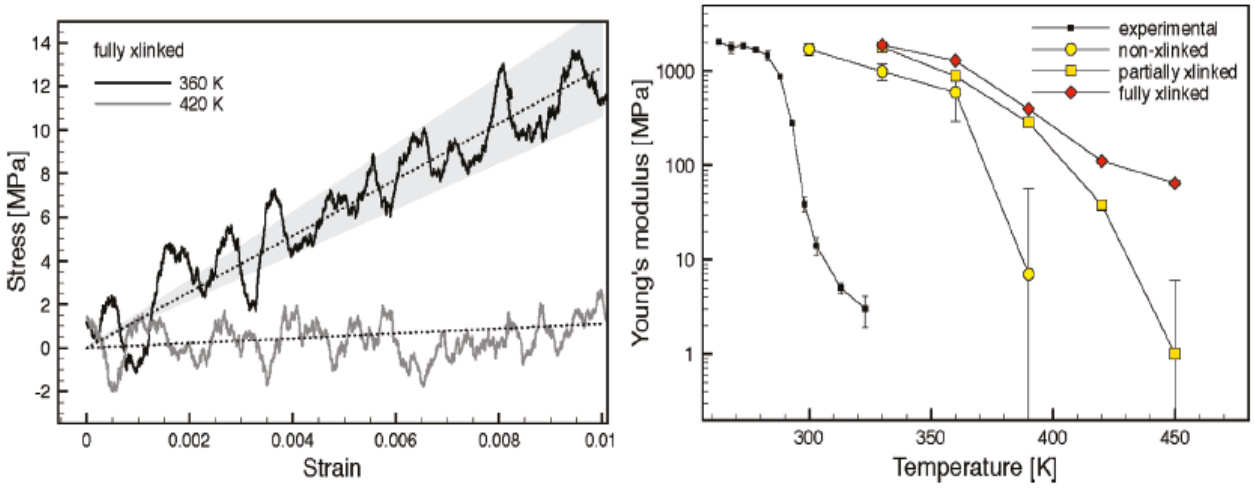

Figure 24 Stress-strain curves for fully cross-linked samples at different T, with linear fit curves used and Young's moduli calculated for different T. Reprinted with permission of (16), Copyright © 2011, American Chemical Society.

Mechanical reinforcements induced by the dispersion of nanofillers in the resin, which mutual interactions can be realistically captured by MARTINI, is under investigation. According to *Rossi et a*l. (16), this CG approach, initially aimed to bio-MD simulations, will be applicable to a large variety of polymer systems. However, it requires a recalibration for describing the elastic properties of CNTs.

Epoxy (EPN-BPA) MARTINI-based model

S. Yang et al. (23) developed a CG model for simulations of an epoxy phenol Novolac and phenolic curing agents system (EPN-BPA), adopting an iterative optimization approach, starting from MARTINI force field and implementing bond rupture in it, in order to model material failure. Monomers are chains of three or four backbone beads. Each of one has one reactive branching bead, where there is epoxy ring. Curing agents have two reactive beads, which represents amine groups, and one centre bead. LJ potentials describe inter-bead non-bonded potentials truncated at 2.5σ, while bonded interactions are a sum of a pure repulsive LJ truncated at $2^{1/6}\sigma$ and a quartic potential, accounting also for bond rupture:

$$U_b(r) = U_0 + k_4(r - r_c)^2(r - b_1 - r_c)(r - r_c)H(r_c - r) + 4\varepsilon\left[\left(\frac{\sigma}{r}\right)^{12} - \left(\frac{\sigma}{r}\right)^{6} + \frac{1}{4}\right]H\left(2^{1/6}\sigma - r\right)H((r_c - r)$$

Where $H(x)$ is the Heaviside step function of x, $k_4 = 1434.5\frac{\varepsilon}{\sigma^4}$ $b_1 = -0.7589\sigma$ and $U_0 = 67.2234\varepsilon$. Heaviside step function is defined as the integral of the Dirac delta and can be seen as the cumulate of a probability density function (PDF) of a sure event corresponding to the x in which $\delta(x)$ is equal to 1:

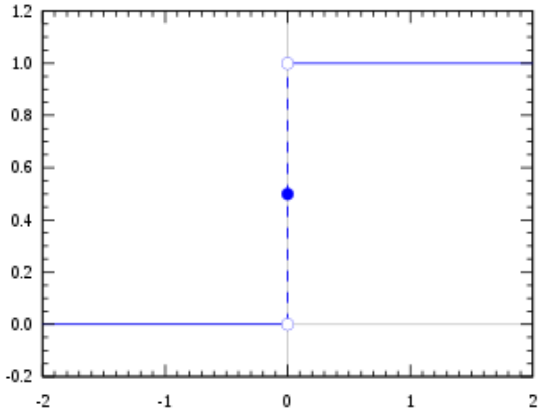

Figure 25 Heaviside step function H(x) (own work, MATLAB)

$$H(x) = \int_{-\infty}^{x} \delta(x')dx'$$

In addition, angular bending interaction is described by a typical harmonic function, for three different angle type:

- Angle between three beads in an epoxy monomer, with equilibrium $\vartheta_0^{(1)} = 100°$
- Epoxy branching bead/curing agent reactive bead, with equilibrium $\vartheta_0^{(2)} = 180°$
- All the angles formed within curing agent, with equilibrium $\vartheta_0^{(3)} = 180°$

Cross-linking process starts from a network structure epoxy and hardener monomers in a liquid mixture equilibrated in NPT controlled by Nosè-Hoover thermostat and barostat. During the simulations, if an epoxy branching bead is within a 1.3σ distance from a hardener reactive bead, there is 1% of probability to have a bond between the two. Simulations stop when the system reaches the desired degree of cross-linking, which is typically high for this problem, about 90%, taking up to 500000 steps. All the parameters above mentioned are optimized through Particle Swarm Optimization (PSO), a population-based stochastic method also used to simulate animal behaviours. The aim is to find a solution x_0 that satisfies the condition of $f(x_0) \leq f(x)$ for any x in the space.

Thus, once a vector of all the optimized parameters is computed $\mathbf{x} = \{M, \varepsilon, \sigma, r_c, k_\vartheta^{(1)}, k_\vartheta^{(2)}, k_\vartheta^{(3)}\}$, the objective function is defined as:

$$f(x) = \sum_{i=1}^{N} \left[\frac{g_i(\mathbf{x})}{y_i} - 1\right]^2$$

Where g_i is the set of N parameters calculated by the CG model, while y_i is the same set of known physical properties for the system considered, which can be the ones calculated by the full atomistic models available. Size of search space for each parameters can be subject of optimization by

empirical considerations or by conducting some parametric studies to guess the weight of each parameters on the potential and force field calculation.

Epoxy with improved crosslinking algorithm

A. Aramoon et al. (24) studied a CG model for a DGEBA-DAB (diaminobutane) epoxy resin focusing on the fact that existing cross-linking algorithms are not efficient and have severe computational limitations, since, in large epoxy systems, rate of reaction decrease quickly when gel point is reached and cross-linking process goes on very slowly. Thus, for systems having a large number of atoms, or a high degree of cross-linking as epoxy does, such algorithms provide bad results, with lower degrees of cross-linking and non-uniform distribution of curing bonds. In order to overcome these issues, groups of partially cross-linked chains of DGEBA monomers and curing agents are considered. This is to avoid chains longer than expected, and get uniformity in cross-links. Moreover, to speed up the reaction, the velocities of beads in regions where there is an excess of curing agents concentration varies in order to have like concentration gradient, which moves active groups towards lower concentration zones. Therefore, a redistribution algorithm, which mimics the process of shaking the simulation box, has been implemented. Beads velocities correction follows, to keep constant the temperature of the system. Bond formation control is also necessary, because the transportation of beads in regions with a very high concentration of active beads could be very slow. For this reason, there is a curing rate control in every region, by modulating the probability of bond formation, defining an acceptance rate a.

Acceptance rate is dynamically calculated, according to this formula:

$$a = a_{min} + H(\chi_{target} - \chi_{local})\left(\frac{\chi_{cell}}{\chi_{target}}\right) a_{max}\left(\frac{\chi_{cell}}{\chi_{local}}\right)$$

Where $H(x)$ is the Heaviside step function, χ is the degree of cross-linking, calculated as the ratio between available pairs of reactive beads ad number of bonds formed. With this equation, the more the average degree of cross-linking in the simulation box is closer to the desired one, the higher is

the probability that active group pairs form bonds. In addition, it decreases the local probability of bond formation in zones with higher local degree of cross-linking.

With respect to traditional algorithms, in the first 250000 steps, the system reaches a lower cross-linking degree, due to the beads redistribution, but increasing number of steps is possible to reach desirable values beyond 90% in about 750000 steps. This new algorithm is also included in the libraries of LAMMPS, in USER-MISC package.

Epoxy (EPN-BPA) under Couette and Poiseuille flow conditions

Y. Fu et al. (25) studied the structural behaviour of EPN-BPA melt, for different cross-linking degrees, under Couette and Poiseuille flow conditions, employing a Non-Equilibrium CGMD model. In this work, a 21000 beads system is defined, with 3 backbone beads for epoxy, each linked to a branching bead (epoxy active group), and one centre bead plus two reactive beads for hardener. Cross-linking procedure implements the probability of 1% to have a bond between reactive beads, if the distance between them is within 1.3σ, and the potential definition is the same of *S. Yang et al.* (23) (LJ for non-bonded and quartic potential for bonded) with a fixed value of cut-off distance $r_c = 1.343\sigma$. An Epoxy liquid mixture with an epoxy/curing agents ratio of 66.6:33.3, is equilibrated under NPT for 200000 steps with a time step of 6.48 [fs], using LAMMPS. Shear viscosity η is evaluated through SLLOD algorithm, under laminar Couette flow conditions. Couette flow is defined as the flow of a viscous fluid in the space between one fixed plate and one surface moving tangentially relatively to the other. A deforming cube representation of the Lees-Edward BCs, which is equivalent to the sliding-brick representation, is used. Nosè-Hoover thermostat is applied to remove dissipative heat generation in the fluid and keep the temperature constant at 612.2 [K]. Laminar flow conditions are ensured by the small size of the system (Reynolds number around 10 for highest shear rates considered).

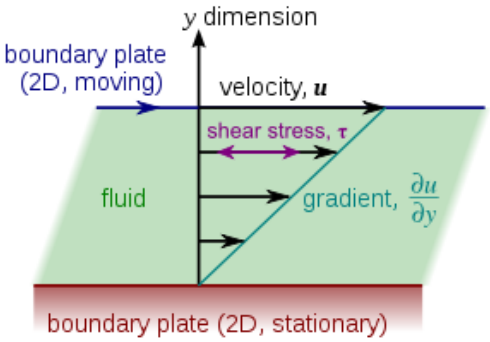

Figure 26 Velocity profile under Couette flow condition

Epoxy system experiments a homogeneous shear and the equations of motion of the i^{th} particle are two: velocity and acceleration expressed as first and second order time dierivative of the position:

$$\frac{d\boldsymbol{r}^i}{dt} = \frac{\boldsymbol{p}^i}{m} + \hat{\boldsymbol{x}}\dot{\gamma}y^i$$

$$\frac{d\boldsymbol{p}^i}{dt} = \boldsymbol{f}^i - \hat{\boldsymbol{x}}\dot{\gamma}p_y^i - \zeta\boldsymbol{p}^i$$

Where $\boldsymbol{r}^i$ and $\boldsymbol{p}^i$ are respectively position and momentum of i^{th} particle, $\hat{\boldsymbol{x}}$ is a versor for x direction, $\dot{\gamma}$ is the homogeneous shear rate of the system and ζ is the friction parameter of Nosè-Hoover thermostat. Time evolution of the latter is the following:

$$\frac{d\zeta}{dt} = \frac{1}{\tau_0^2}\sum_{i=1}^{N}\left(\frac{\left(\boldsymbol{p}^i\right)^2}{f_T m^i k_B T^*} - 1\right)$$

The relaxation time of the thermostat is τ_0, f_T is the number of DOF in the thermoset region, k_B the Boltzmann constant and T^* the target temperature.

As initial conditions, a linear velocity profile is imposed $(t = 0)$:

$$\boldsymbol{v}^i = \boldsymbol{v}_0^i + \hat{\boldsymbol{x}}\dot{\gamma}y^i$$

Then, the system experiments a homogenous shear rates with periodic BCs in all direction and the model periodically provides velocity profiles until there are no significant changes between two subsequent profiles. During the process, pressure terms p and p_0 give information on rotation of the distorted microstructure and nonlinear bulk deformation. In particular, if different from zero indicate the presence of non-Newtonian behaviour. In fact, viscosity depends on shear rate in this case, with different laws depending on shear rate value.

X. *Xu et al.* (26) established that the variation of the shear viscosity as a function of the shear rate could be separated into three regions by two values, the Non-Newtonian transition shear rate $\dot{\gamma}_{nt}$ and the critical shear rate $\dot{\gamma}_{cr}$. They respectively indicate the transition from non-Newtonian to Newtonian region, and the transition from the non-Newtonian to a third region which follows another law, characterized by high shear rate, where is meaningless for this study to evaluate viscosity, since bond breaking occurs. Cross-linking shifts $\dot{\gamma}_{nt}$ towards lower values, and Newtonian region almost disappears for 60% cross-linked configurations. For this reason, the reference material, characterized in practice by crosslinking degree beyond 90%, material is always non-Newtonian. In non-Newtonian region, shear-thinning effect occurs. Shear thinning is a common behavioural deviation from Newtonian fluid observed for polymer melts under shear flow, which produces a viscosity decrease with increasing shear rate. Cross-linking process increase the viscosity, but at same time enhance shear-thinning effect, by deviating the fluid from Newtonian behaviour. Moreover, is observed that crosslinked epoxy has a higher-level alignment of the chains along the shear direction, than the not crosslinked one. Typically, well-aligned structures present less inter-layer interactions, and reduced shear viscosity. Thus, enhanced shear-thinning behaviour is prevalent for cross-linking degree increase, leading to a decrease of shear viscosity as final effect.

Simulations under Poiseuille flow are suitable to evaluate the possible influence of the presence of carbon fibres during the curing process. It is defined as a laminar flow between two infinite parallel plates (e.g. duct or pipe), separated by a distance H. Solid walls atoms are grouped in identical beads as those of the epoxy branching beads, forming two surface put on top and bottom of the system

in *y* direction. Walls' beads interact with epoxy reactive beads through LJ potential, and Langevin thermostat controls temperature. A gravity force in *x* direction is imposed to ensure the flow of the melt.

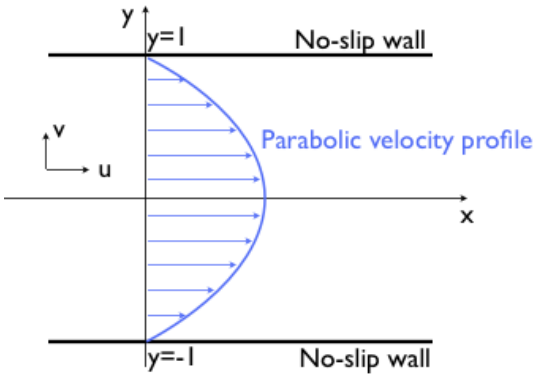

Figure 27 Velocity profile under Poiseuille flow conditions

The parabolic velocity profile obtained, under non-slip BCs, is given by the analytical solutions of Navier-Stokes equations for a Poiseuille flow, and also known as Poiseuille Law:

$$v(y) = \frac{4yv_m}{H}\left(1 - \frac{y}{H}\right)$$

Where H is the duct height and v_m is the maximum velocity evaluated, starting from density ρ and viscosity η, by applying a gravity force:

$$v_m = \rho g \frac{H^2}{8\eta}$$

Viscosity depends on crosslinking degree, while density profile is much less sensitive to it. Hence, an increasing degree of cross-linking will lead to less pronounced velocity profiles and increasing viscosity of the melt, at the same driving gravity force.

1.2.5 STRAIN ENERGY CONSERVATION BASED METHODS

Methods based on the strain energy conservation between CG and MD models, have been already applied successfully to carry out CNTs elastic behaviour. *B. Arash et al.* (27) developed a CG model to calculate mechanical properties of carbon nanotube reinforced polymer nanocomposites (CFRP). In particular, materials under investigation are poly(methyl-methacrylate) PMMA and single wall CNTs (SWCNT) with chiral vector (5,5). Bonded and non-bonded potential functions make up the force field. Therefore, the total potential energy is a sum of energy terms corresponding to the various potentials:

$$E_{tot} = E_0 + \sum_i E_{b,i}(r) + \sum_j E_{a,j}(\theta) + \sum_k E_{d,k}(\phi) + \sum_{lm} E_{vdW,l}(r)$$

Where U_0 is the constant free energy of the system, $E_{b,i}(r)$ are the stretching potentials, $E_{a,k}(\theta)$ are the bending angle potentials, $E_{d,k}(\phi)$ are the dihedral angle potentials and $E_{vdW,lm}(r)$ are the Van Der Waals interaction potentials. All these potentials are the ones of classical MD, harmonic for bonded and Lennard-Jones for Van der Waals interactions, with the same formulations already seen before.

Carbon reinforced polymer: Mapping and Parametrization

In order to simplify the structure and reduce the number of DOF, CG of PMMA and CNTs are performed. Concerning PMMA matrix, single monomers of methyl methacrylate ($C_5O_2H_8$) are considered as super-atoms called P beads (mass 100.12 [amu] and radius 2.15 [Å]) for a 15-fold decrease in DOF, while for CNTs each particle, called C bead, is composed by 5 atomic ring (mass 600.55 [amu] and radius 3.96 [Å]), for a 50-fold decrease in DOF.

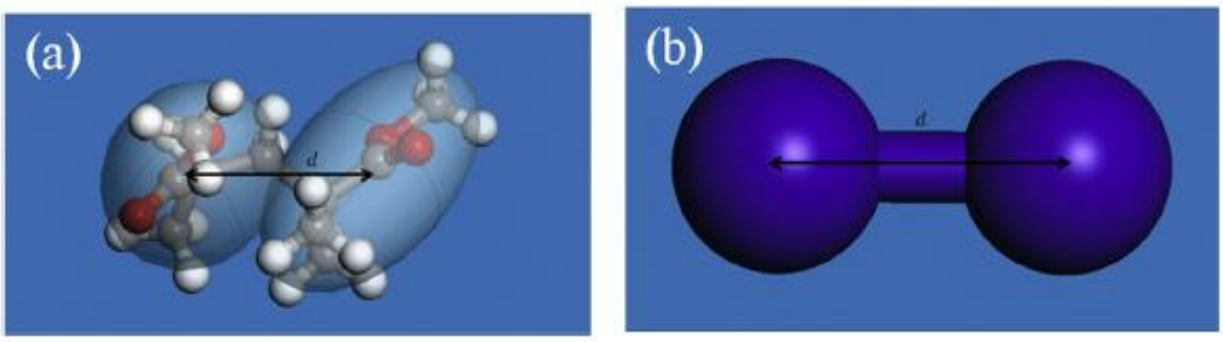

Figure 28 CG of two PMMA monomers (27). Reprinted with permission of the publisher (License N. 4784330453369)

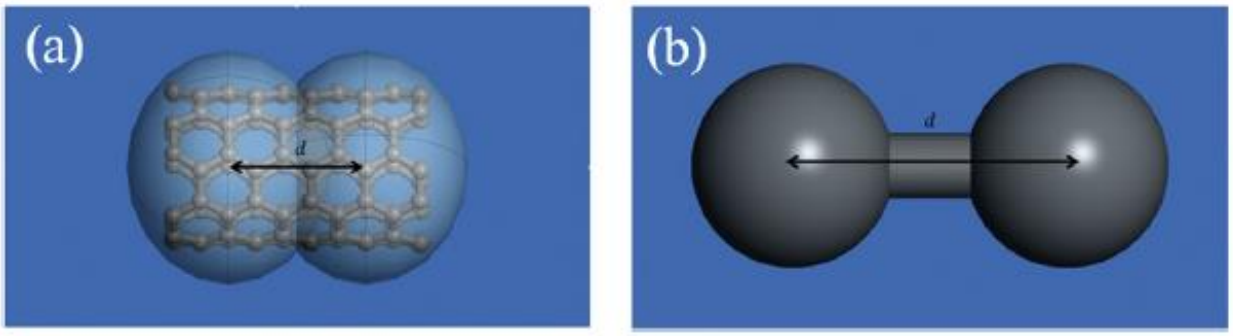

Figure 29 CG of ten atomic rings of (5,5) SWCNT (27). Reprinted with permission of the publisher (License N. 4784330453369)

Equilibrium distances and angles for bonded potentials calculation are measured and available in literature, while spring constants are the second derivatives of the potential energy with respect to the bond lengths or angles.

For vdW potentials, LJ parameters like equilibrium well depth D_0 and equilibrium distance r_0 are determined. D_0 is the minimum value of the cohesive energy, defined as the difference between the total vdW energy of the atomistic system and the vdW energy of each isolated monomer (P-P vdW potential). Table 6 summarizes all these information.

	BONDED						**NON-BONDED**	
	STRETCHING		**BENDING**		**DIHEDRAL**		**vdW**	
	d_0 [Å]	**k_d [kcal/mol/Å^2]**	**θ_0 [°]**	**k_θ [kcal/mol/rad^2]**	**φ_0 [Å]**	**k_φ [kcal/mol]**	**D_0 [kcal/mol]**	**r_0 [Å]**
P beads	4.02	194.61	89.6	794.89	0	42.05	1.34	6.53
C beads	6.03	161024	180	66148.01	0	14858.8	2.8	7.71

Table 6 CG beads equilibrium distances and spring constants for potentials calculation (data from (27))

The calibrated CG force field parameters are then validated though a comparison with MD results, revealing a percentage difference of 3.3% for the equivalent spring constant of PMMA and less than 0.5% for the one of CNTs.

Carbon Reinforced polymer: mechanical properties computation

A simulation unit cell with a size of 5x5x5 [nm^3] and periodic boundary conditions, containing a (5, 5) CNT bundle, is initially constructed. 30 monomers of PMMA are packed in a cubic lattice with a predefined mass density of 1 [g/cm^3]. A Monte Carlo code builds the molecules space distribution,

by minimizing close contacts between atoms. The considered system contains 11144 atoms, and after the CG process number of particles is reduced at 684 (16.29-fold decrease in DOF).

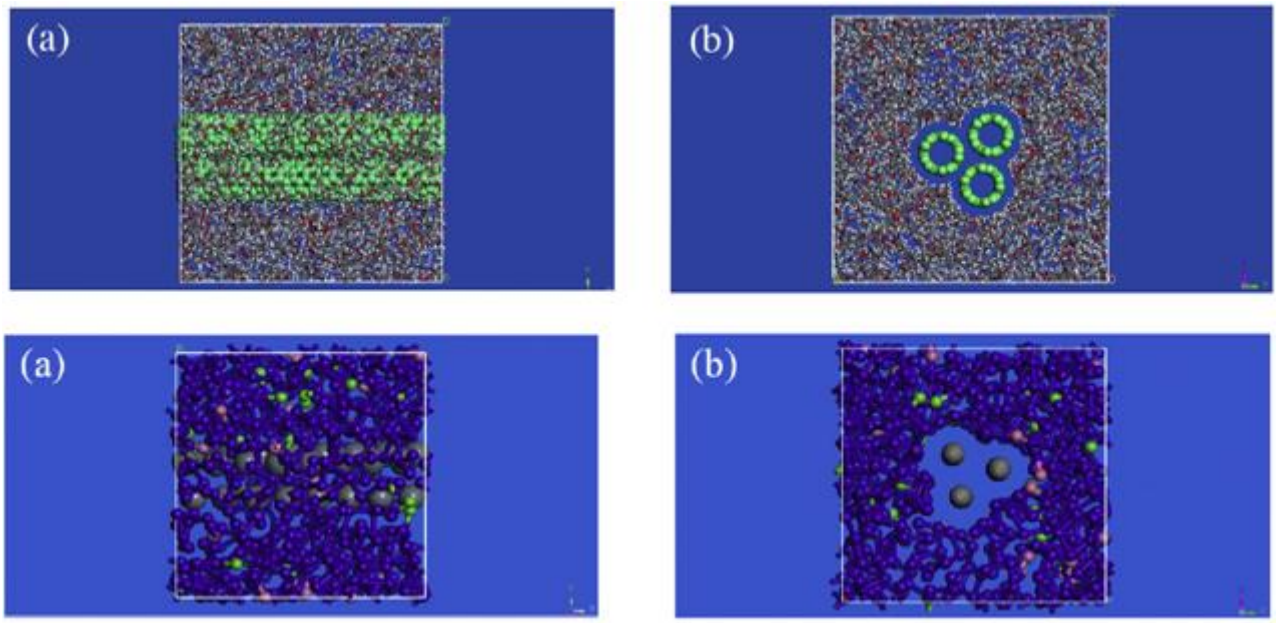

Figure 30 Atomistic and CG RVE of PMMA matrix reinforced with (5,5) SWCNT, (a) side view (b) top view (27). Reprinted with permission of the publisher (License N. 4784330453369)

Energy minimization with the convergence criteria of 1e-5 [kcal/mol] is performed and then the system is allowed to equilibrate over the NPT ensemble at 298 [K] and atmospheric pressure for 2 [ns], using Andersen feedback thermostat and Berendsen barostat and with time step set to 1 [fs] (MD) and 10 [fs] (CG). A further energy minimization follows, in order to eliminate internal stresses and the CNT/PMMA concludes the composite preparation.

The mass density of the composite predicted by CG and MD models are respectively 1.023 [g/cm^3] and 1.021 [g/cm^3], with a percentage difference of 0.2%.

Then, the system experiments a constant-strain minimization method, by imposing a 0.1% strain in the longitudinal direction (x). This take place by uniformly expanding of the RVD dimensions in direction of the deformation and rescaling the new coordinates of the atoms to fit within the new dimensions. After each increment of the applied strain, energy is re-minimized keeping the lattice parameters fixed.

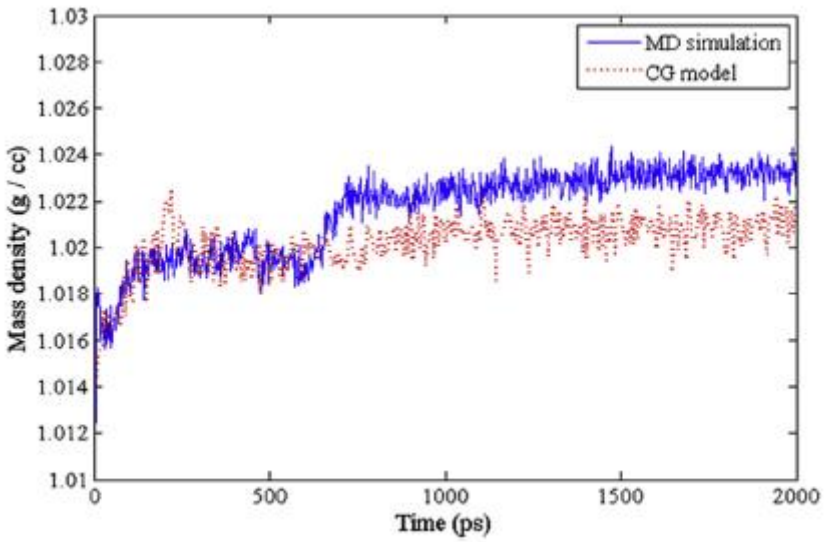

Figure 31 Mass density versus time of PMMA matrix reinforced with (5, 5) SWCNT (27). Reprinted with permission of the publisher (License N. 4784330453369)

Finally, the variation of the measured energies versus applied strain is used to calculate Young's modulus as:

$$E = \frac{1}{V}\left(\frac{\partial^2 U}{\partial \varepsilon^2}\right)$$

Where U is the potential energy, V is volume of the cell and ε is the strain.

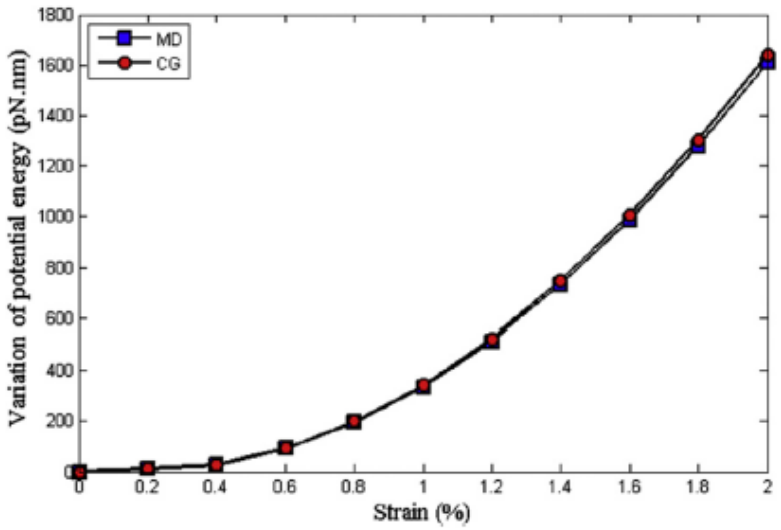

Figure 32 Potential energy versus strain applied (27). Reprinted with permission of the publisher (License N. 4784330453369)

Young's moduli obtained are 72.54 GPa (MD) and 73.39 GPa (CG), with a percentage difference of 1.17%.

1.2.6 DISSIPATIVE PARTICLE DYNAMICS (DPD)

Maiti et al. (28) investigated on a multi-scale study for CFRPs, basing on a method incorporated in Accelrys Materials Studio software. In DPD functional groups are represented with a single bead, to decrease DOFs, but, instead of LJ potentials, for non-bonded interactions a simple soft pairwise conservative potential which embodies all the essential chemistry of the system and determines CNT dispersion in the polymer matrix. In DPD, beads follow Newton's equations, where, for the sake of simplicity, all masses are normalized to 1:

$$\frac{d\boldsymbol{r_i}}{dt} = \boldsymbol{v_i} \qquad \frac{d\boldsymbol{v_i}}{dt} = \boldsymbol{f}_i = \sum_{i \neq j} \boldsymbol{f_{ij}^C} + \boldsymbol{f_{ij}^D} + \boldsymbol{f_{ij}^R}$$

$\boldsymbol{f_i}$ contains three contributions: $\boldsymbol{f_{ij}^D}$ and $\boldsymbol{f_{ij}^R}$ represents respectively dissipative and random forces, while $\boldsymbol{f_{ij}^C}$ is the conservative soft repulsion between beads i and j, acting along the joining line. *Groot and Warren* proposed the following expression:

$$\boldsymbol{f_{ij}^C} = \begin{cases} a_{ij}\left(1 - \dfrac{r}{R_C}\right) & |\boldsymbol{r}| = r \leq R_C \\ 0 & r > R_C \end{cases}$$

R_C is the interaction range that sets the length-scale of the system and is defined as the side of a cube containing an average beads density $\bar{\rho}$ (dimensionless density).

$$R_C = (\bar{\rho} V_b)^{1/3}$$

Where V_b is the volume of one bead, reciprocal of the density.

The basic assumption of the model is that, also for systems with several different species, V_b is the same for each bead. a_{ij} terms are the DPD interaction parameters, depending to underlying atomistic interactions, conventionally used in dimensionless form:

$$\bar{a} = \frac{aR_C}{kT} \; [-]$$

If all the beads have the same volume it's possible to state that intra-species interaction are the same for all species $\overline{a_{AA}} = \overline{a_{BB}}$, so the fundamental parameter to determine how two components will mix is the excess cross-species interaction $\Delta\bar{a} = \overline{a_{AB}} - \overline{a_{AA}}$.

A parallelism is possible with Flory-Huggins (FH) theory for polymers in solution, in particular between $\Delta\bar{a}$ and FH-χ parameters. In fact, according to FH, for a homogenous mixture:

$$\chi = 2\alpha\bar{\rho}\Delta\bar{a}$$

With α roughly constant equal to 0.1. Using computed volume fraction of the minority component of the homogenous mixture, *Groot and Warren* determine a linear fit for a monomer-monomer mixture, while *Wijmans-Smit-Groot* determine a non-linear fit. GW linear laws follow:

$$\begin{cases} \chi = 0{,}286\Delta\bar{a} & for\ \bar{\rho} = 3 \\ \chi = 0{,}689\Delta\bar{a} & for\ \bar{\rho} = 5 \end{cases}$$

These are appropriate only for a not too high value of χ (about 10). For higher values, a way to compute it from solubility parameters is:

$$\chi_{AB} = \frac{V_b}{kT}(\delta_A - \delta_B)$$

Where δ_A and δ_B are solubility parameters of systems A and B, defined as square roots of the cohesive energy densities, V_b is still the volume of beads, k is the Boltzmann constant ($1{,}38 \cdot 10^{-23}$ $\left[{}^{J}/_{K}\right]$) and T is the absolute temperature.

Thus, all DPD interaction parameters can be determined after calibrating the value of intra-species interactions for a specific system (GW chose water).

As a concrete example, DPD modelling of a mixture of PMMA polymer and (15, 15) CNTs is conducted. One PMMA monomer is a bead, so that V_b is the equilibrium volume occupied by it at room temperature, about 145 [Å^3].

Using UFF-computed solubility parameter equal to 15.7 [(J/cm^3)$^{1/2}$] for (15, 15) CNT and SYNTHIA-computed value of 18.9 [(J/cm^3)$^{1/2}$] for PMMA are carried out. Basing on a dimensionless density $\bar{\rho} = 3$, interaction parameters are computed as $\overline{a_{AA}} = 25$ and $\overline{a_{BB}} = 26{,}3$.

In addition to conservative soft-repulsive interactions, polymeric systems require more potentials to describe covalent bonding between consecutive beads. Accelrys DPD code implements Hook's potentials, as in classical MD and in models previously shown.

Medium-scale CG models with structure and force-potential derived from full-atom MD simulation results can be a good compromise between computational efficiency and precision, enabling to extend time and space scales by reducing the number of degree of freedom (DOF), but maintaining the molecular details.

1.3 Continuum Models of Epoxy in literature

Although MD simulations provided a good detail of the chemical structures. For this reason, many characterizations, not possible at the nanoscale via experiments, become feasible. However, they are limited to a few micrometres in size and up to microseconds in simulation time. This literature review focuses on continuum models for mechanical properties computation.

In continuum-based approaches, composites are homogenized materials. For example, having in input transversely isotropic stiffness matrixes of neat polymer and nanofillers, give in output a homogenized stiffness matrix for the nanocomposite.

To do this, a way is to build a Representative Volume Element (RVE) in which are included all the characteristics of the material, e.g. a certain grade of reinforcement or a certain disposition, and then evaluate the homogenized properties by integrating it over space and time, applying the so called Finite Element Method (FEM).

1.3.1 FEM-BASED MODELS

Doagou-Ead's model

S. Doagou-Ead et al. (29) purposed a multiscale model including FE, aiming to study elastic behaviour of nanocomposites with single or combination of carbonic fillers (G, CNT). In this model, characteristics of the constituents come from the statistical microscopy investigations. Properties acquired are included in the performed MD simulations, which provide the stiffness matrix of nanofillers. The latter is implemented into micromechanical Mori-Tanaka and FE models, with RVD construction methods in order to get a comparison. Materials considered are polyamide nylon as polymer matrix and MWCNTs and GNP as nanofillers.

The core of this approach is the construction of a series of 3D computational models, through RVEs generation using a developed Python code, which is an input for FE software (e.g. ABAQUS, DIGIMAT etc.).

MWCNT are implemented by a chain system of models. A prepared FORTRAN code uses stiffness matrixes of polymer and reinforcements, type, volume fraction and geometrical aspects of the nanofillers as input parameters. Then the following procedure is performed:

1. Three random numbers define coordinates of initial point of each nano-filler inside the cell.

2. Two random angles (0÷360°) are generated to define a new point.

3. Following turning point is defined by two new random angles (-60÷60°)

4. Round sections of given diameter were swept through the array of points to create a nanofiber.

Similarly, GNPs construction follows these steps:

1. A random number defines the centre of the circle plane inside the cell.

2. Discs extrusion by adding the defined thickness.

3. Random vector (module 0÷length of RVD) translates discs into the box.

4. Random axis direction and angle (0÷180) are generate to rotate them.

In order to add subsequent nanofillers, Random Sequential Absorption (RSA) algorithm is implemented. RSA for snake-shaped inclusions consists of sequential addition of randomly oriented reinforcements to a unit cell to guarantee there is no overlapping.

Distances between new points and all the available ones are checked at each step; if they are closer than a certain tolerance, the algorithm discards them and generates another point. So does also for line segments; if they coincide, the second point of a line segment is generated again.

The developed program provides two meshing typology: geometry based mesh, suitable when the number of nodes and nanofillers aspect ratio (width/height) are limited and embedding element mesh, needed for more complex structures. Quadratic tetrahedral elements (C3D10) are used to mesh the model. Experimental observations from TEM and SEM micrographs of thin cross section of the produced composites inspire RVEs constructions.

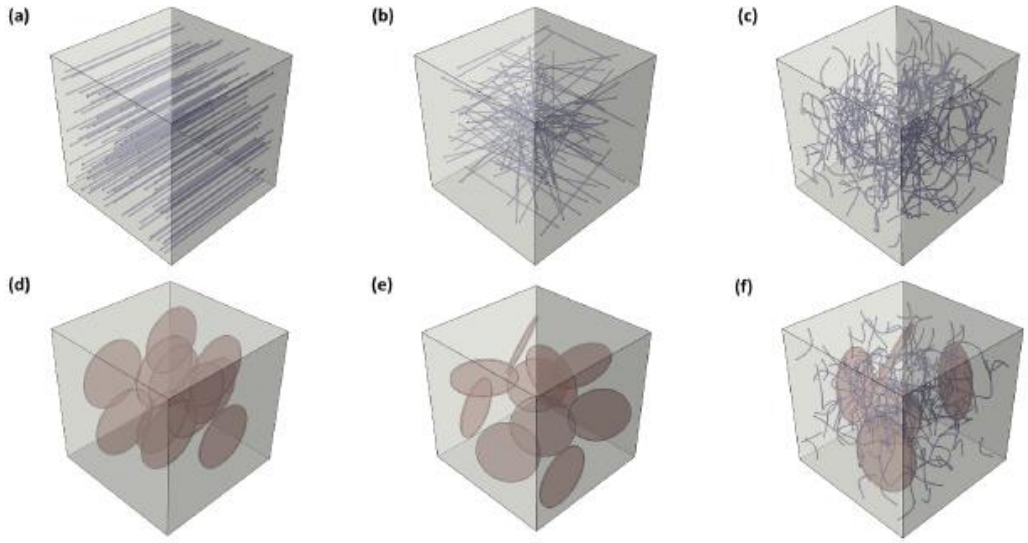

Figure 33 RVEs of different configurations (a) aligned straight CNTs (b) random straight CNTs (c) random curved CNTs (d) aligned GNPs (e) random GNPs (f) random CNTs-GNPs hybrid (29). Reprinted with permission of the publisher (License N. 4784331244738)

Is very important to observe that a random homogenized composite structure model with a sufficient number of nanofillers represents the morphology independently from randomness within the RVE, leading to similar homogeneous and isotropic behaviour. Based on sensitivity analysis, in this case 1-2 µm cell lengths lead to stable homogenized results. Elastic modulus in the three directions is carried out by applying 0.3% uniform strain on the corresponding surfaces, in particular reaction force on the opposite surface is calculated to obtain the stress in the volume element, while the other two normal directions are kept constant. ABAQUS continuously updates the variable coordinate systems, in order to ensure anisotropy of the fillers, since stiffness matrix varies on global coordinates.

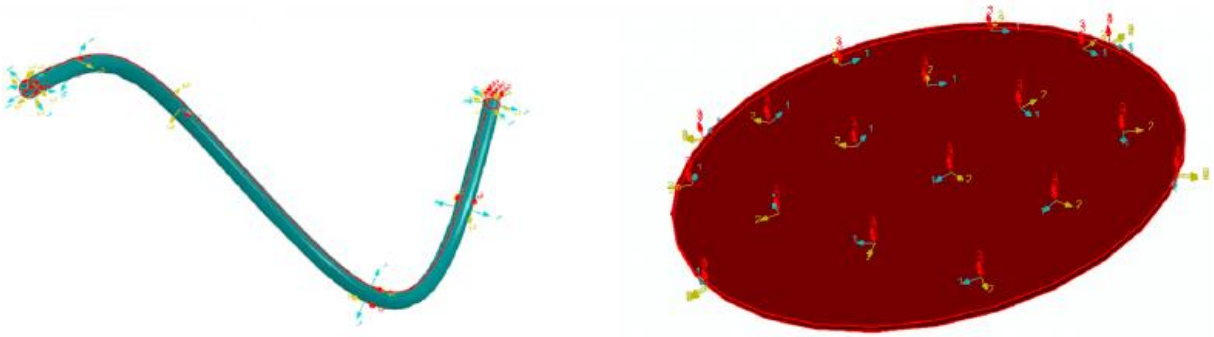

Figure 34 Variable coordinate systems in CNT and GNP (29). Reprinted with permission of the publisher (License N. 4784331244738)

Acquiring minimum standard deviation of E in the three directions is the determinant parameter to find the required number of nanofillers and the length of unit cell. RVEs modifications are possible in order to be more realistic and closer to SEM observations, by adding a random curvature to the fibres. Electron microscopic investigations show that GNP are not bent or curved like CNTs, but a number of agglomerates for higher content of graphene is observable. This is due to the manufacturing process, in particular to the injection moulding process, where nanocomposite melts experiment high shear forces, leading to non-homogeneities. *Doagou-Ead et al.* have represented this aspect, stacking 30% of GNPs into group of four. There is a good matching between model and experimental data.

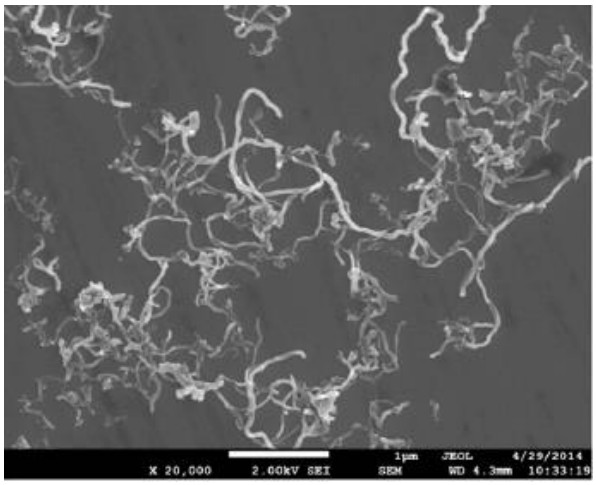

Figure 35 SEM representation of CNTs (30). Reprinted with the permission of the publisher (License N. 4784331423925)

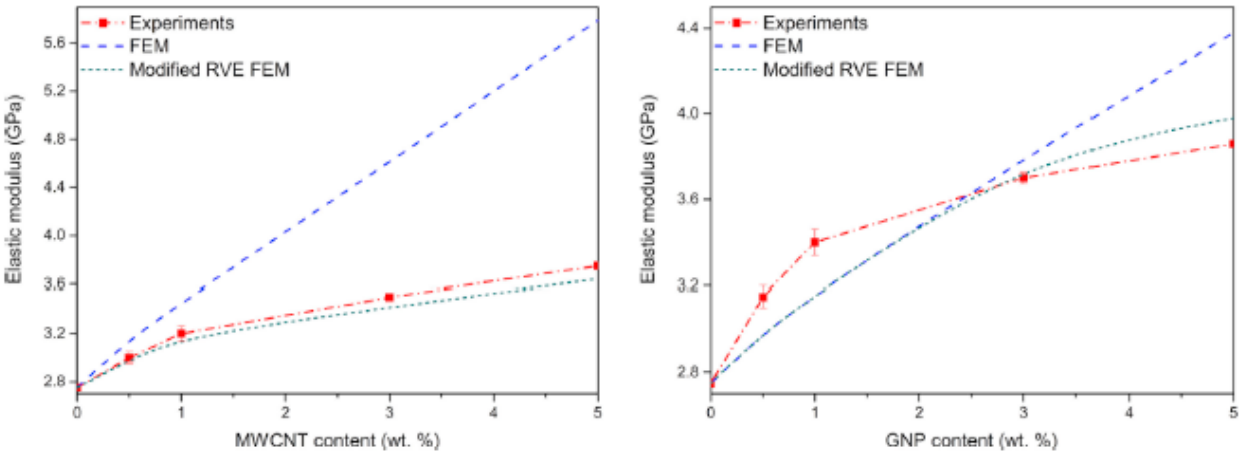

Figure 36 Young's modulus versus CNT and GNP content by Doagou et al. (25). Reprinted with permission of the publisher (License N. 4784331244738)

Pontefisso et al. (30) developed another approach to model re-stacking on nanoplates. According to it, after a RVE generation, an interaction radius is defined from the centre of each filler. For each filler, if another filler centre exists within its interaction radius, the couple of fillers is marked, for generating a stack. If a branched chain of fillers is marked for re-stacking, this chain gives rise to a thicker stack. Stack columns are generated, separated by a distance, which defines a new material phase called intra-stack. The position and orientation of these stacks depend on the original orientation of the constituents, modifications are possible in case of overlapping issues. Not considering the stacking effect will lead to an overestimation of the Young's modulus.

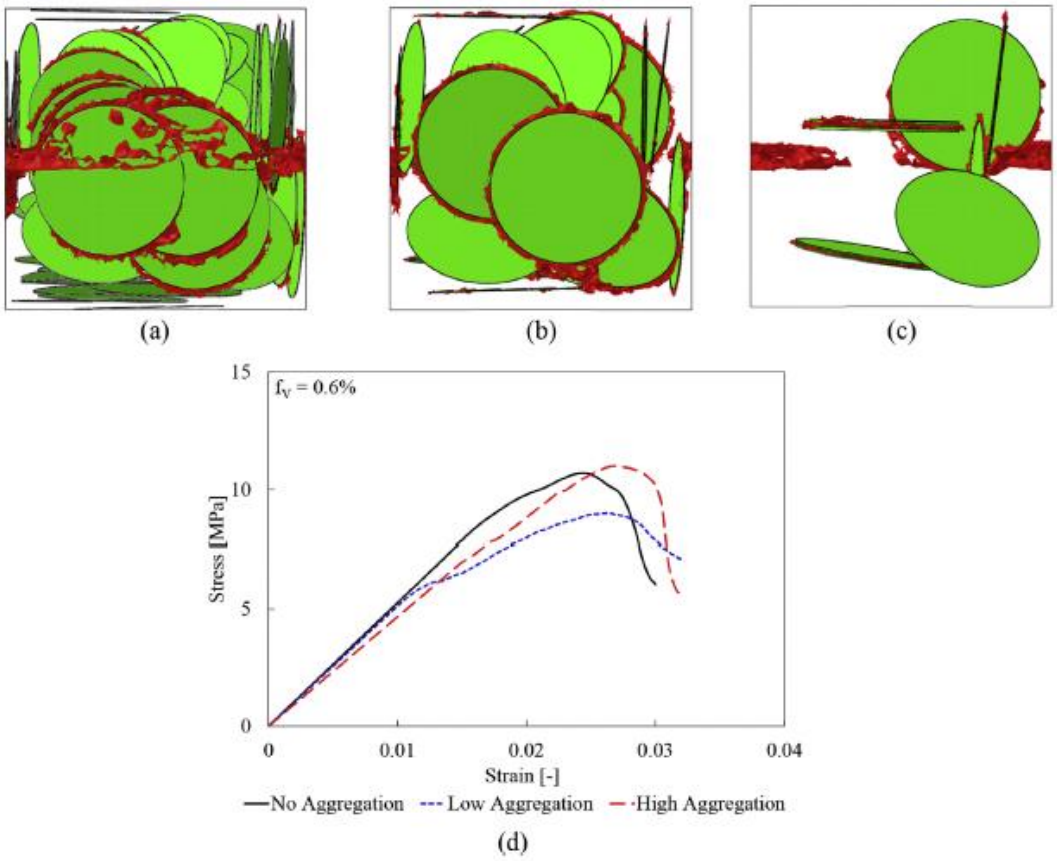

Figure 37 (a-c) damage evolution (in red) and stress-strain curves (d) for different stacking grades (30). . Reprinted with the permission of the publisher (License N. 4784331423925)

M. Lidgett et al. (31) proposed a model focused on high rates of strain for military Armoured Fighting Vehicles (AFV), dealing with materials with lower density with respect to common steels, but very good structural and blast performance. The materials investigated is a 65% S2glass-8552 epoxy, through ABAQUS scripting interface. The microstructure has been idealized into a regular hexagonal

packing arrangement, and the overall dimensions of the cell are taken from *Hull and Clyne* equations:

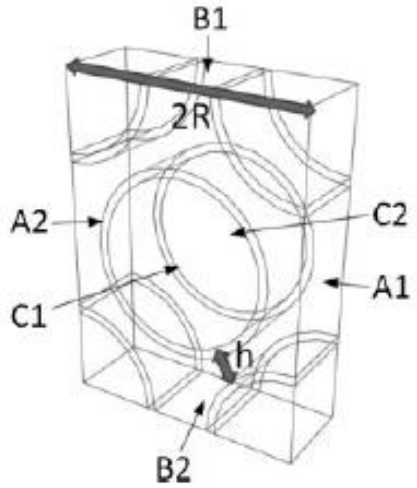

Figure 38 Regular hexagonal packing (27)

$$R = \frac{r}{\sqrt{\frac{2f\sqrt{3}}{\pi}}}$$

$$h = 2r\left[\left(\frac{\pi}{2f\sqrt{3}}\right)^{0,5} - 1\right]$$

Where the centre-to-centre semi-distance is R, h is the inter-fibres spacing, r is the fibre radius (set 5 [μm] and equal to unit cell depth), f is the fibre volume fraction (set 65%). Interface thickness is 1/10 of fibre radius, half taken by polymer matrix and half from the fibre itself. Boundary conditions are applied on the basis of a translational symmetry method, by taking two point in the unit cell O and P, and their image point in another cell O' and P', following steps are performed:

1. Displacements equalization in each direction:

$$\begin{cases} u_P{}' - u_O{}' = u_P - u_O \\ v_P{}' - v_O{}' = v_P - v_O \\ w_P{}' - w_O{}' = w_P - w_O \end{cases} \rightarrow \begin{cases} u_P{}' - u_P = u_O{}' - u_O \\ v_P{}' - v_P = v_O{}' - v_O \\ w_P{}' - w_P = w_O{}' - w_O \end{cases}$$

2. Relationship between macroscopic strains and relative displacements, introducing a Cartesian system of coordinates:

$$\begin{cases} u' - u = (x - x')\varepsilon_x + (y' - y)\gamma_{xy} + (z' - z)\gamma_{xz} \\ v' - v = (y' - y)\varepsilon_y + (z' - z)\gamma_{yz} \\ u' - u = (z' - z)\varepsilon_z \end{cases}$$

3. Translational symmetry transformations A, B and C, Considering i, j, k as number of unit cells per direction and a, b, c, respectively as semi-width, semi-height and semi-depth of a unit cell.

$$\begin{cases} x' - x = A(i,j,k) = 2ai \\ y' - y = B(i,j,k) = 2bj \\ z' - z = C(i,j,k) = 2ck \end{cases}$$

4. Transformed strains-relative displacements relationship:

$$\begin{cases} u' - u = 2ai\varepsilon_x + 2bj\gamma_{xy} + 2ck\gamma_{xz} \\ v' - v = 2bj\varepsilon_y + 2ck\gamma_{yz} \\ u' - u = 2ck\varepsilon_z \end{cases}$$

From this set of equations, BCs can be derived, on for each of the 6 faces, 12 edges and 8 corners of the unit cell.

Faces	Edges 1–4	Edges 5–8	Edges 9–12
$i=1,\ j=0,\ k=0$	$i=0,\ j=1,\ k=0$	$i=0,\ j=1,\ k=0$	$i=1,\ j=0,\ k=0$
$u_{A2}-u_{A1}=2a\varepsilon_x$	$u_{E2}-u_{E1}=2b\varepsilon_{xy}$	$u_{E6}-u_{E5}=2b\varepsilon_{xy}$	$u_{E10}-u_{E9}=2a\varepsilon_x$
$v_{A2}-v_{A1}=0$	$v_{E2}-v_{E1}=2b\varepsilon_y$	$v_{E6}-v_{E5}=2b\varepsilon_y$	$v_{E10}-v_{E9}=0$
$w_{A2}-w_{A1}=0$	$w_{E2}-w_{E1}=0$	$w_{E6}-w_{E5}=0$	$w_{E10}-w_{E9}=0$
$i=0,\ j=1,\ k=0$	$i=1,\ j=1,\ k=0$	$i=0,\ j=1,\ k=1$	$i=1,\ j=0,\ k=1$
$u_{B2}-u_{B1}=2b\varepsilon_{xy}$	$u_{E3}-u_{E1}=2a\varepsilon_x+2b\varepsilon_{xy}$	$u_{E7}-u_{E5}=2b\varepsilon_{xy}+2c\varepsilon_{xz}$	$u_{E11}-u_{E9}=2a\varepsilon_x+2c\varepsilon_{xz}$
$v_{B2}-v_{B1}=2b\varepsilon_y$	$v_{E3}-v_{E1}=2b\varepsilon_y$	$v_{E7}-v_{E5}=2b\varepsilon_y+2c\varepsilon_{yz}$	$v_{E11}-v_{E9}=2c\varepsilon_{yz}$
$w_{B2}-w_{B1}=0$	$w_{E3}-w_{E1}=0$	$w_{E7}-w_{E5}=2c\varepsilon_z$	$w_{E11}-w_{E9}=2c\varepsilon_z$
$i=0,\ j=0,\ k=1$	$i=1,\ j=0,\ k=0$	$i=0,\ j=0,\ k=1$	$i=0,\ j=0,\ k=1$
$u_{C2}-u_{C1}=2c\varepsilon_{xz}$	$u_{E4}-u_{E1}=2a\varepsilon_x$	$u_{E8}-u_{E5}=2c\varepsilon_{xz}$	$u_{E12}-u_{E9}=2c\varepsilon_{xz}$
$v_{C2}-v_{C1}=2c\varepsilon_{yz}$	$v_{E4}-v_{E1}=0$	$v_{E8}-v_{E5}=2c\varepsilon_{yz}$	$v_{E12}-v_{E9}=2c\varepsilon_{yz}$
$w_{C2}-w_{C1}=2c\varepsilon_z$	$w_{E4}-w_{E1}=0$	$w_{E8}-w_{E5}=2c\varepsilon_z$	$w_{E12}-w_{E9}=2c\varepsilon_z$

Corners	
$i=0,\ j=1$ and $k=0$	$i=0,\ j=1$ and $k=1$
$u_{V2}-u_{V1}=2b\varepsilon_{xy}$	$u_{V6}-u_{V1}=2b\varepsilon_{xy}+2c\varepsilon_{xz}$
$v_{V2}-v_{V1}=2b\varepsilon_y$	$v_{V6}-v_{V1}=2b\varepsilon_y+2c\varepsilon_{yz}$
$w_{V2}-w_{V1}=0$	$w_{V6}-w_{V1}=2c\varepsilon_z$
$i=1,\ j=1$ and $k=0$	$i=1,\ j=1$ and $k=1$
$u_{V3}-u_{V1}=2a\varepsilon_x+2b\varepsilon_{xy}$	$u_{V7}-u_{V1}=2a\varepsilon_x+2b\varepsilon_{xy}+2c\varepsilon_{xz}$
$v_{V3}-v_{V1}=2b\varepsilon_y$	$v_{V7}-v_{V1}=2b\varepsilon_y+2c\varepsilon_{yz}$
$w_{V3}-w_{V1}=0$	$w_{V7}-w_{V1}=2c\varepsilon_z$
$i=1,\ j=0$ and $k=0$	$i=1,\ j=0$ and $k=1$
$u_{V4}-u_{V1}=2a\varepsilon_x$	$u_{V8}-u_{V1}=2a\varepsilon_x+2c\varepsilon_{xz}$
$v_{V4}-v_{V1}=0$	$v_{V8}-v_{V1}=2c\varepsilon_{yz}$
$w_{V4}-w_{V1}=0$	$w_{V8}-w_{V1}=2c\varepsilon_z$
$i=0,\ j=0$ and $k=1$	
$u_{V5}-u_{V1}=2c\varepsilon_{xz}$	
$v_{V5}-v_{V1}=2c\varepsilon_{yz}$	
$w_{V5}-w_{V1}=2c\varepsilon_z$	

Table 7 Boundary conditions for a unit cell (31)

ABAQUS interface is utilised to identify the nodes, with the knowledge of the unit cell size, through linear equation constraints, used to link a node on one face/edge/corner of the unit cell to the corresponding node on the other face/edge/corner.

Macroscopic strains are represented by generating also some dummy nodes, linked to faces edges and corners through linear equation constraint, so that is possible to directly apply a strain to the unit cell, by applying a displacement to a dummy node.

Results for transversal compression at 2000 Hz match with experimental ones of *Vural et al.* on the same material and load.

Considering the relationship between Young' modulus E and material stiffness k_E:

$$k_E = \frac{A}{L}E$$

Where A is the surface area of the resistant section, and L is the length of the element, FE model derived a stiffness of 32.5 [GPa] (+81% with respect to *Vural*) and a UTS of 236 MPa, in fair accordance with experimental results.

Zuberi's Model

M.J.S. Zuberi et al. (32) investigated on CFRPs with SWCNTs, starting from the point that is the best configuration, since MWCNTs possess lower mechanical, electrical and thermal properties because in practice the concentric nanotubes slide past each other during axial tensile loading.

In particular, they focused on the effect of nanotubes diameter and chirality on the Young's modulus and Poisson's ratio of a SWNT/epoxy composite.

Thus, *Zuberi et al.* propose a 3D FE model, using cylindrical RVEs constructed in three different stages: SWCNT in the inner part, surrounded by an interface region and the polymer matrix. The software is MSC.Marc2010, a multi-physics tool for non-linear FE analysis of static and dynamic problems.

Concerning CNT structure, each C-C bond in the is replaced with an equivalent 3D beam according to *Li and Chou* approach, which establish a correlation between interatomic potential energies and mechanical strain energies, by linking potentials spring constants to mechanical properties as follows:

$$k_r = \frac{EA}{L} \qquad k_\theta = \frac{EI}{L} \qquad k_\tau = \frac{GJ}{L}$$

Where k_r, k_θ and k_τ are the bonded spring constant (stretching, bending, torsion), L is the length of C-C bond (0.142 nm), A is the cross-sectional area, I and J are respectively moment of inertia, and polar moment of inertia, E and G are respectively Young's modulus and shear modulus.

For the polymer matrix, assigned epoxy is selected. Epoxy resins form strong bonds with almost all surfaces except a few nonpolar substrates, which make them suitable for CNT dispersion with high adhesion. Volume fraction of SWCNT is from 3% to 5%, but volume of polymer is much larger compared to SWCNTs in molecular scale and molecular polymer chains are relatively tighter providing a high-density space. Thus, polymer matrix is simulated as a continuum medium and solid elements can be used for the simulations. Assigned values of Young's modulus and Poisson ratio are respectively 10 [GPa] and 0.3.

Simulation of the interface region plays a critical role in this model, because it is responsible of the load transfer between the two materials. *Ayatollahi et al.* found that a value of Young's modulus of 20 [GPa] has a low influence on axial stiffness on the RVE (10%).

There are two main approaches to simulate interface region: a non-bonded model and a perfect bonding model.

In the non-bonded model, Interactions between CNT and epoxy are weak non-bonded, vdW-type. In this case, vdW are preferred with respect to functionalization, which consists in introducing covalent cross-links between C atoms of SWCNT and the molecules of the polymer matrix to enhance load transfer capability, causing also defects in SWCNT's structure. In this case, interface region is modelled using truss/spring elements connecting C atoms of discrete SWCNTs to the nodes

of continuum polymer matrix, through already seen LJ potentials, imposing a cut-off distance of 0.85 [nm]. For stress-strain behaviour evaluation, RVE is restrained from one extremity, with the other one fixed, with displacements ranging from 0.1 [nm] to 1 [nm]. Then, the slope of the resulting curve is evaluated as Young's modulus, in this case 52,04 [GPa], in good matching with *Raflee et al.* experimental results, in particular for small strains (up to 1%).

In the perfect bonding model, bonding is covalent between SWNT and the polymer matrix. *Karimzadeh et al.* demonstrate that the possibility of having such a strong bond between SWCNT and polymer matrix exists. Therefore, this model is developed, under the assumptions of continuity and linear elasticity, isotropy and homogeneity of all the regions, with given values of E and ν.

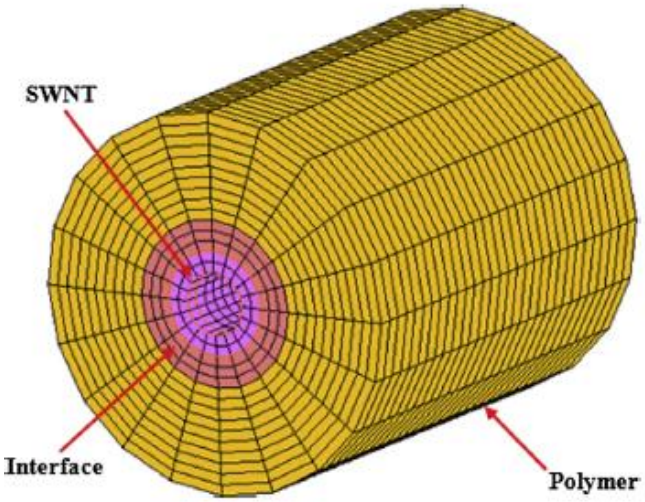

Figure 39 view of continuum RVE (32). *Reprinted with the permission of the publisher (License N. 4784340513963)*

The effective Young's modulus in this case is:

$$E_{RVE} = \frac{\sigma_{RVE}}{\varepsilon_{RVE}} = \frac{F_{RVE} L_{RVE}}{A_{RVE} \Delta \mathrm{L}_{RVE}}$$

The initial length of RVE is L_{RVE}, ΔL_{RVE} is the axial displacement, A_{RVE} is the cross section of RVE and F_{RVE} is the reaction force in axial direction. The value obtained for E_{RVE} is 54.47 [GPa], in fair accordance with the other validated approach. A comparison with continuum rule of mixtures validates both models.

Reference	Approach	V_f (%)	E_{RVE} (GPa)
Karimzadeh et al	Perfect bonding	3	53.46
Rafiee et al.	Perfect bonding	5	56.47
Shokrieh and Rafiee	Non-bonded interaction	5	58.59
Wernik and Meguid	Non-bonded interaction	5	50.30
RVE-1	Non-bonded interaction	5	52.04
RVE-2	Perfect bonding	5	54.47
Rule of mixtures	–	5	53.65

Table 8 Results comparison on RVEs with armchair (10, 10) reinforcements (32). Reprinted with the permission of the publisher (License N. 4784340513963)

M.J.S. Zuberi (32) used the approach of perfect bonding in the interface region, in order to guess the effect of geometrical characteristics of SWCNT on mechanical properties.

Three geometrical parameters define a SWCNT:

- Diameter of the nanotube cross section.

- Chirality is a property that describes the way in which the graphene plate is rolled up to form CNT, through a chiral vector $\boldsymbol{C_h} = n\boldsymbol{a_1} + m\boldsymbol{a_2}$, by two plane versors $\boldsymbol{a_1}$ and $\boldsymbol{a_2}$. If n=m, SWCNT is in the so-called armchair configuration, while if m=0 it is in zigzag configuration.

- Rolling angle ϑ, which is the angle that $\boldsymbol{C_h}$ forms with the zigzag direction. In general, SWCNTs are defined chiral if ϑ is between 0° and 30°.

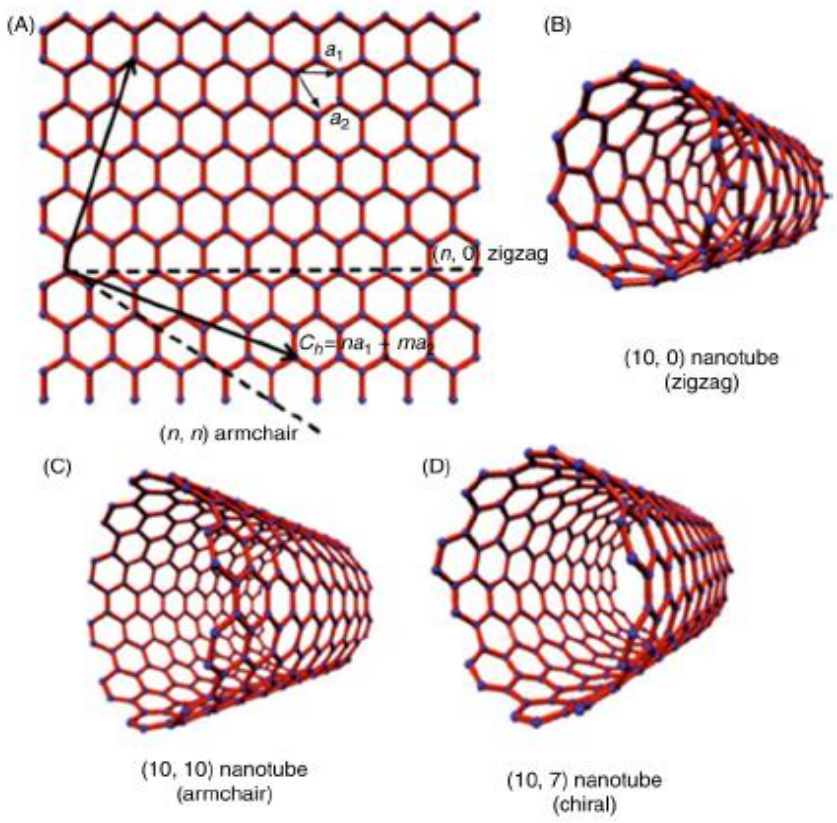

Figure 40 Ways to roll up a graphene plate to form CNT structure

Li and Chou (33) demonstrate that Young's modulus E increases with diameter due to the decrease of CNT curvature, ant lower distortion of C-C bonds. It increases speeder for small diameters, up to about 5 [nm], and then, it increases with lower slope. Moreover, the armchair configuration guarantees a higher Young's modulus, so is possible to state that E grows with ϑ up to 30°, which corresponds to armchair configuration.

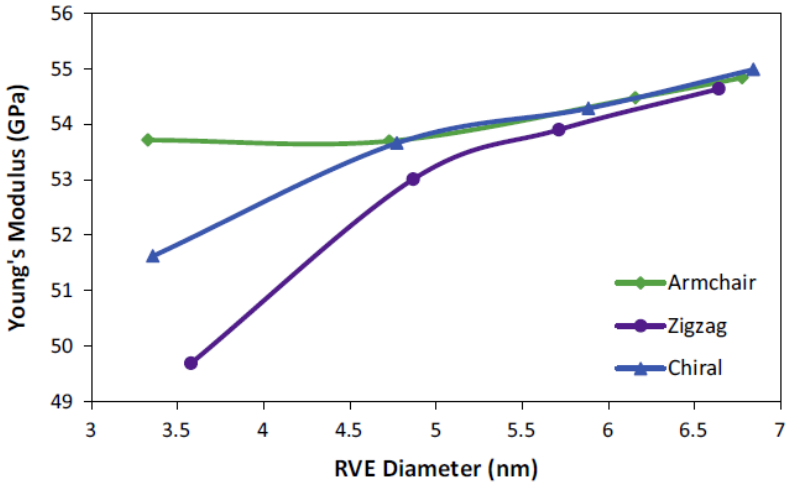

Figure 41 Young's modulus vs representative volume element diameter for different chirality (32), Reprinted with the permission of the publisher (License N. 4784340513963)

Concerning Poisson ratio ν of the RVE, an axial displacement of 2 [nm] is applied to each node in longitudinal direction at one end, keeping the other completely restrained. Changes in diameter and length of RVE due to the axial deformation are evaluated, and ν is calculated as the ratio between transversal and longitudinal deformation:

$$\nu_{RVE} = -\frac{\varepsilon_y}{\varepsilon_x} - \frac{\Delta \mathrm{d}_{RVE}}{d_{RVE}} \frac{L_{RVE}}{\Delta \mathrm{L}_{RVE}}$$

Where d_{RVE} and L_{RVE} are respectively initial diameter and length of the RVE, while $\Delta \mathrm{d}_{RVE}$ and $\Delta \mathrm{L}_{RVE}$ are their variation.

Independently by the chirality, ν decreases with diameter, due to the fact that polymers strains more than the reinforcements, and for higher diameter a bigger part of CNT has to be strained.

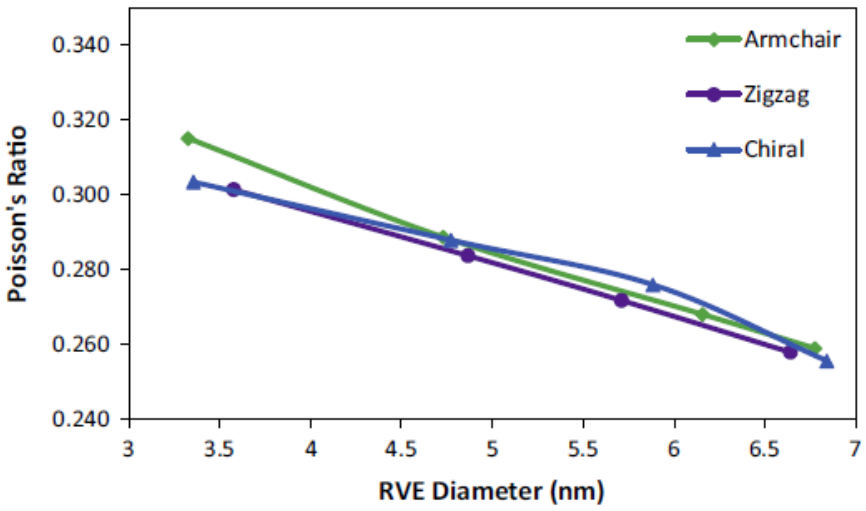

Figure 42 Poisson's ratio vs representative volume element diameter for different chirality (32). Reprinted with the permission of the publisher (License N. 4784340513963)

FE modelling is a versatile tool, it could include many of the elements missing in analytical models, even if is still quite simplistic with respect to the complex structure of the nanocomposites, considering that properties of the latter are strongly dependent on the morphology.

On the other hand, it provides the advantage to implement complex morphology and microstructures of different components systematically.

1.4 Analytical Models of epoxy in the literature

1.4.1 RULE OF MIXTURES

One of the most common techniques used to validate the results of theoretical works is the continuum rule of mixtures. Composite can be modelled as an elastic, isotropic matrix filled with aligned fibres that span the full length of composite. According to this rule, the following equation provides the Young's Modulus of a composite material:

$$E_c = EV_f + E_m(1 - V_f)$$

Where E and E_m are respectively the Young's moduli of SWCNT and polymer matrix and V_f is the reinforcements volume fraction. In Table 8 rule of mixtures is used to compare results of several models and validate them.

1.4.2 ESHELBY-MORI-TANAKA THEORY

S. Doagou-Rad et al. (29) implemented a continuum model base on Eshelby-Mori-Tanaka theory, to obtain the effective stiffness tensor of the two-phase nanocomposite. The equation is:

$$C = C_m + c_r\langle(C_r - C_m)A_r\rangle[(1 - c_r)I + c_r\langle A_r\rangle]^{-1}$$

Where C, C_m and C_m are respectively nanocomposite, neat polymer and reinforcement stiffness tensors, c_r is the reinforcement volume fraction, I is the identity tensor and A_r represents the dilute mechanical strain concentration tensor, defined as:

$$A_r = [I + S(C_m)^{-1}(C_r - C_m)]^{-1}$$

Where S is the Eshelby tensor, which is tabulated from Mura's theory for long cylindrical inclusions (CNTs) and thin penny shapes (GNPs) as follows (29):

$$S_{2222} = S_{3333} = \frac{5-4\nu_m}{8(1-\nu_m)},\ S_{2233} \qquad S_{1212} = S_{3131} = \frac{1}{2},$$
$$= S_{3322}\frac{4\nu_m-1}{8(1-\nu_m)},$$
$$S_{3311} = S_{1122} = \frac{\nu_m}{2(1-\nu_m)}, \qquad S_{3311} = S_{1122} = \frac{\nu_m}{1-\nu_m},$$
$$S_{1212} = S_{3131} = \frac{1}{4},\ S_{2323} = \frac{3-4\nu_m}{8(1-\nu_m)} \qquad S_{1111} = 1$$

Where ν_m is the neat polymer Poisson's ratio.

When acquiring global stiffness matrix in the defined principal directions, nanofillers that are oriented in other directions can be included using transformation matrices.

Thus, stiffness matrix is a function of transversely isotropic stiffness matrix C and Euler angles transformation matrices N_ϑ and N_φ:

$$C^* = N_\vartheta^T N_\varphi^T C N_\varphi N_\vartheta$$

Therefore, the integration of the stiffness matrix C^* in the span of $[-\pi, \pi]$ results in the global matrix of a nanocomposite comprising reinforcements in all direction in the three dimensions.

Comparing results with FEM models and experimental evidences is possible to notice that the modelling predictions are higher than experimental results, due to manufacturing process, which causes anisotropy. In fact, reinforcement's disposition is not aligned, but not even perfectly random, it follows some patterns due in particular to the mounding process, which are observable by electron microscope, but that are difficult to model.

The overestimation of Young's modulus is larger for higher reinforcement's volume (and weight) fraction.

Nanofiller type	Wt(%)	FEM		Mori-Tanaka		Experiments
		Aligned	Random	Aligned	Random	
CNT	0.5	4.04	3.15	4.42	3.04	3.0
	1.0	4.95	3.45	6.10	3.34	3.2
	3.0	10.24	4.61	12.8	4.52	3.5
	5.0	15.83	5.79	19.5	5.71	3.75
GNP	0.5	3.03	2.98	4.69	3.71	3.15
	1.0	3.28	3.09	6.63	4.71	3.4
	3.0	4.23	3.62	13.94	8.34	3.7
	5.0	4.97	4.42	21.4	12.10	3.86

Table 9 Young's modulus [GPa] for different reinforcement grade (29)

1.5 Target of the thesis

After the multiscale overview on epoxy modelling, the objective of the thesis is to apply a new model to compute thermo-physical, mechanical and thermal properties of a system, for which, as in my knowledge, there are still no investigations available in the literature.

The system is a DGEBA/DICY/DETA epoxy, with a mass composition of respectively 70%, 20% and 10%.

Within the SMARTFAN project, in WP 5, the aim is to build a model to compute mechanical properties of a composite including this epoxy and carbon-based nanofillers, in particular its stiffness matrix, as an input for a continuum model. The material is of interest for racing cars, in particular front wings (Figure 43), since it can reach stiffness values comparable to the steel one with lower weight, allowing improved driving performances, without affecting aerodynamics and driver safety. In addition, glass transition temperature is computed, since polymers present a dramatic change of mechanical behaviour above T_g and is important to predict it, in order to provide eventually some restrictions in the applications of the material.

Figure 43 FIA Formula 3 car, Dallara front wing, 2019 (34)

Besides mechanical behaviour, thermal properties have been computed, since there are not modelling results available in literature, concerning this material, while several other epoxies are widely used also for electrical insulation of processors or other electronic components (Figures 44-45). The unique combination between high mechanical stiffness and low thermal conductivity may be of interest for many applications in different fields. The possibility to enhance its properties by using it as a polymer matrix in for a nanocomposite material with carbon-based nanofillers, combined with a relatively low density, can make him a valid lightweight substitute of steel or common structural materials, in applications where weight is a limitation, e. g. aerospace, motorsport, electronics etc.

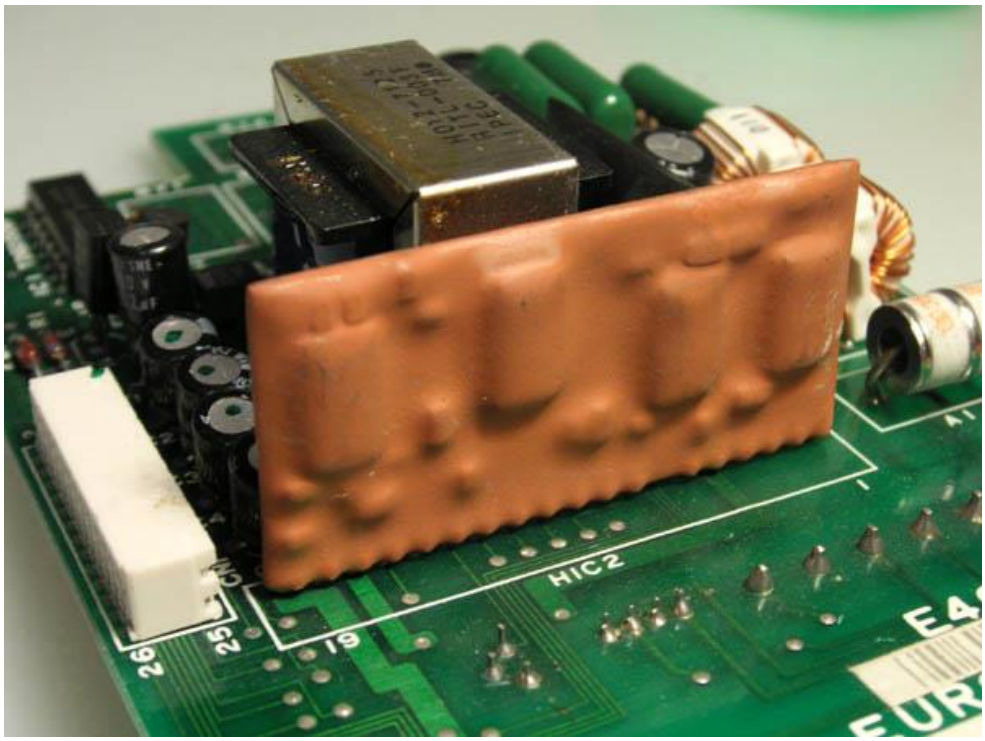

Figure 44 A hybrid integrated circuit (orange), encapsulated in epoxy resin.

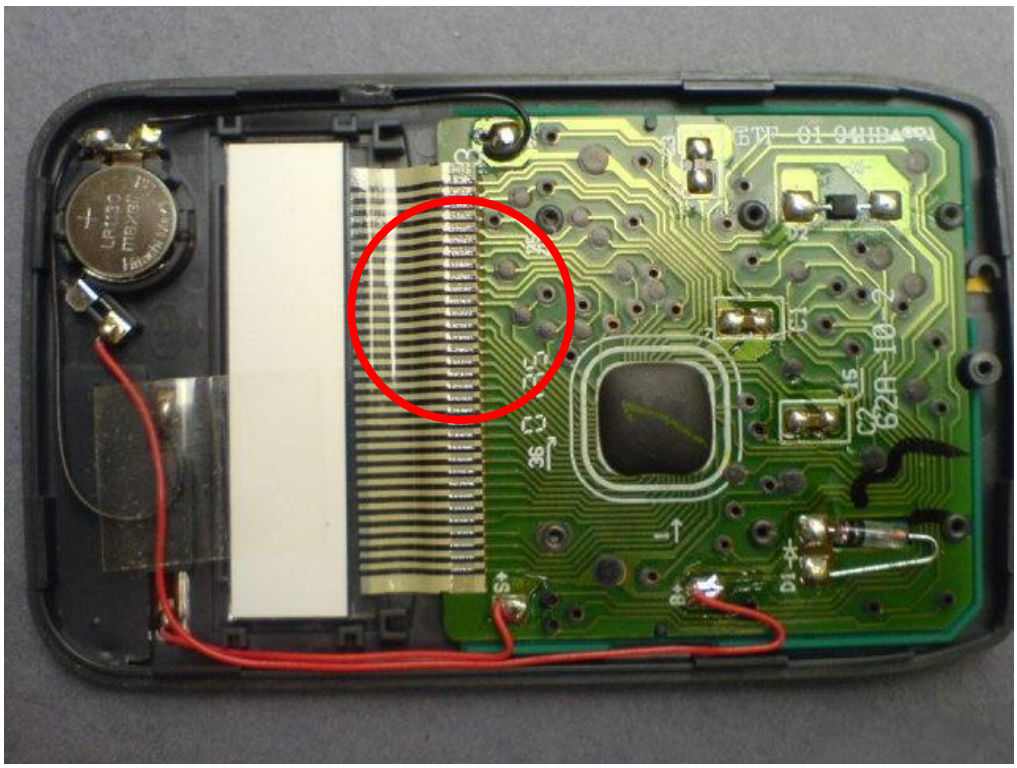

Figure 45 Interior of a pocket calculator. The dark lump of epoxy in the centre covers the processor chip

2. METHODS

In this chapter, all the procedures adopted to get the results are shown and explained step-by-step. First of all, there is a pre-processing phase in which all the information required to run the simulation are carried out and collected in input files

The pre-processing consists of two main steps. The first is the definition of the topology of the problem, which is composed by the mapping that describes how particles are coarse-grained and the characteristics of every single bead, and the force field, including all the laws and all the parameters that rule the interactions between them.

After that, the simulation procedures are presented, starting from the deposition on the particles in the simulation box and continuing with the various equilibration steps and properties computations.

2.1 Topology

Topology is a fundamental characteristic of the system. It affects a lot of crucial parameters for the simulations, such as the number and size of particles, size of initial box, forces acting among the particles, with effect both on the simulation performance in terms of time step and on simulation results' accuracy.

The system under investigation presents a high variety of particles and structures, compared with other polymers, which may have a single repetitive unit. In addition, crosslinking process increases the number of parameters involved and the variety of particles, bonds and angles, so that the system is even more complicated after crosslinking. For these reasons, atomistic simulations require a high computational power for this system and can run with severe limitations on time step and cross-linking degree.

The mapping of the CG system is a critical task, since the coarser are the grains, the less are the particles involved and the parameters related to them, the simpler is the system and the higher is the time step for the simulations. On the other hand, the simpler is the system, the lower is the captured chemical detail and the hardest is to predict properties with accuracy.

The force field is the second main ingredient, and also here there are many possibility to model the various interactions between beads and every configuration may works better with some force fields, and worse with others.

Thus, there is a trade-off in the choice of CG mapping, between chemical detail and computational cost, with an eye on the force field adopted.

2.1.1 CG MAPPING

Technological Institute of Aragon (ITAINNOVA) has developed one possible coarse-grained configuration for DGEBA/DICY/DETA epoxy resin. This configuration is characterized by thirteen bead types, nine bond types, and thirty-five angle types.

Not crosslinked system

Before crosslinking reactions take place, the CG configuration includes just seven beads types, four bond types and four angle types. DGEBA monomer is symmetric with respect to one central dimethyl group (bead B), and has two oxyphenylene groups (beads G) and two epoxy ring groups (beads E), one per side. Central bead is electrically neutral, while E and G are polar.

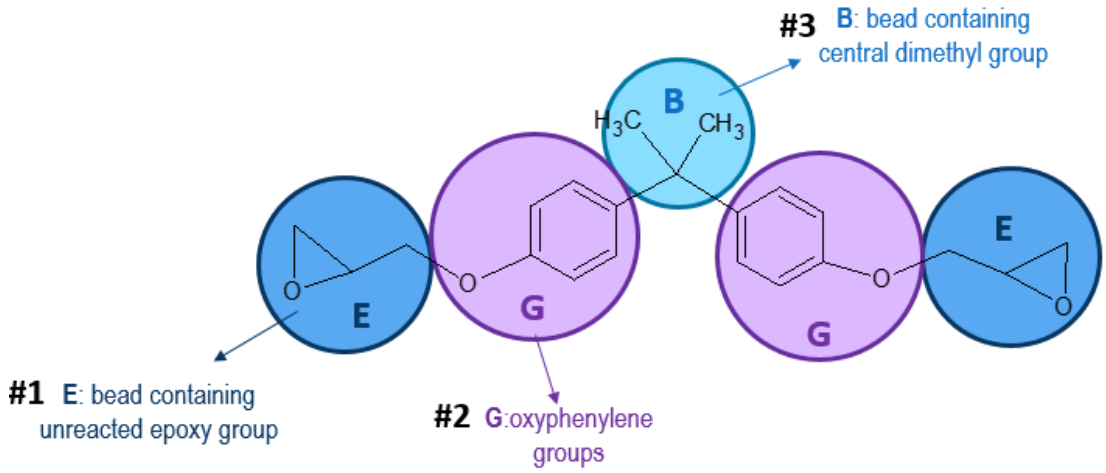

Figure 46 DGEBA CG configuration (developed by ITA (35))

DICY and DETA molecules are three-bead configurations with one central backbone bead and two amine-based arms. DICY has a central non-amine group (bead Y), bonded with two primary amines (beads Ay), while in DETA central bead is itself a secondary amine (bead Ae), bonded with other two primary amines (beads Ad). All hardener's beads are electrically neutral before the cross-linking.

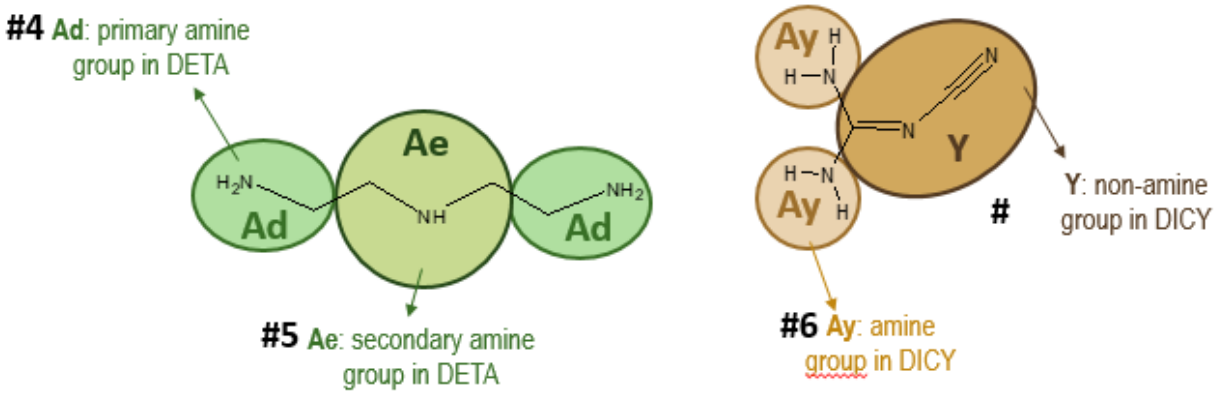

Figure 47 DETA and DICY CG configurations (developed by ITA (35))

Bead number, ID, mass and partial charge values are the beads attributes, since atom_style has been set with the "full" keyword in the data files (details on the software are in the section dedicated 2.2.1, while data file sample is in Appendix B.

Bead No.	Molecule	ID	Bead Mass [g/mol]	Charge [C]	Atoms
1	DGEBA	E	57.07270	+0.16	1 O, 3 C
2	DGEBA	G	92.09818	-0.16	1 O, 6 C
3	DGEBA	B	42.08127	0.00	6 H, 3 C
4	DETA	Ad	30.04973	0.00	2 H, 1 C, 1 N
5	DETA	Ae	43.06885	0.00	1 H, 2 C, 1 N
6	DICY	Ay	16.02264	0.00	2 H, 1 N
7	DICY	Y	52.03570	0.00	2 N

Table 10 Beads general information in not-crosslinked CG configuration

Concerning inter-beads bonds, there are two E_G (bond 1) and two G_B (bond 2) bonds per DGEBA monomer, two Ay_Y (bond 4) per DICY molecule and two Ae_Ad (bond 3) per DETA molecule. Bond number and ID, as involved two beads IDs joined by underscore, define bonds.

Bond No.	ID
1	E_G
2	G_B
3	Ad_Ae
4	Ay_Y

Table 11 Bonds classification

Finally, there are two E_G_B (angle 1) and one G_B_G (angle 2) angles per DGEBA monomer, one Ad_Ae_Ad (angle 4) per DICY molecule and one Ay_Y_Ay (angle 3) per DETA molecule. Angle number and ID, as involved three beads joined by underscore where central bead is the vertex, define angles.

Angle No.	ID
1	E_G_B
2	G_B_G
3	Ay_Y_Ay
4	Ad_Ae_Ad

Table 12 Angles classification

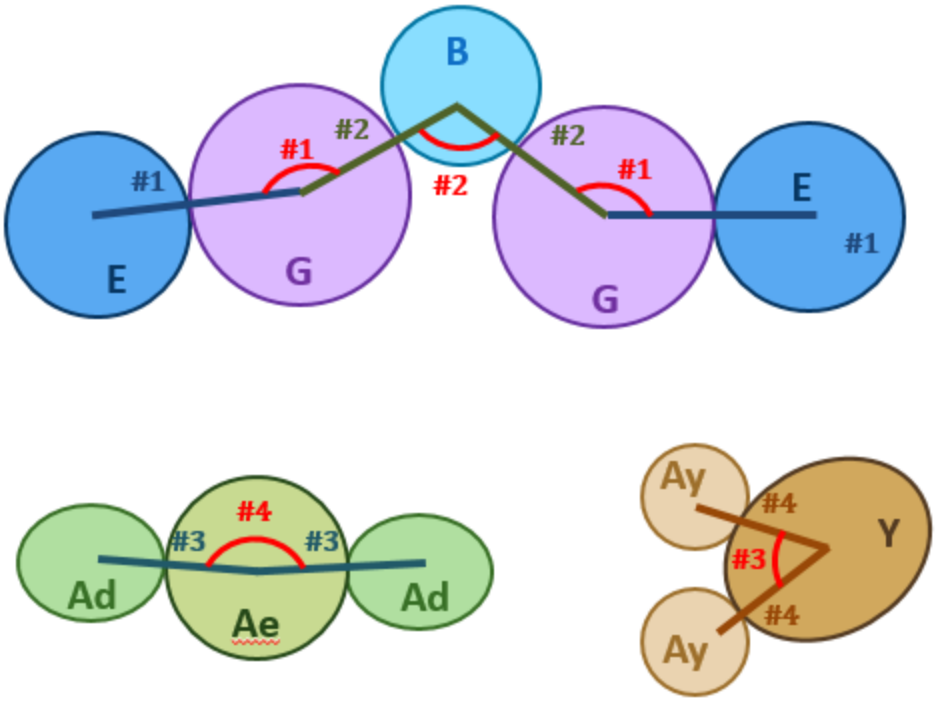

Figure 48 DGEBA, DETA and DICY bonds and angles representation in not-crosslinked CG configuration (developed by ITA (35))

Crosslinked system

Crosslinking process involves DGEBA, DICY and DETA reactive beads, which are the epoxy ring groups (E), primary amine groups in DICY (Ay) and both primary and secondary amine groups in DETA (Ad and Ae). In particular, primary amine groups Ad and Ay are reactive twice, since they have still two H atoms that can bond with O from opened epoxy rings forming hydroxyl, while secondary amine group Ae is once reactive, since it has only one H atoms remaining. Therefore, epoxy ring groups are reactive once, since they have only one epoxy ring. Details on crosslinking reactions are in the chapter dedicated (1.1.3).

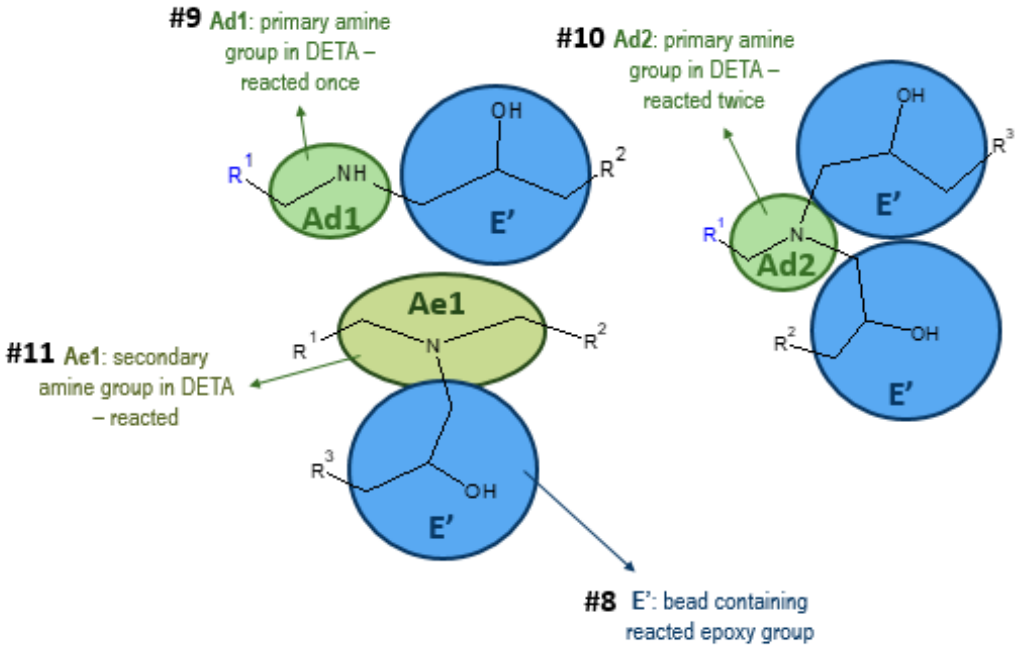

Figure 49 DGEBA-DETA crosslinking reactions (developed by ITA (35))

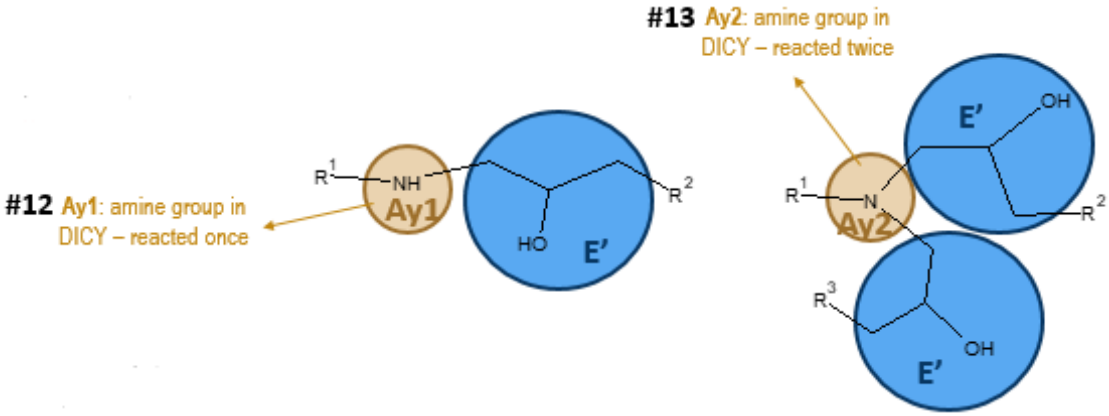

Figure 50 DGEBA-DICY crosslinking reactions (developed by ITA (35))

Thus, new bonds are forming during crosslinking between E beads and hardener beads, but every time a new reaction takes place and a new bond forms, the two involved beads change their mass and charge. For this reason, not only new bond, but also new bead and consequentially new angle definitions will be necessary. In particular, bead mass will change depending on the mass redistribution among reactant bead after the reaction, and so does charge.

The new so-defined beads have the same name as before, followed by a number N, which is the number of carried out reactions (1 or 2). This leads to the definition of six new beads, which are one or twice reacted beads. Reacted beads are all polar and present slight mass redistribution with respect to not crosslinked configuration.

Bead No.	ID	Bead Mass [g/mol]	Charge [C]	Atoms
8	E1	58.08067	+0.2427	1H 1O 3C
9	Ad1	29.04176	-0.0827	1H 1C 1N
10	Ad2	28.03379	-0.1654	1C 1N
11	Ae1	42.06088	-0.0827	2C 1N
12	Ay1	15.01467	-0.0827	1H 1N
13	Ay2	14.00670	0.1654	1N

Table 13 Reacted beads classification

Bond No.	ID
5	E1_Ad1
6	E1_Ad2
7	E1_Ae1
8	E1_Ay1
9	E1_Ay2

Table 14 Crosslinking bonds classification

Considering all the possible intermediate and/or complete crosslinked configuration that may occur in the system, is possible to identify up to thirty-one new angle types. In fact, each time a new bond forms, involved beads change their ID and so do all the angles involving them, leading to several possible configurations.

Angle No.	ID	Angle No.	ID	Angle No.	ID
5	E1_Ad1_Ae	16	E1_Ay2_Y	27	Ad_Ae1_Ad
6	E1_Ad1_Ae	17	G_E1_Ay1	28	Ad_Ae1_Ad2
7	E1_Ad2_Ae	18	G_E1_Ay1	29	Ad1_Ae_Ad
8	E1_Ad2_Ae1	19	E1_G_B	30	Ad2_Ae1_Ad2
9	E1_Ae1_Ad	20	Ay2_Y_Ay	31	Ad_Ae_Ad2
10	E1_Ae1_Ad1	21	Ay1_Y_Ay	32	Ad1_Ae1_Ad2
11	E1_Ae1_Ad2	22	Ay1_Y_Ay1	33	Ad2_Ae_Ad1
12	G_E1_Ad1	23	Ay1_Y_Ay2	34	Ad_Ae1_Ad1
13	G_E1_Ad2	24	Ay2_Y_Ay2	35	Ad2_Ae_Ad2
14	G_E1_Ae1	25	E1_Ad2_E1	36	Ad1_Ae1_Ad1
15	E1_Ay1_Y	26	E1_Ay2_E1	37	Ad1_Ae_Ad1

Table 15 Crosslinked system new angles classification

Once the mapping of the system is complete including crosslinking modifications, is possible to deposit the beads in a simulation box, apply the force field and start some simulations in order to get an equilibrated initial system with proper density and internal energy. Is noteworthy that in the final crosslinked configuration, crosslinking degree is not perfectly homogeneous along the box three directions and this leads to a system in which there are both several possible partially crosslinked chains and totally crosslinked groups. This limits or makes more difficult to achieve high global crosslinking degree (more than 90%). Further details on crosslinking procedure adopted are in the dedicated section (2.2.4), while implemented crosslinking algorithms are in Appendix B.

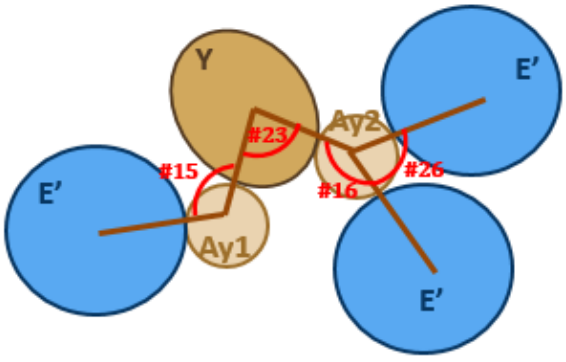

Figure 51 Possible DICY crosslinked structure (developed by ITA (35))

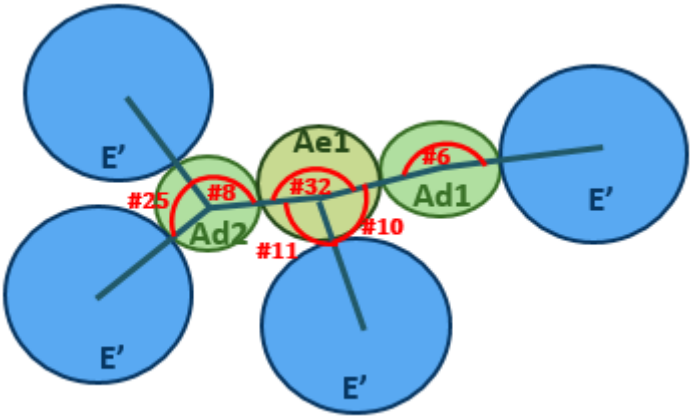

Figure 52 Possible DETA crosslinked structure (developed by ITA (35))

Due to the complexity of the system and to the high number of parameters to be set in the force field, improper dihedral and torsional potential are not taken into account. Concerning improper potential, planar epoxy groups are already packed into E and E1 beads, so they are just considered in the potential evaluation and there are no more planar groups in the CG configuration. Proper dihedral or torsional potentials are neglected to simplify the force field.

In other words is possible to consider all the beads as full homogenous spheres and bonds as mono-directional springs, forgetting about what particular atom inside the bead is bonding and where it is, in the spirit of CG procedures, so that beads are free to rotate without affecting final trajectories.

2.1.2 FORCE FIELD

In addition to the CG Mapping, ITA developed a force field, through the Iterative Boltzmann Inversion (IBI) method, starting from atomistic simulations of the same system. Details on force fields parameters are in the Appendix A, while more on IBI is in the chapter dedicated (1.2.3). This CG force field has been carried out by optimizing the IBI on the RDFs, which indicates the density variation in function of the distance from a certain point. In other words, it is built to have a beads spatial distribution similar to the atoms distribution of the original atomistic system. This is done for potentials corresponding to each degree of freedom taken into account: stretching, bending and non-bonded interactions. This method provides a series of point that are fitted by linear interpolation to obtain tables of 1000 points.

Only for non-bonded potentials, beads modifications due to the crosslinking reactions are not taken into account, so that:

- E1==E
- Ad1==Ad
- Ad2==Ad
- Ae1==Ae
- Ay1==Ay
- Ay2==Ay

Long-range Van Der Waals tail correction terms are set, while long-range Coulombic interactions are computed by means of Ewald solver with 0.01% of desired relative error in forces.

Neighbour list are built with bin algorithm and all the beads pair within a neighbour cut-off distance equal to their force cut-off plus a skin distance set to 2.260777 [Å].

2.2 Simulations

2.2.1 LAMMPS

All the simulations are conducted in LAMMPS (36)(Large Atomic/Molecular Massively Parallel Simulator), an open source software written in C++, developed by Sandia National Laboratories, part of the Department of Energy in USA.

LAMMPS performs the Newton's equations integration for large discrete systems with many particles, which can be atoms, electrons, molecules, beads or other groups. It uses neighbour lists to monitor continuously nearby particles, optimized for short-range repulsive interaction to avoid high local densities and overlapping. One of the main features of LAMMPS is that it can be run in parallel machines, in order to exploit the computational power spend. In particular, the domain is divided in several sub-domains of equal computational cost assigned to each processor employed,

while processors communicate and store information of the atoms exceeding their sub-domains, by means of the Message Passing Interface (MPI) protocol.

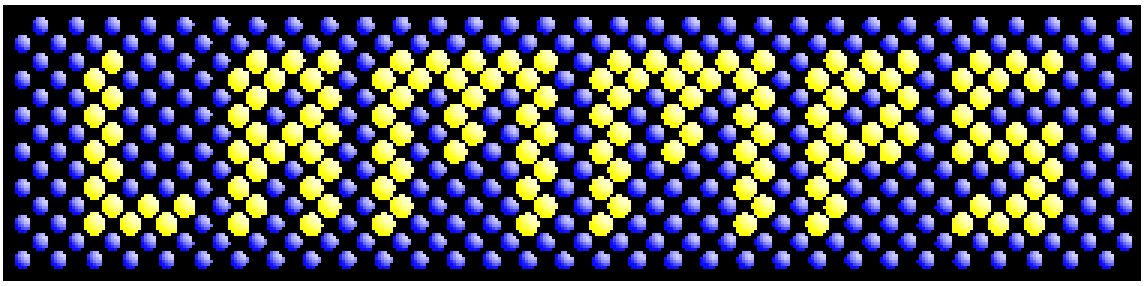

Figure 53 LAMMPS logo, by LAMMPS manual (36)

To run LAMMPS several input files are necessary, while it provides a log file in output with all the information about the run, in addition to all the prescribed output.

Concerning input files, data file contains the information about bond, angles and eventually dihedrals number and types, the dimensions of the box and exact position, mass, partial charge and type of each particle present in the system. Typically, there is one potential file, which contain all the information about the force field, including type and parameters of each bonded and non-bonded interaction, in addition to parameters of long-range solvers, and neighbour lists building.

Usually, these input files are referred to in a main input script, which contains initialization settings as units and time-step for the runs, output customization options and all the simulation commands.

As an example of data file, the one related to 70% crosslinked system is reported in Appendix B: .data, with all the potentials files .ff and the input scripts .in.

2.2.2 INITIAL SYSTEM

The first task is to get an initial system of the crosslinked structure at minimum energy and with a proper density, in order to compute properties starting from a realistic bulk of material.

To do this, a multi-step crosslinking procedure is adopted, similar to the one described by *A. Gavrielides et al.* (37) for a DGEBA-EDA system.

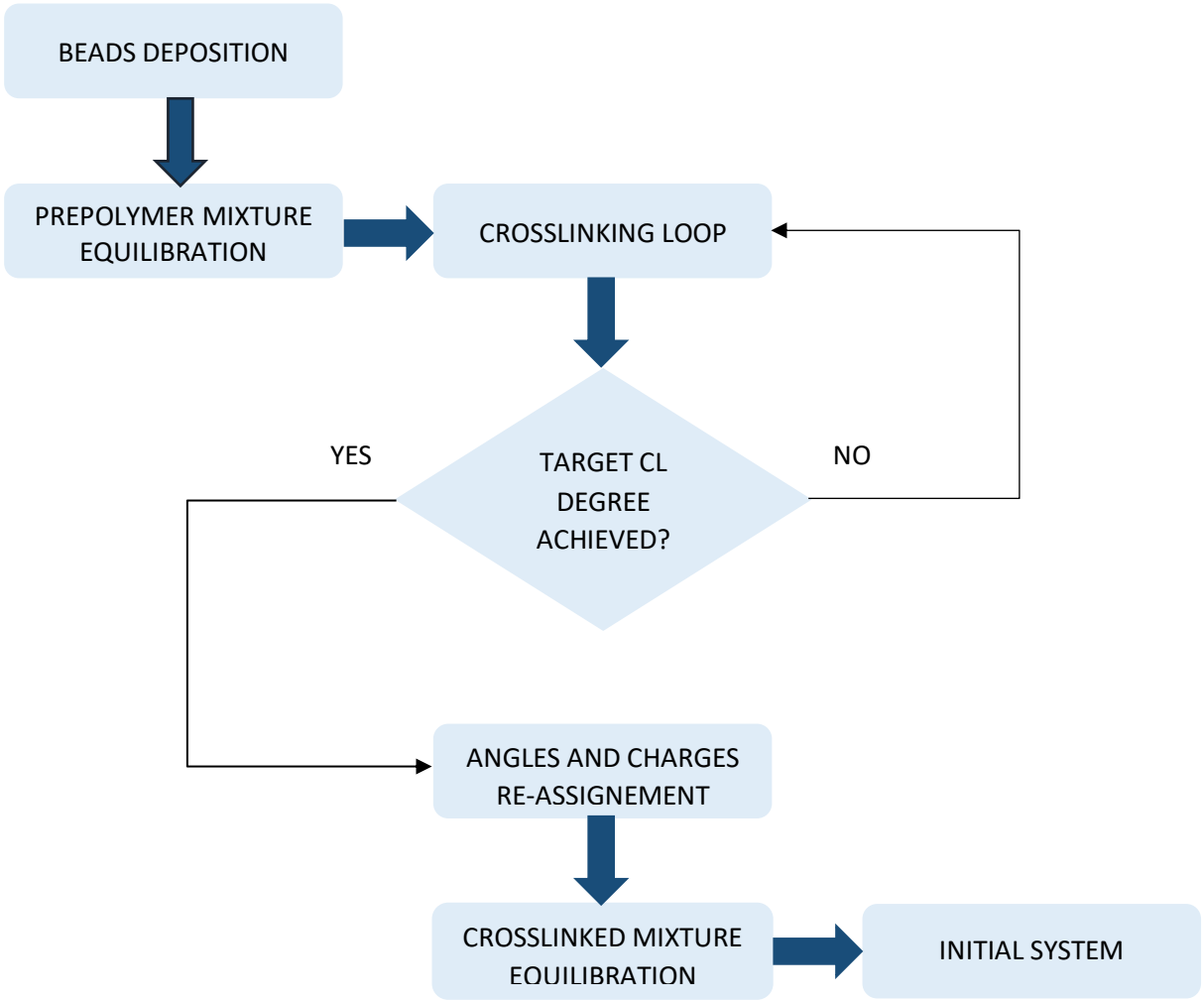

Figure 54 Multistep-crosslinking procedure flowchart

2.2.3 BEADS DEPOSITION AND PRE-POLYMER MIXTURE EQUILIBRATION

These two steps can be seen as one macro-step, since, as explained below, they establish a single optimization problem. In other words parameters of the first step affect the second one and vice-versa, so it is necessary to consider them as a whole.

Beads deposition takes place in a cubic orthogonal simulation box with periodic boundary conditions in all direction, in order to get a bulk of material. The dimensions of the box are $L_x = L_y = L_z$. The origin is a box vertex and each time a bead's spatial coordinate L_i overcomes one box dimension or goes below 0, it is immediately set respectively to 0 or L_i.

After the box creation, beads are grouped in three molecule units, which are the real DGEBA, DICY and DETA molecules of the pre-polymer system. Each molecule is then deposited into the box with different random seeds, keeping the typical 70:30 matrix-hardeners composition adopted in real systems (in this case 70% DGEBA, 20% DICY and 10% DETA in weight).

However, the system is not still equilibrated and if crosslinking procedure started now, it would be difficult to obtain high crosslinking degrees (>60%), because molecule are not uniformly distributed and there would be some regions with no crosslinking reactions and saturated regions with too much reactive beads.

On the other hand, an equilibrated pre-polymer mixture can hinder the crosslinking reactions as well, since beads swings around equilibrium positions. The crosslinking algorithm adopted does not include dynamic detection of new reactive beads according to the local reactive beads concentration, so a certain mobility is necessary to make new bonds, otherwise a saturation condition in several regions of the box could occur easily.

For these reasons, this step has to be optimized to go on with the procedure.

In order to frame the problem effectively, it is possible to look at it as a multi-objective multi-variable optimization problem, in which the goals are: maximize the cross-linking degree γ_{CL}, minimize the computational cost and minimize the standard deviation of the computed density with respect to the actual value.

In addition, there are several design variables to modulate:

- time step $(0.1 - 2.0\ fs)$
- number of beads deposited $(10^3 - 10^4\ atoms)$
- box dimensions $(20 - 70\ nm)$
- number and length of equilibration steps $(\sim\ ns, 1 - 5\ steps)$
- thermodynamic conditions of equilibration steps $(T = 275 - 500\ K, p \simeq 1\ atm)$
- cut-off distance for crosslinking reactions $(4 - 8\ \text{Å})$

For example crosslinking cut-off distance, which is the distance within which the search of other reactive beads is performed at each step during the crosslinking, has been studied though a sensitivity analysis. Keeping constant all the other parameters, equilibration and crosslinking procedures are performed varying cut-off, to investigate on its effect on the maximum γ_{CL}

achievable. For low values of cutoff (about one fifth of the box side), it is generally hard to find other reactants and is possible to achieve only very low values of γ_{CL}. Same result for high value (about half of the box side), because many bonds are formed in the first steps, and saturated regions occur before the system is able to relax. Higher values of γ_{CL} are obtained for a crosslinking cutoff of about $6 - 7$ Å.

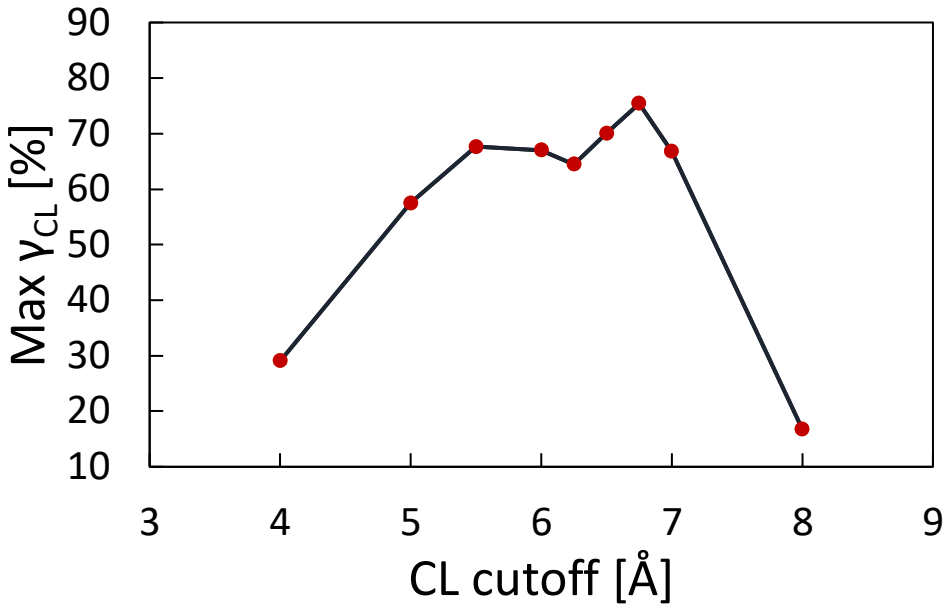

Figure 55 Maximum crosslinking degree achieved with different crosslinking cut-off radii

Similarly, also box dimension, number of particles and thermodynamic conditions have been optimized so that a set of fixed parameters is built to reduce the number of design variables. The fixed parameters are the following:

- 15062 beads, 3430 molecules (2401 DGEBA, 686 DICY,343 DETA), 86779 atoms
- simulation box with about 20 nm per side (it is changing during NPT runs)
- crosslinking cut-off set to 6.75 [Å]
- initial thermodynamic conditions are about standard conditions (T=300 [K], p=1 [atm])
- time step in this phase is set to 1.0 [fs]

The approach is not to look for the best solution because the problem is very complex and it is not needed for the goals of the present work. For this reason, design variables have been iteratively

adjusted to get an initial system with proper density, sufficiently high crosslinking degree (at least 70%) and suitable to compute mechanical and thermal properties, in a reasonable time.

2.2.4 CROSSLINKING PROCEDURE

Crosslinking process is simulated by means of a loop consisting of the formation of bonds and NVT run. In particular, for each of the five crosslinking bond types described in the CG mapping section, couples of the involved bead types are searched within the prescribed cut-off radius and if they are present, a new bond is formed. An energy minimization step follows each bond type creation, and after all the types, a NVT run at 300K ends the loop. Crosslinking script need three parameters in input: target crosslinking degree, number of initial bonds in the system and number of epoxy rings (E beads) in the system. At the beginning of the loop, it computes the total number of bonds and then calculates the crosslinking degree as the ratio between the increase of bonds and the number of E beads, since 100% is achieved when all the E beads react:

$$\gamma_{CL} = \frac{N_{bond} - N_{bond0}}{N_E}$$

When the crosslinking degree value reaches the target, the loop is broken and the final crosslinked configuration is provided in output.

The code also modify the types of the involved beads, since mass and charge distribution change as already explained. Conversely, angles are not automatically updated because when a new bond is formed, several new angles occur and is not possible to define a priori the type of those angles without information on the thirds beads involved. For this reason, for angles update a further step is necessary. Concerning charges, is possible to set new types one by one directly inside the code, after the crosslinking loop, or to proceed as for the angles.

2.2.5 ANGLES AND CHARGES UPDATE

The crosslinking output configuration present all the new angles of one type and all the charges unchanged, so it is necessary to update them. A MATLAB script does this, by iteratively searching beads corresponding to crosslinking angles in the angles list and substituting the angle type with the correct one. Angles with the same central bead and inverted lateral beads are considered as the same angle, while, as a simplification, two angles, for which potential is not available from the adopted force field, are considered as respectively type 29 and 33, which are composed by the same beads, but with different reactivity. Angle 36 (Ad1_Ae1_Ad1) is assumed as 29 (Ad1_Ae_Ad); while angle 37 (Ad1_Ae_Ad1) is assumed as 33 (Ad2_Ae_Ad1). Once angles and charges have been updated, a complete crosslinked data file is provided for the final equilibration.

2.2.6 CROSSLINKED MIXTURE EQUILIBRATION

The crosslinked configuration is still not at minimum energy and density is still lower than the actual one, since the space of the box is not filled uniformly and there are some voids and/or some region with high beads concentration, which determines the high energy of the system. The equilibration script is made by subsequent step of minimize, NVE, NVT, NPT ensemble runs up to one nanosecond. During these runs density slowly increase due to the box size adjustment combined with redistribution of the beads inside the box. When beads are distributed uniformly, a smaller box is needed to contain the system, so the volume is lower and the density increases. At the same time, the total energy of the system decreases since all the bonds, angles and interactions approach their potential minima. At the end of this phase, is possible to compute the density with standard deviation.

The final configuration has been reached following three different procedures: P1, P2 and P3. Then the most efficient has been selected for going on with the properties computation.

- P1: sample equilibration, replication and direct crosslinking

For the first procedure, the idea is to equilibrate first a small box with few beads, then to replicate this pattern in the three directions, to get a homogenous system and perform crosslinking starting from it. In particular, ten molecules (seven DGEBA monomers, two DICY and one DETA molecules) are deposited in a small box with 2.5 nm per side.

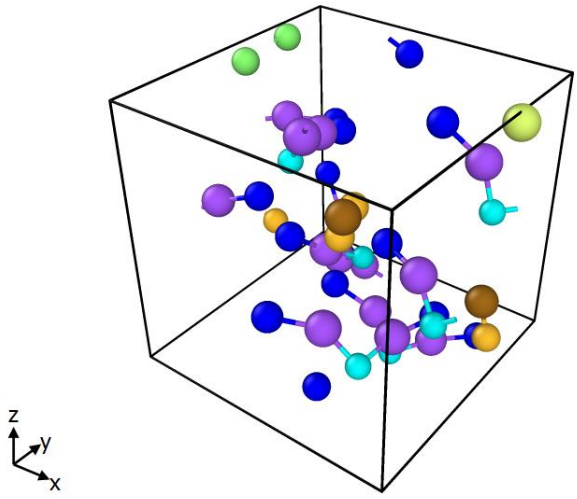

Figure 56 P1: deposition of ten molecules equilibrated sample (OVITO)

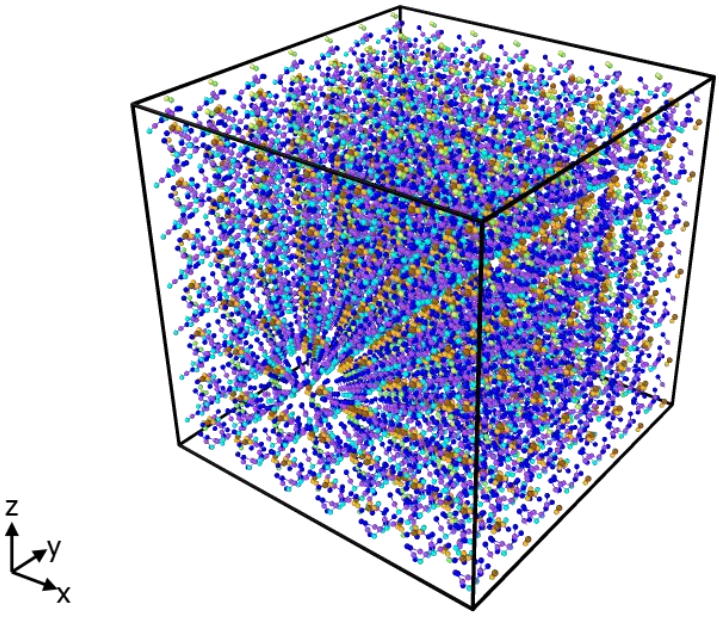

Figure 57 P1: Deposition of ten molecules sample box replicated 7x7x7 (OVITO)

This procedure leads immediately to high values of γ_{CL}, thanks to the homogeneous distribution of beads, but after the first wave of bonds, a saturation condition is established and crosslinking proceeds very slowly. In addition, the post-crosslinking equilibration is problematic, since many bonds formed just in the very first steps and there several voids.

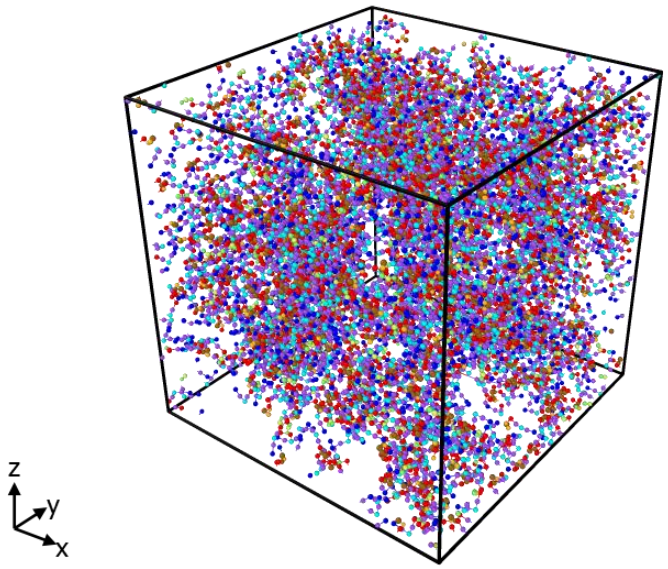

Figure 58 P1: maximum γ_{CL} crosslinked system before final equilibration (OVITO). Red beads are reacted epoxy rings (E1 beads).

- P2 sample equilibration, replication, partial equilibration and crosslinking

In the second procedure, the first part is the same of the first procedure: ten molecules (seven DGEBA monomers, two DICY and one DETA molecules) are deposited in a small box with 2.5 nm per side. Then the sample is replicated seven times in each dimension. A partial equilibration run for 20000 steps in NVE ensemble and 50000 steps in NVT ensemble at 700K, before crosslinking. This partial pre-crosslinking equilibration just remove the artifice of the sample replication slightly mixing the system, in order to facilitate the crosslinking process.

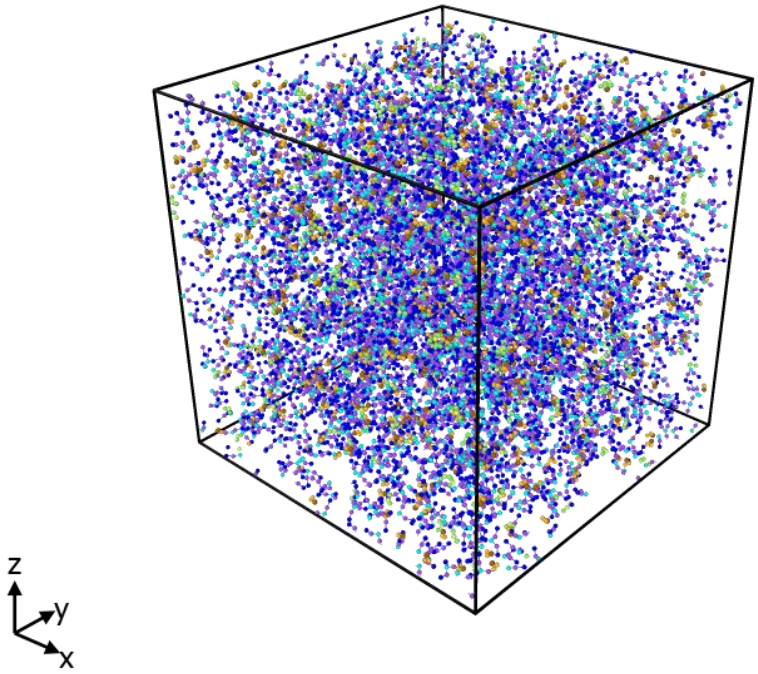

Figure 59 P2: Deposition and partial equilibration of ten molecules sample replicated 7x7x7 (OVITO)

This configuration allows reaching $\gamma_{CL} = 85\%$. This value is suitable to carry out properties, since is near to actual values of the most common epoxies of about 90%. Beyond this value, saturation condition is established and γ_{CL} grows slow as already seen for P1. Post-crosslinking equilibration is efficient, because is still space for the system to relax and, at the same time, not too much bonds are already formed, resulting in higher mobility for the beads to fill the voids. This is the best procedure to compute the density.

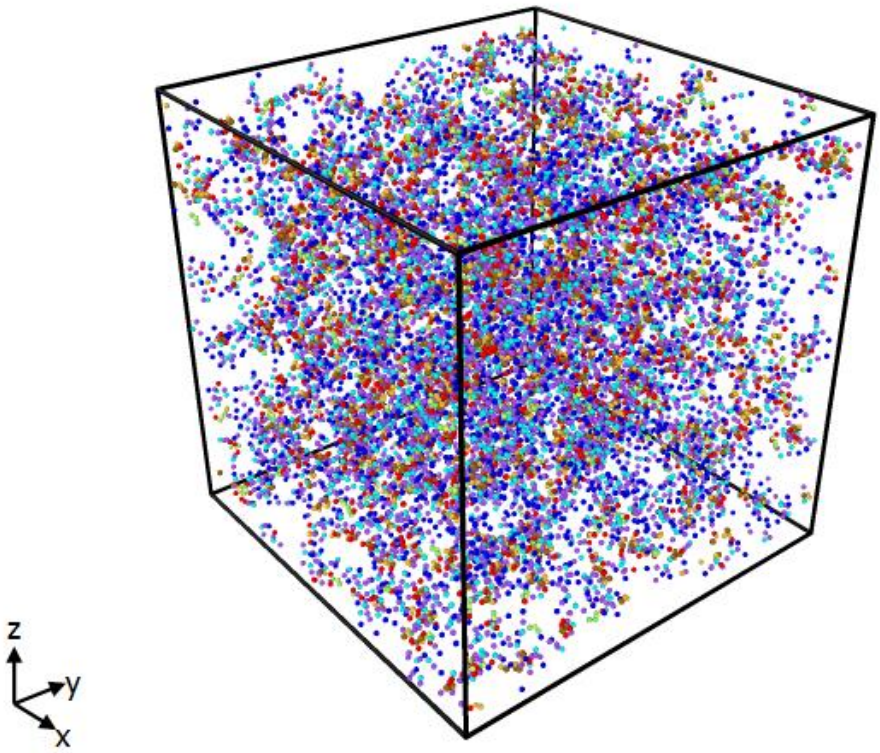

Figure 60 P2: maximum γCL crosslinked system before final equilibration (OVITO). Red beads are reacted epoxy rings (E1 beads).

- P3: Direct deposition in the final box, crosslinking and equilibration

In the third procedure, 3430 molecules (2000 DGEBA, 571 DICY, 343 DETA) are deposited directly in a 200x200x200 nm box without any replication, and then equilibrated in NVE for 100000 steps, in NPT for 100000 steps and finally in NPT at 300K for 1 nanosecond. Then, crosslinking procedure is performed as for P1 and P2.

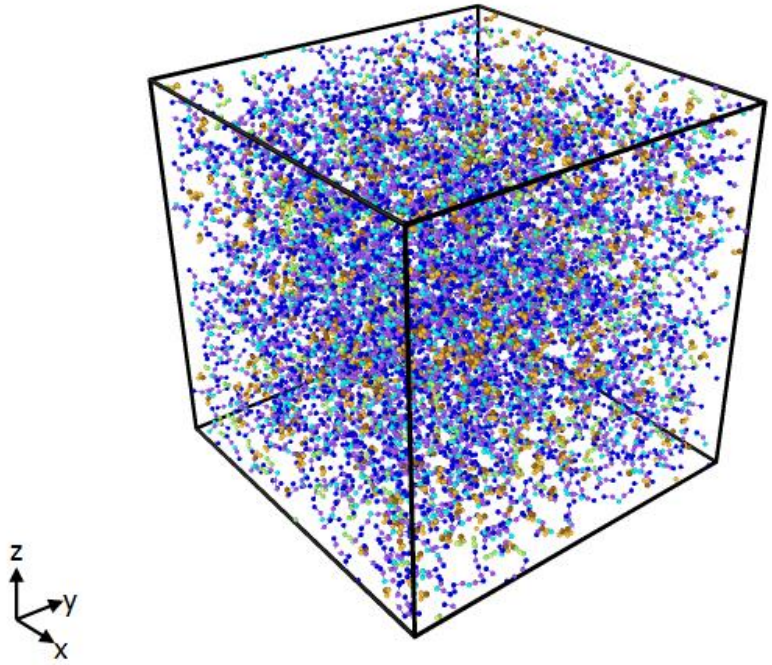

Figure 61 P3: Direct random deposition of 3430 molecules (2000 DGEBA, 571 DICY, and 343 DETA)

In P3, and in general in all configuration in which all the beads are randomly deposited directly in the final box, big agglomerates of particles are formed, leaving space to very big voids, as shown in figure.

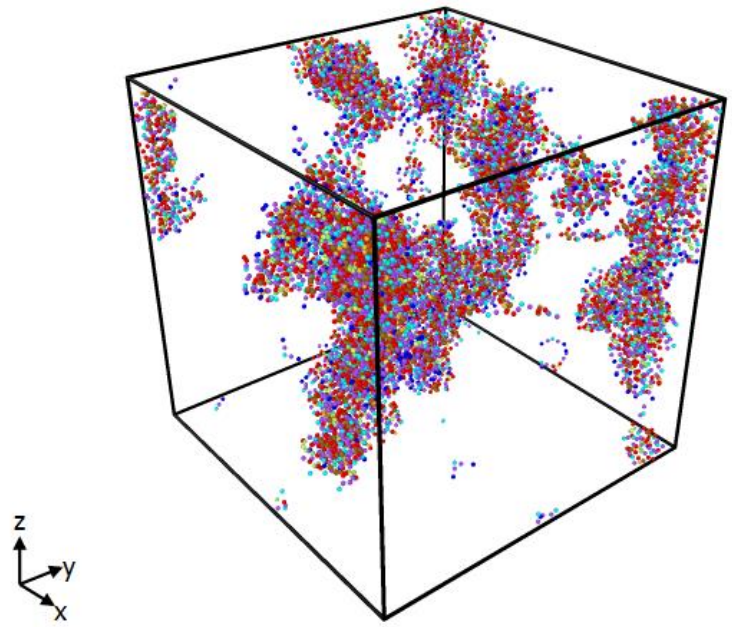

Figure 62 P3: maximum γ_{CL} crosslinked system before final equilibration (OVITO). Red beads are reacted epoxy rings (E1 beads).

This configuration is very difficult to equilibrate since beads are strongly connected to the agglomerates and cannot move to fill the voids, resulting in few big macro-beads moving inside the box, without mixing.

P2 is most efficient among these procedures and it has been implemented for all the properties computation.

3. RESULTS

3.1 Density

Concerning the pre-polymer mixture, the density computed is 1.10729 ± 0.26% [g/cm^3], while the final total internal energy is 8656.74 [Kcal/mol] and fluctuations on temperature are lower than 0.2%, which means that system is equilibrated. At the end of this run, crosslinking process begins.

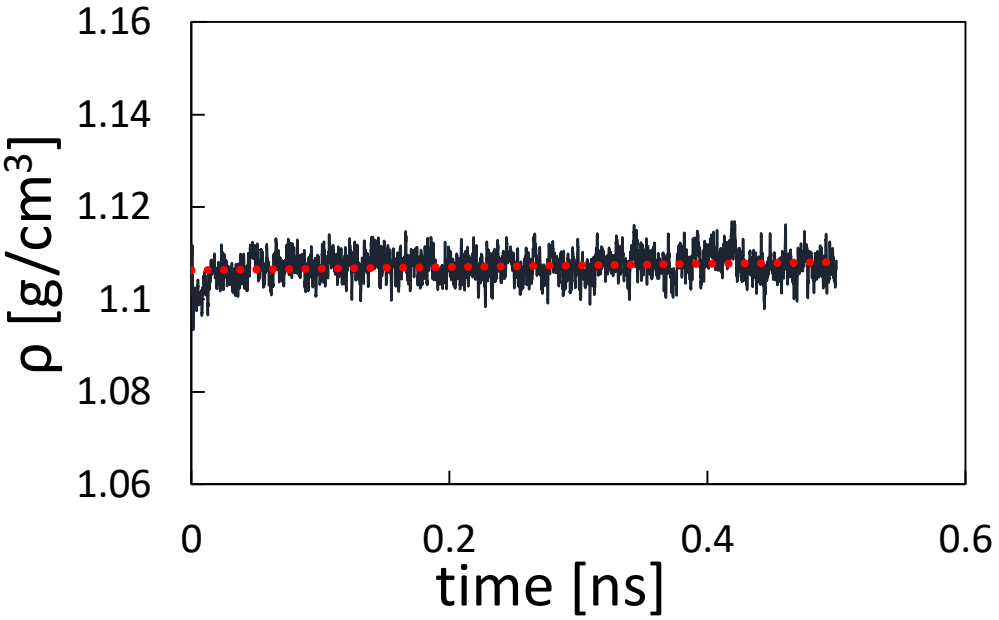

Figure 63 Density time evolution in pre-polymer mixture

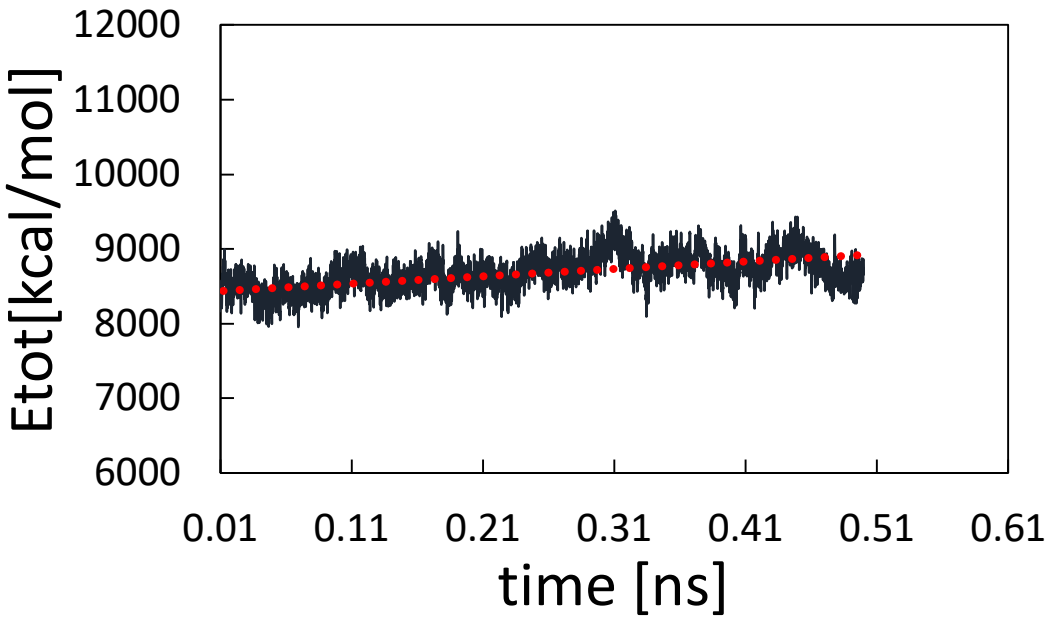

Figure 64 Total internal energy time evolution in pre-polymer mixture

Density has been computed for five different values of γ_{CL}, in addition to the 0% crosslinked one, which is the pre-polymer mixture. In figure, the equilibrated 75% crosslinked configuration is shown as an example, while density and internal energy time evolutions are plotted, started from the end of the crosslinking process.

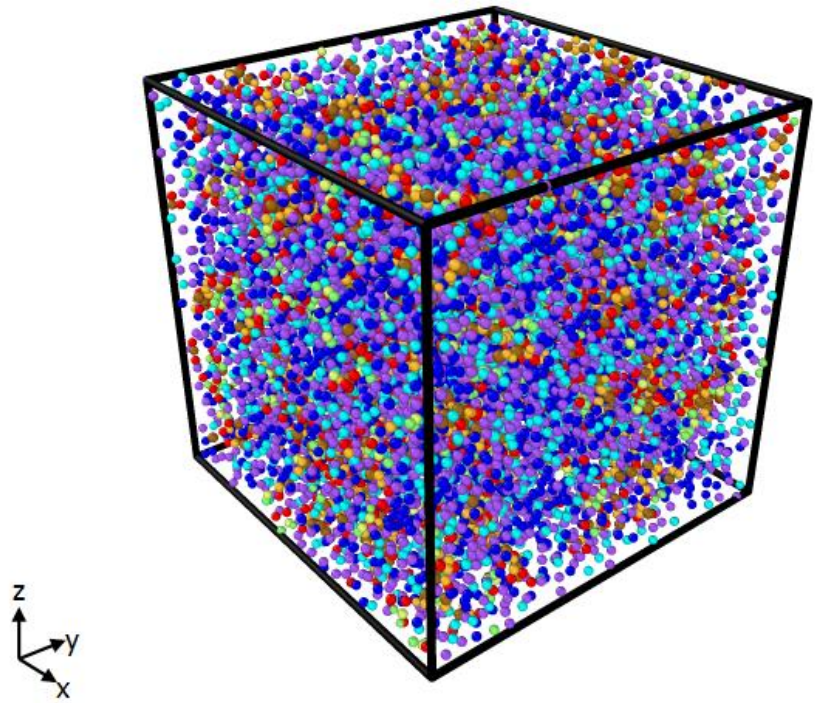

Figure 65 Equilibrated 75% crosslinked configuration. Red beads are reacted epoxy rings (E1 beads).

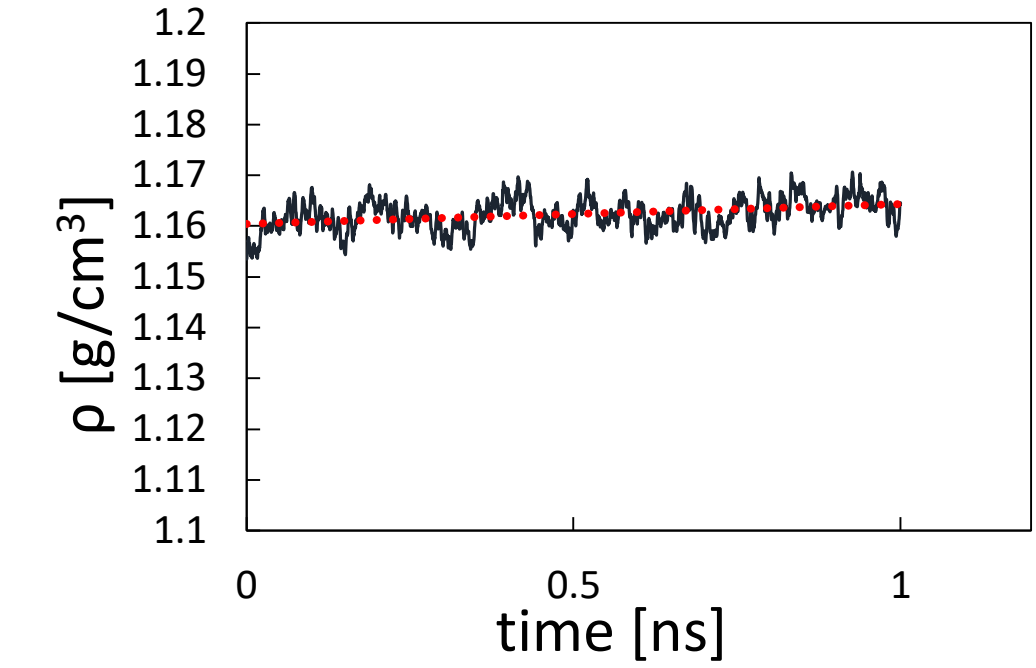

Figure 66 Density time evolution in 75% crosslinked system

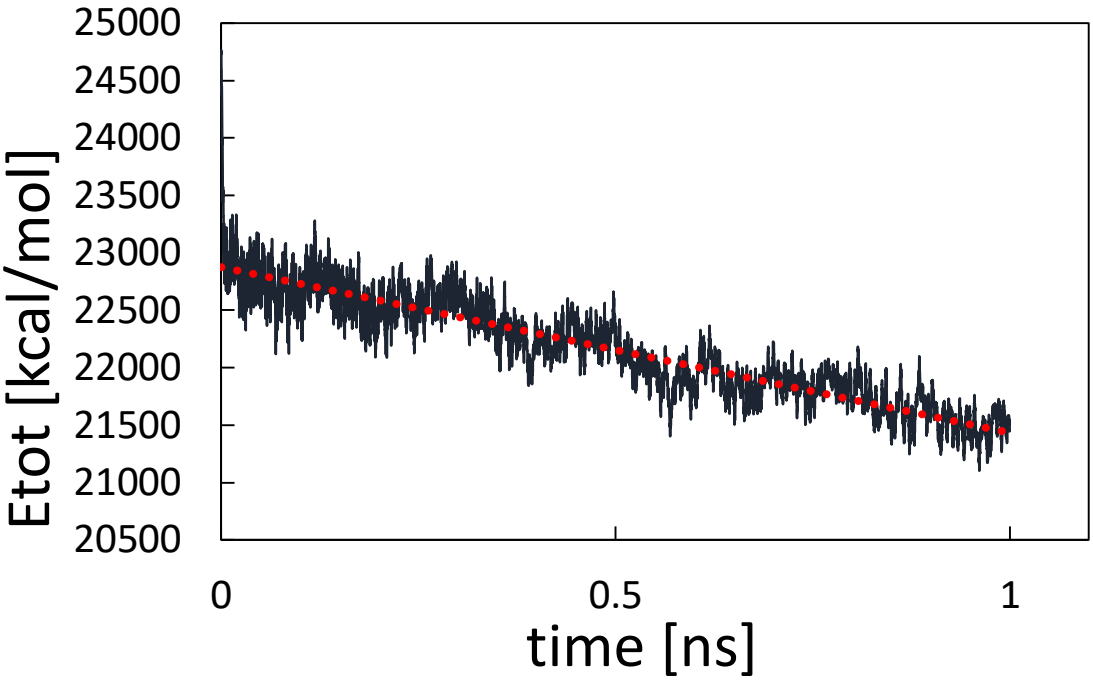

Figure 67 Total internal energy time evolution in 75% crosslinked system

For 75% crosslinked system, the computed density is 1.1624 ± 0.26% [g/cm3], while internal energy decreases up to 21500 [Kcal/mol], after the increase due to the crosslinking process. Temperature fluctuations are lower than 0.2% after 0.5 [ns].

Similar outputs are obtained for the others crosslinking degree considered: 63%, 70%, 81%, and 85%.

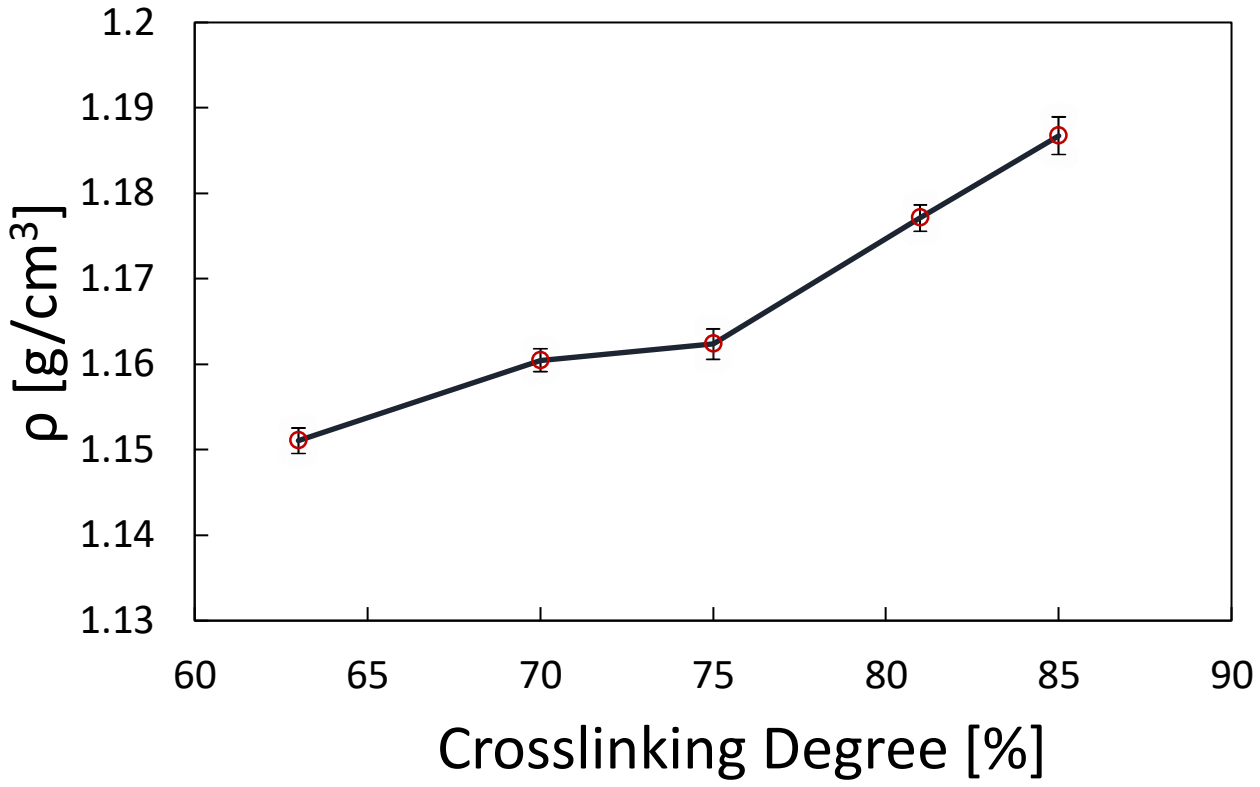

Figure 68 Density computed for different crosslinking degrees

As expected, density increases with crosslinking degree. Considering the whole process, for an 85% crosslinked system, volume reduces by a 6-7% starting from the pre-polymer mixture. This is because, as well shown in P3 procedure, new crosslinking bonds tends to agglomerate the molecules, and this reduces their mobility and the occupied volume. Using P2 procedure is possible to investigate only on systems beyond 60% crosslinked, because this percentage is reached in the very first step, then it grows slowly. Other procedures are more suitable to get less crosslinked systems, but, as already explained, these are the most interesting and realistic values.

Density results are in good agreement with values found in different works on DGEBA-based epoxy resins (38) (39) and with those found from the atomistic simulation within the SMARTFAN project (35). Matching is good also with values from online databases (40).

3.2 Glass Transition Temperature

Glass transition temperature T_g is an important property for thermosetting polymers as epoxy resins, since in correspondence of it there is a change of mechanical behaviour of the material. Below T_g the material is in the glassy state and acts like a crystalline solid, while beyond T_g it is in the rubbery state, pliable and soft. Knowing the value of T_g of a polymer, with an eye on its final use, is fundamental for the correct material selection.

Density varies with temperature, but is possible to observe that the slope below and above T_g are different. Glass transition temperature (T_g) was determined at discontinuity position on the density with respect to temperature profile (41). Hence, is possible to predict T_g through MD simulations, by computing density of several system equilibrated at different temperatures, in parallel. Each density computed is a point on a density-temperature chart. Then points are divided in two groups with different slopes and linearly fitted in MATLAB via cftool.

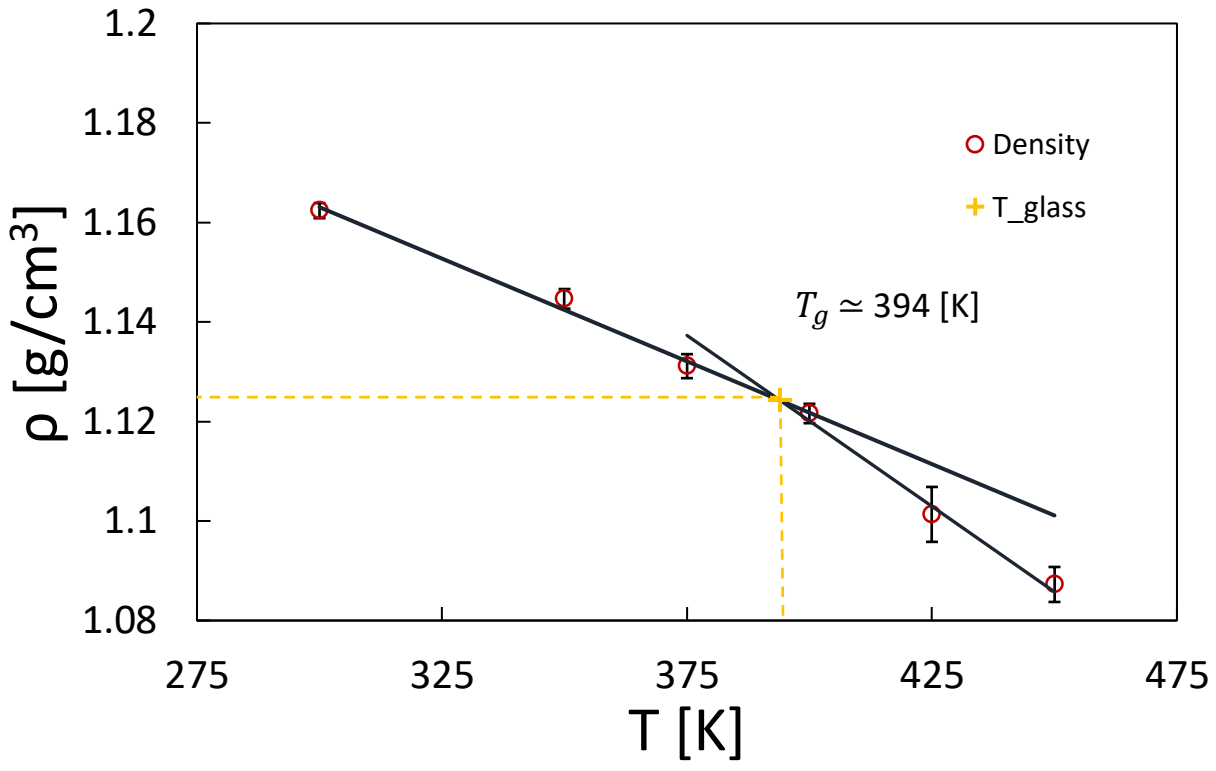

Figure 69 Density computed at different temperatures and glass transition temperature evaluation

Density decreases with temperature faster above glass transition temperature than below glass transition temperature. Thus, it is possible to identify two different slopes within the trend. The abscissa of the intersection of the two fitting straight lines is the computed T_g, in this case is about 394 [K].

3.3 Mechanical Properties

Starting from the equilibrated crosslinked initial system obtained through P2 procedure, is possible to compute mechanical properties and predict the mechanical behaviour of the resin under stresses due to external loads. The main mechanical properties of interest are Young's Modulus and Stiffness Ratio. From these is possible to obtain also Shear Modulus, Bulk Modulus and in general is possible to build the stiffness matrix of the linear elastic problem, to characterize the material and for macroscale study, which is one goal of multi-scale studies.

The fundamental hypothesis adopted is the isotropy of the material. It is justified by the space distribution of beads in the equilibrated crosslinked system, which is a homogenous bulk of material and does not present any particular directional pattern, so it is possible to assess that mechanical properties does not depend on directions. The similarity between stress-strain curves of the same system in different directions will enforce this hypothesis as well. For the same reason, the bulk can be considered homogeneous and computed properties are constant in space.

Hence, is possible to write six equations for the six deformation components for a linear elastic, isotropic and homogeneous solid, by deriving elastic potential with respect to six strain components. The resulting equations are writable in a matrix form:

$$[\sigma] = [H][\varepsilon]$$

Where $[\varepsilon]$ is the strains vector, $[\sigma]$ is the stresses vector and $[H]$ is the stiffness matrix of the material, which operates 2nd order derivatives of the elastic potential with respect to strain components, since elastic potential itself, developed according to MacLaurin, is composed by 1st order derivatives, while the analogy with the harmonic oscillator potential well is applied. According to this analogy $[\sigma]$ corresponds to the derivative of the elastic potential with respect to one

direction, spring stiffness k corresponds to the stiffness matrix $[H]$ and the spring elongation is corresponds to $[\varepsilon]$ (42).

The resulting stiffness matrix is a Hessian matrix and, since the undeformed state is the absolute minimum of the elastic potential function, it has to be positive-definite. This means that his determinant is positive, all the principal minors' determinants are positives and the matrix is invertible, allowing writing the equation in the most common form, which is:

$$[\varepsilon] = [H]^{-1}[\sigma]$$

$[H]^{-1}$ is the inverse of the stiffness matrix of the material. It contains Young's modulus E, Poisson's ratio ν and shear modulus G.

$$\begin{bmatrix} \varepsilon_{xx} \\ \varepsilon_{yy} \\ \varepsilon_{zz} \\ \gamma_{xy} \\ \gamma_{xz} \\ \gamma_{yz} \end{bmatrix} = \begin{bmatrix} 1/E & -\nu/E & -\nu/E & 0 & 0 & 0 \\ -\nu/E & 1/E & -\nu/E & 0 & 0 & 0 \\ -\nu/E & -\nu/E & 1/E & 0 & 0 & 0 \\ 0 & 0 & 0 & 1/G & 0 & 0 \\ 0 & 0 & 0 & 0 & 1/G & 0 \\ 0 & 0 & 0 & 0 & 0 & 1/G \end{bmatrix} \begin{bmatrix} \sigma_{xx} \\ \sigma_{yy} \\ \sigma_{zz} \\ \tau_{xy} \\ \tau_{xz} \\ \tau_{yz} \end{bmatrix}$$

The form with the stiffness matrix $[H]$ is less common and is as follows:

$$\frac{1}{2G}\begin{bmatrix} \sigma_{xx} \\ \sigma_{yy} \\ \sigma_{zz} \\ \tau_{xy} \\ \tau_{xz} \\ \tau_{yz} \end{bmatrix} = \begin{bmatrix} \frac{1-\nu}{1-2\nu} & \frac{\nu}{1-2\nu} & \frac{\nu}{1-2\nu} & 0 & 0 & 0 \\ \frac{\nu}{1-2\nu} & \frac{1-\nu}{1-2\nu} & \frac{\nu}{1-2\nu} & 0 & 0 & 0 \\ \frac{\nu}{1-2\nu} & \frac{\nu}{1-2\nu} & \frac{1-\nu}{1-2\nu} & 0 & 0 & 0 \\ 0 & 0 & 0 & 1/2 & 0 & 0 \\ 0 & 0 & 0 & 0 & 1/2 & 0 \\ 0 & 0 & 0 & 0 & 0 & 1/2 \end{bmatrix} \begin{bmatrix} \varepsilon_{xx} \\ \varepsilon_{yy} \\ \varepsilon_{zz} \\ \gamma_{xy} \\ \gamma_{xz} \\ \gamma_{yz} \end{bmatrix}$$

In order to compute stiffness matrix or its inverse, is necessary to compute at least two properties among Young's modulus, Poisson's Ratio and shear modulus. In this case, the first two have been computed, and then the other one is calculated.

Young's Modulus E $[GPa]$

Also called Modulus of Elasticity, it is defined as the ratio between stress and strain or the factor of proportionality of the unidirectional Hooke's Law with perfect elastic behaviour hypothesis (linear Hooke's Law).

$$E = \frac{\partial \sigma(\varepsilon)}{\partial \varepsilon}\bigg|_{\varepsilon=0} \; [GPa]$$

It describes the elastic properties of a solid under unidirectional tension or compression conditions. In other words, it is a measure of the capability of a material to withstand deformations under external loads. Its evaluation is very important, in particular for mechanical components, structural components or protection devices.). From the linear elasticity theory is known that E must be always positive, by imposing the Hessian stiffness matrix to be positive-definition, which means that all its principal minors' determinants are positive. Typical values for construction materials are about 205 [GPa] for steel and about 25 [GPa] for concrete, while polymers goes from the order of [MPa] for highly elastic polymers to 4÷5 [GPa] for thermosetting ones.

It is calculated from the stress-strain curve, often obtained from uniaxial tensile test. During this test, a sample bar of material is subjected to a controlled tension until failure occurs, frequently measuring the stretch. Each stretch value, coupled with the tension, provide a point in a stress-strain chart, and more points compose the stress-strain curve. For ductile materials, these curves have a linear part until a yield strength value, when plasticization starts, cross-area starts reducing (necking) and deformation increases faster until failure occurs. The strain value corresponding to yield strength is the boundary between elastic and plastic regions. Sometimes is also possible to observe a resonance zone called "deformation plateau" near the elastic-plastic transition. The main difference between the two regions is that if the external load is removed still in the elastic region, the component returns at his initial shape, while, if plastic region is reached, a permanent deformation is observed.

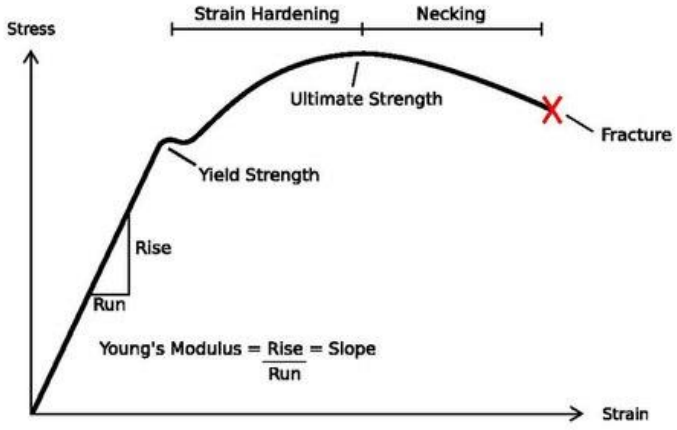

Figure 70 Example of stress-strain curve of a low carbon steel (11)

Young's modulus is usually calculated as the slope of the linear part of the stress-strain curve obtained by uniaxial tensile tests.

In MD, one possibility is to simulate these conditions by deforming the simulation box in one direction, carrying out stress-strain curves and then measuring the initial slope to predict Young's modulus.

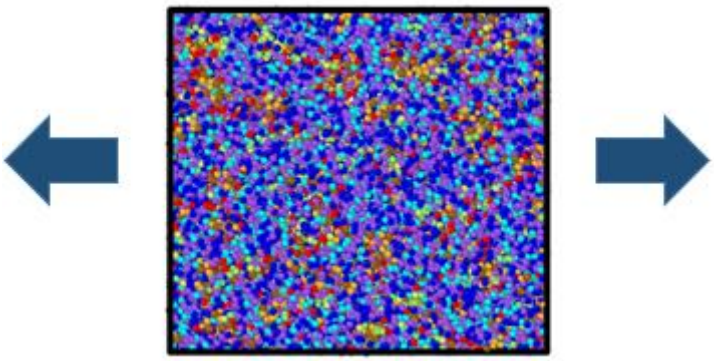

Figure 71 75% crosslinked system under X unidirectional tensile stress (x-y space).

A two-steps procedure has been performed. First, a further equilibration for 0.1 [ns] in NPT at 300 [K] and 0 [atm] is performed to remove possible crosslinking residual internal stresses which may obstacle the axial deformation of the box. A drag coefficient of 0.2 is applied in order to damp pressure and temperature oscillations.

Then, the box is deformed in x direction with a deformation rate of 0.01 [Å/fs], while time integration is performed in NVT ensemble at 300 K. All the components of pressure tensor pxx, pyy, pzz, pxy, pxz and pyz are computed and the script provides them in output for each deformation step.

Strain ε [-] is calculated with the typical engineering definition:

$$\varepsilon = \frac{l - l_0}{l_0} \; [-]$$

Where l and l_0 are respectively the current and initial box dimension in the deformation direction. Stress σ is the output value of the simulation, properly converted in from [atm] to [GPa]. With these data is possible to compute the x direction stress-strain curve.

Since the potentials of the adopted force field do not foresee rupture, failure is not visible, but, in correspondence of failure conditions, is possible to observe the beginning of an oscillatory trend. In other words, the system deforms until failure conditions, but instead of break, the box starts to showily expand and compress because bonds and angles are moving towards high potential values, high forces occur and system diverges. However, until rupture, the computed curve has the typical shape and this is sufficient to compute E.

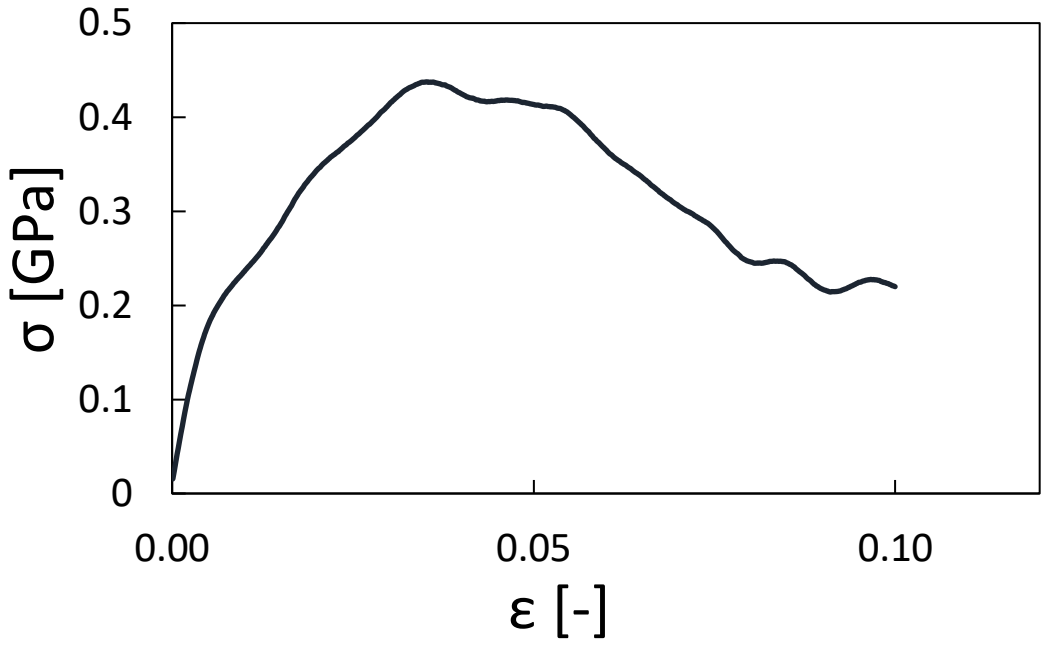

Figure 72 Stress-Strain curve in x direction for 75% crosslinked system

Zooming in the zone of small strains, in particular in the order of magnitude of the strain rate, is possible to isolate the linear part, whose slope is the Young's modulus, calculated as the derivative of the straight-line equation.

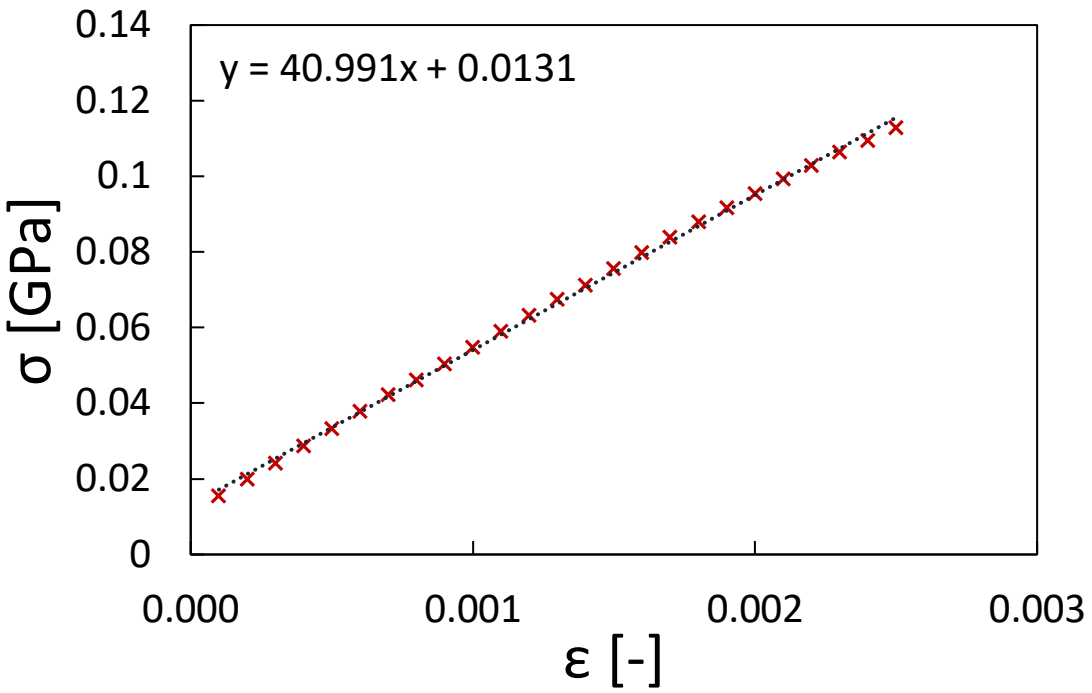

Figure 73 Elastic stress-strain curve of 75% crosslinked system. Zoom on small strains zone.

The procedure is repeated for all directions, and provides similar stress-strain curves in output. Three curves of the same system in different directions are the equivalent of three different random configuration of the same box. Moreover, their similarity supports the validity of the results besides enforcing the isotropy hypothesis, as explained above.

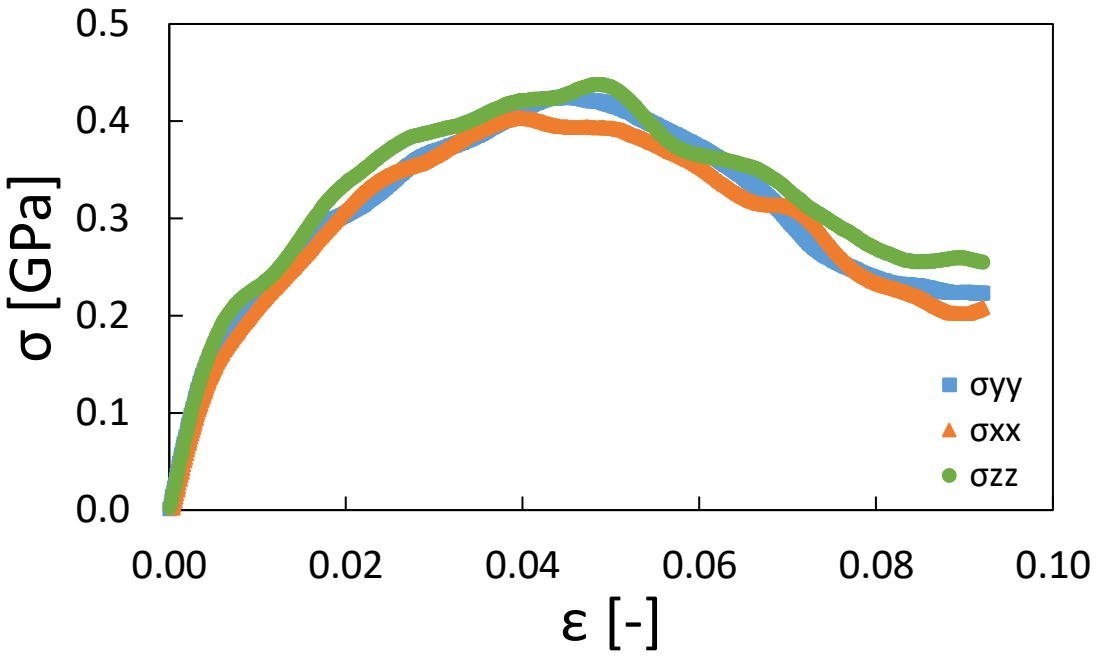

Figure 74 Stress-strain curves in x, y and z directions of 75% crosslinked system

Stress-strain curves are carried out for five different crosslinking degrees, as for density computation and Young's modulus is calculated for each configuration. Different values obtained in different direction size the error bars.

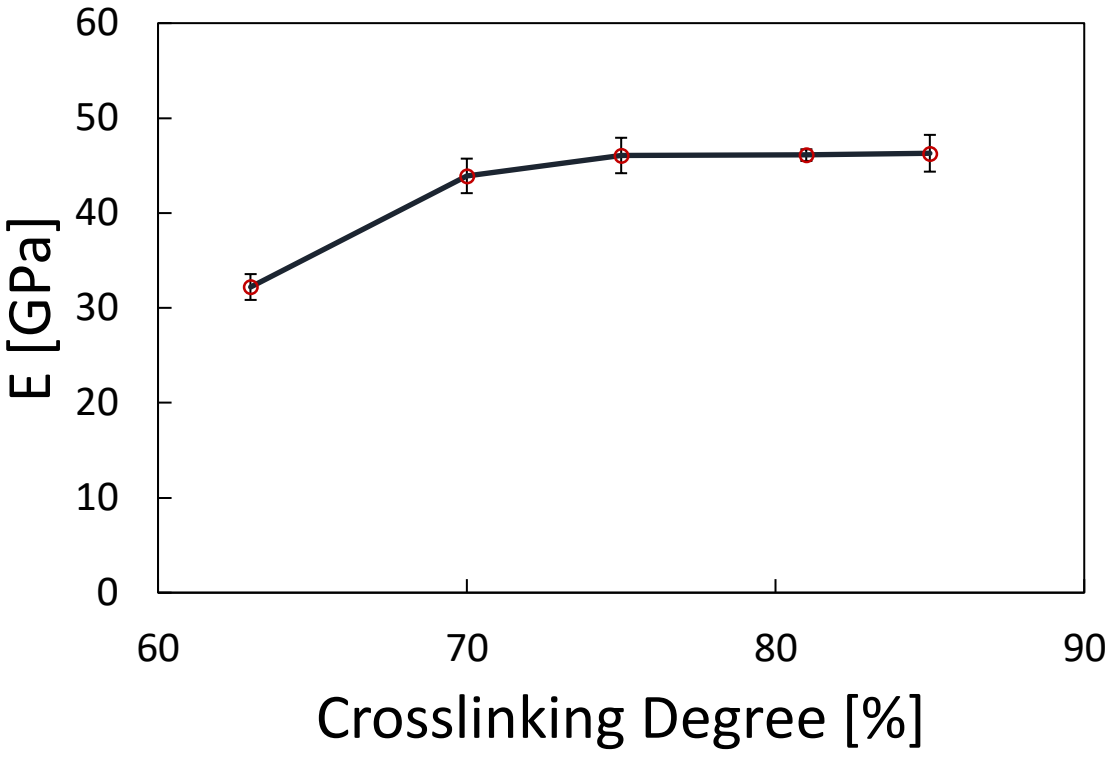

Figure 75 Young's modulus computed for different crosslinking degrees

As expected, Young's modulus increases with crosslinking degree, since crosslinking process contributes to make the material stiffer, by means of new bonds. It increases faster below 70% of crosslinking, then it stabilizes at about 46 [GPa].

POISSON RATIO ν $[-]$

The Poisson's Ratio measures the phenomenon for which the materials tend to contract in the direction perpendicular to the stretching or to expand in the direction perpendicular to the compression. Once a traction/compression load is applied in for example x direction, Poisson's ratio is defined as the ratio between the deformations in the two orthogonal directions and the deformation in the load direction:

$$\nu = \left|\frac{\varepsilon_y}{\varepsilon_x}\right| = \left|\frac{\varepsilon_z}{\varepsilon_x}\right| \ [-]$$

Linear elasticity theory states that ν must be among -1 and +0.5 due to the positive-definite condition of the Hessian stiffness matrix as already explained for E. However, experimentally orthogonal deformations result have always opposite signs, so it is possible to state that in practice $0 < \nu < 0.5$. Typical values for construction materials are about 0.3 for steel and 0.15 for concrete, while for polymers the range is 0.25-0.45 and it is lower for thermoplastics and higher for thermosetting ones (42).

Since the simulation box is a bulk of material with boundary condition and not a finite sample with external interfaces, it is not possible to evaluate ν by simply computing longitudinal and transversal deformations. In fact, the box deforms only in one direction keeping constant the other two.

For this reason, ν is carried out from the linear elastic problem equations. As an example, in the case of x-direction load, in isotropy conditions is possible to write the following three equations:

$$\varepsilon_{xx} = \frac{1}{E}(+\sigma_{xx} - \nu\sigma_{yy} - \nu\sigma_{zz})$$

$$\varepsilon_{yy} = \frac{1}{E}(-\nu\sigma_{xx} + \sigma_{yy} - \nu\sigma_{zz})$$

$$\varepsilon_{zz} = \frac{1}{E}(-\nu\sigma_{xx} - \nu\sigma_{yy} + \sigma_{zz})$$

For each step of the x-deformation simulation σ_{xx}, σ_{yy} and σ_{zz} are in output, then is sufficient to solve one of the equations related to the transversal deformations, in y or z directions, imposing null deformation. In particular, v has been carried out always from both the transversal direction equations and then averaged, for x, y and z load directions.

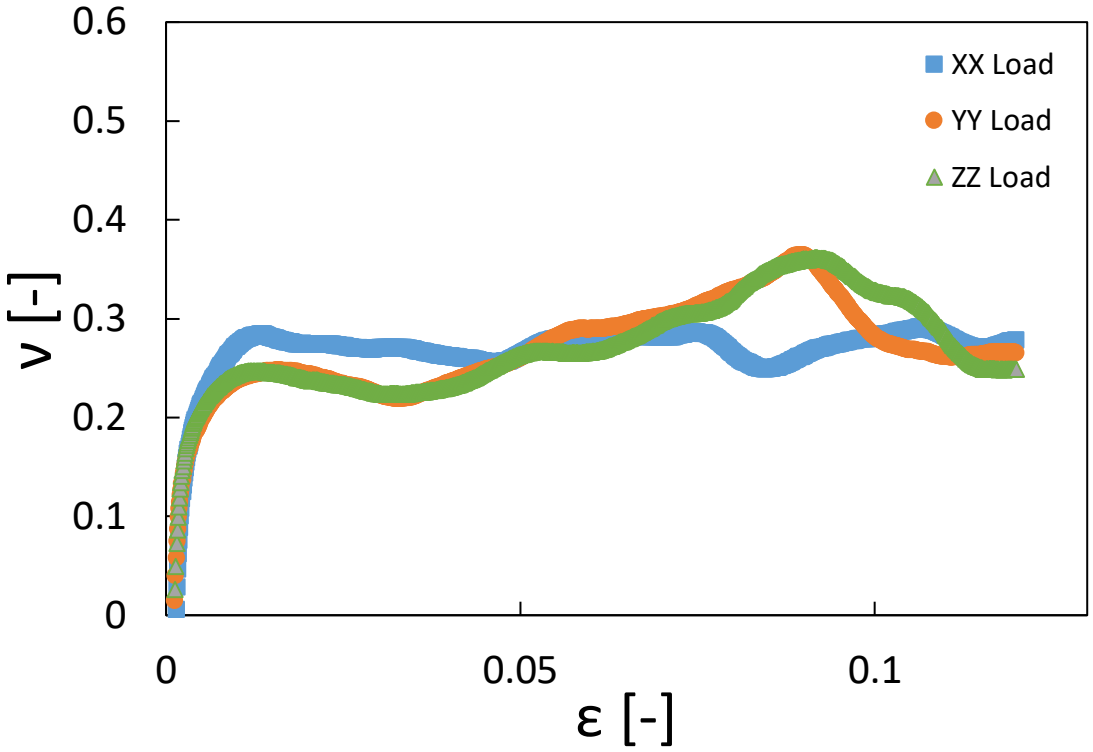

Figure 76 Poisson's ratio evolution during deformation for three different deformation directions for 63% crosslinked system

This is repeated for different values of crosslinking degree as for Young's Modulus, to summarize the results in a graph in which different load directions results for a single crosslinking degree determines the SD and the size of the error bars.

Poisson's Ratio is decreasing for crosslinking degree increases, as expected, since the formation of new bond will limit the tangential sliding of the beads, and it decreases faster beyond the 70% of crosslinking degree.

Once E and ν are known, the mechanical behaviour is characterized and is possible to carry out the other properties from them.

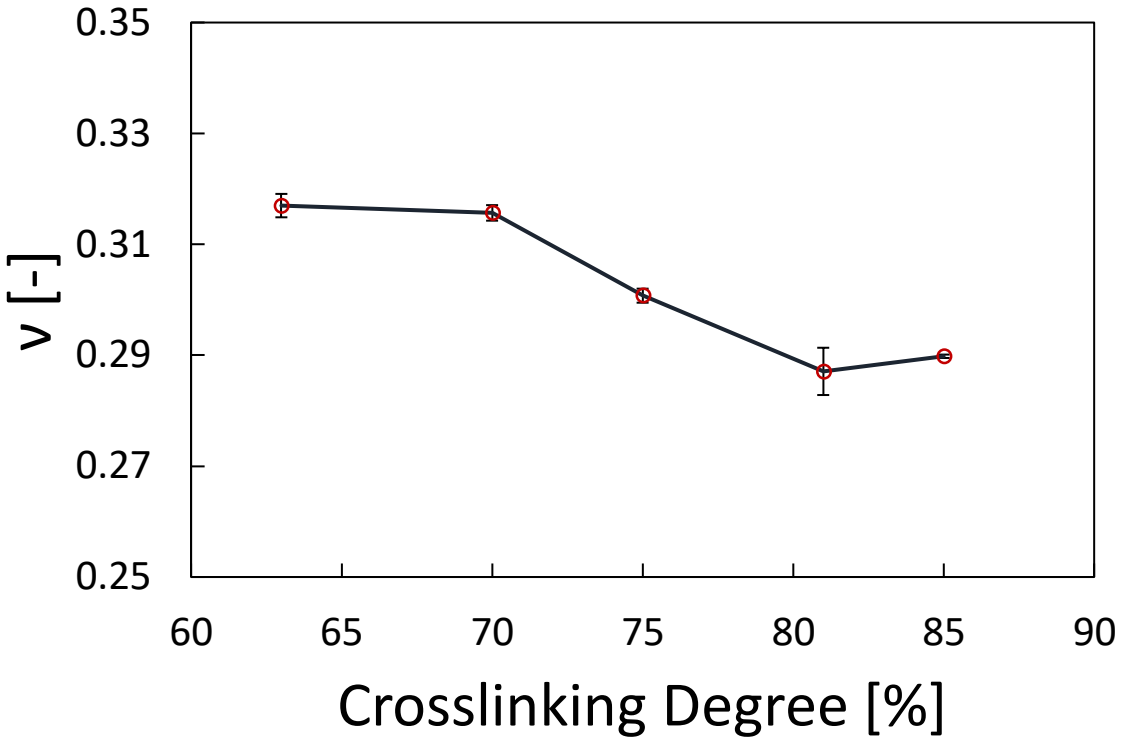

Figure 77 Young's modulus computed for different crosslinking degrees

Shear Modulus G $[GPa]$

The Shear modulus represents the stiffness the solid opposes to angular sliding and it is the ratio between tangential stresses and corresponding transversal strains, when a longitudinal load is applied:

$$G = \frac{\partial \tau(\gamma)}{\partial \gamma}\Big|_{\gamma=0} \; [GPa]$$

Linear elasticity theory states that G must be positive as for Young's modulus (42), while G, E and ν are linked by the following relationship:

$$G = \frac{E}{2(1+\nu)} \; [GPa]$$

Thus, shear modulus is calculated directly from Young's modulus and Poisson's ratio, and the different load directions for a single crosslinking degree size the error bars through linear error propagation in the formula.

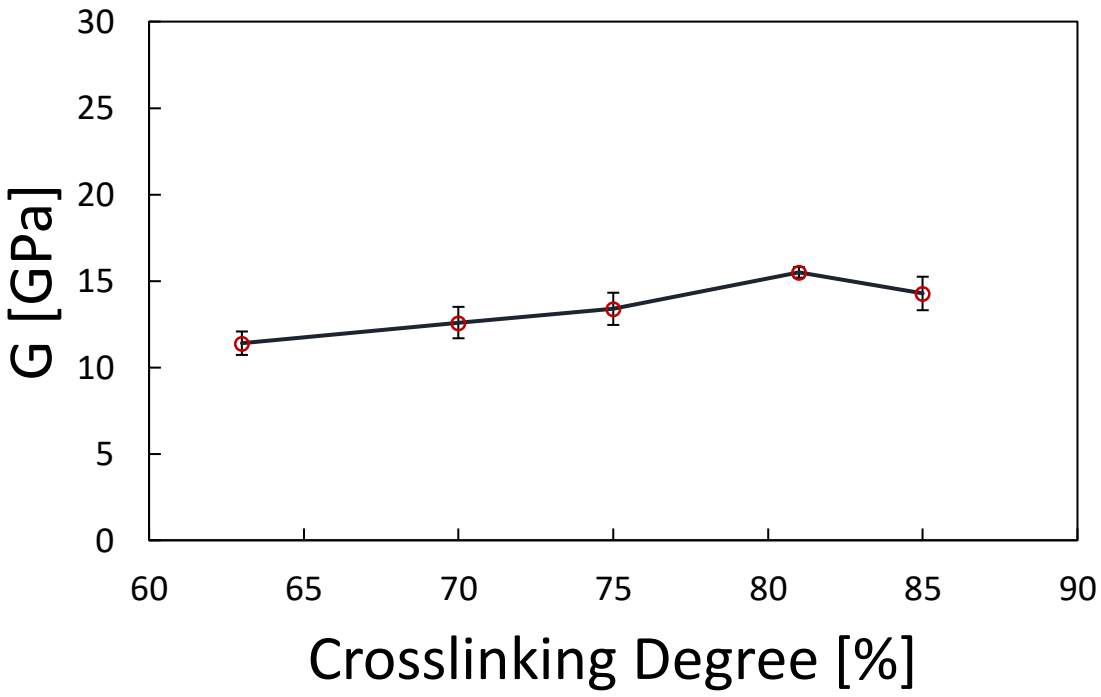

Figure 78 Shear Modulus computed for different crosslinking degrees

Bulk Modulus K $[GPa]$

The Bulk Modulus or Volume modulus measures how easily a fluid can change its volume by changing the pressure working upon it. It is the ratio between the infinitesimal pressure increase and the resulting relative volume decrease:

$$K = -V\frac{\partial p}{\partial V}\ [GPa]$$

Bulk modulus is de reciprocal of typical liquid compressibility β. Typical values of K are about 160 [GPa] for steel, 30÷50 [GPa] for glasses, up to 442 [GPa] for carbon in diamond state (42).

As for Shear modulus, Bulk modulus is calculated directly from Young's modulus and Poisson's ratio, by means of the following formula:

$$K = \frac{E}{3(1-2\nu)}\ [GPa]$$

As for Poisson's Ratio and Shear Modulus, error bars dimension depends on the linear error propagation from ν, in the formula.

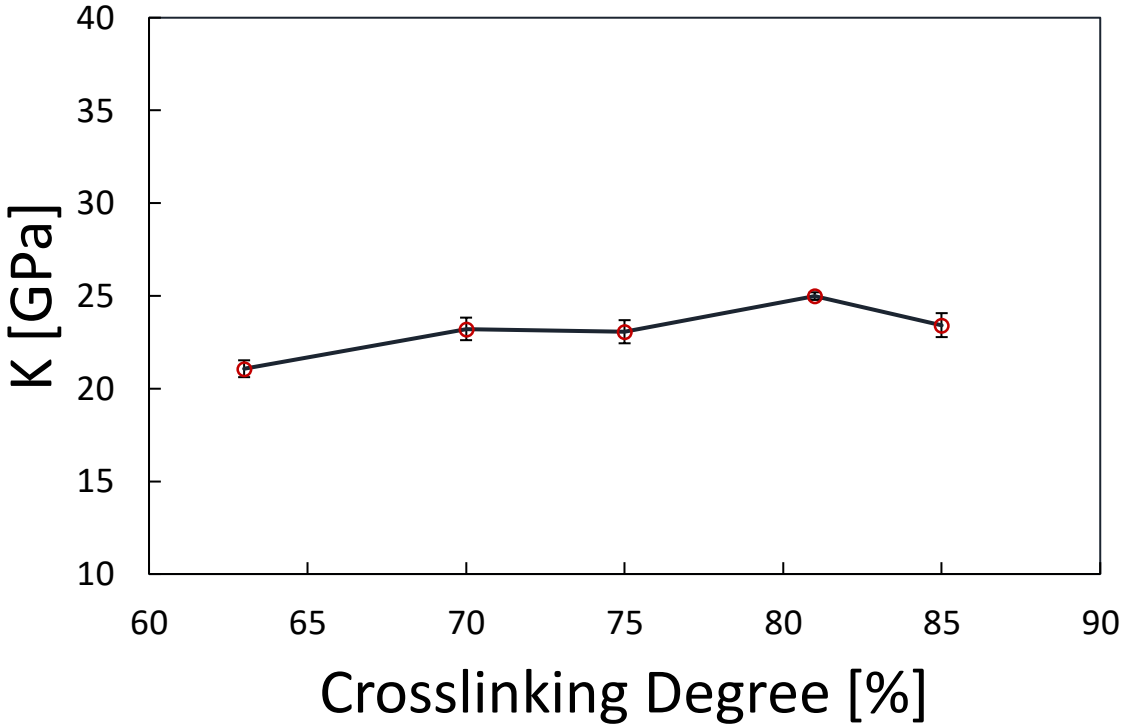

Figure 79 Bulk Modulus computed for different crosslinking degrees

3.4 Thermal Properties

Starting from P2 crosslinked initial system, the goal is to study the response of the material to a thermal load and predict the thermal conductivity.

Starting from the most general form of the Heat Conduction Equation by heat transfer theory, in which figure both spatial and temporal derivatives of the temperature:

$$\rho c_p \frac{\partial T}{\partial t} = \nabla \cdot (k \nabla T) + \sum_i q_{vol,i} \left[\frac{W}{m^3}\right]$$

Where ρ is the density, c_p is the specific heat and k is the thermal conductivity of the material, while the summation term is the net volumetric heat flux including heat sources and sinks. Assuming

linearity, which means that k does not depend on temperature, is possible to bring it out of the outer nabla operator, and group the two Nabla operators in a Laplacian operator ∇^2.

$$\rho c_p \frac{\partial T}{\partial t} = k\nabla^2 T + \sum_i q_{vol,i} \left[\frac{W}{m^3}\right]$$

Considering a Cartesian 1D steady-state linear problem with a volumetric heat source, the problem's equation is the following Ordinary Differential Equation (ODE):

$$k \frac{d^2 T}{dx^2} = -q_{vol} \quad \left[\frac{W}{m^3}\right]$$

The shape of the solution $T(x)$ depends on the presence of internal heat sources or sinks and on the boundary conditions adopted. For example with internal volumetric heat generation, the temperature profile is quadratic, while it is linear without it.

In the macroscopic scale, possible heat sources could be current flows, by Joule effect, or particular exothermic reactions like nuclear fission, while constant temperature, constant heat flux or convective heat flux can be imposed as boundary conditions respectively of Dirichlet, Neumann and Robin type.

In MD, the system is a periodic simulation box, while the temperature profile is just a macroscopic effect of the beads velocity distribution. The Energy Equipartition Theorem links velocity and temperature:

$$E_k = \frac{f}{2} k_b T \ [J]$$

Where E_k is the total kinetic energy, f is the number of the degrees of freedom (in this case equal to three), k_b is the Boltzmann constant and T is the temperature in Kelvin.

In order to simulate thermal loads, some Non-Equilibrium Molecular Dynamics (NEMD) simulations are performed. In these simulations, it is necessary to act on beads velocity, since it is not possible

to directly apply heat sources/sinks and boundary condition. In particular, Müller-Plathè (43) (44) algorithm is implemented. It modifies iteratively beads velocities, in order to compute the thermal conductivity, starting from a velocity profile and exchanged kinetic energy between different zones of the box.

First, a thermalization run is performed in NVT ensemble at 300 [K] for 100 [ps] and in NVE ensemble for other 100 [ps], starting from a velocity profile adjusted so that the aggregate linear momentum is zero. The temperature of each atom is calculated as:

$$T = \frac{2}{3}\frac{E_k}{k_b} \ [K]$$

Then, the box is divided in several layers along one direction and for each layer the average temperature is calculated, in order to build a 1D-temperature profile.

Müller-Plathè algorithm performs some velocity swaps between the hottest beads on the first layer and the coldest beads in the central layer. Even if masses are different, kinetic energy conservation is ensured, since in this case an exchange of velocities relative to the centre of mass motion of the two beads is performed (36). The total kinetic energy transferred by these swaps is stored and it is the output. This happens at each step, while time integration in NVE ensemble is performed for 1 [ns]. In other words, an artificial heat flux is applied, by means of velocities swaps, and a temperature gradient is inducted along one box direction.

After an initial transient in which it grows up quickly, the imposed heat flux stabilizes and the system reaches steady state conditions at about 45 [pW/Å^2].

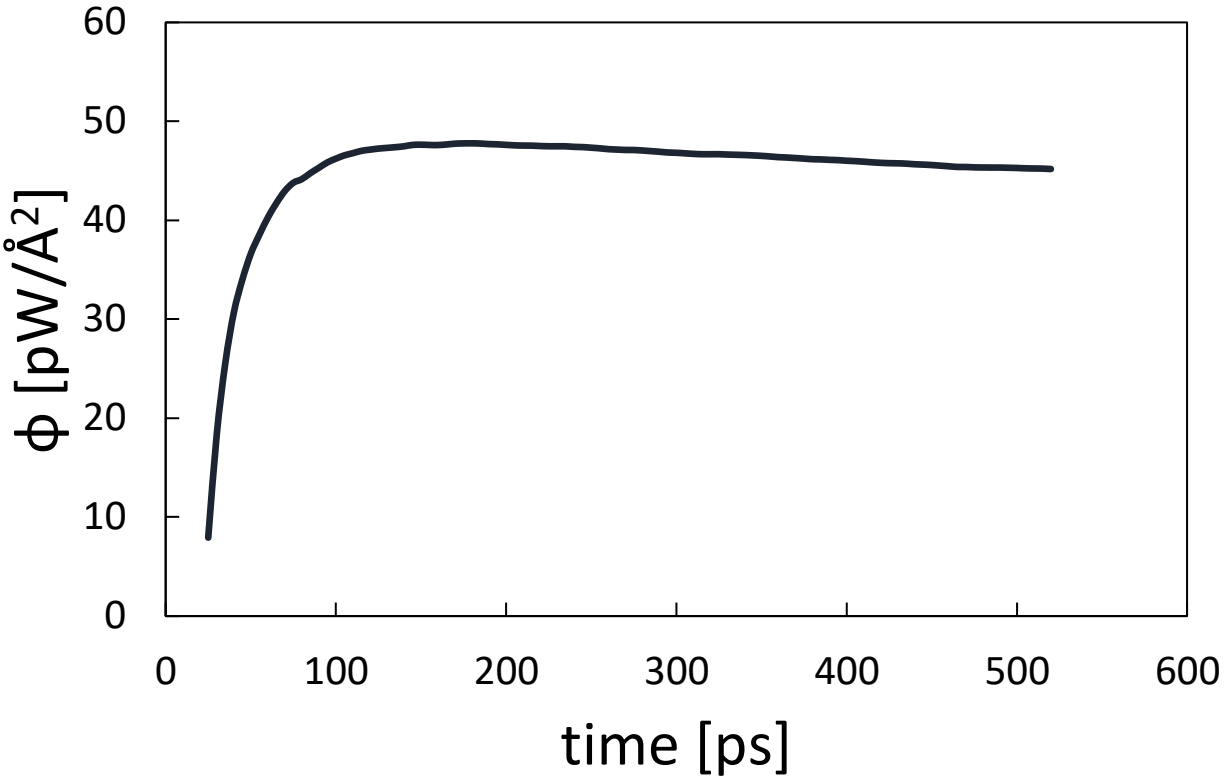

Figure 80 Muller-Plathè heat flux transient and stabilization

Heat flux's magnitude depends on the number of swaps per step performed. Starting from the exchanged kinetic energy $E_{k,ex}$ is possible to calculate the heat flux as:

$$\varphi = \frac{2 * E_{k,ex}\left[\frac{kcal}{mol}\right] * 4186\ \left[\frac{J}{kcal}\right] * N_s\left[\frac{beads}{step}\right]}{N_A\left[\frac{beads}{mol}\right] * \Delta t\ \left[\frac{fs}{step}\right] * 10^{-15}\left[\frac{s}{fs}\right] * L_t^2[\text{Å}^2] * 10^{-20}\left[\frac{m^2}{\text{Å}^2}\right]} \quad \left[\frac{W}{m^2}\right]$$

The number of swapped beads per step is N_s, L_t^2 is the cross-section area and N_A is the Avogadro's number (6.022e23 [beads/mol]). Two multiplies heat flux because, with periodic boundary conditions, it is going in two directions and it is not possible two impose it all in one direction.

In 1D steady state condition, is possible to evaluate the thermal conductivity from the 1D temperature profile. Y-direction temperature profile of a 70% crosslinked system is shown as an example.

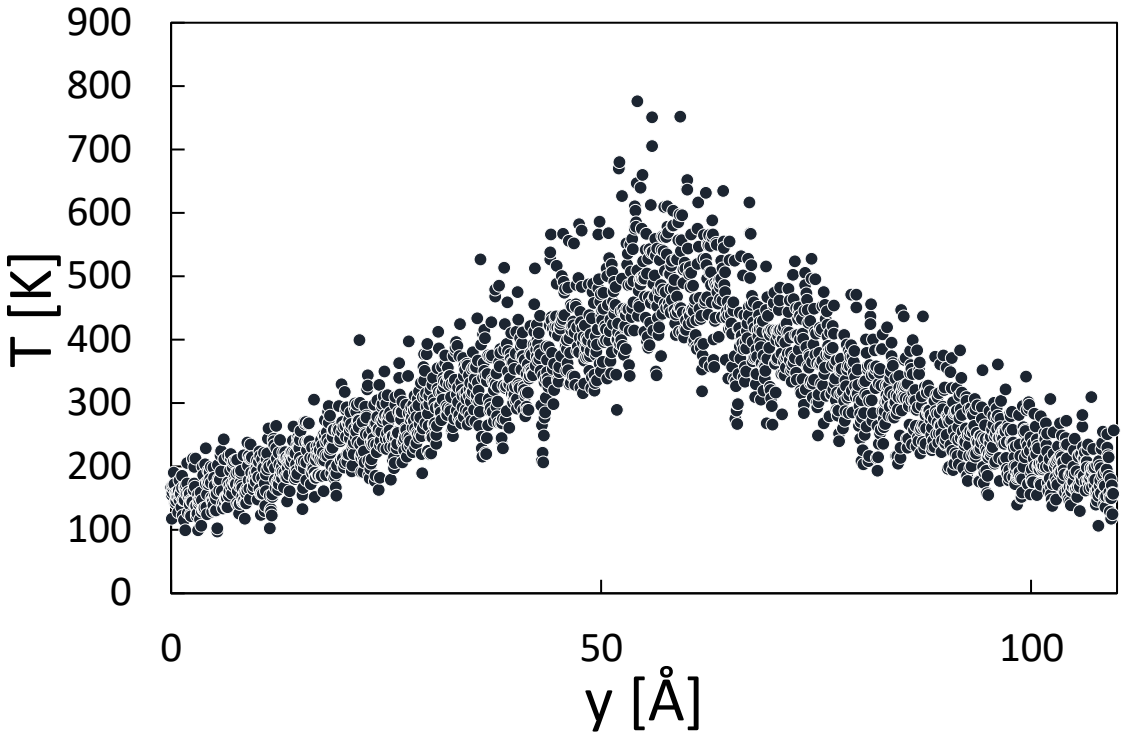

Figure 81 1D-Temperature profile in y-direction, inducted by Muller-Plathè velocity swaps, for a 70% crosslinked system

The profile is about linear, with the maximum temperature at half of L_y as expected (Figure 81), since the algorithm performs velocity swaps between the first and the central layers.

After a linear fitting on the first half and the second half, is possible to evaluate the slope of the temperature profile as the mean value of the two halves slopes (Figure 82). Boundary and central layers are not included because is where velocity swaps take place, while in the other layers beads are more free to move according to their thermodynamic conditions. Thermal conductivity k is computed by the Fourier's Law, dividing heat flux by the slope of the temperature profile (36):

$$k = \frac{\varphi}{dT/dx} \quad \left[\frac{W}{m \cdot K}\right]$$

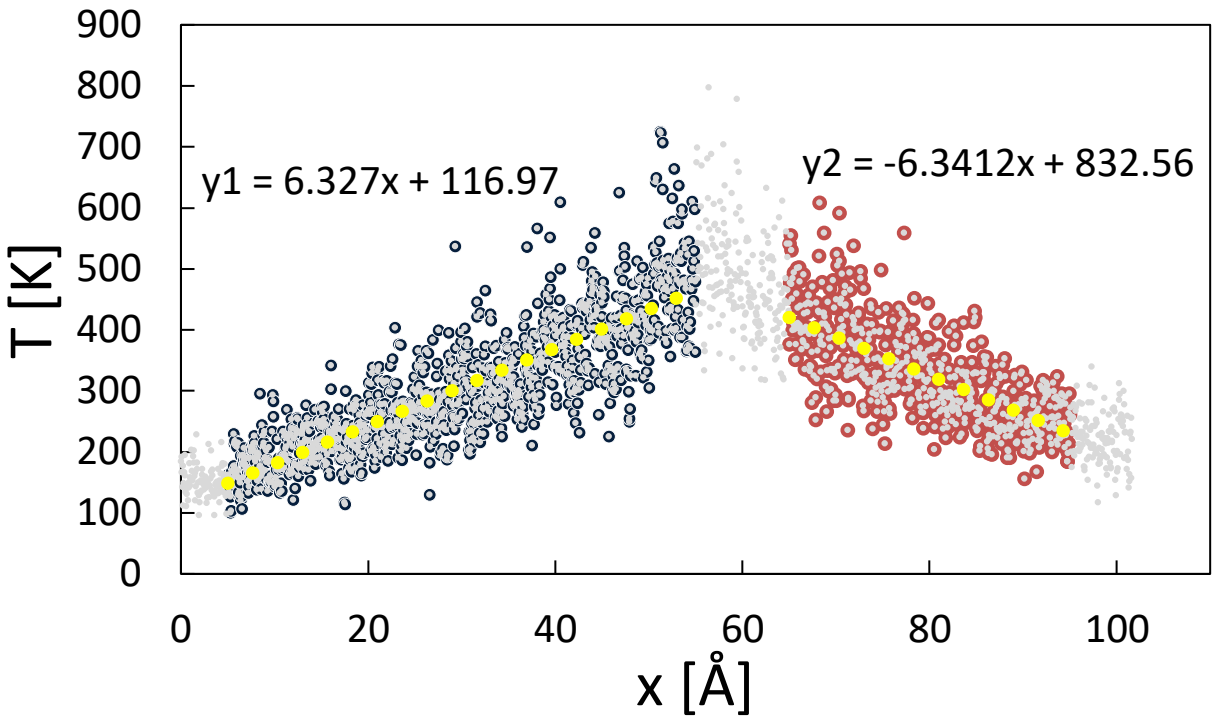

Figure 82 1D-Temperature profile in x-direction, inducted by Muller-Plathè velocity swaps, for a 63% crosslinked system, with linear fittings.

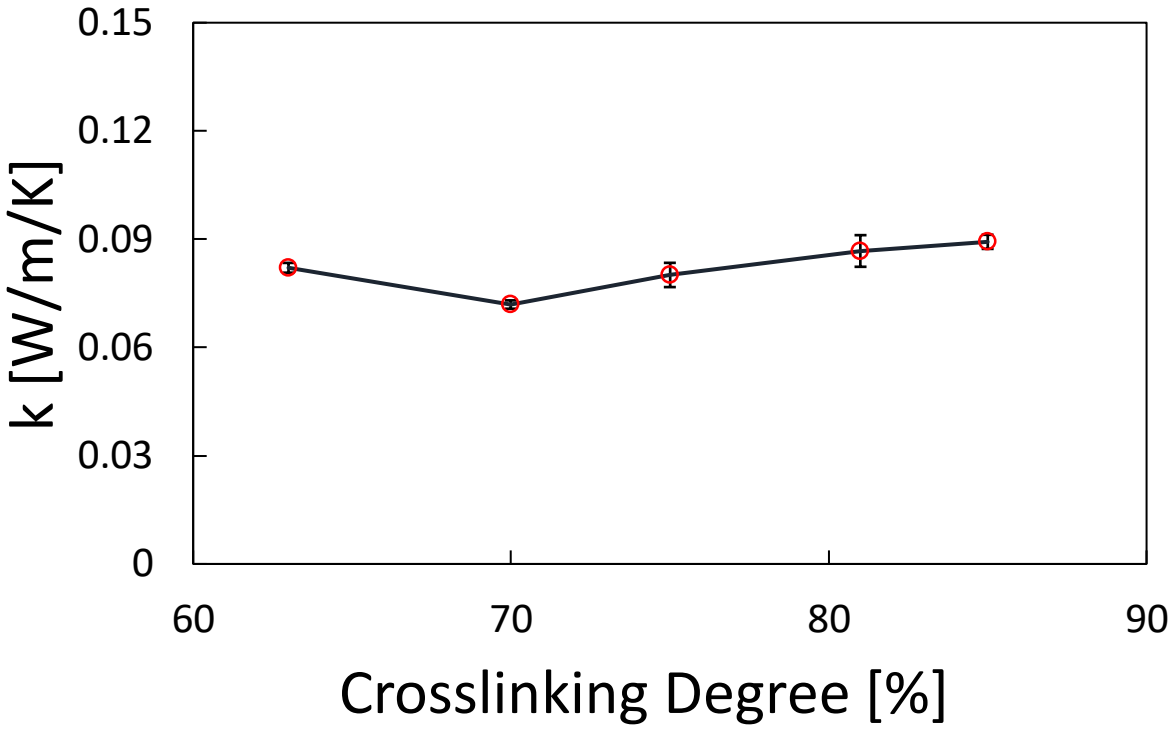

Figure 83 Computed thermal conductivity for different crosslinking degrees

The procedure is repeated in the three directions x, y and z and for five crosslinking degrees. For each crosslinking degree, three values of conductivity are carried out, one per direction, and these determine a mean value and a SD as error bars size. Results are not strongly dependent on crosslinking degree, since probably in this case crosslinking bonds do not affect too much phonons transmission, while the isotropy of the material, already verified for mechanical properties (3.3), is confirmed by the relatively small error bars. Computed values are of the order of 0.1[W/m/K].

3.5 Comparison with Literature and Open Issues

Density results are in good agreement with values found in different works on DGEBA-based epoxy resins (38) (39) and with those found from the atomistic simulation within the SMARTFAN project (35). Matching is good also with values from online databases (40).

Glass Transition Temperature is in good agreement with the value found by *F. Khameneh et al.* (44) (385-395 [K]) and *A. Gavrielides et al.* (37) (391 [K]) for others DGEBA-based systems. There is a good matching also with experimental results (45) (46) (38) (47) by means of Differential Scanning Calorimetry (DSC).

Concerning mechanical properties, Poisson's Ratio is in good agreement with *F. Khameneh et al.* (44) for DGEBA/TEDTA system (0.25-0.30), with *S. Saseendran et al.* (48) for a commercial LY5052 and with EPO-TEK Company Technical Tips brochure (49). On the other hand, stress-strain curves shapes are acceptable, but the procedure leads to a Young's Modulus overestimation by an order of magnitude with respect to other works. For example, results from systems with similar epoxies like *N. Saleh et al.* (50) (3-3.5 [GPa]) for DGEBA/DDM system and experimental results by *S. Dalle Vacche et al.* (47) (~3 [GPa]) for DGEBA/DICY system, through a universal testing machine (UTM, LFM-125 kN, Walter&Bai). This overestimation propagates also in Bulk Modulus and Shear Modulus, which are calculated from it.

Thermal conductivity is slightly underestimated, but in the same order of magnitude with respect to *A. Sammani et al.* (51) for a DGEBA/NOVOLAC system (~0.18 [W/m/K] at 300 [K]) and

experimental results by *T. Zhou* (52) for a DGEBA/EMI-2.4 system ((~0.2 [W/m/K] for the neat polymer).

According to the results, the main open issue is the overestimation of the Young's Modulus by an order of magnitude. This can be due to several factors, for example, the force field adopted may not be optimized for the mechanical properties computation, even if it gives good results for other properties. In addition, is almost always not possible to run simulations longer than 1 [ns] with at least 1 [fs] of time step, due to the high number of potentials (9 bond types, 35 angle types) and in particular to the crosslinking procedure which produces a non-homogeneous system, difficult to equilibrate. For this reason, to get all the results in a proper time, not all of them present the same accuracy, depending on the achievable length of the simulation. However, error bars in every property's computation attest an acceptable accuracy for all the results, with SDs of the order of 0.1%, up to 1% in some particular cases.

Other force fields have been implemented to get a good matching also for Young's Modulus, like MARTINI-based CG force field and two hybrids among MARTINI CG and ITA's CG force fields. For the MARTINI parametrization, values from *Aramoon et al.* (24) for a new DGEBA parametrization have been implemented, combined with both ITA's 3-beads CG of DICY and DETA and 2-beads CG of DAB. Simulations run quicker and the system is more stable due to the lower number of particles and potentials and to the higher mass of central DGEBA beads, which makes the bonds stiffer. However, results matching is worse than pure ITA's force field.

CONCLUSIONS

Molecular Dynamics (MD) simulations can be a valid tool for thermo-physical properties prediction starting from the nanoscale, even for materials characterized by a complex chemical structure, like epoxy resin. Concerning the latter, mesoscale models like Coarse-Grained Molecular Dynamics (CGMD) are suitable to face the high variety and complexity of the system and perform sufficiently long simulations in acceptable times.

In a more general multi-scale study framework, nano and meso-scale modelling can be the first screening for new materials testing. Once thermo-physical properties are predicted, continuum modelling completes the study by implementing new materials behaviour in macroscale simulation of components in various mechanical or thermal load conditions.

There are many advantages in developing and implementing simulation protocols for properties computation, like the possibility to study new materials, or new combination of existing ones, even if they are not yet available in the market. In the case of thermoset polymers, this is particularly of interest, since there are infinite combinations between monomers and curing agents and several possible mixing ratios.

A good matching with modelling and experimental results has been already achieved with mesoscale modelling of thermo-plastic polymers like PP and PLA for both mechanical and thermal properties and it has been proven that nanofillers produce an important stiffening effect, besides a slight thermal conductivity increase. Concerning thermoset polymers, like the epoxy resin subject of this thesis, a good matching is achieved for density, glass transition temperature, thermal conductivity and Poisson's Ratio.

With the force field adopted, stress-strain curves obtained after the one-direction box deformation have the typical shape observed in other models and experimental results but with a different slope of the elastic part, which produces an overestimation of the Young's Modulus of about one order of magnitude.

For future investigations, there is the possibility to study a nanocomposite material, with this system as polymer matrix and carbon-based nanofillers like Graphene sheets (G), Graphene Oxide (GO) or reduced Graphene Oxide (rGO), in order to enhance mechanical properties.

The aim is to get an order of magnitude of 102 [GPa], in the range of steels, with a relatively light material. Within the SMARTFAN project, this has been already performed for some thermo-plastic polymers like Poly-Propylene (PP) and Poly-Lactic Acid (PLA) with encouraging results (53) in good accordance with literature modelling and experimental results.

BIBLIOGRAPHY

1. Kindahl, Thoma. *Generic structure of an epoxide.* s.l. : Own Work.

2. May, Clayton A. *Epoxy resins: chemistry and technology.* s.l. : CRC Press, 1987.

3. Jean-Pierre Pascault, Roberto Williams. *Epoxy Polymers, New Materials and Innovations.* Weinheim : WILEY-VCH, 2010.

4. *Ciba catalogue.* BASF, Germany.

5. *Selector guide for composite resin systems.* Huntsman co., Switzerland.

6. *Ethyleneamines brochure.* Huntsman co., Switzerland.

7. *Molecular modelling of epoxy resin crosslinking experimentally validated by near-infrared spectroscopy.* R. Unger, U. Braun, J. Fankhanel, B. Daum, B. Arash, R. Rolfes. 2019, Computational Materials Science 161.

8. Strehmel, V. *Bildung un struktur vernetzer temperatutstabiler polymerer materlialien.* 2000.

9. *Computational Methodology for Modelling Fracture in Fiber-Reinforced Polymer Composites.* A.A. Benzerga, X. Poulain, K. A. Chowdhury, R. Talreja. 2009, Journal of Aerospace Engineering, July.

10. *Tempco catalogue.* Tempco srl, Desio (MB), Italy.

11. Harper, Charles A. *Handbook of Plastics, Elastomers & Composites.* s.l. : McGraw-Hills, 2002.

12. *Failure phenomena in two-dimensional multi-fibre microcomposites—3. A raman spectroscopy study of the influence of interfacial debonding on stress concentrations.* P.W.J Van Den Heuvel, T. Peijs, R.J. Young. 58, s.l. : ELSEVIER, 1998, Vol. Composites Science and Technology.

13. Raflee, R. *Carbon nanotube-reinforced polymers, from nanoscale to macroscale.* s.l. : Elsevier, 2011.

14. *Conformational properties of Sodium Polystyrenesulfonate in Water: insights from a coarse-grained model with explicit solvent.* S. Mantha, A. Yethiraj. 2015, The Journal of Physical CHemistry B.

15. *The power of coarse graining in biomolecular simulations.* H. I. Ingolfsson, C. A. Lopez, J.J Uusitalo, D.F. de Jong, S.M. Gopal, X. Periole, S.J. Marrink. 2014, Vol. WIREs Comput Mol Sci. doi: 10.1002/wcms.1169.

16. *A MARTINI coarse-grained model of a thermoset polyester coating.* G. Rossi, I. Giannakopoulos, L. Monticelli, N.K.J. Rostedt, S.R. Puisto, C. Loew, A.C. Taylor, I. Vattulainen, T.A. Nissila. 2011, Macromolecules.

17. *A comparison of united atom, explicit atom and coarse-grained simulation models for poly(ethylene oxide).* C. Chen, P. Depa, V.G. Sakai, J.K. Maranas, J.W. Lynn, I. Peral, J.R.D. Copley. 2006, The Journal of Chemical Physics 124.

18. Deserno, Markus. The Henderson Theorem. *cmu.edu.* [Online] 23 08 2018. https://www.cmu.edu/biolphys/deserno/pdf/henderson.pdf.

19. *The MARTINI Force Field: Coarse Grained Model for Biomolecular Simulations.* S.J. Marrink, H.J. Risselada, S. Yefimov, D. P. Tieleman, A.H. de Vries. 2007, Vol. The Journal of Physical Chemistry B.

20. Luca Monticelli, Emppu Salonen. *Biomolecular Simulations: Methods and Protocols, Methods in Molecular Biology.* New York : Springer Science+Business Media, 2013.

21. *Martini Coarse Grain forcefield for Biomolecules.* [Online] http://cgmartini.nl/index.php/about.

22. *The MARTINI coarse-grained force field: Extension to proteins.* L. Monticelli, S.K. Kandasamy, X. Periole, R.G. Larson, D.P. Tieleman, S.J. Marrink. 2008, Journal of chemical Theory and Computation.

23. *A coarse-grained model for epoxy molding compound.* S. Yang, Z. Cui, J. Qu. 2014, The Journal of Physical Chemistry B.

24. *coarse-grained molecular dynamics study of the curing and properties of highly cross-linked epoxy polymers.* A. Aramoon, T.D. Breitzman, C. Wookward, J.A. El-Awady. 2016, The Journal of Physical Chemistry B.

25. *Coarse-grained molecular dynamics simulation of epoxy resin during the curing process.* Y. Fu, J. Michopoulos, J.H. Song. 2015, Computational Materials Science 107.

26. *Shear thinning behavior of linear polymer melts under shear flow via non-equilibrium molecular dynamics.* X. Xu, J. Chen, L. An. 2014, The Journal of Chamical Physics 140.

27. *Mechanical properties of carbon nanotube reinforced polymer nanocomposites: A coarse-grained model.* B. Arash, H.S. Park, T. Rabczuk. 2015, Composites Part B.

28. *Nanotube-polumer composites: insights from Flory-Huggins Theory and mesoscale simulations.* A. Maiti, J. Wescott, P. Kung. 2005, Molecular Simulation.

29. *Multiscale molecular dynamics-FE modeling of polymeric nanocomposites reinforced with carbon nanotubes and graphene.* S. Doagou-Rad, J.S. Jensena, A. Islama, L. Mishnaevsky Jr. 2019, Composite Structures.

30. *Nanomorphology of graphene and CNT reinforced polymer and its effect on damage: Micromechanical numerical study.* A. Pontefisso, L. Mishnaevsky Jr. 2013, Composites .

31. *Virtual modelling of microscopic damage in polymer compiste materials at high rates of strain.* M. Lidgett, R. Brooks, N. Warrior, K.A. Brown. 2013, Plastics, Rubber and Composites.

32. *Investigating the mechanical properties of single walled carbon nanotube reinforced epoxy composite through finite element modelling.* M.J.S. Zuberi, V. Esat. 2015, Composites Part B.

33. C. Li, T. W. Chou. Modeling of Carbon Nanotubes and Their Composites. [aut. libro] P.M. Anderson, M.K. Wu, S. Hsieh T.J. Chuang. *Nanomechanics of materials and structures.* s.l. : Springer, 2006.

34. Racecar Engineering. [Online] https://www.racecar-engineering.com/featured/f3-2019-car-revealed/.

35. C.Saenz, F. Bellussi, A. Chiminelli. *Determination of interface properties from atomistic models.* s.l. : SMARTFAN deliverable by ITAINNOVA, 2019.

36. Sandia Corporation. LAMMPS Manual. [Online] https://lammps.sandia.gov/doc/Intro_overview.html.

37. *Model of the DGEBA-EDA Epoxy polymer: Experiments and simulation using classical molecular dynamics.* A. Gavrielides, T. Duguet, M. Aufray, C. Lacaze.Dufaure. 2019, Internationa Journal of Polymer Science.

38. *Structur, microparametes and properties of crosslinked DGEBA/MTHPA: A molecular dynamics simulation.* Q. Xie, S. Liang, B. Liu, K. Fu, Z. Zhan, L. Lu, X. Yang, F. Lu, Z. Huang. 2018, AIP Advances 8.

39. *Influeance of tubber on the curing kinetics of DGEBA epoxy and the effect on the morphology and hardness of the composites.* A. Romo-Uribe, J.A. Arcos-Casarrubias, A. Flores, C. Valerio-Cardenas, A. E. Gonzalez. 2014, Polymer Bulletin 71(5).

40. Polymer database. [Online] www.polymerdatabase.com.

41. *Thermal Expansion and Diffusion Coefficients of Carbon Nanotube-Polymer Composites.* C. Wei, D. Srivastava, K. Cho. 2002, Vol. Nano Letters, vol. 2, pp. 647-650.

42. Carpinteri, Alberto. *Scienza delle Costruzioni.* Bologna : Pitagora Editrice, 1992.

43. *Out-of-plane thermal conductivity of polycrystalline silicon nanofilm by molecular dynamics simulation.* S. Ju, X. Liang, X. Xu. 110(5), September 2011, Vol. Journal of Applied Physics.

44. *Thermal Conductivities of Molecular Liquids by Reverse Nonequilibrium Molecular.* Meimei Zhang, Enrico Lussetti, Luis E. S. de Souza, Florian Muller-Plathè. 2005, Vol. J. Phys. Chem. B 109.

45. *Comparative investigation of thermal and mechanical properties of cross-linked epoxy polymers with different curing agents by Molecular Dynamics Simulation.* F. Khameneh, G. Alahyarizadeh, B. Arab. 2015, Journal ofmolecular graphics & modelling.

46. *Diffusion control on the cure kinetics of DGEBA with ethylenediamines.* G. Prolongo, F. Mikes, J. C. Cabanelas, S. Paz-Abuin, J. Baselga. 2003, Journal of Materials Processing Technology.

47. *Mechanical properties of epoxy networks based on DGEBA with ethylenediamines.* G.F. Gonzalez, S.B.G., P.V.J, R.R.S., S. Ruben, R. Jacques. 2003, Journal of Materials Processing Technology.

48. *Curing kinetics and thermomechanical properties of latent, IOP Conf. Series: Materials Science and Engineering 139.* S. Dalle Vacche, V. Michaud, M. Demierre, P-E. Bourban, J-A. E Manson. 2016.

49. *Cure-state dependent viscoelastic Poisson's ratio of LY5052 epoxy resin.* S. Saseendran, M. Wysocki, J.Varna. s.l. : Taylor&Francis, 2017, Vol. Advanced Manufacturing: Polymer & Composites Science, Vol.3.

50. EPO-TEK®. Technical Tips 19. *https://www.epotek.com/site/technical-material/technical-tips.html.* [Online]

51. *A study mechanical properties of epoxy resin cured at constante curing time and temperature with different hardeners.* N. Saleh, A. A. A. Razak, M. Tooma. January 2011, Vol. Eng. & Tech. Journal, Vol.29, No.9.

52. *Thermal properties of Epoxy (DGEBA)/phenolic resin (NOVOLAC) blends.* A. Sammani, N. Al-Muaikel. April 2010, Vol. ARABIAN JOURNAL FOR SCIENCE AND ENGINEERING .

53. *Improving the thermal conductivity of epoxy resin by the.* T. Zhou, , X. Wang, P. Cheng, T. Wang. 2016, Vol. eXPRESS Polymer Letters Vol.7, No.7.

54. Muhammad, A. Master thesis, Relator: Prof. P. Asinari, Co-Relator: Prof. R. Srivastava. *Modelling thermo-physical properties carbon reinforced polymer Composites.* Politecnico di Torino : s.n., 2019.

55. *An introduction to classical molecular dynamics modelling.* M. Fasano, E. Chiavazzo. 2018, Accumulo e trasporto di energia.

56. *Small but strong: a review of the mechanical properties of carbon nanotube-polymer composites.* J.N. Coleman, U. Kahn, W.J. Blau, Y.K. Gun'ko. 2006, Carbon 44.

57. *A review on carbon nanotubes and graphene as fillers in reinforced polymer nanocomposites.* G. Mittal, V. Dhand, K.Y.Rhee, S.J. Park, W.E. Lee. 2014, Journal of Industrial and Engineering Chemistry.

58. *Fast relaxation of coarse-grained models of polymer interphases by hybrid particle-field molecular dynamics: Polystyrene-silica nanocomposites as an example.* A. De Nicola, T. Kowakatsu, Muller-Plathe, G. Milano. 2016, The European Physical Journal.

59. Cai, Hark Lee and Wei. *Ewald Summation for Coulomb Interactions in a Periodic Supercell.* Department of Mechanical Engineering, Stanford University, CA 94305-4040 : s.n., January 10, 2009.

APPENDIX A: FORCE FIELD POTENTIALS

Bond potentials

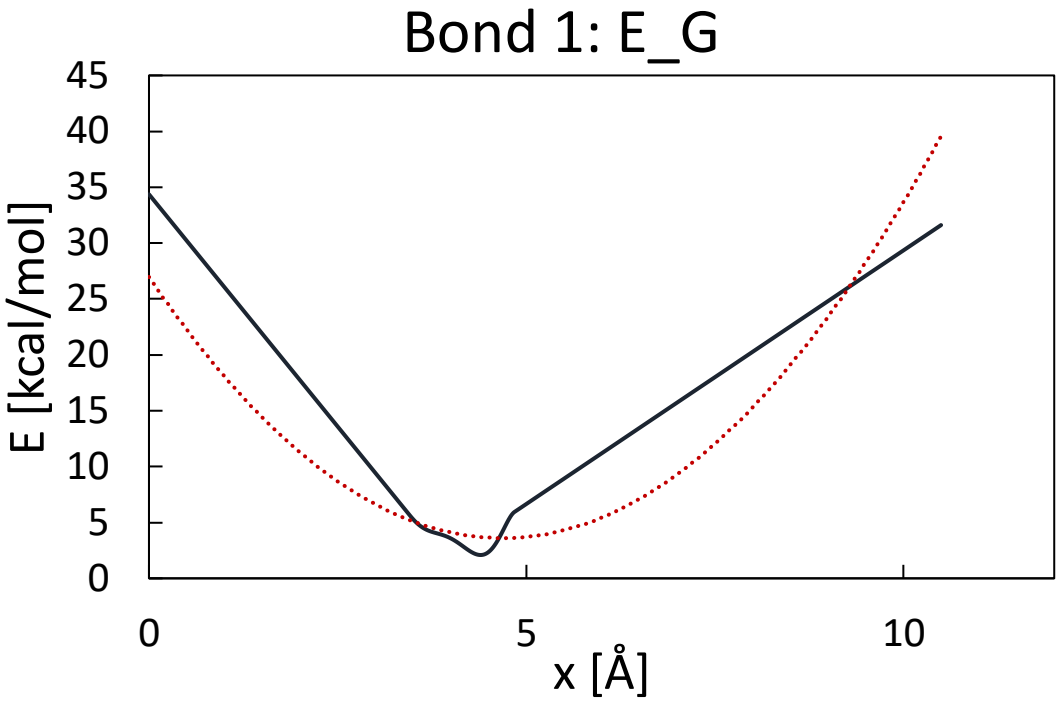

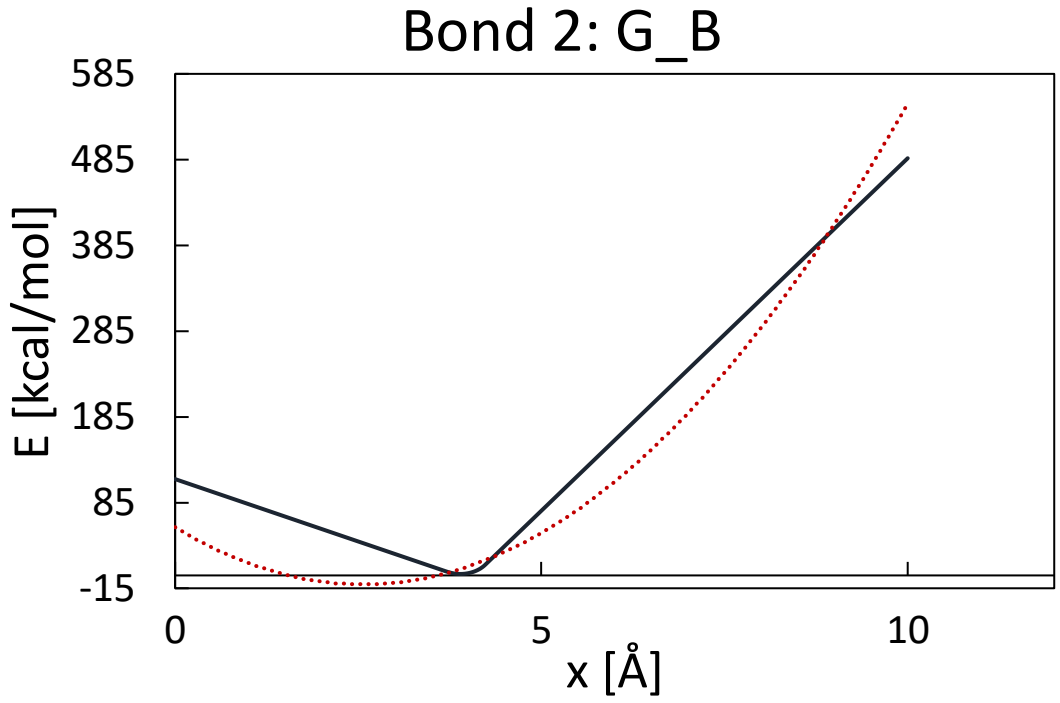

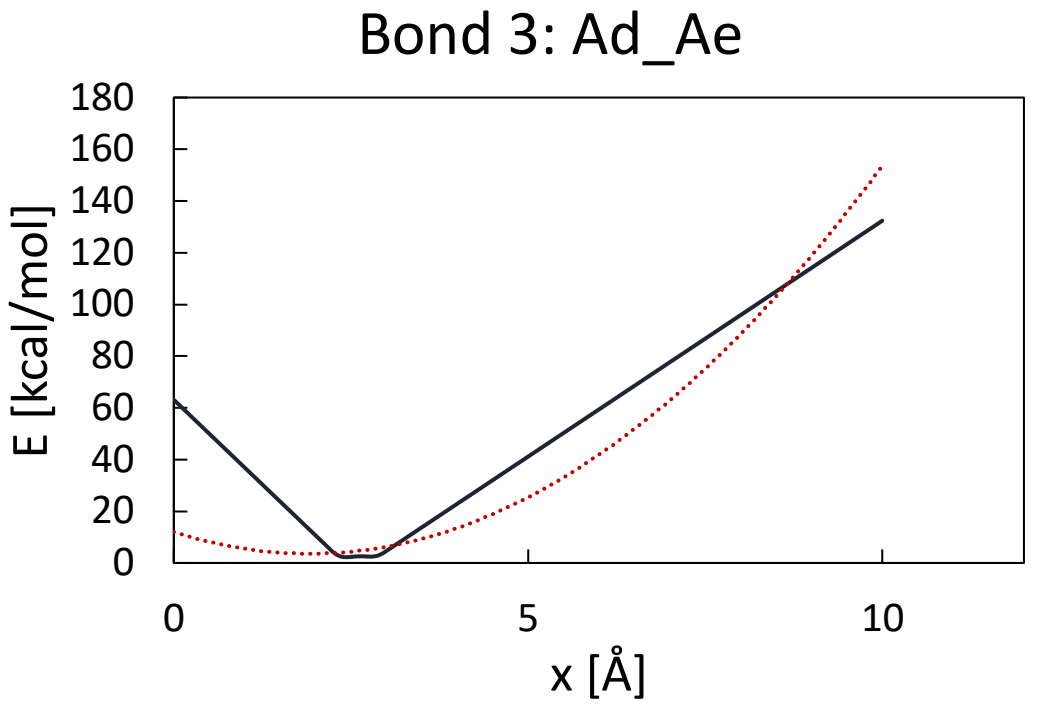
Bond 3: Ad_Ae
E [kcal/mol]
180
160
140
120
100
80
60
40
20
0
0
5
10
x [Å]

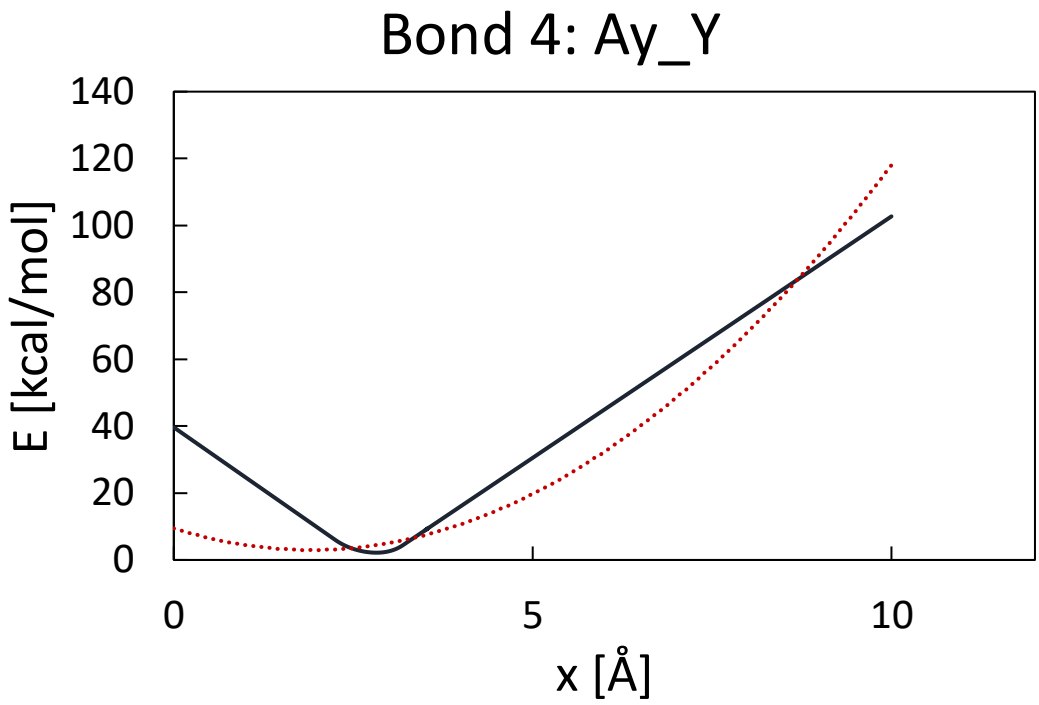
Bond 4: Ay_Y
E [kcal/mol]
140
120
100
80
60
40
20
0
0
5
10
x [Å]

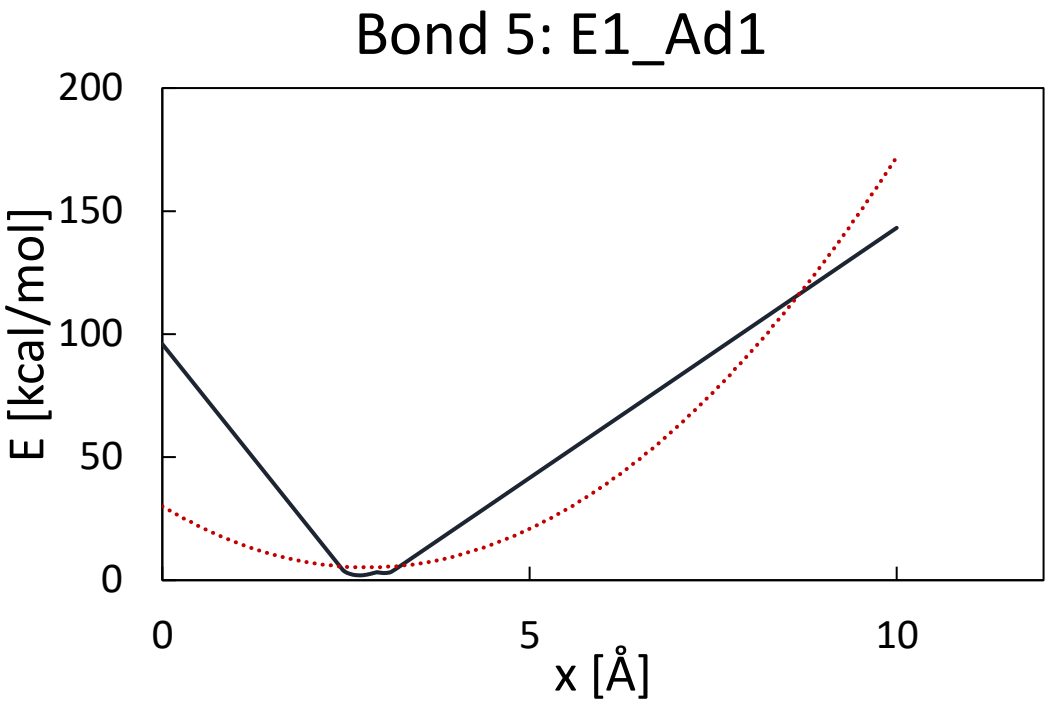
Bond 5: E1_Ad1
200
150
100
50
0
E [kcal/mol]
0
5
10
x [Å]

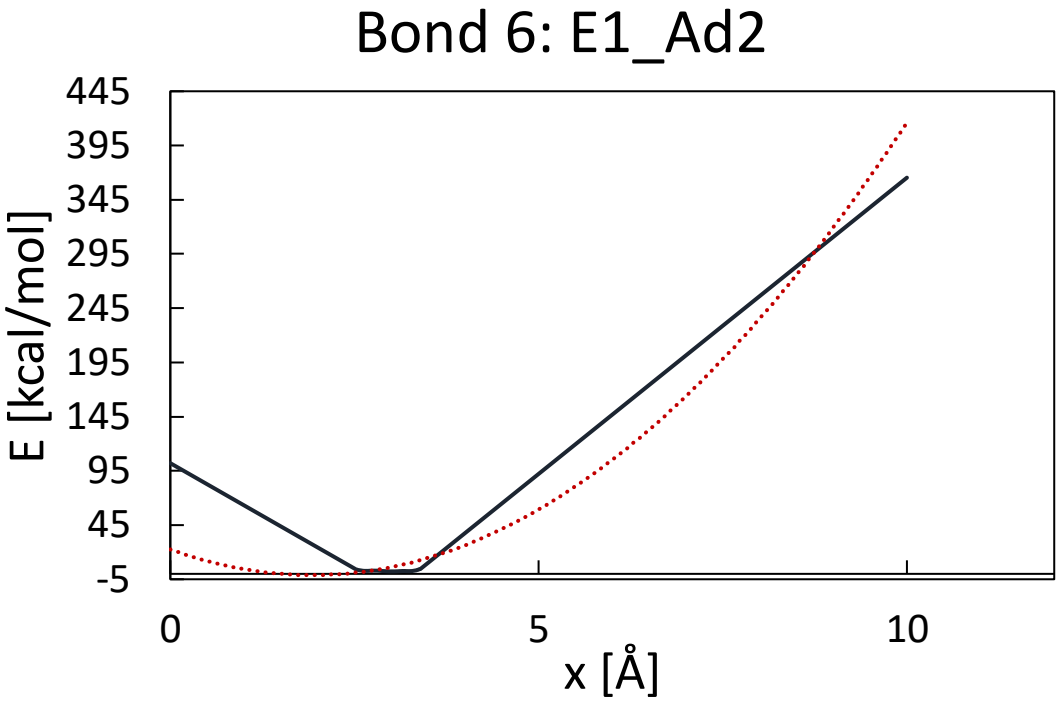
Bond 6: E1_Ad2
445
395
345
295
245
195
145
95
45
-5
E [kcal/mol]
0
5
10
x [Å]

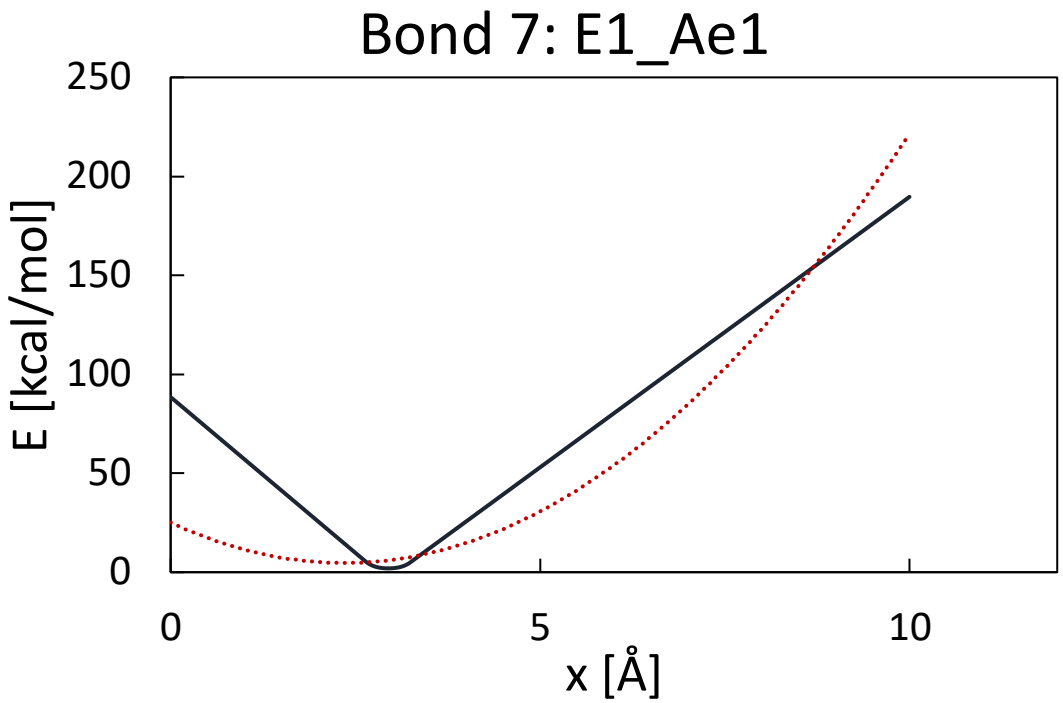
Bond 7: E1_Ae1
250
200
150
100
50
0
E [kcal/mol]
0
5
10
x [Å]

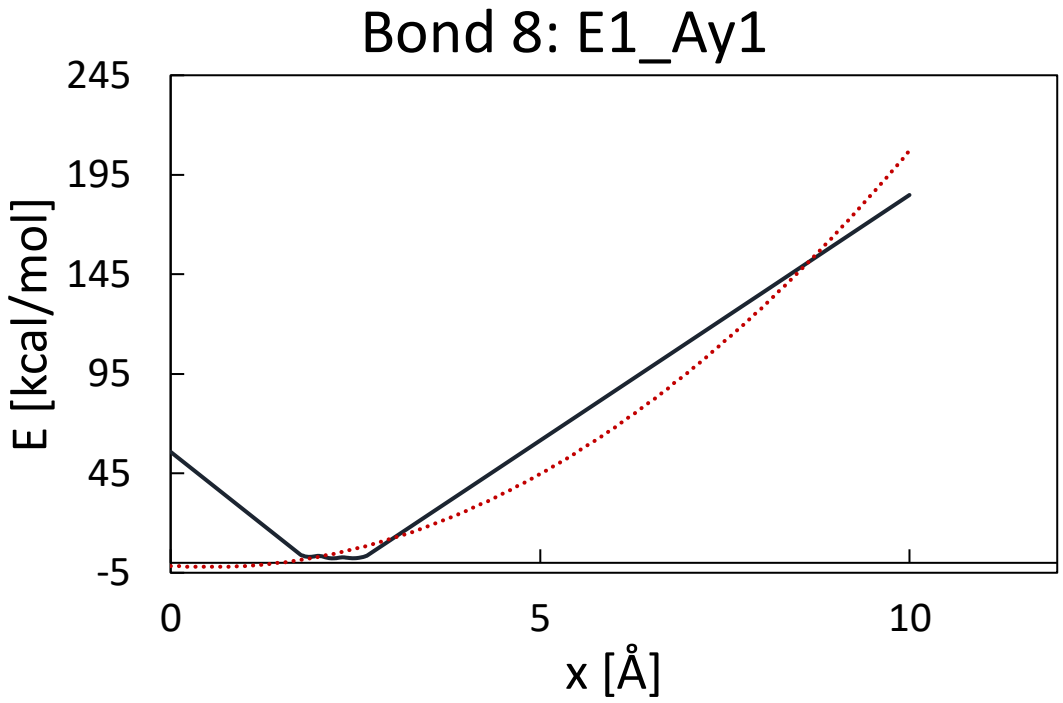
Bond 8: E1_Ay1
245
195
145
95
45
-5
E [kcal/mol]
0
5
10
x [Å]

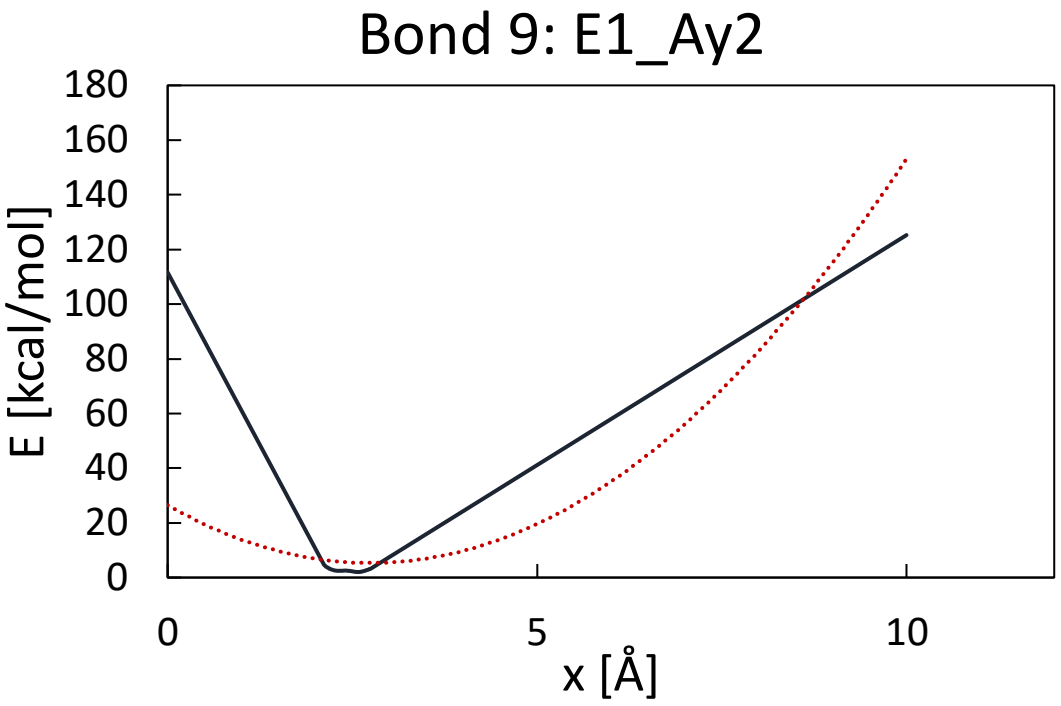

Angle potentials

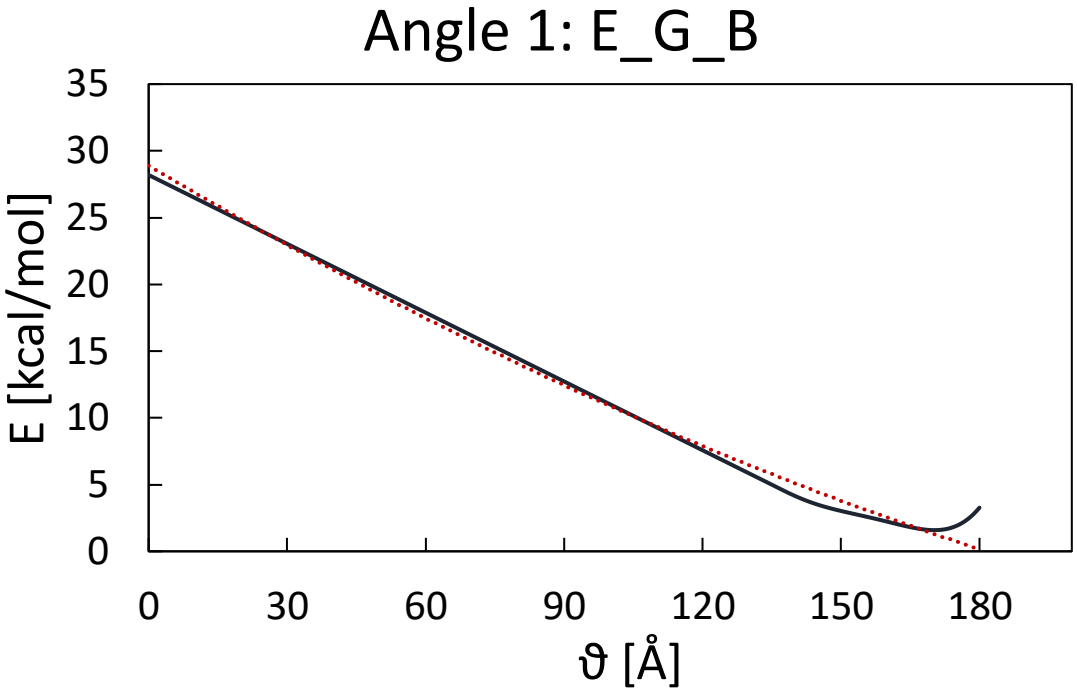

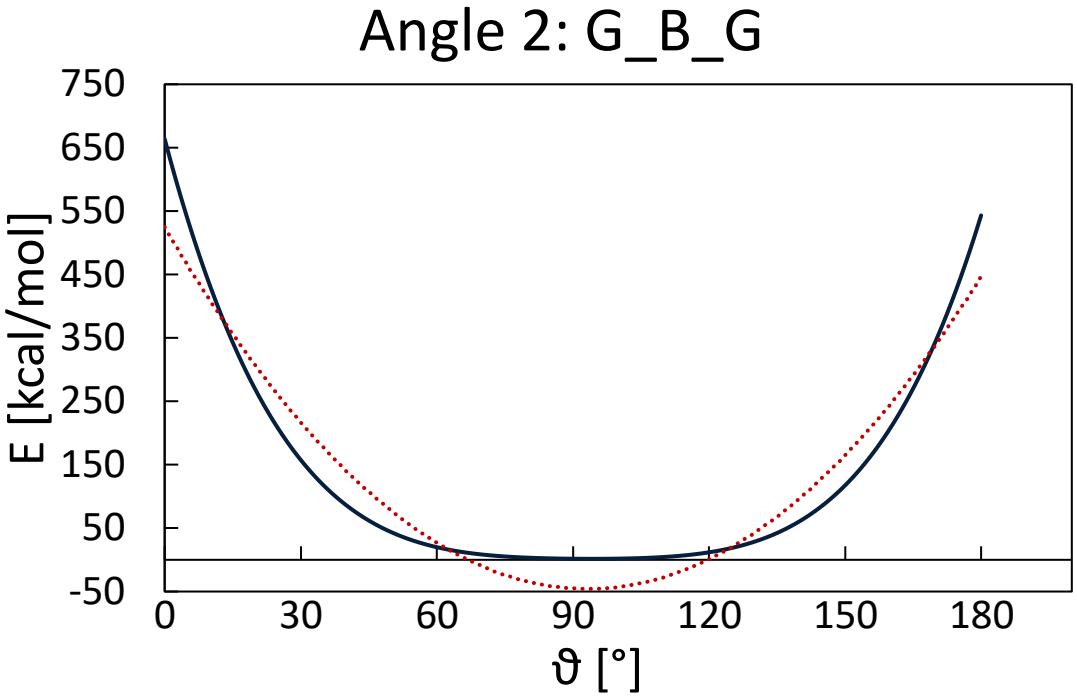
Angle 2: G_B_G
750
650
550
450
350
250
150
50
-50
E [kcal/mol]
0
30
60
90
120
150
180
ϑ [°]

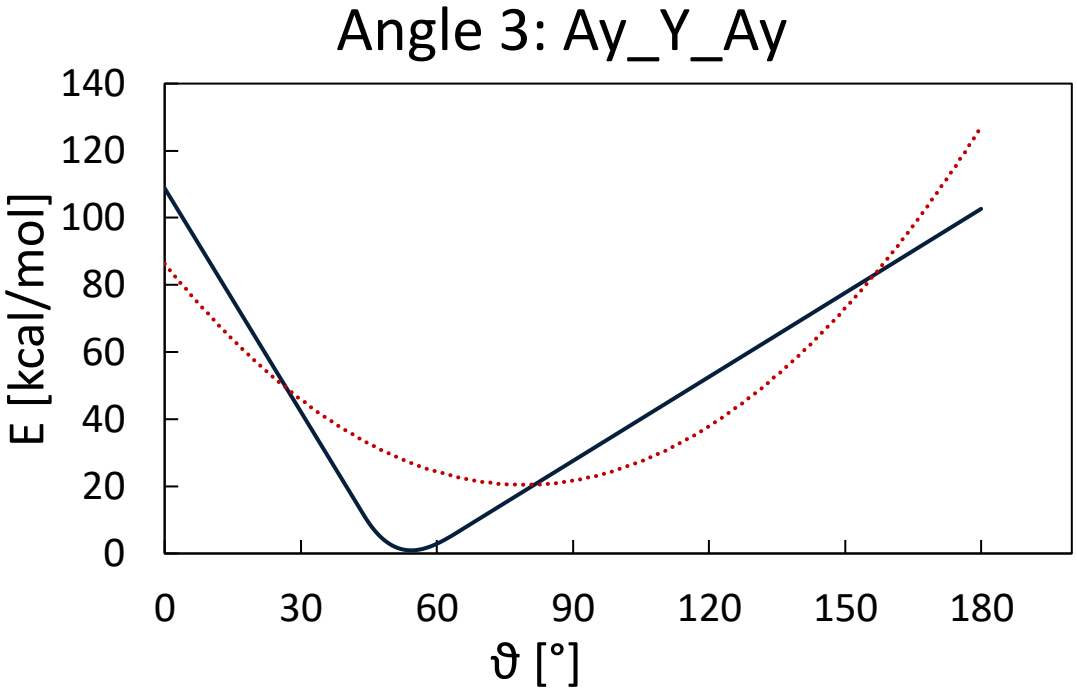
Angle 3: Ay_Y_Ay
140
120
100
80
60
40
20
0
E [kcal/mol]
0
30
60
90
120
150
180
ϑ [°]

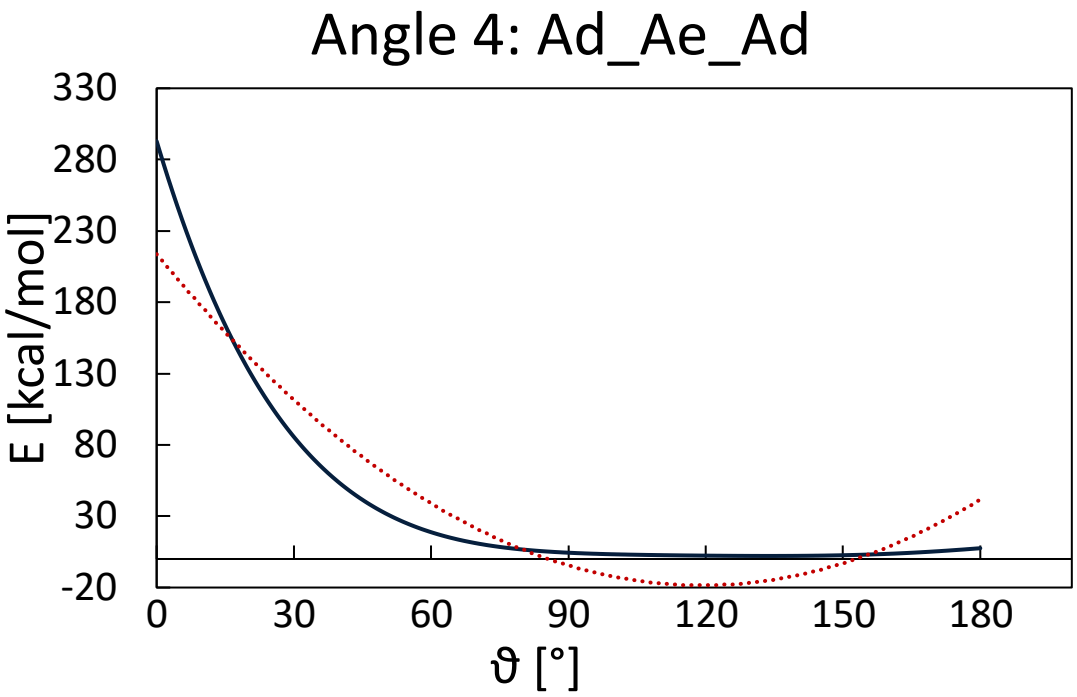
Angle 4: Ad_Ae_Ad
330
280
230
180
130
80
30
-20
E [kcal/mol]
0
30
60
90
120
150
180
ϑ [°]

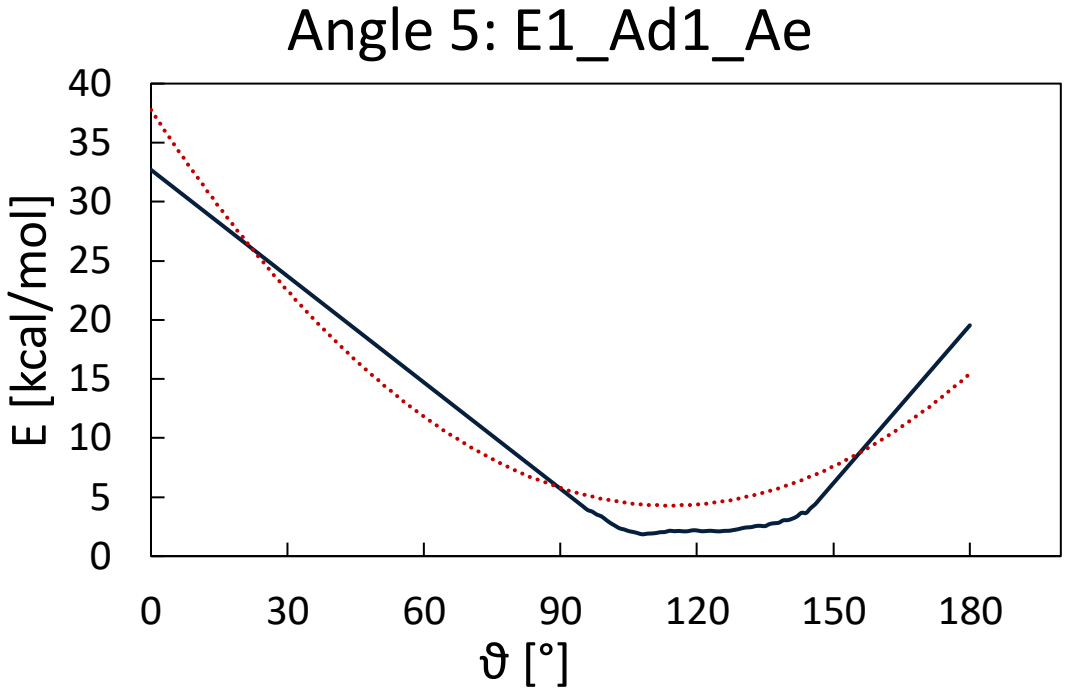
Angle 5: E1_Ad1_Ae
40
35
30
25
20
15
10
5
0
E [kcal/mol]
0
30
60
90
120
150
180
ϑ [°]

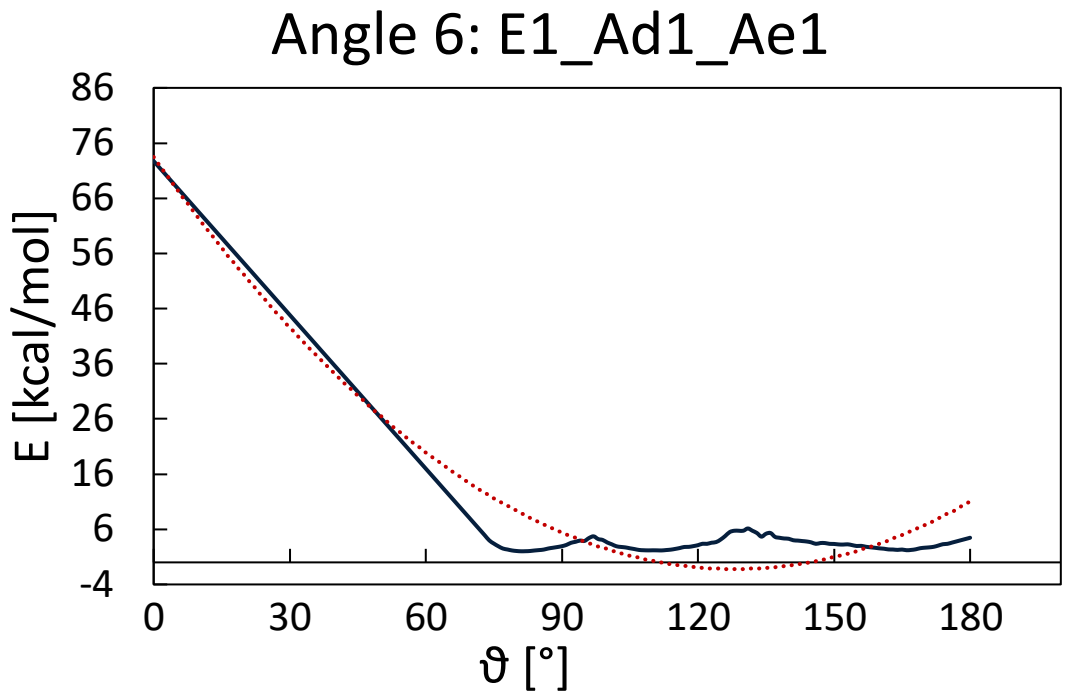
Angle 6: E1_Ad1_Ae1
E [kcal/mol]
86
76
66
56
46
36
26
16
6
-4
0
30
60
90
120
150
180
ϑ [°]

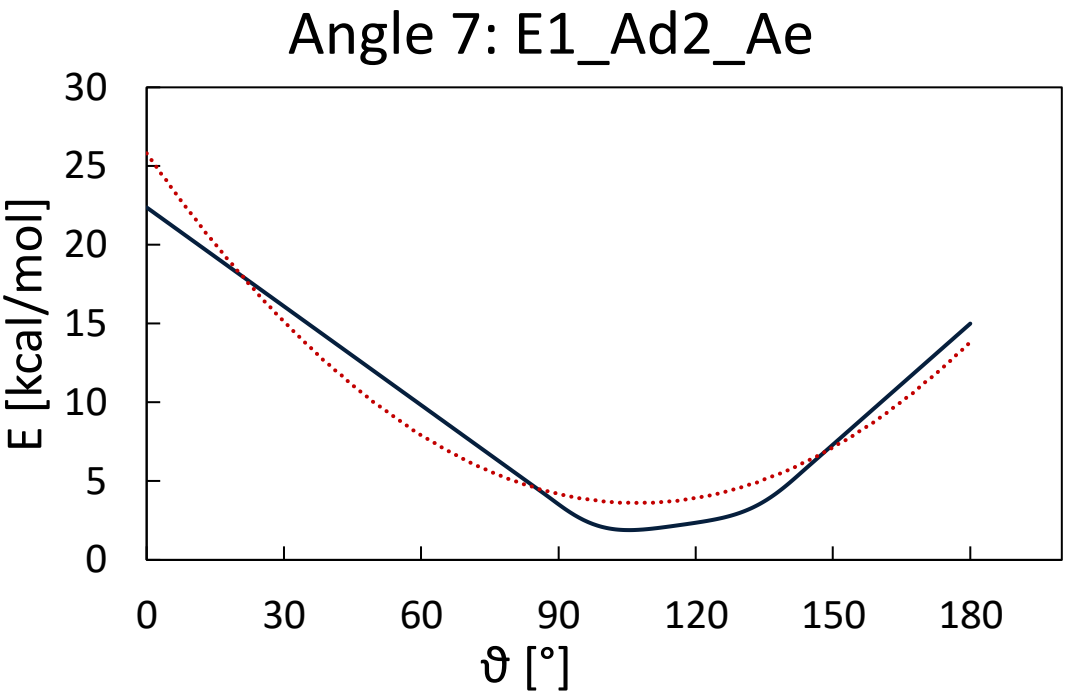
Angle 7: E1_Ad2_Ae
E [kcal/mol]
30
25
20
15
10
5
0
0
30
60
90
120
150
180
ϑ [°]

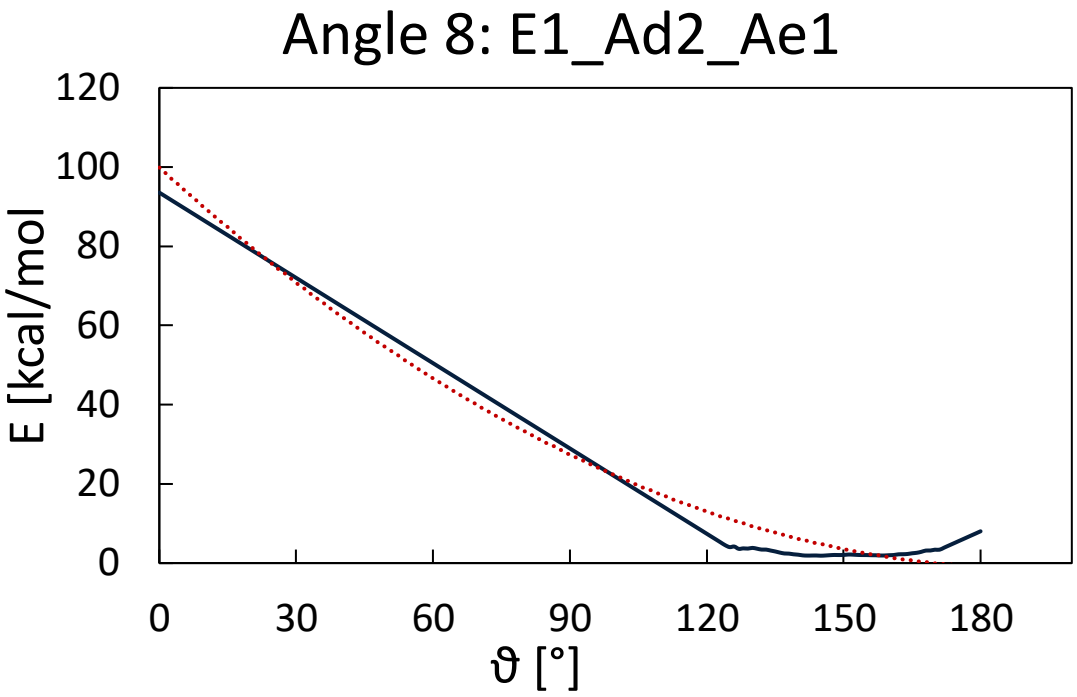
Angle 8: E1_Ad2_Ae1
120
100
80
60
40
20
0
E [kcal/mol
0
30
60
90
120
150
180
ϑ [°]

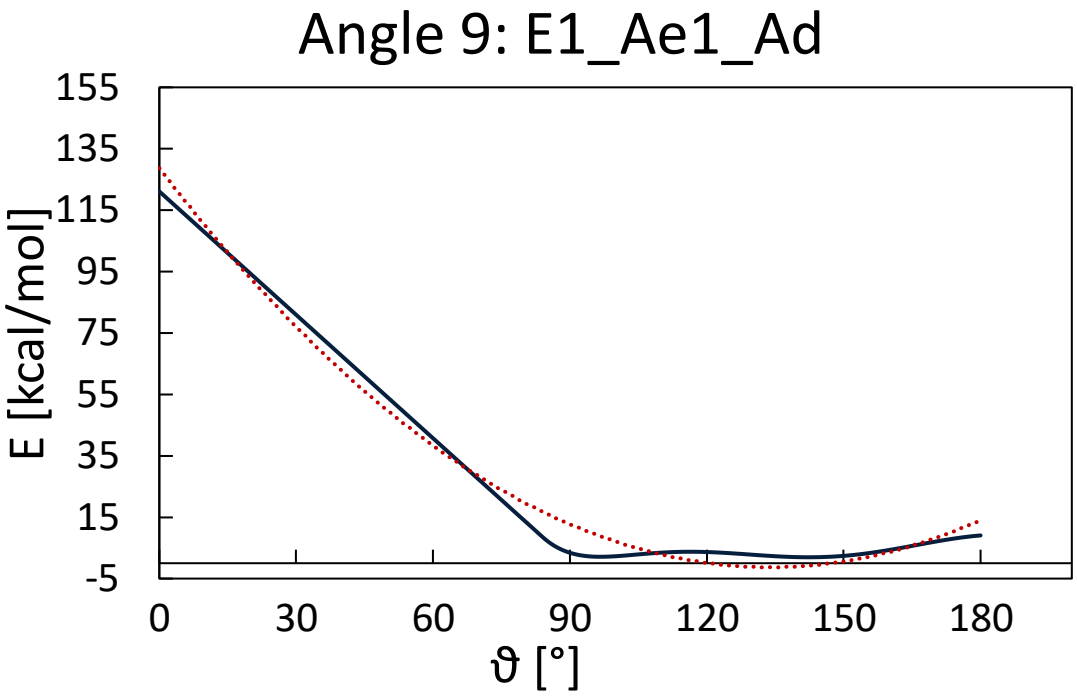
Angle 9: E1_Ae1_Ad
155
135
115
95
75
55
35
15
-5
E [kcal/mol]
0
30
60
90
120
150
180
ϑ [°]

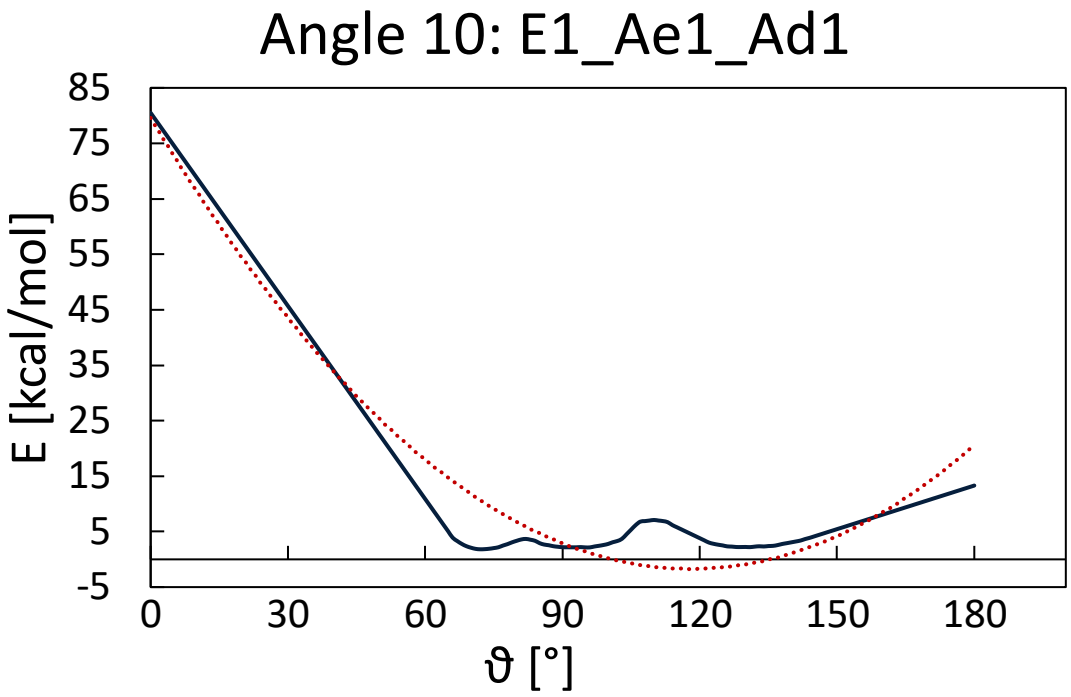
Angle 10: E1_Ae1_Ad1
E [kcal/mol]
85
75
65
55
45
35
25
15
5
-5
0
30
60
90
120
150
180
ϑ [°]

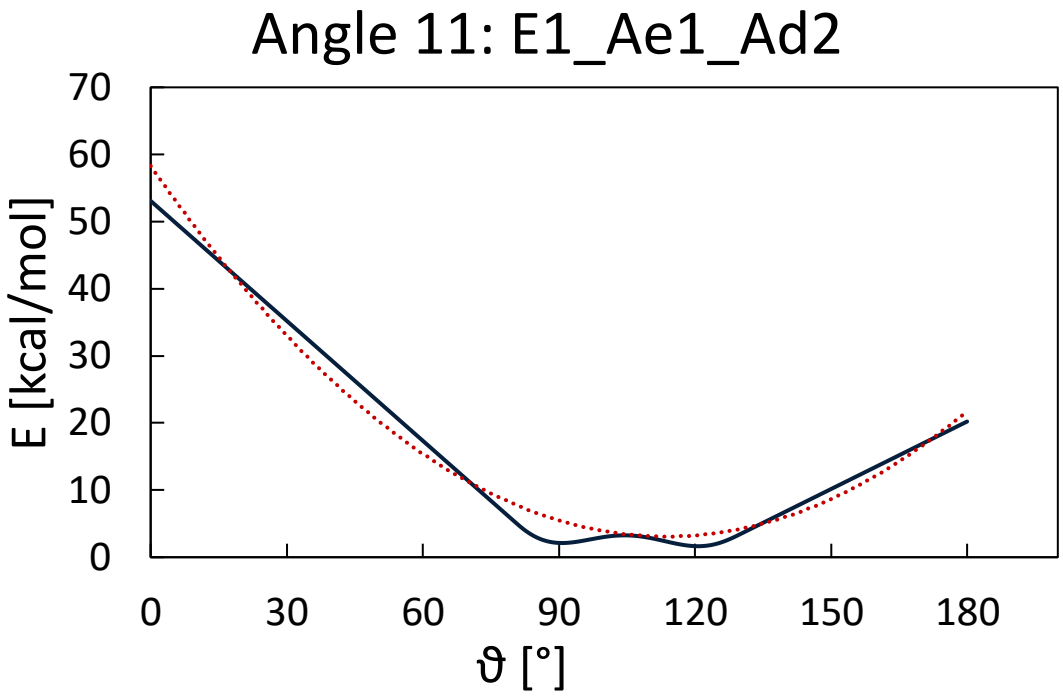
Angle 11: E1_Ae1_Ad2
E [kcal/mol]
70
60
50
40
30
20
10
0
0
30
60
90
120
150
180
ϑ [°]

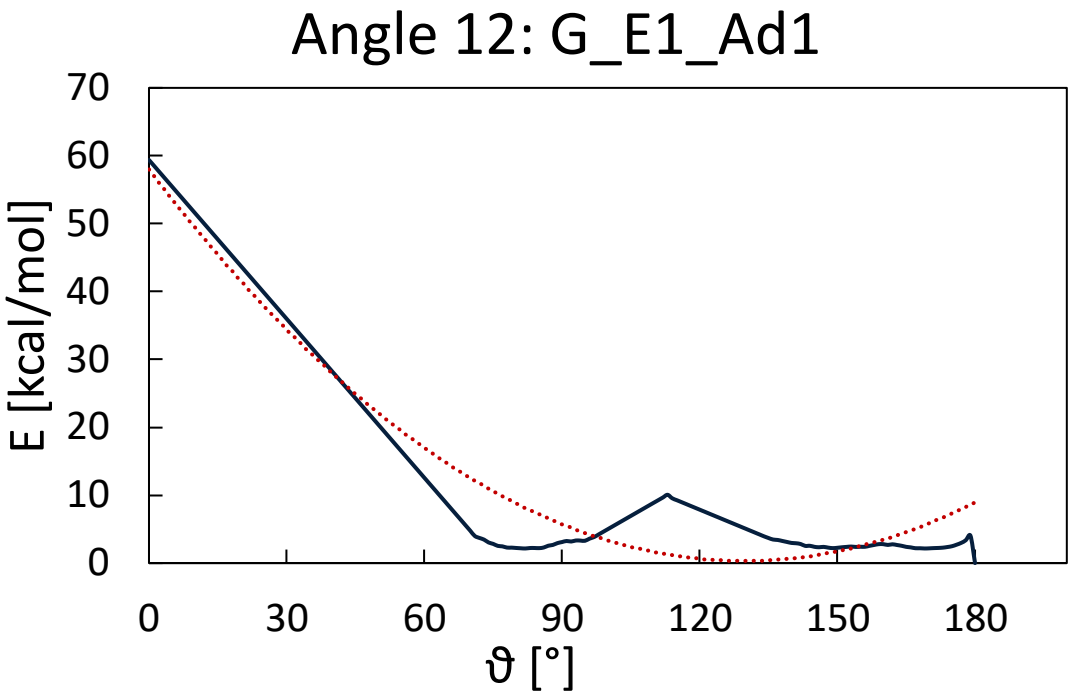
Angle 12: G_E1_Ad1
E [kcal/mol]
70
60
50
40
30
20
10
0
0
30
60
90
120
150
180
ϑ [°]

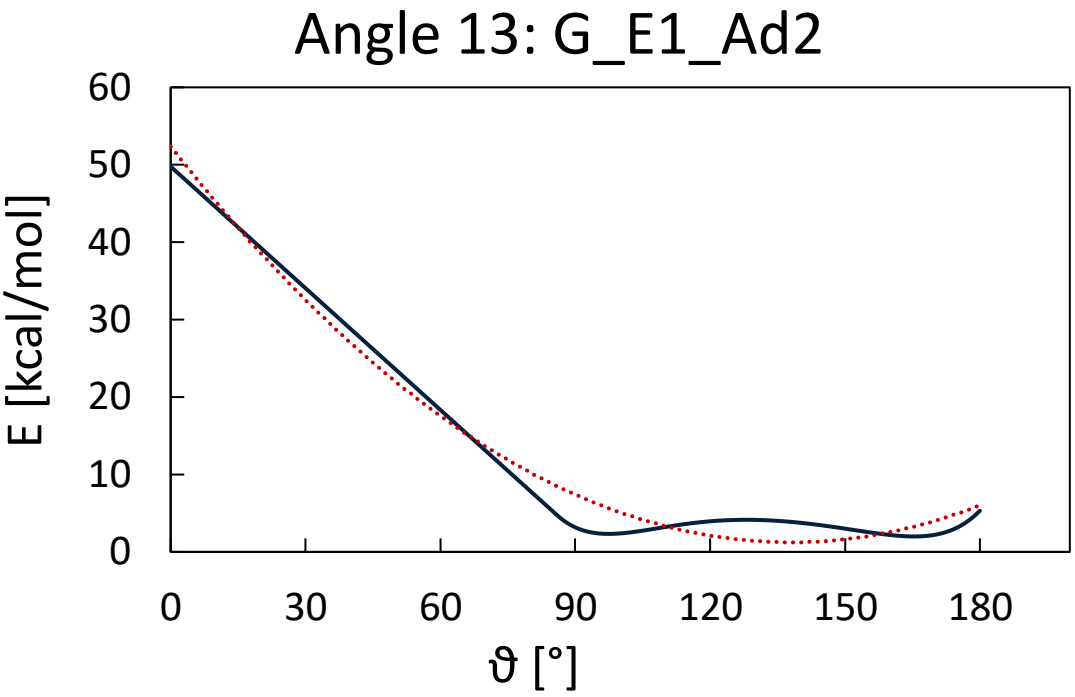
Angle 13: G_E1_Ad2
E [kcal/mol]
60
50
40
30
20
10
0
0
30
60
90
120
150
180
ϑ [°]

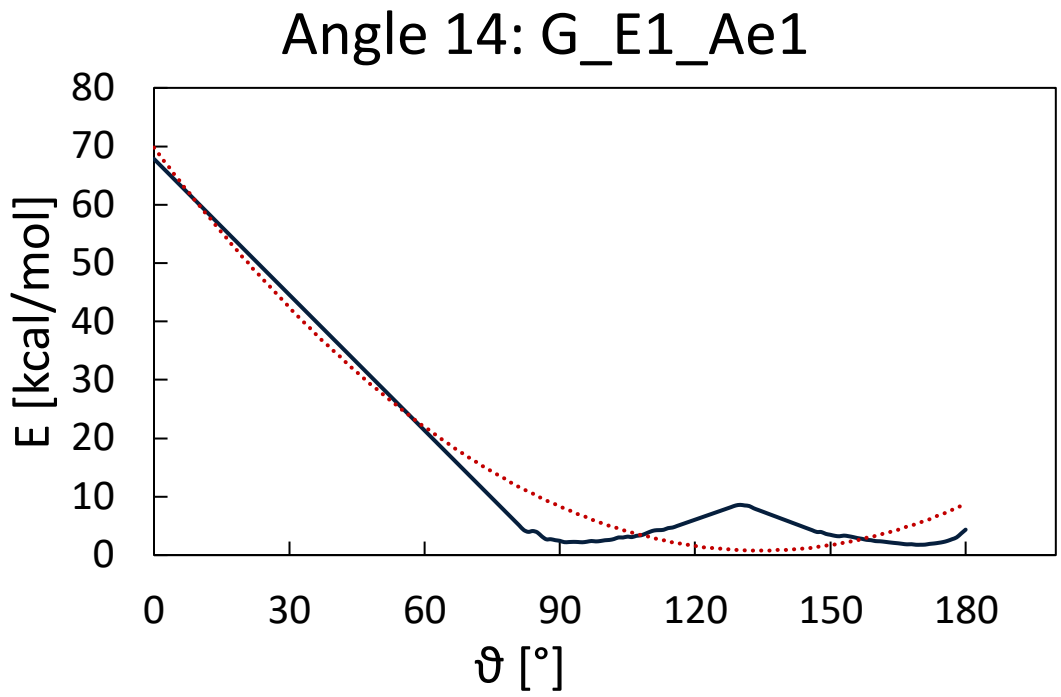
Angle 14: G_E1_Ae1
E [kcal/mol]
80
70
60
50
40
30
20
10
0
0
30
60
90
120
150
180
ϑ [°]

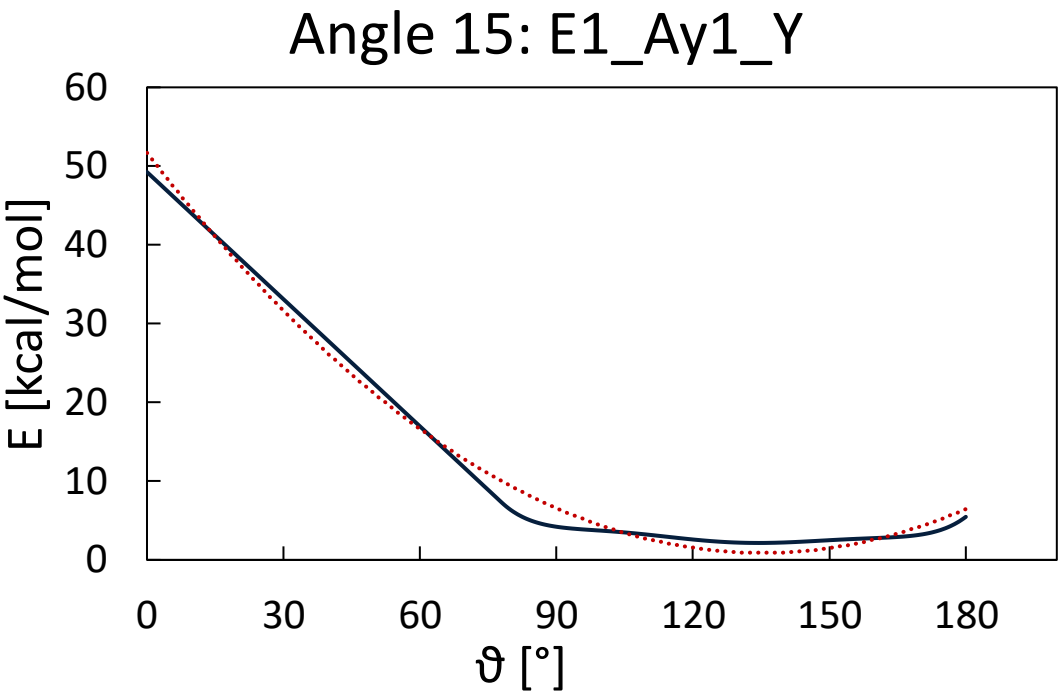
Angle 15: E1_Ay1_Y
E [kcal/mol]
60
50
40
30
20
10
0
0
30
60
90
120
150
180
ϑ [°]

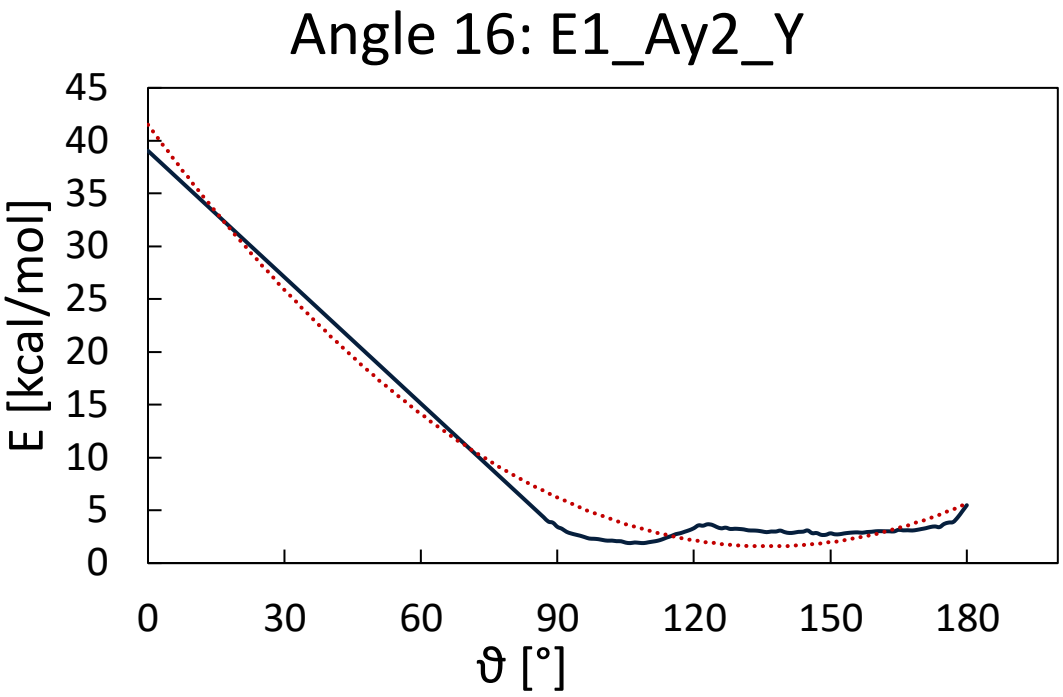
Angle 16: E1_Ay2_Y
E [kcal/mol]
45
40
35
30
25
20
15
10
5
0
0
30
60
90
120
150
180
ϑ [°]

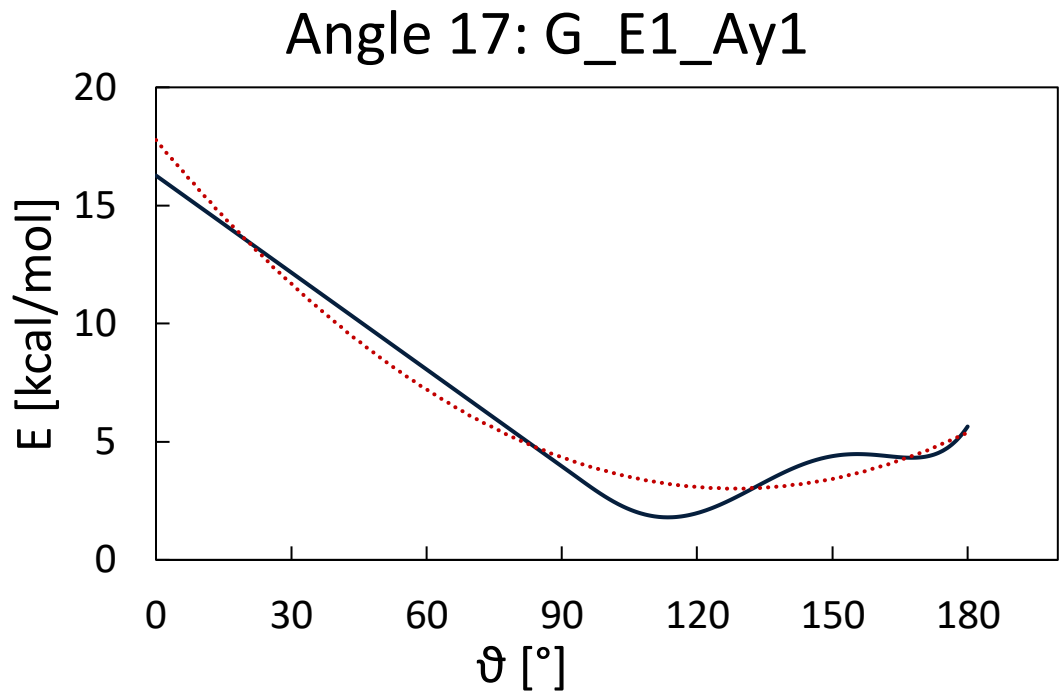
Angle 17: G_E1_Ay1
E [kcal/mol]
20
15
10
5
0
0
30
60
90
120
150
180
ϑ [°]

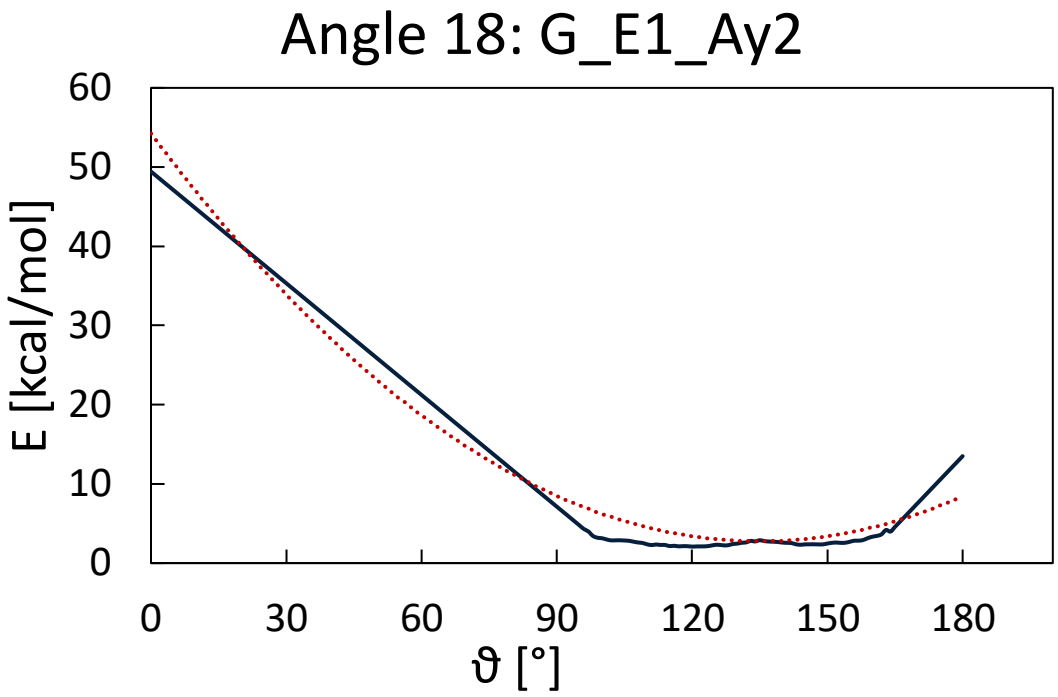
Angle 18: G_E1_Ay2
E [kcal/mol]
60
50
40
30
20
10
0
0
30
60
90
120
150
180
ϑ [°]

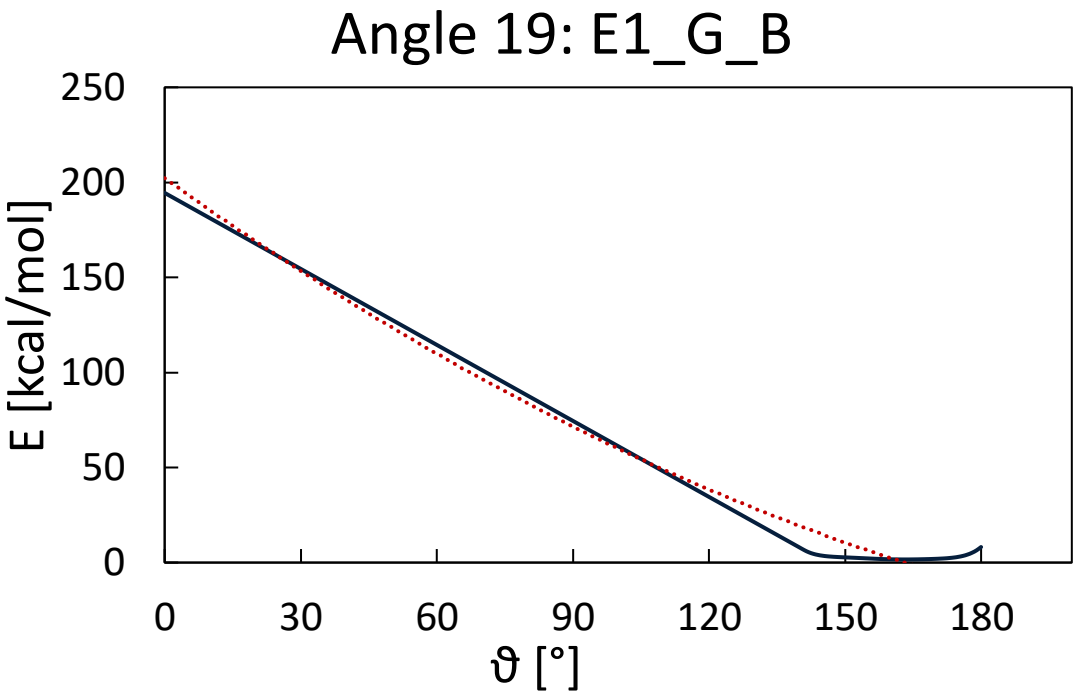
Angle 19: E1_G_B
E [kcal/mol]
250
200
150
100
50
0
0
30
60
90
120
150
180
ϑ [°]

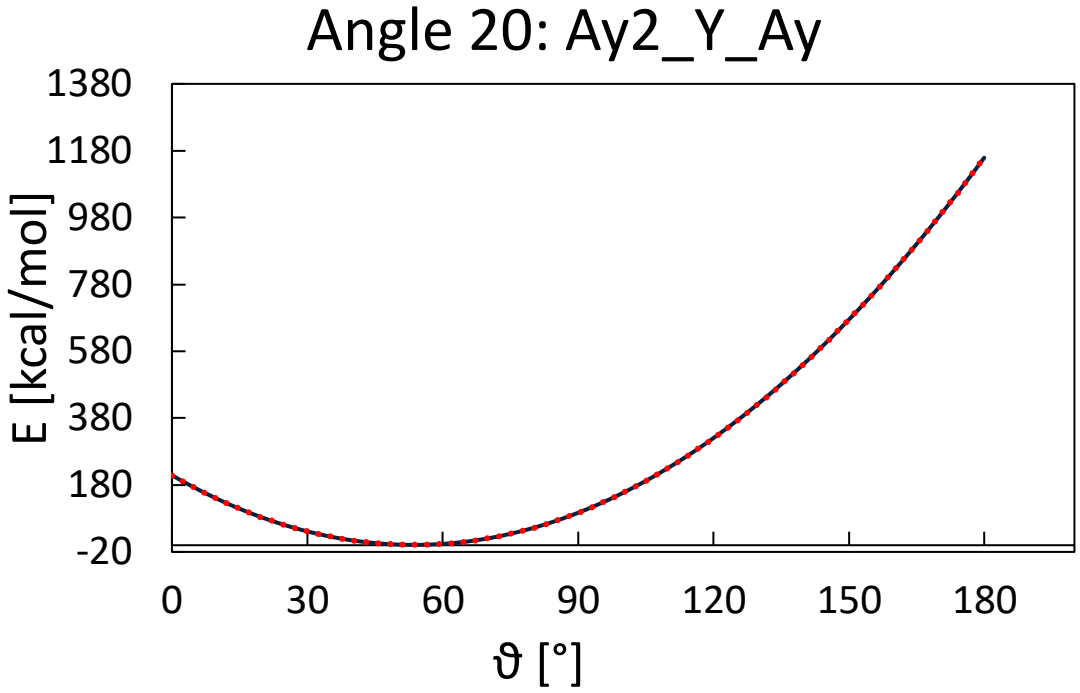
Angle 20: Ay2_Y_Ay
1380
1180
980
780
580
380
180
-20
E [kcal/mol]
0
30
60
90
120
150
180
ϑ [°]

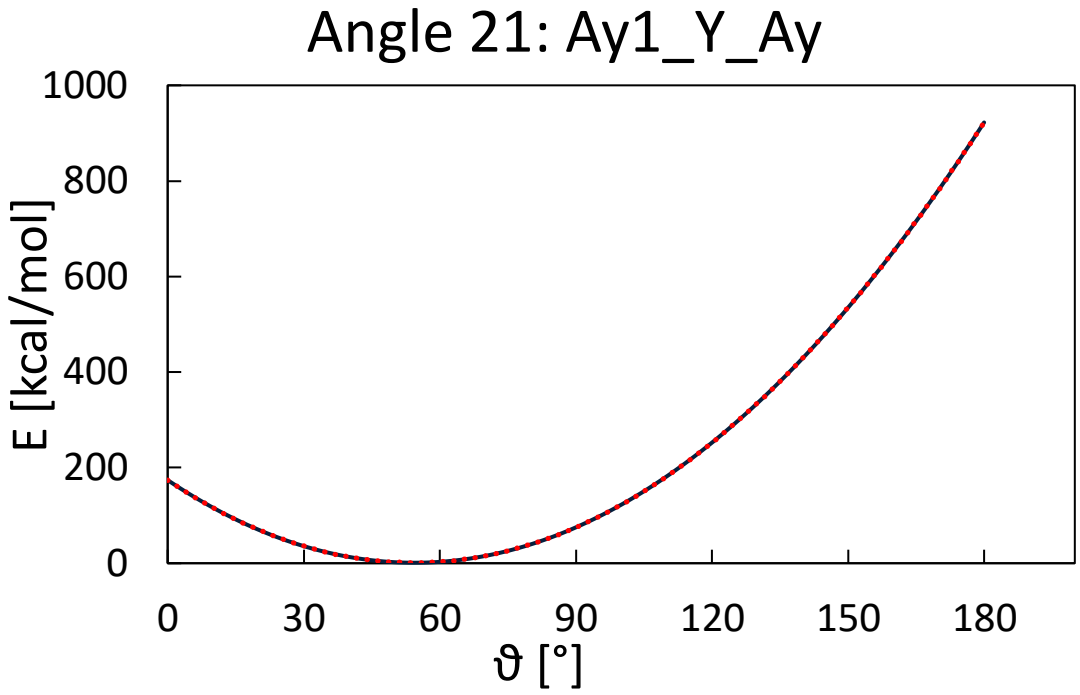
Angle 21: Ay1_Y_Ay
1000
800
600
400
200
0
E [kcal/mol]
0
30
60
90
120
150
180
ϑ [°]

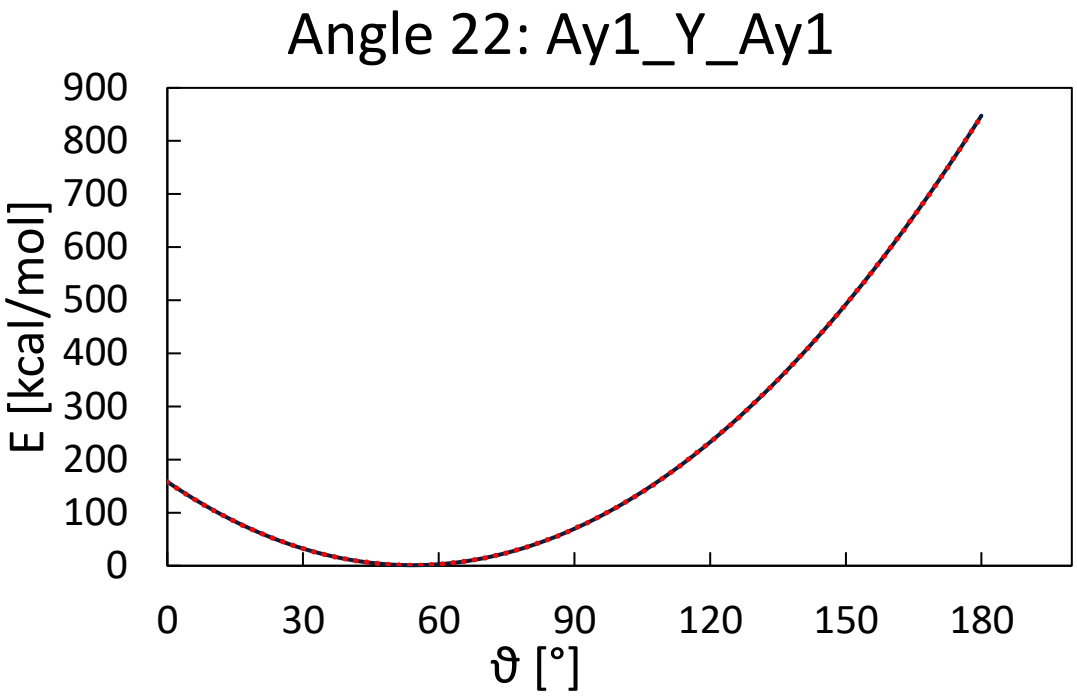
Angle 22: Ay1_Y_Ay1
E [kcal/mol]
900
800
700
600
500
400
300
200
100
0
0
30
60
90
120
150
180
ϑ [°]

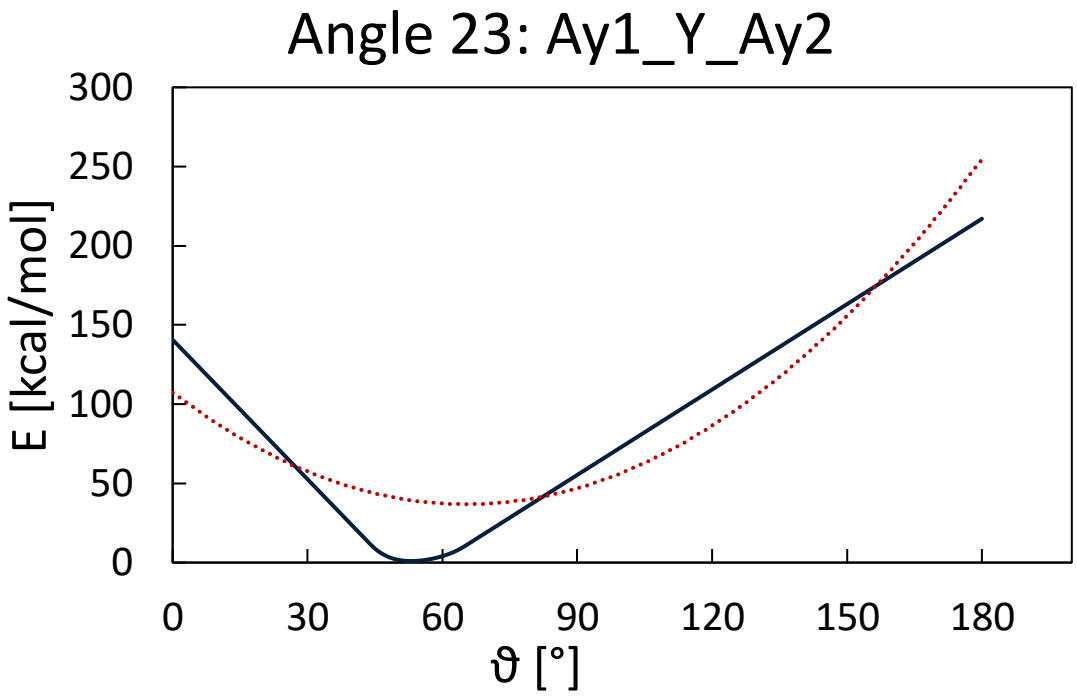
Angle 23: Ay1_Y_Ay2
E [kcal/mol]
300
250
200
150
100
50
0
0
30
60
90
120
150
180
ϑ [°]

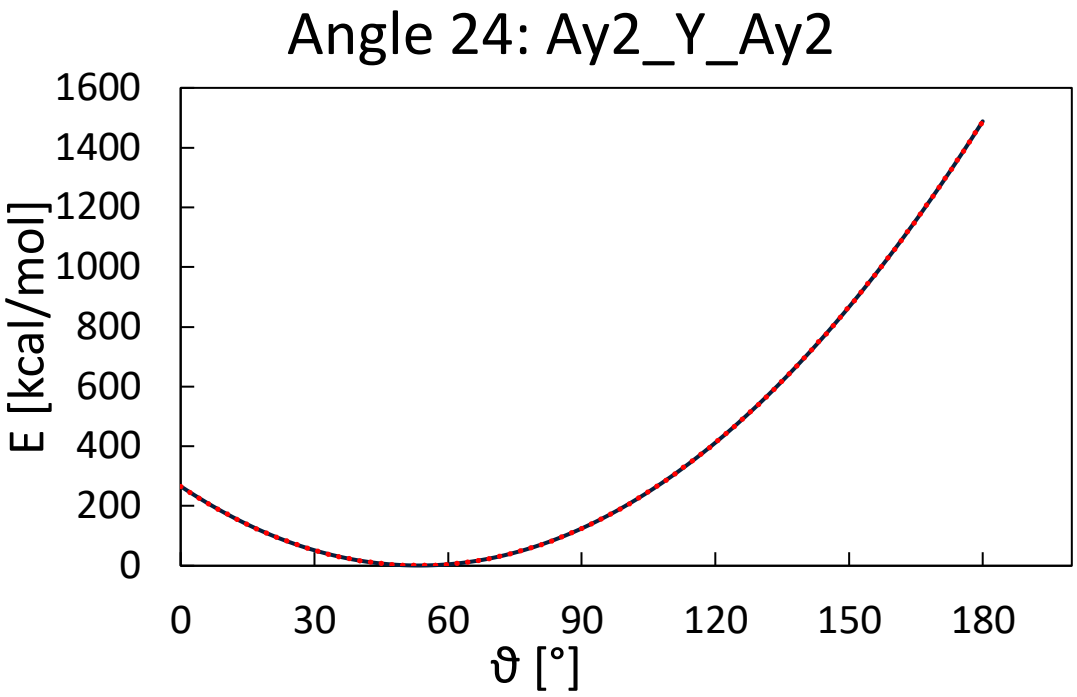
Angle 24: Ay2_Y_Ay2
E [kcal/mol]
1600
1400
1200
1000
800
600
400
200
0
0
30
60
90
120
150
180
ϑ [°]

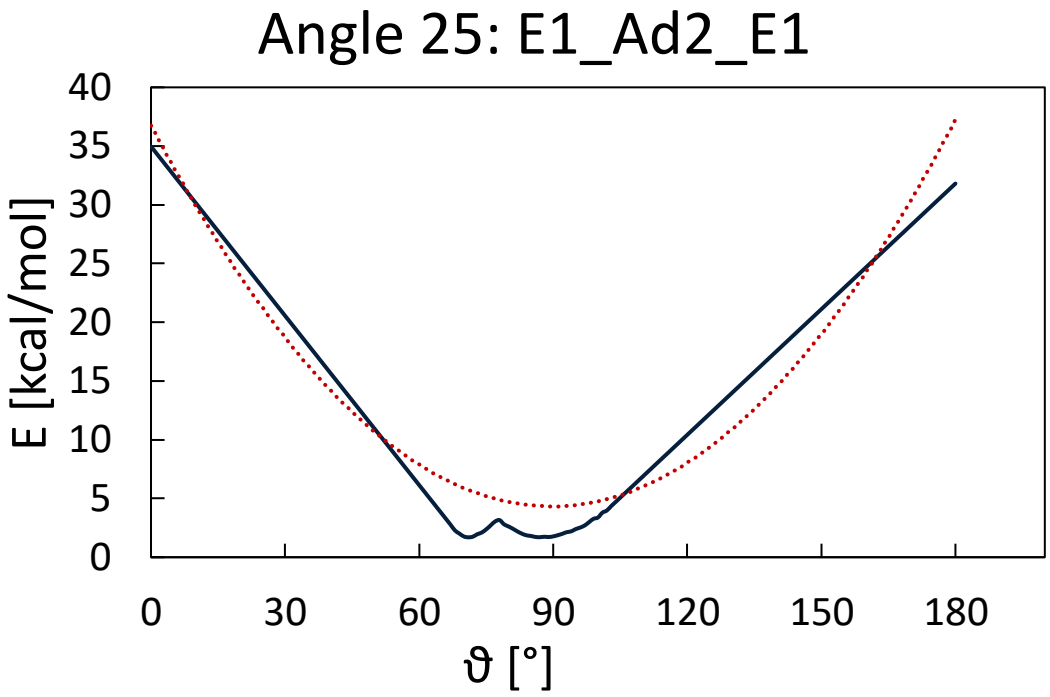
Angle 25: E1_Ad2_E1
E [kcal/mol]
40
35
30
25
20
15
10
5
0
0
30
60
90
120
150
180
ϑ [°]

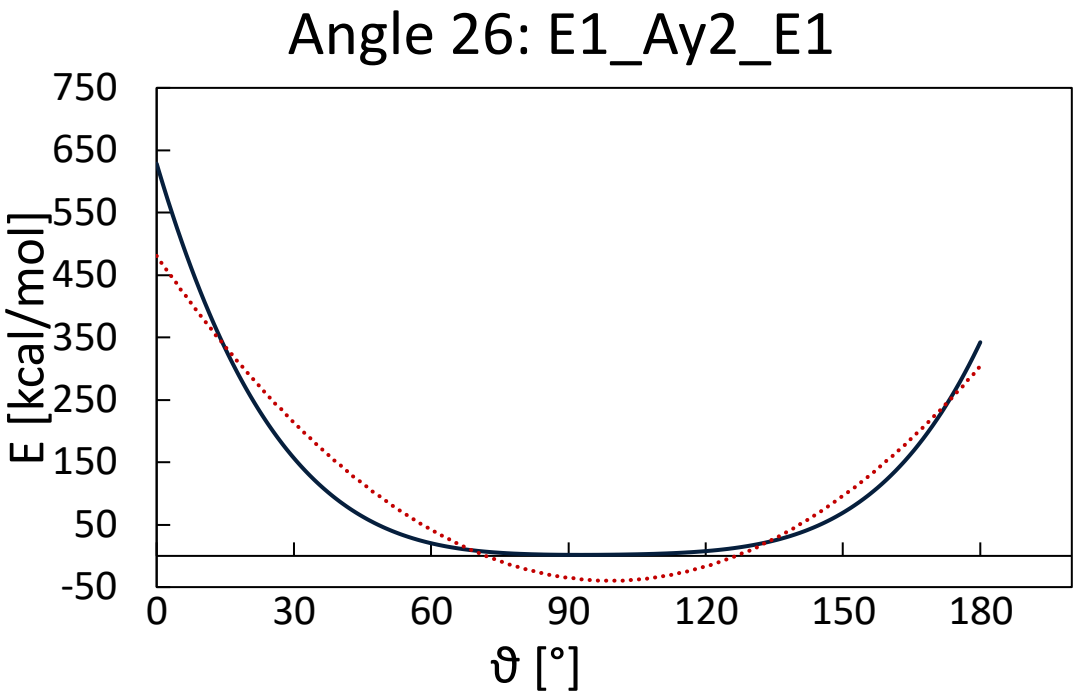
Angle 26: E1_Ay2_E1
750
650
550
450
350
250
150
50
-50
E [kcal/mol]
0
30
60
90
120
150
180
ϑ [°]

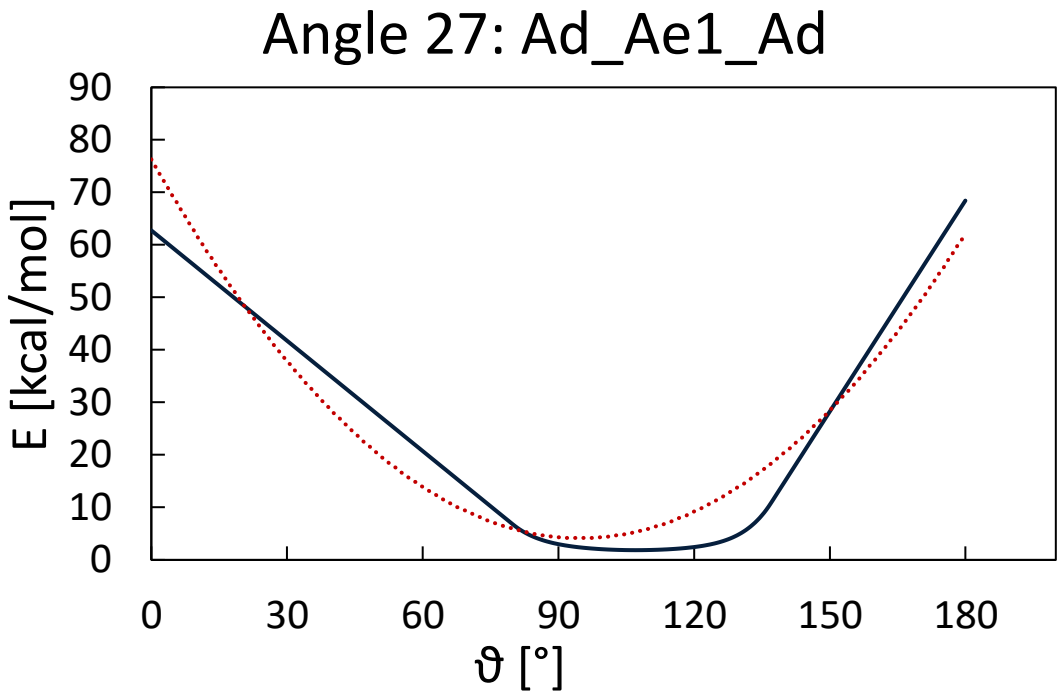
Angle 27: Ad_Ae1_Ad
90
80
70
60
50
40
30
20
10
0
E [kcal/mol]
0
30
60
90
120
150
180
ϑ [°]

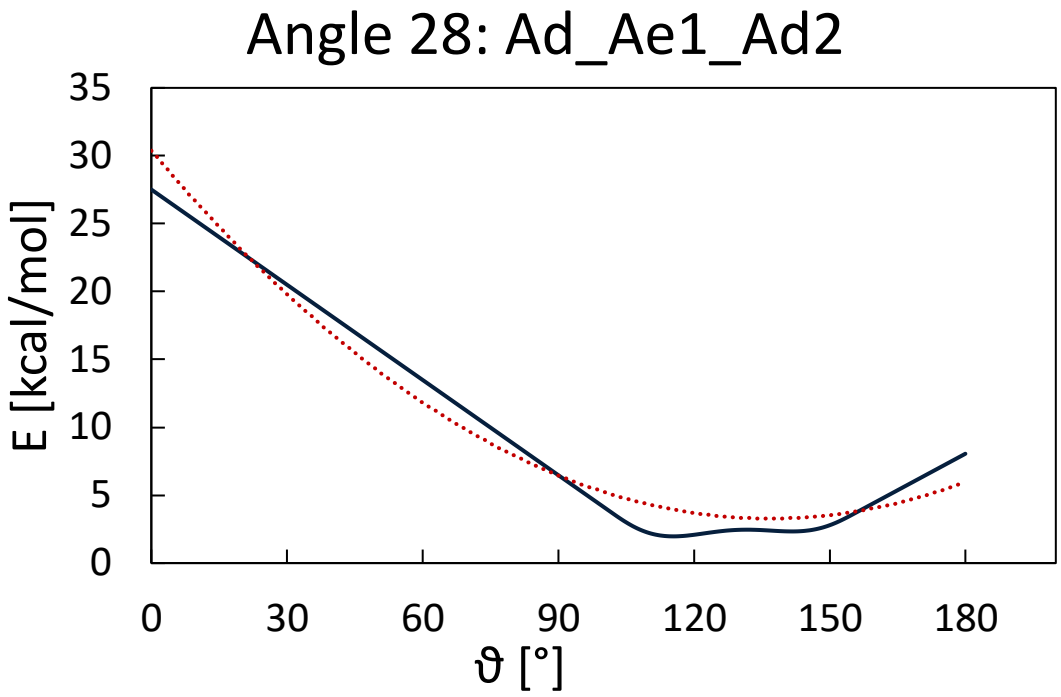
Angle 28: Ad_Ae1_Ad2
E [kcal/mol]
35
30
25
20
15
10
5
0
0
30
60
90
120
150
180
ϑ [°]

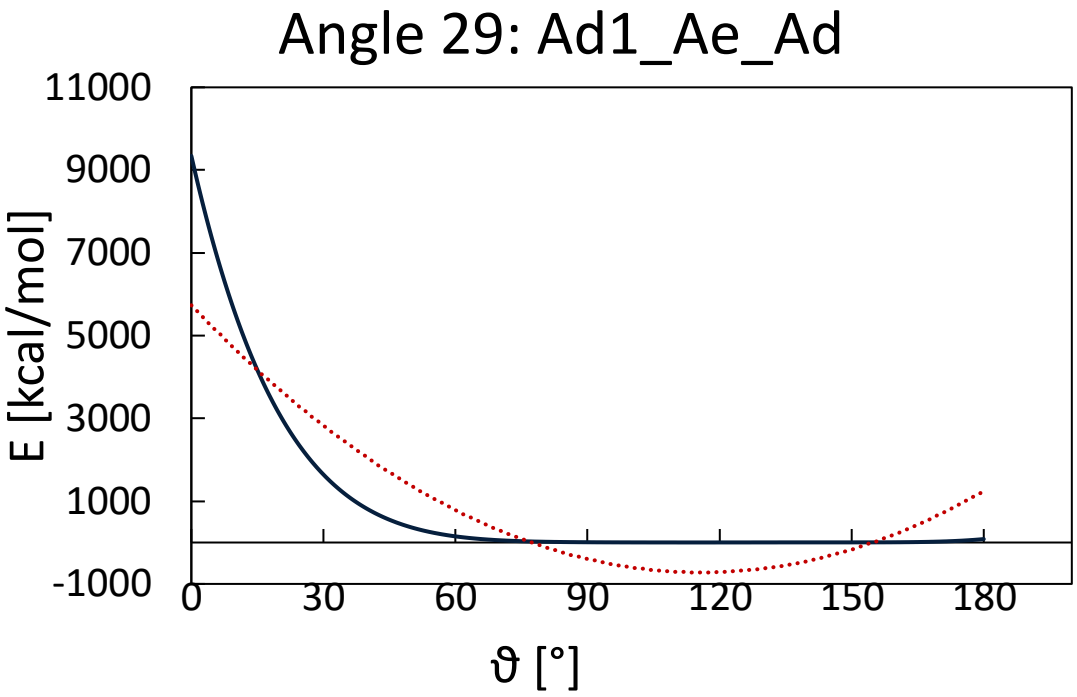
Angle 29: Ad1_Ae_Ad
E [kcal/mol]
11000
9000
7000
5000
3000
1000
-1000
0
30
60
90
120
150
180
ϑ [°]

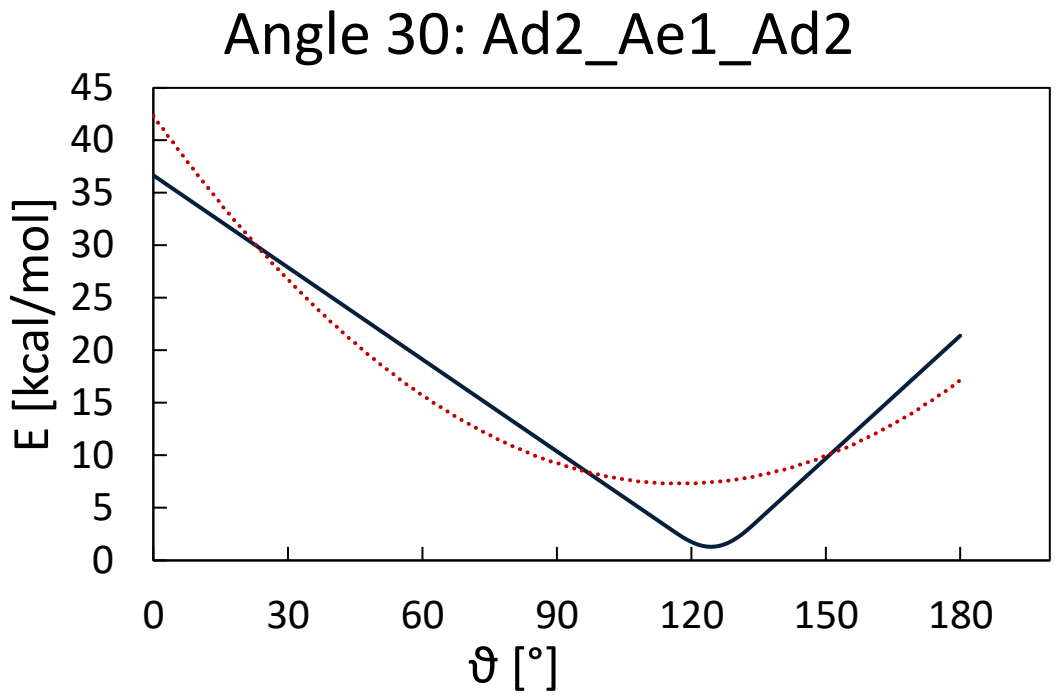
Angle 30: Ad2_Ae1_Ad2
E [kcal/mol]
45
40
35
30
25
20
15
10
5
0
0
30
60
90
120
150
180
ϑ [°]

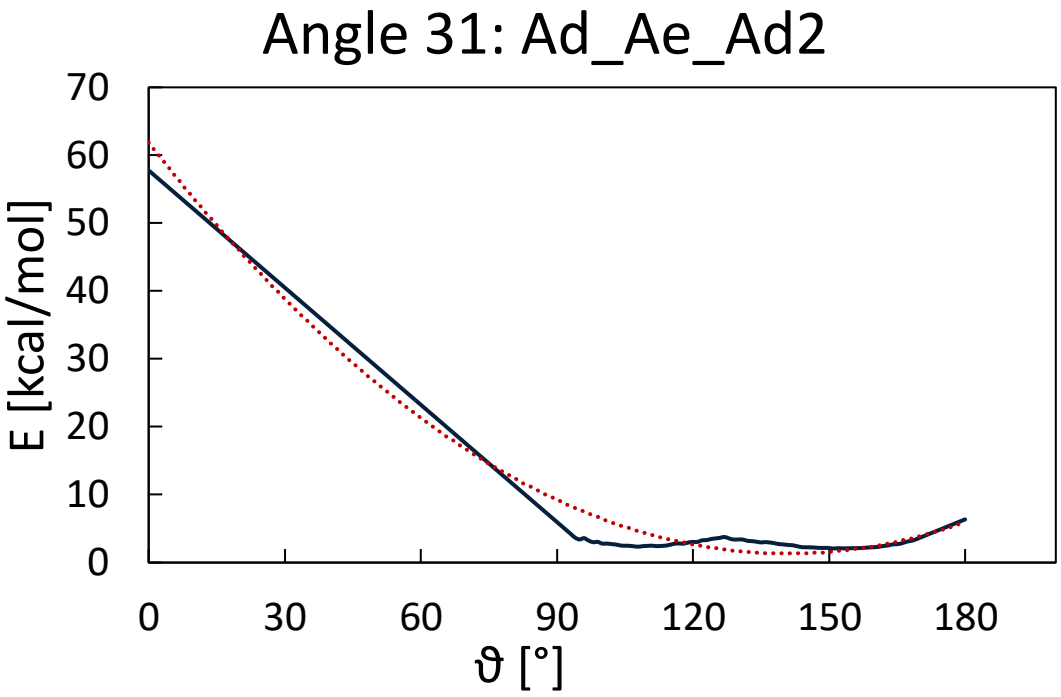
Angle 31: Ad_Ae_Ad2
E [kcal/mol]
70
60
50
40
30
20
10
0
0
30
60
90
120
150
180
ϑ [°]

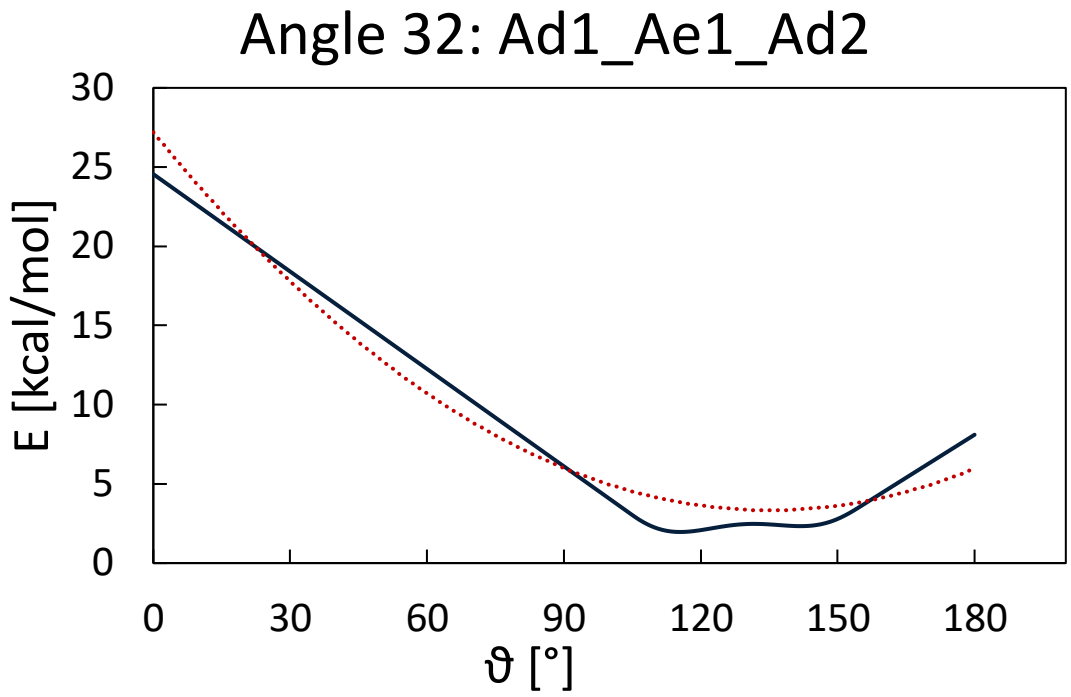
Angle 32: Ad1_Ae1_Ad2
E [kcal/mol]
30
25
20
15
10
5
0
0
30
60
90
120
150
180
ϑ [°]

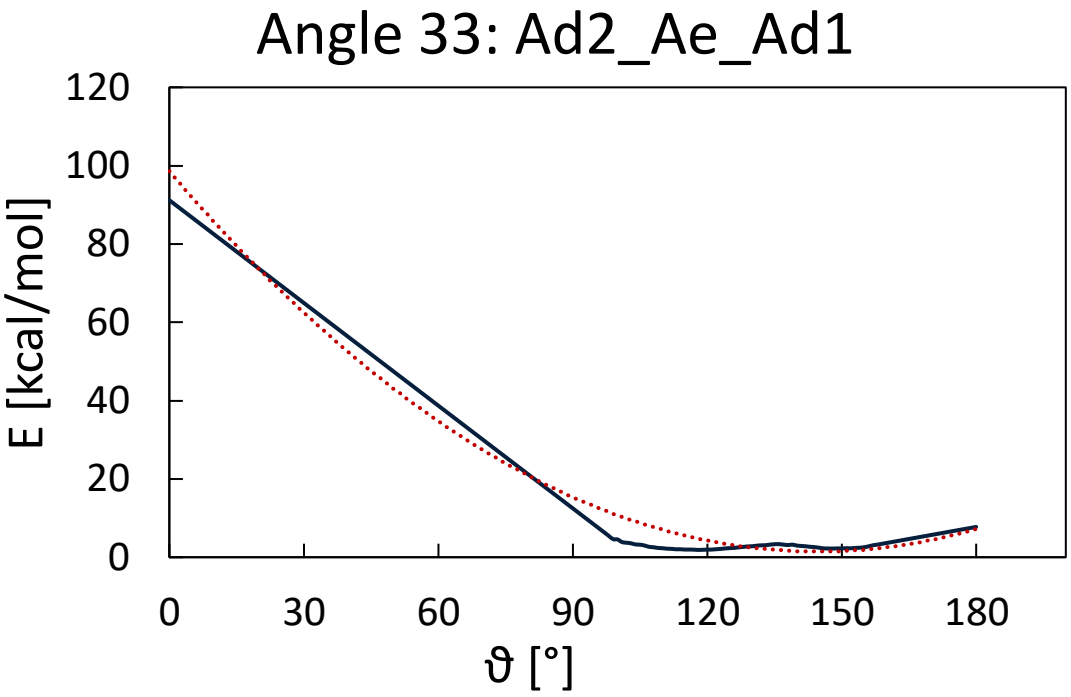
Angle 33: Ad2_Ae_Ad1
E [kcal/mol]
120
100
80
60
40
20
0
0
30
60
90
120
150
180
ϑ [°]

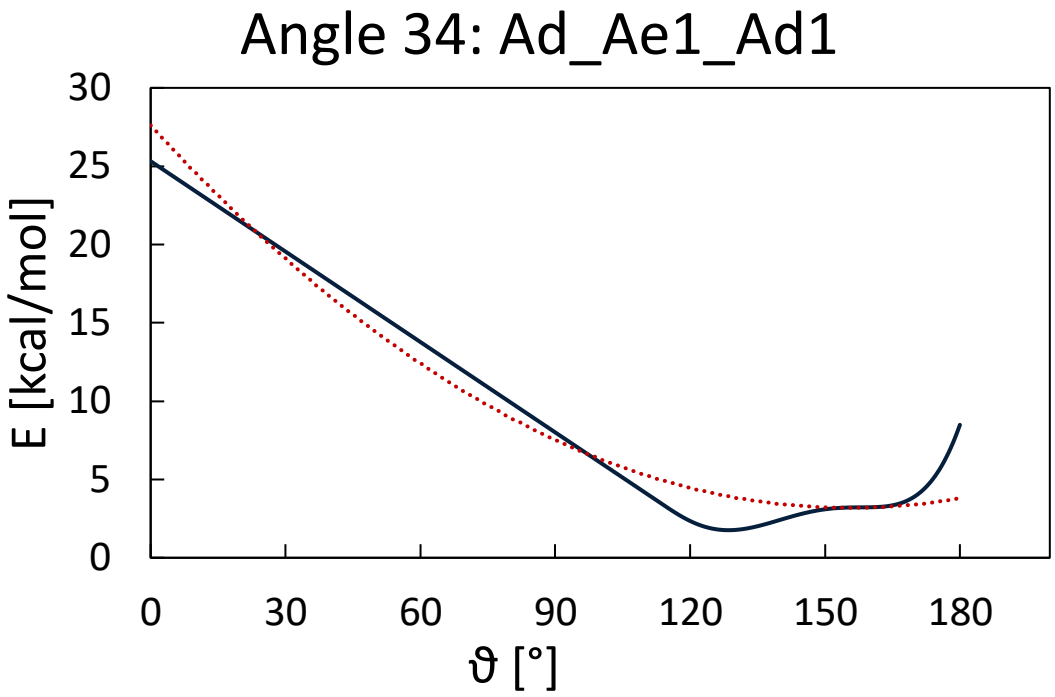
Angle 34: Ad_Ae1_Ad1
E [kcal/mol]
30
25
20
15
10
5
0
0
30
60
90
120
150
180
ϑ [°]

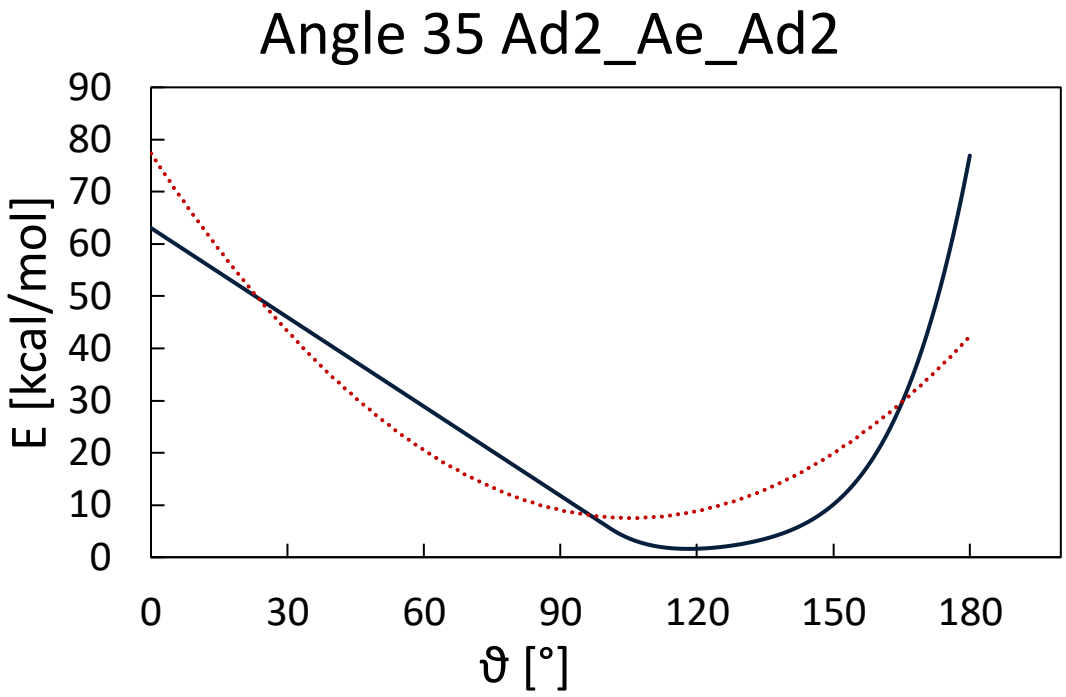
Angle 35 Ad2_Ae_Ad2
E [kcal/mol]
90
80
70
60
50
40
30
20
10
0
0
30
60
90
120
150
180
ϑ [°]

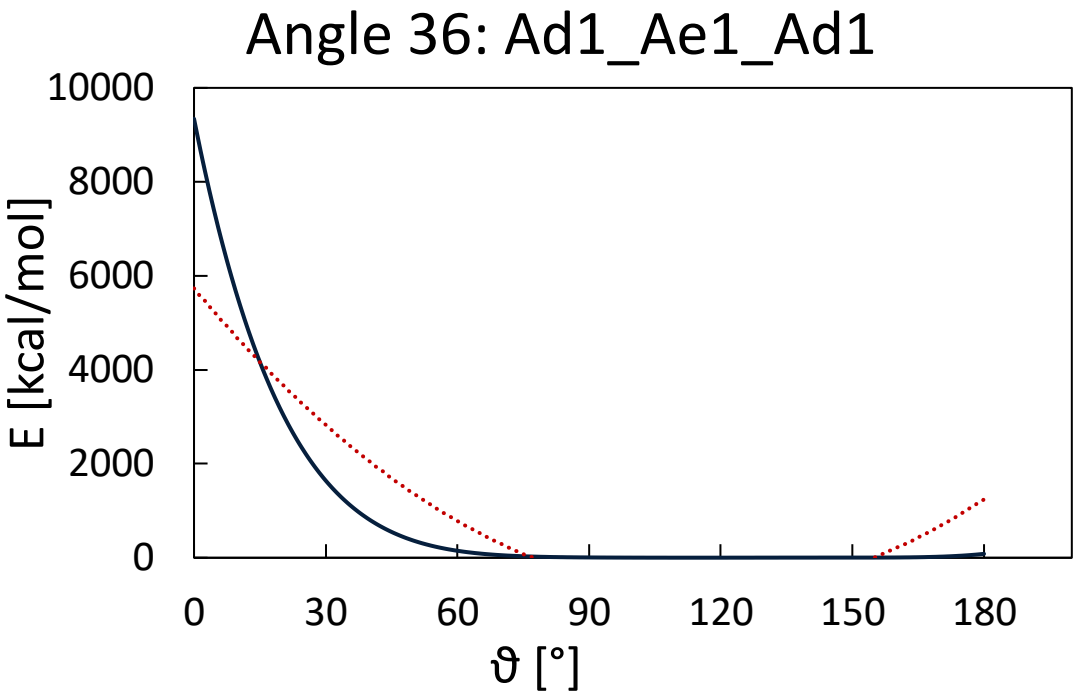
Angle 36: Ad1_Ae1_Ad1
10000
8000
6000
4000
2000
0
E [kcal/mol]
0
30
60
90
120
150
180
ϑ [°]

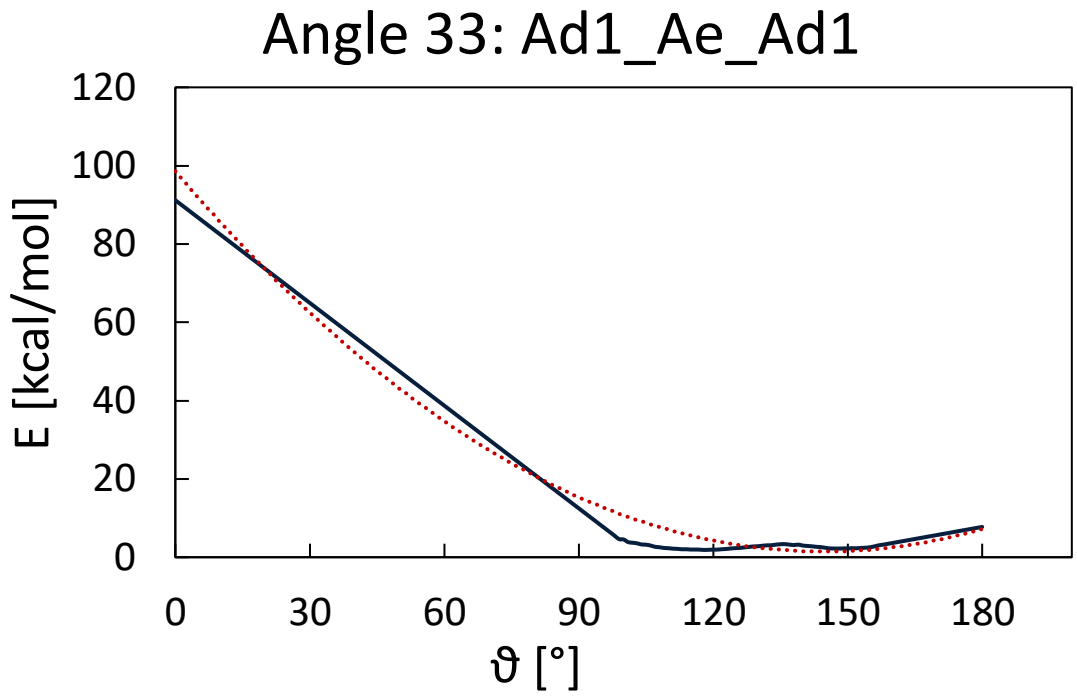
Angle 33: Ad1_Ae_Ad1
120
100
80
60
40
20
0
E [kcal/mol]
0
30
60
90
120
150
180
ϑ [°]

Non-Bonded potentials

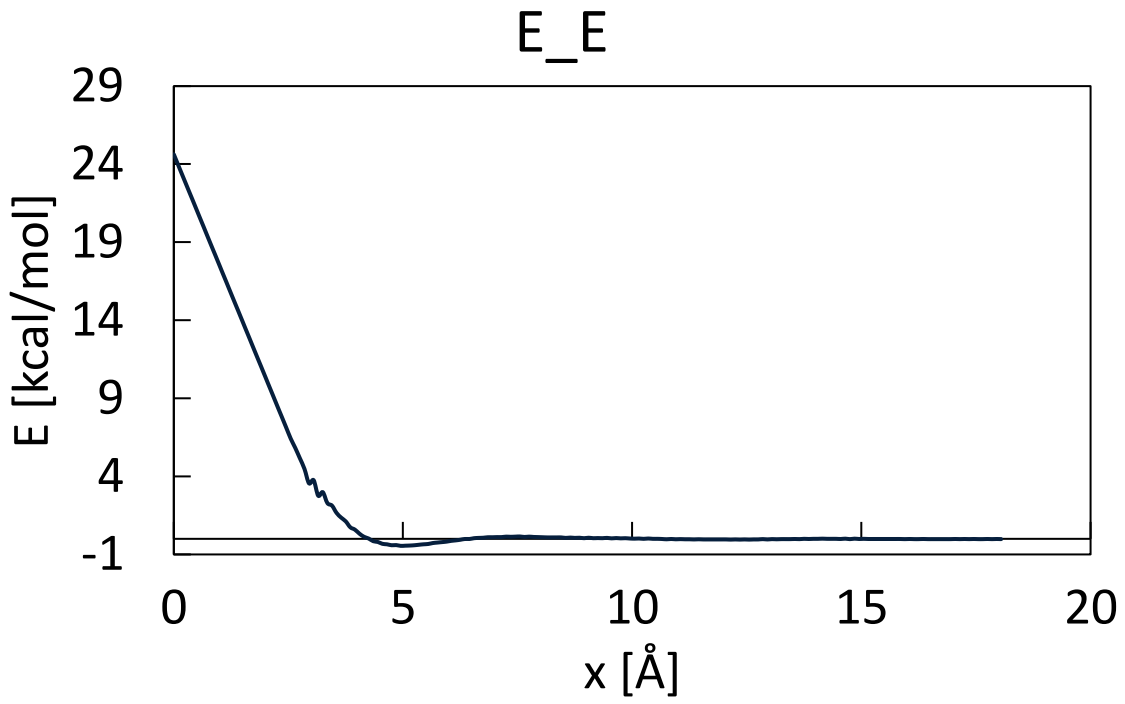

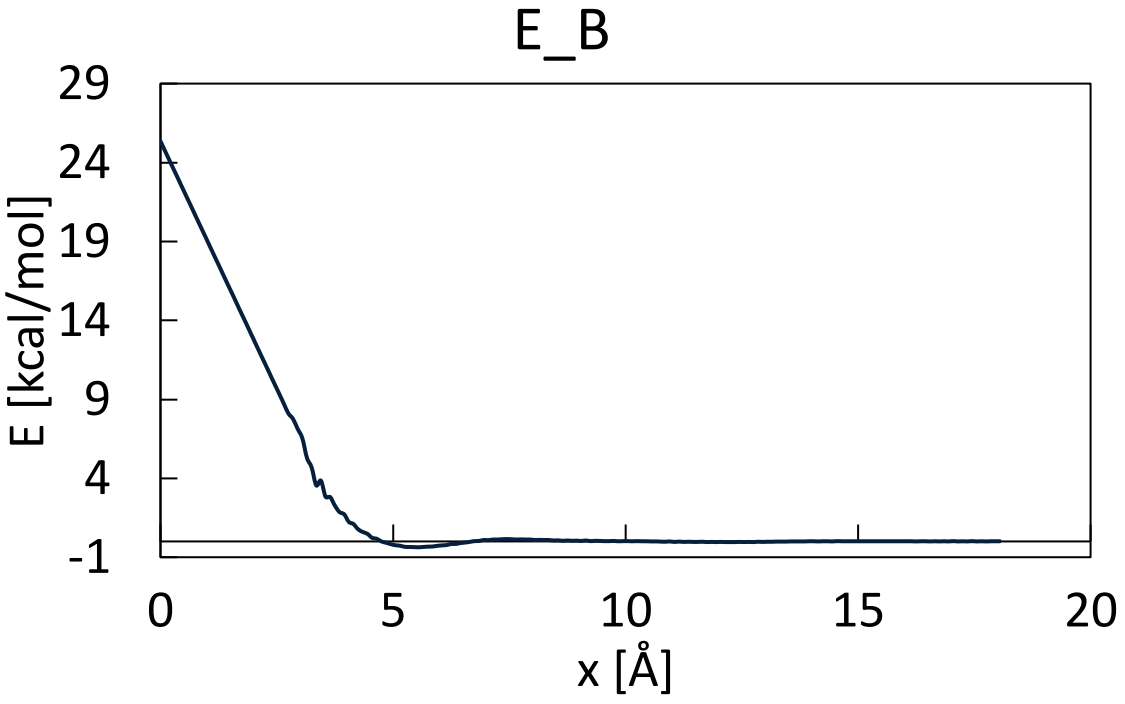

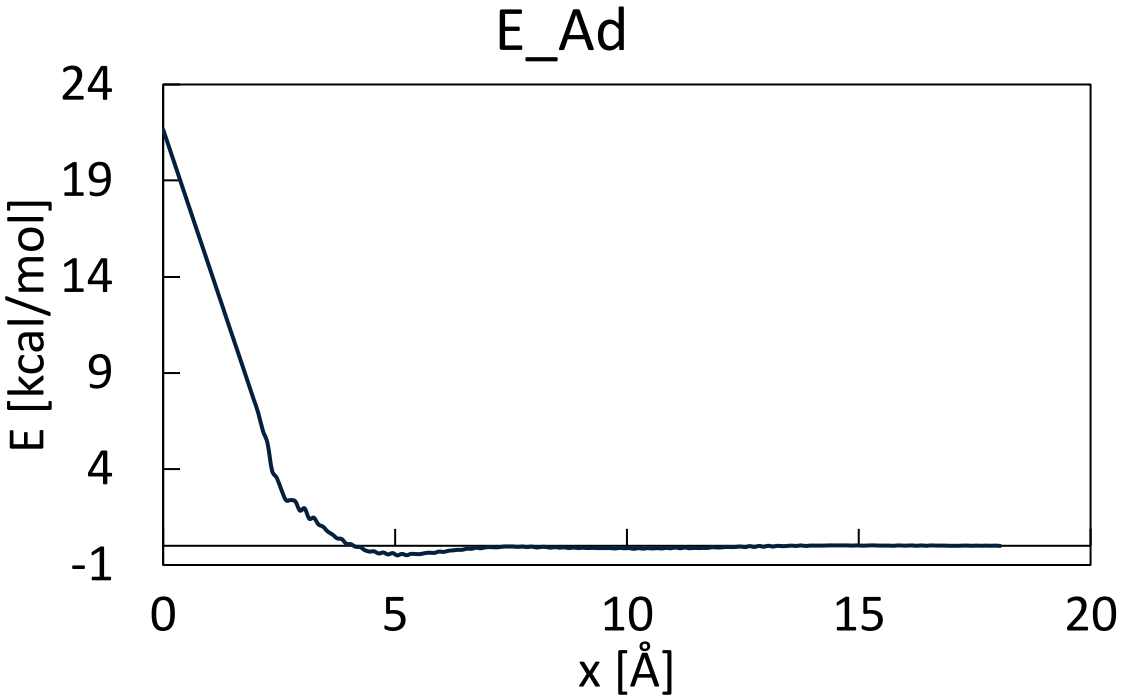
E_Ad
24
19
14
9
4
-1
E [kcal/mol]
0
5
10
15
20
x [Å]

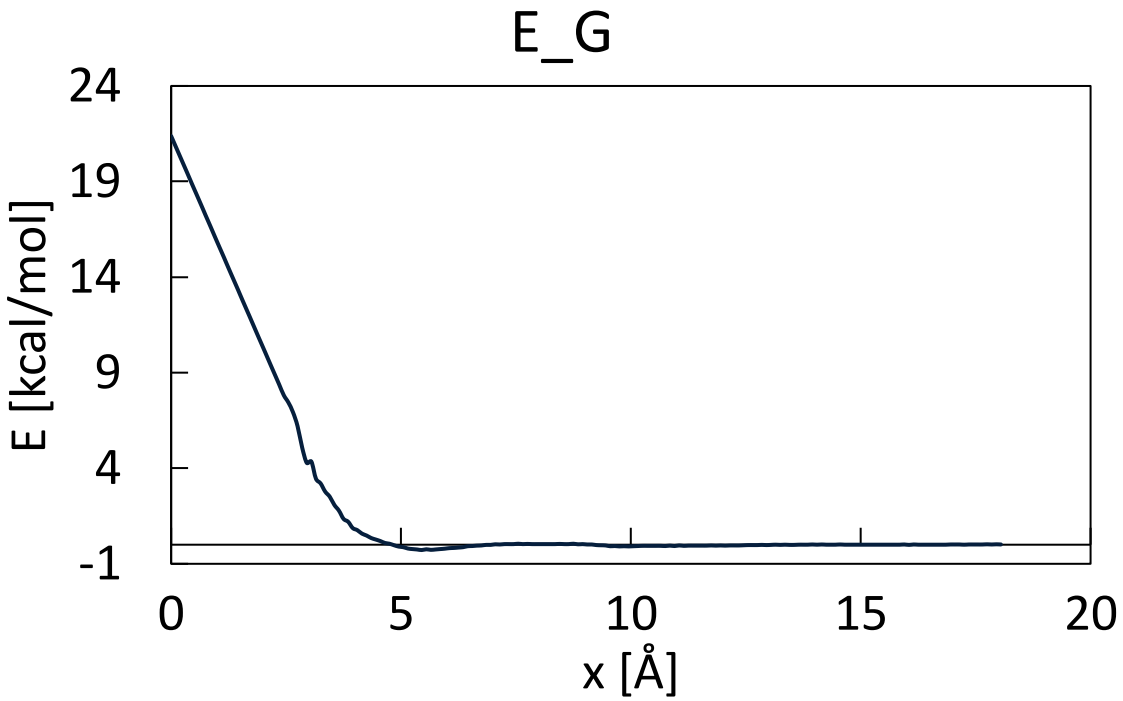
E_G
24
19
14
9
4
-1
E [kcal/mol]
0
5
10
15
20
x [Å]

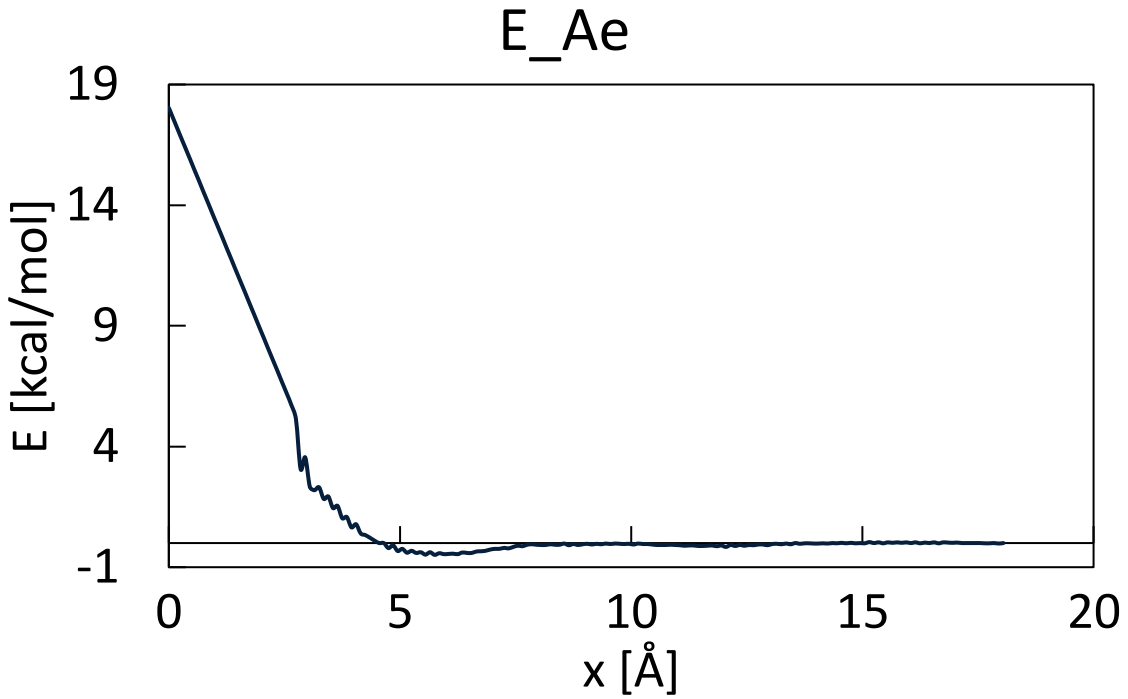
E_Ae
19
14
9
4
-1
E [kcal/mol]
0
5
10
15
20
x [Å]

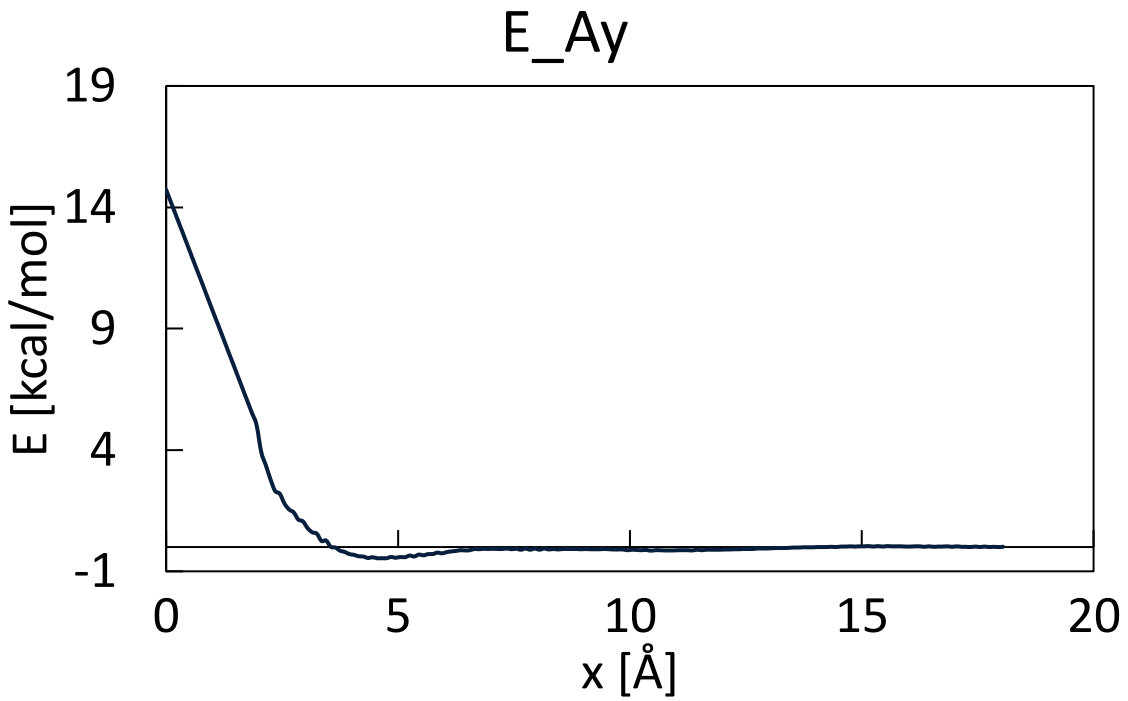
E_Ay
19
14
9
4
-1
E [kcal/mol]
0
5
10
15
20
x [Å]

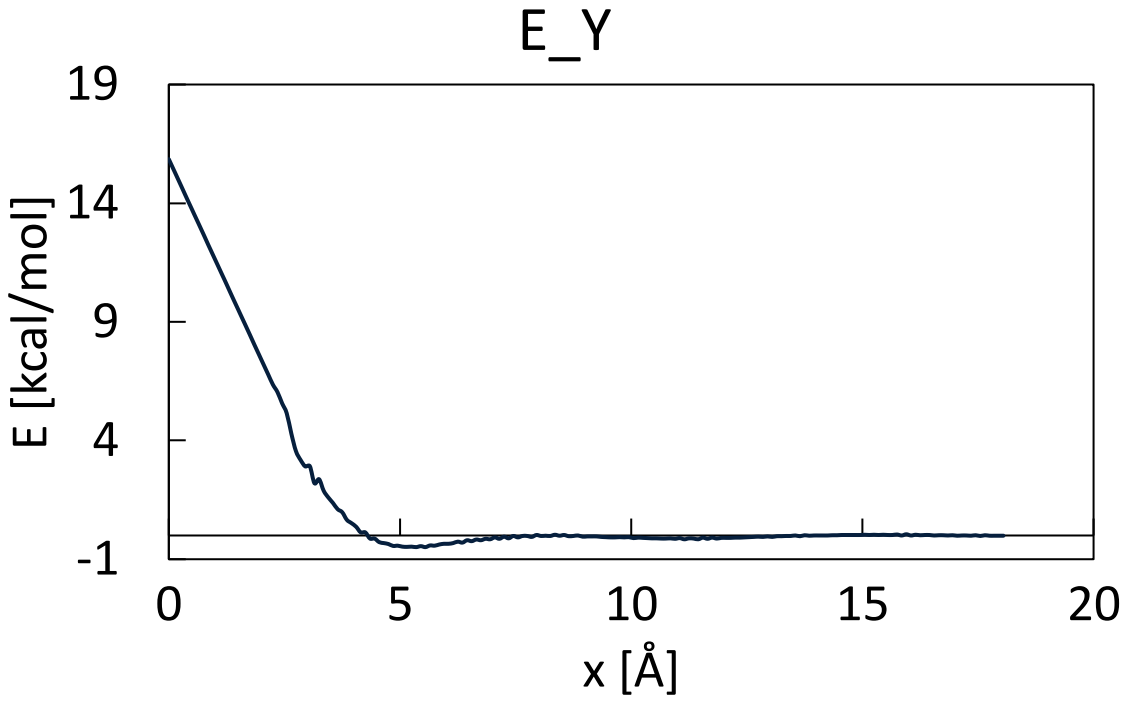
E_Y
19
14
9
4
-1
E [kcal/mol]
0
5
10
15
20
x [Å]

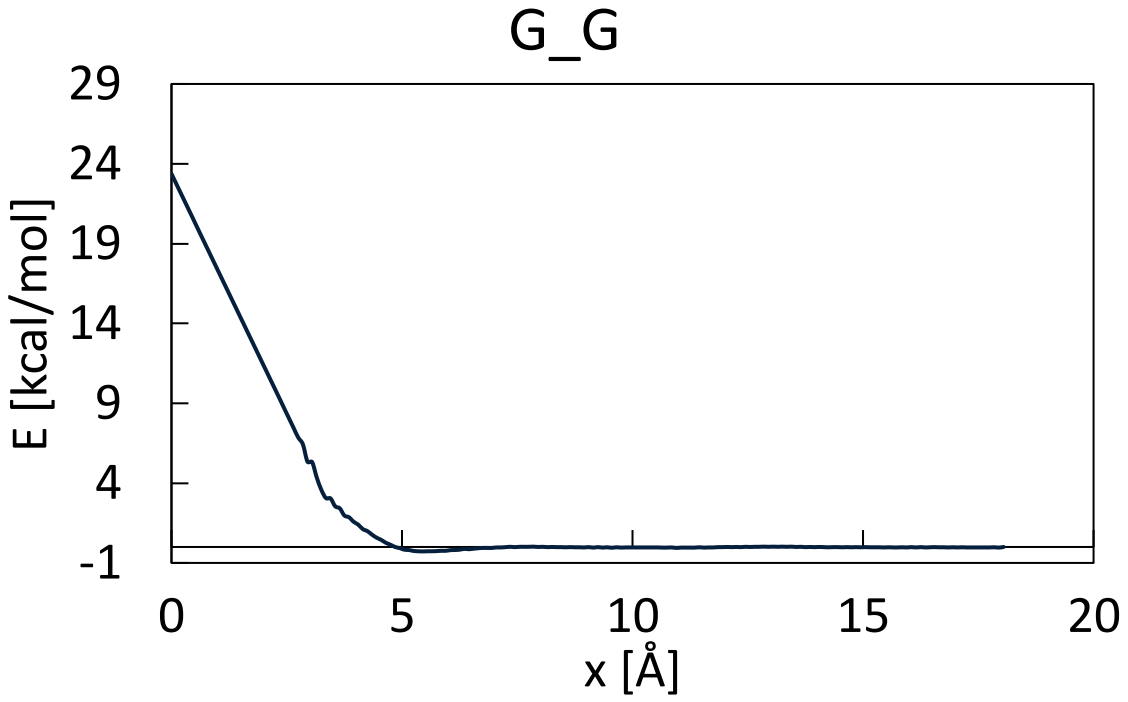
G_G
29
24
19
14
9
4
-1
E [kcal/mol]
0
5
10
15
20
x [Å]

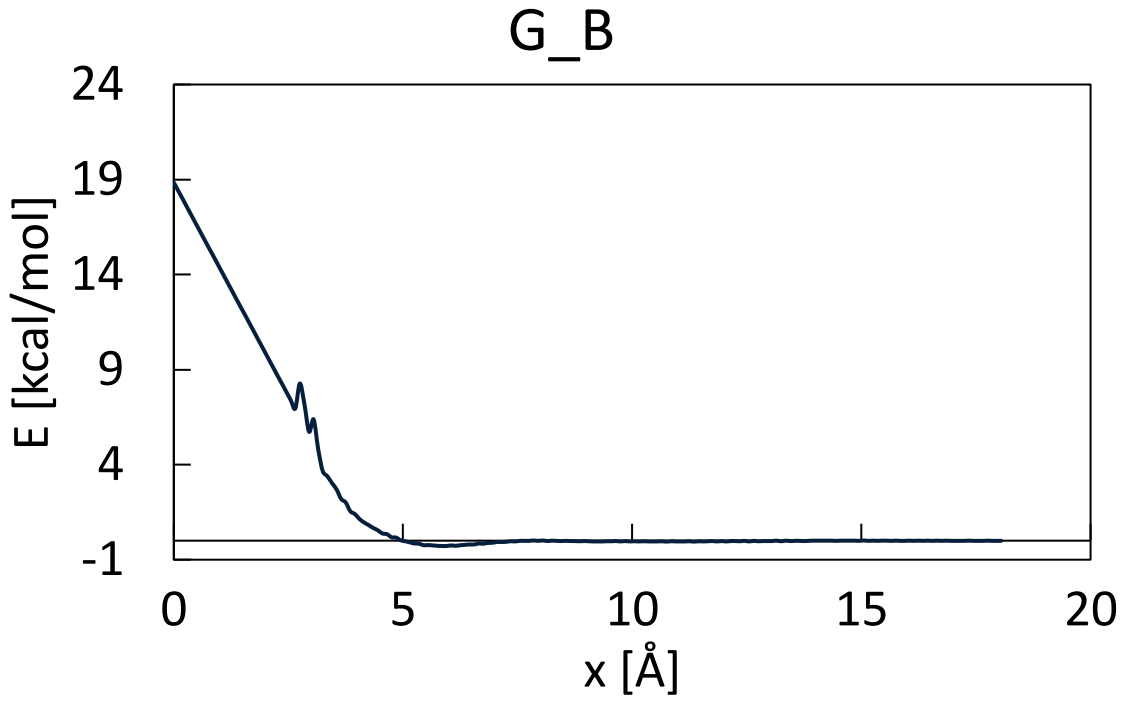
G_B
24
19
14
9
4
-1
E [kcal/mol]
0
5
10
15
20
x [Å]

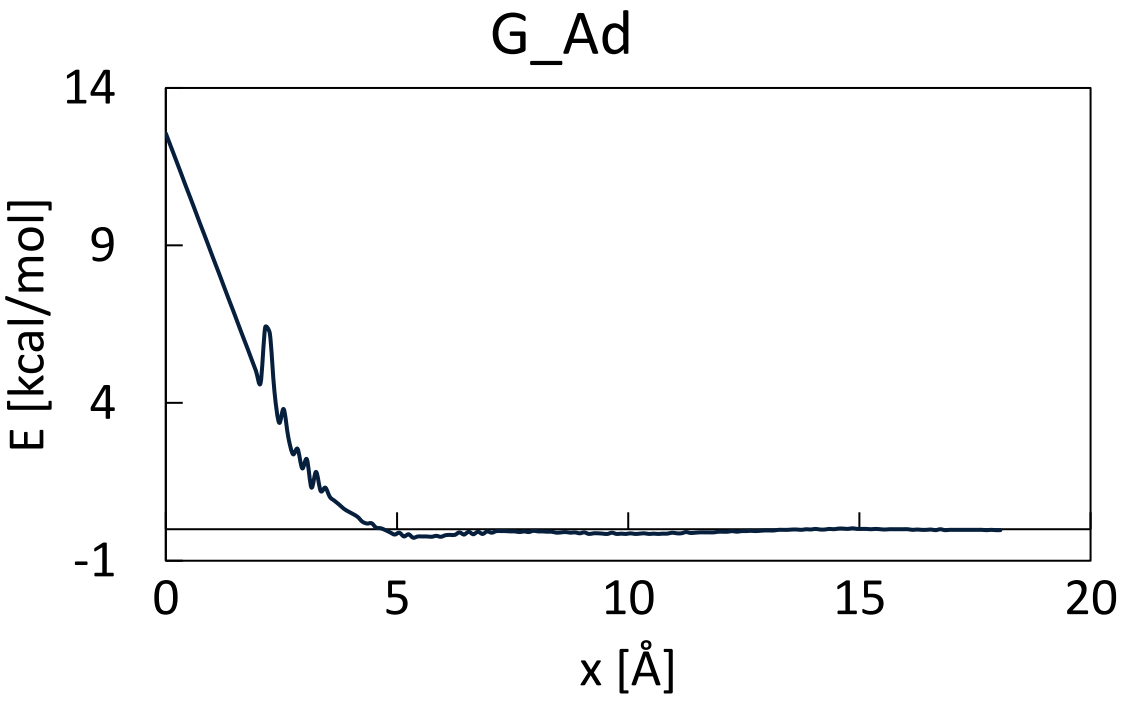
G_Ad
14
9
4
-1
E [kcal/mol]
0
5
10
15
20
x [Å]

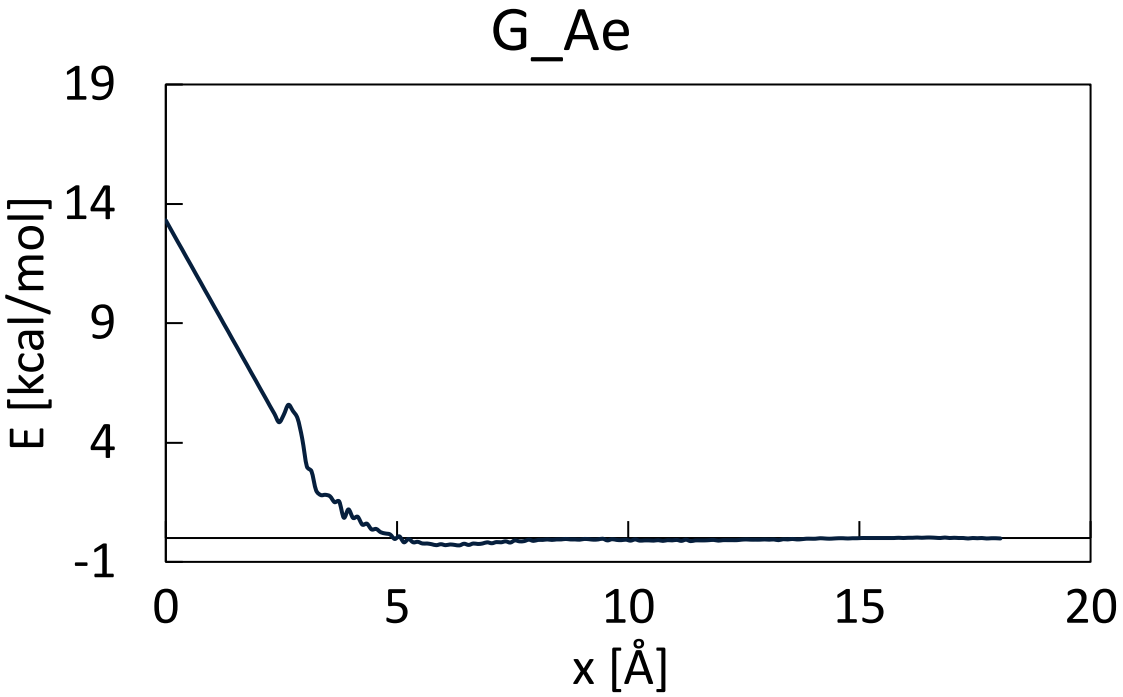
G_Ae
19
14
9
4
-1
E [kcal/mol]
0
5
10
15
20
x [Å]

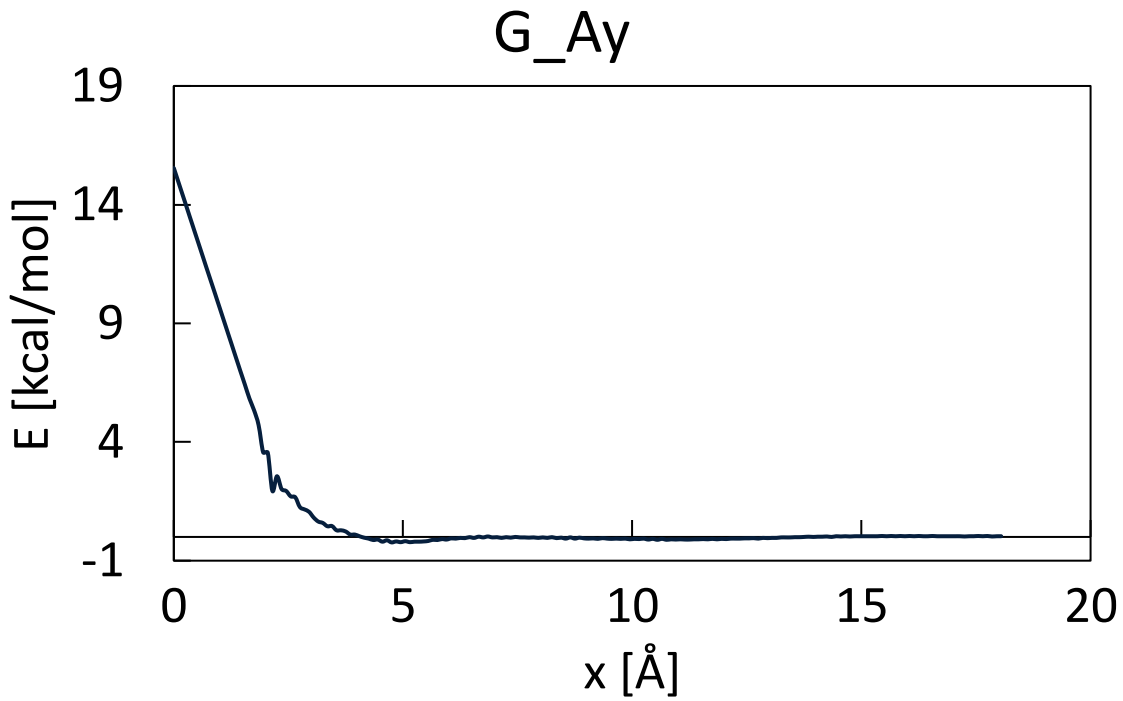
G_Ay
19
14
9
4
-1
E [kcal/mol]
0
5
10
15
20
x [Å]

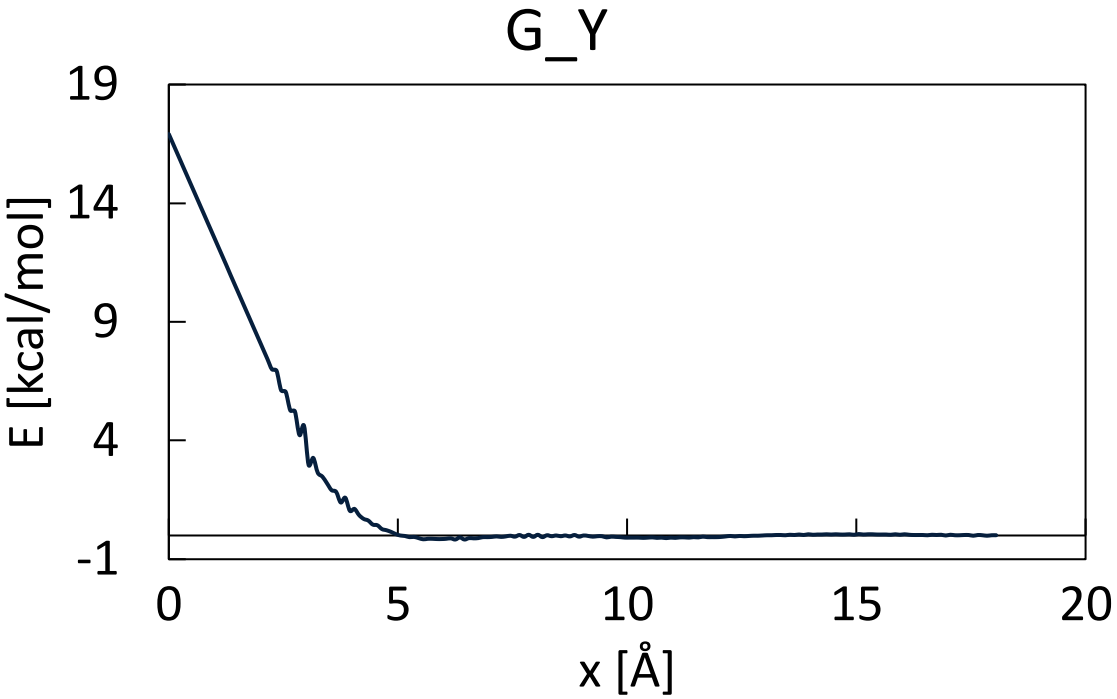
G_Y
19
14
9
4
-1
E [kcal/mol]
0
5
10
15
20
x [Å]

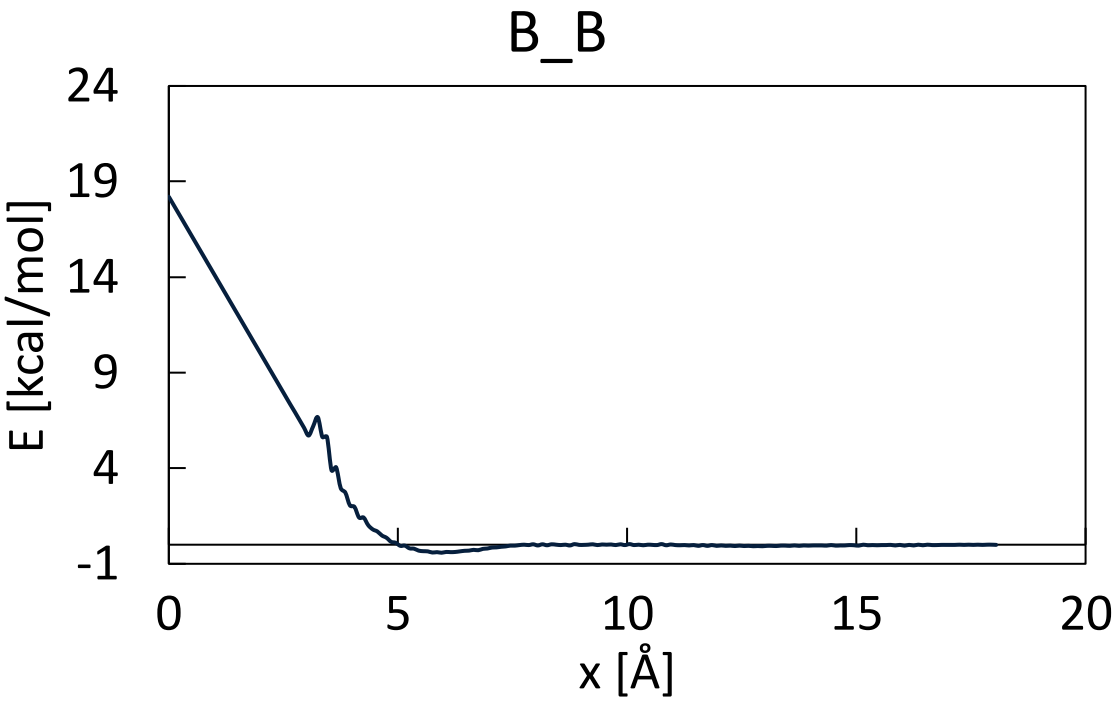
B_B
24
19
14
9
4
-1
E [kcal/mol]
0
5
10
15
20
x [Å]

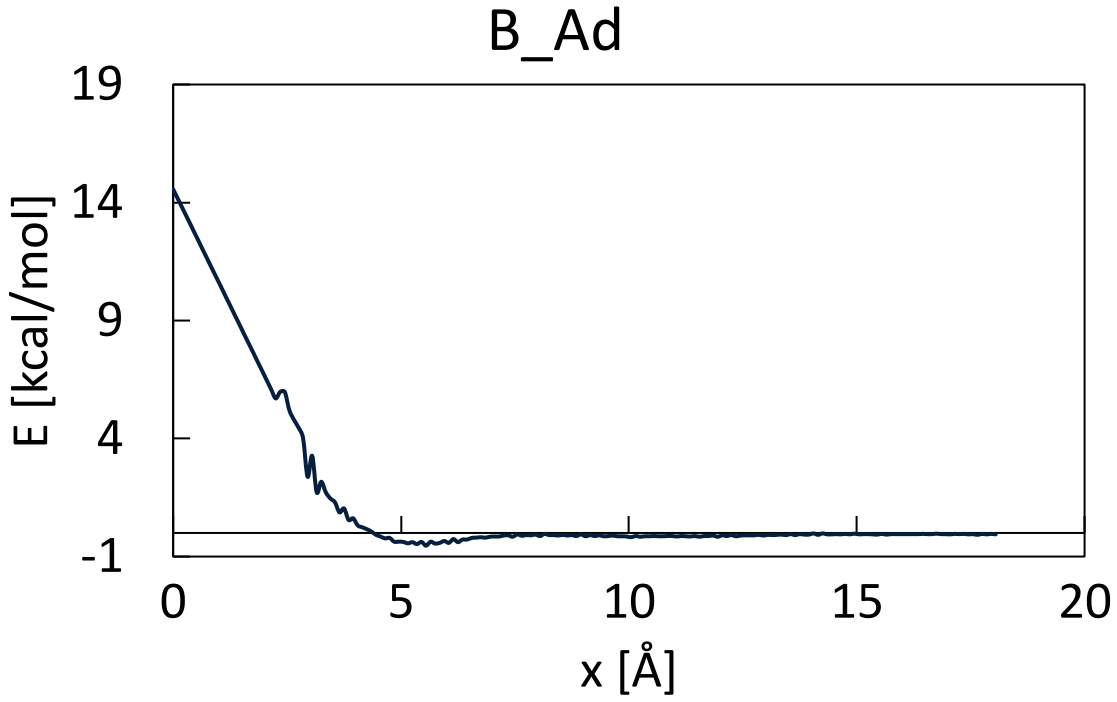
B_Ad
19
14
9
4
-1
E [kcal/mol]
0
5
10
15
20
x [Å]

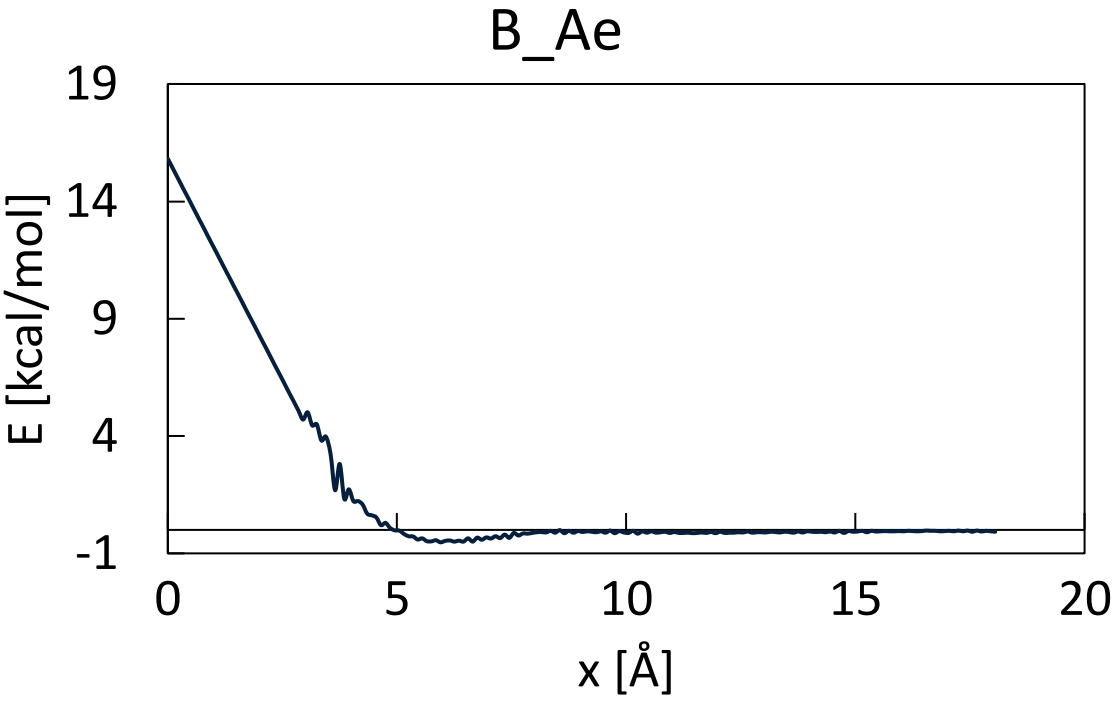
B_Ae
19
14
9
4
-1
E [kcal/mol]
0
5
10
15
20
x [Å]

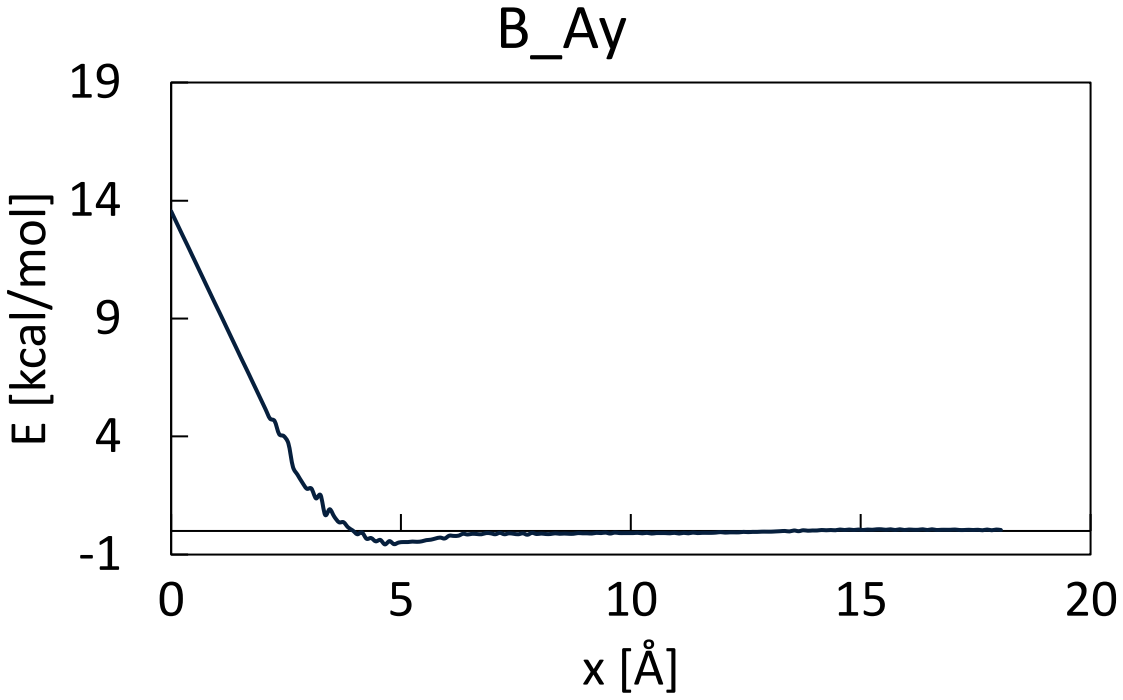
B_Ay
19
14
9
4
-1
E [kcal/mol]
0
5
10
15
20
x [Å]

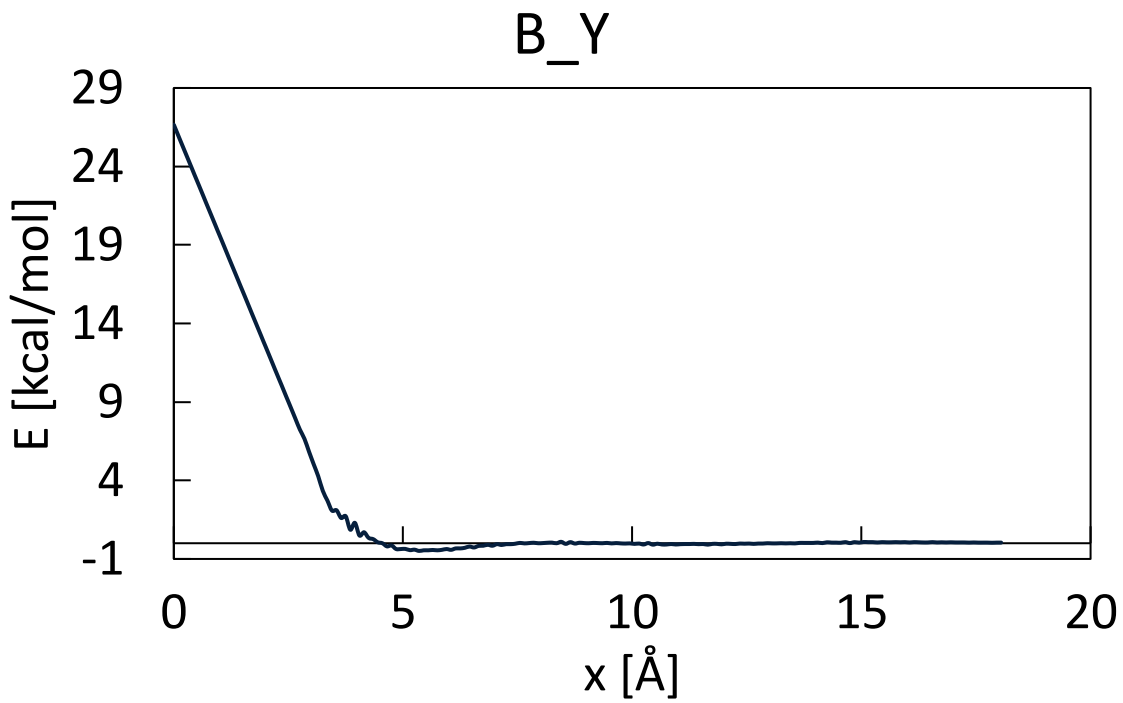
B_Y
29
24
19
14
9
4
-1
E [kcal/mol]
0
5
10
15
20
x [Å]

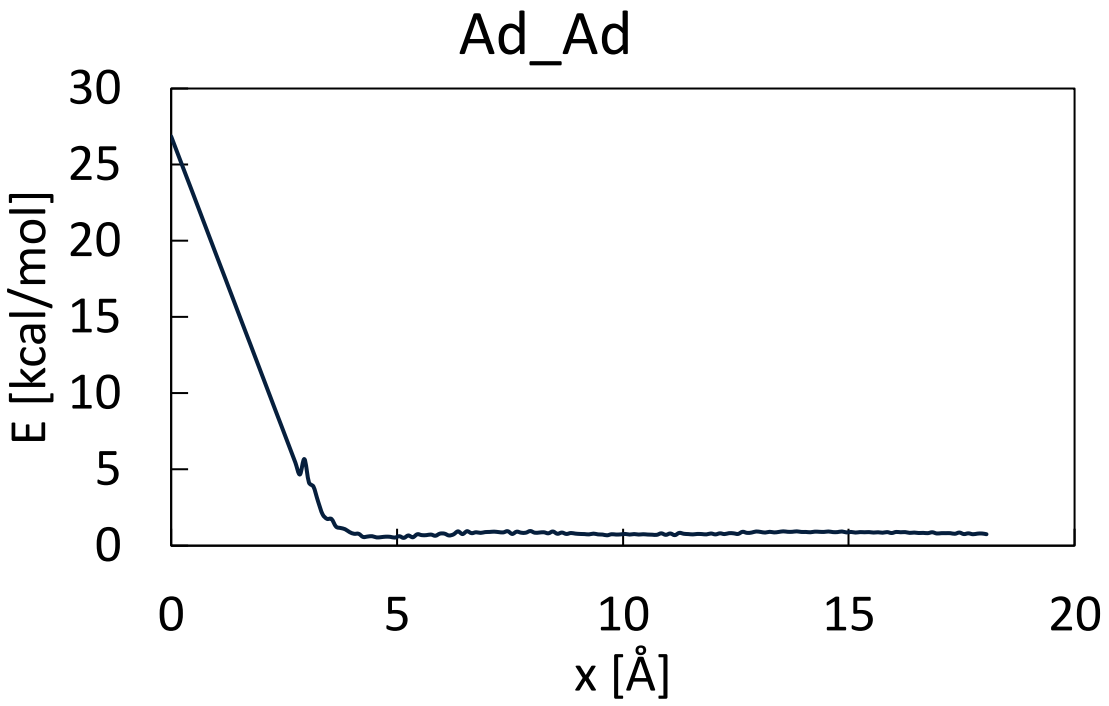
Ad_Ad
E [kcal/mol]
30
25
20
15
10
5
0
0
5
10
15
20
x [Å]

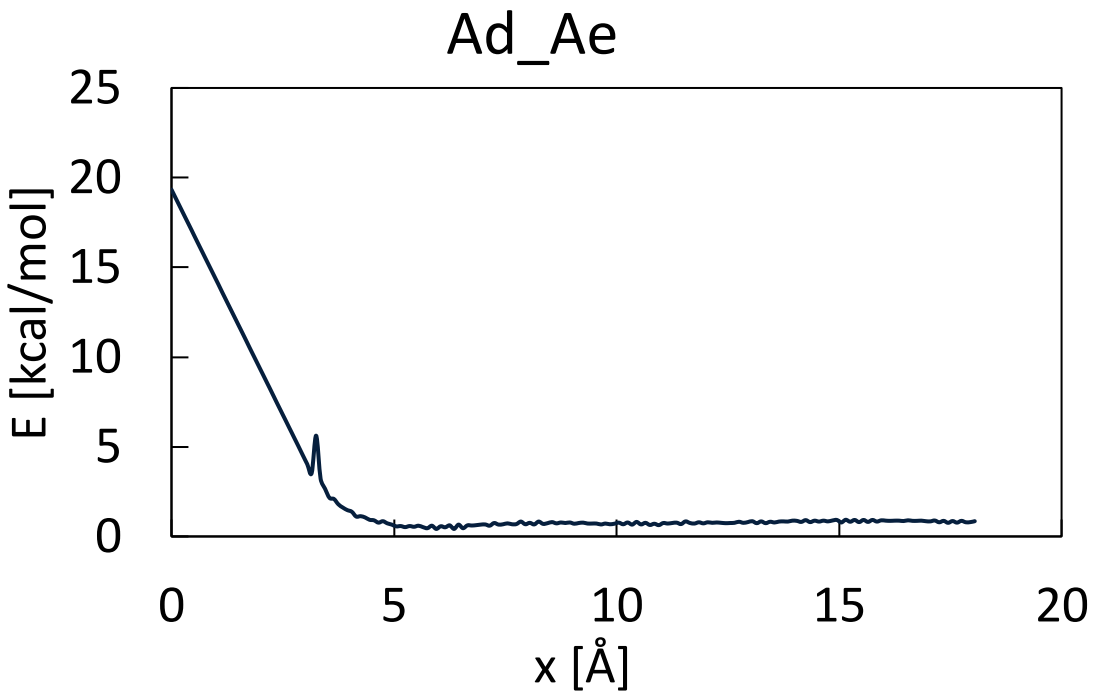
Ad_Ae
E [kcal/mol]
25
20
15
10
5
0
0
5
10
15
20
x [Å]

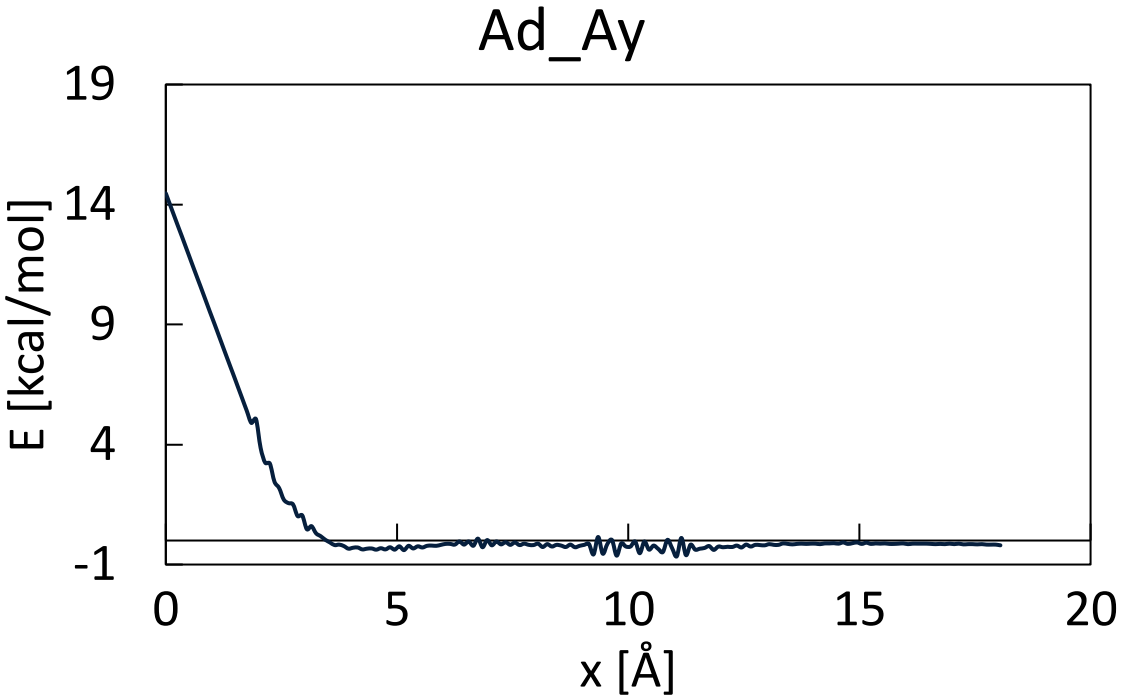
Ad_Ay
19
14
9
4
-1
E [kcal/mol]
0
5
10
15
20
x [Å]

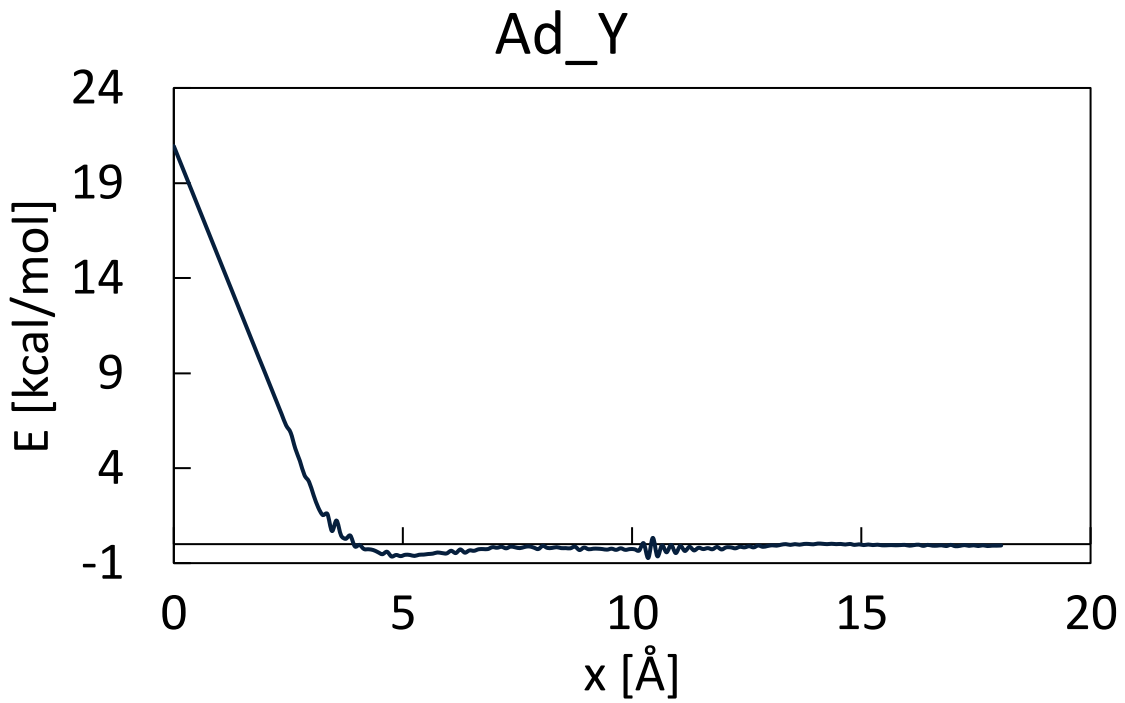
Ad_Y
24
19
14
9
4
-1
E [kcal/mol]
0
5
10
15
20
x [Å]

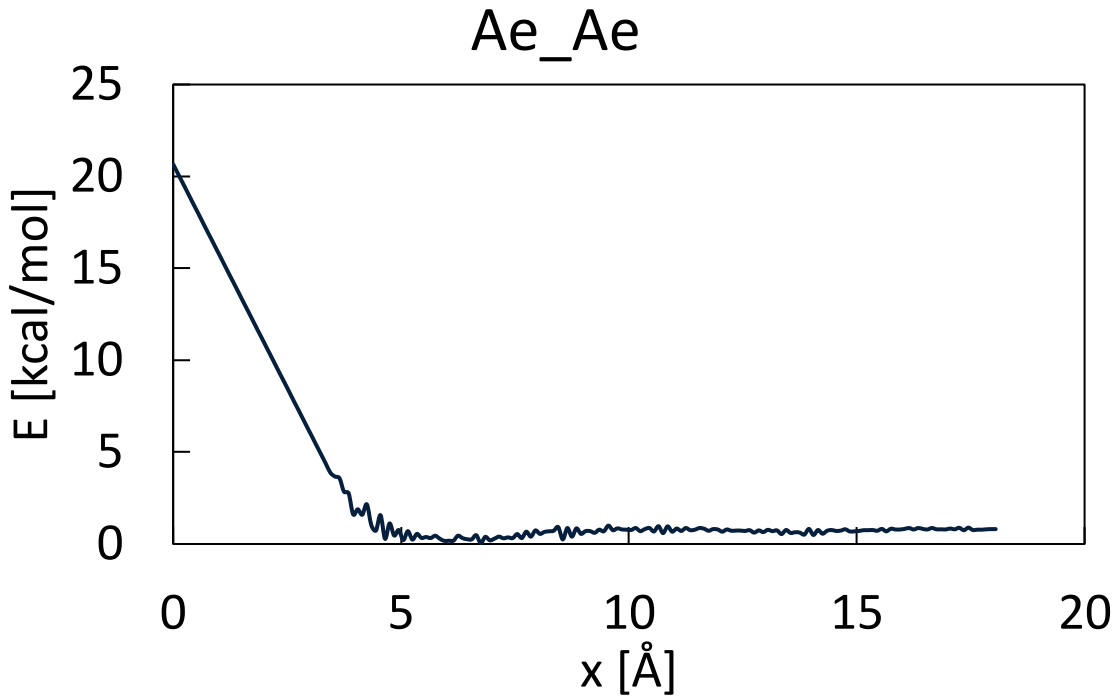
Ae_Ae
25
20
15
10
5
0
E [kcal/mol]
0
5
10
15
20
x [Å]

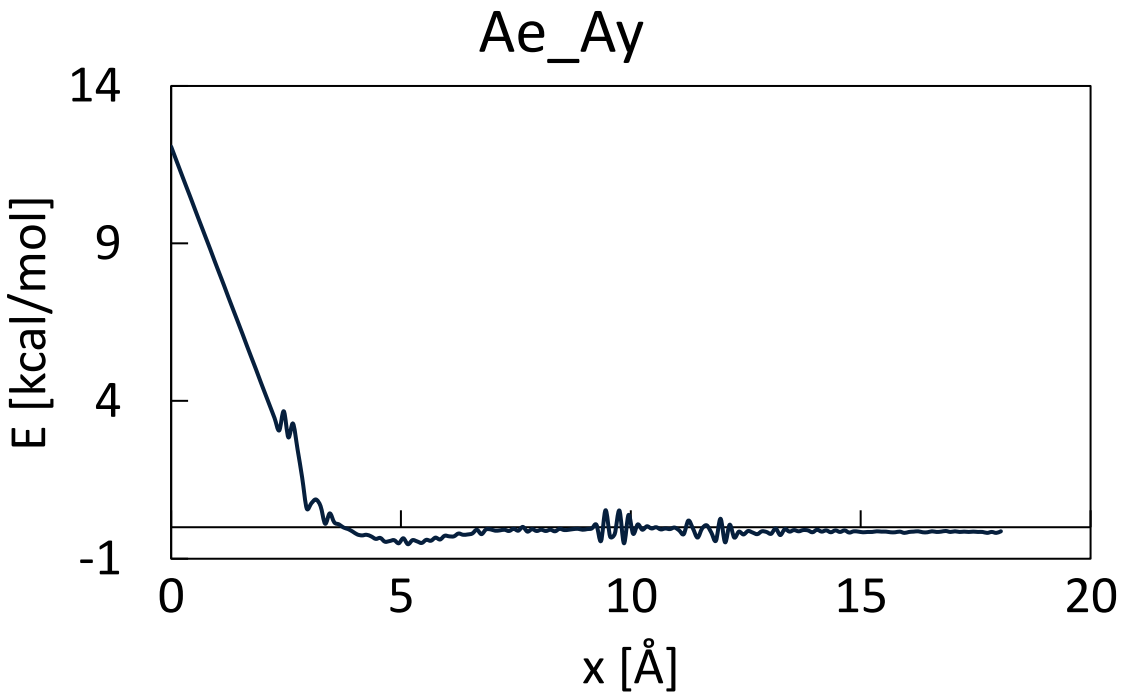
Ae_Ay
14
9
4
-1
E [kcal/mol]
0
5
10
15
20
x [Å]

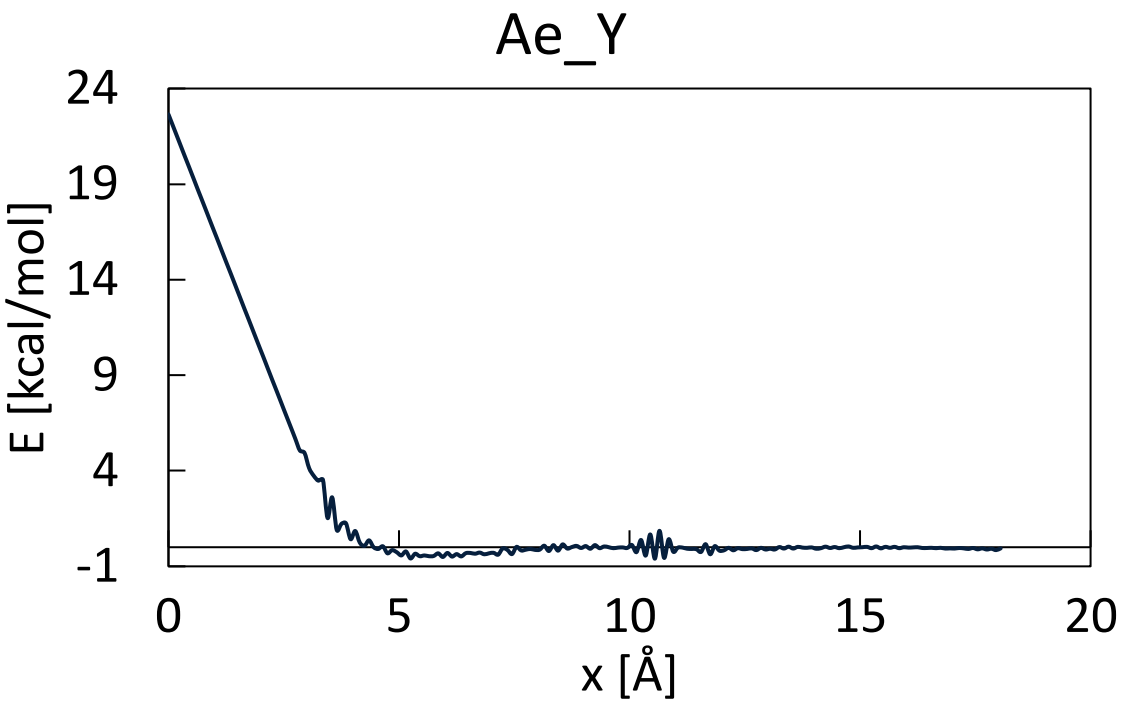
Ae_Y
24
19
14
9
4
-1
E [kcal/mol]
0
5
10
15
20
x [Å]

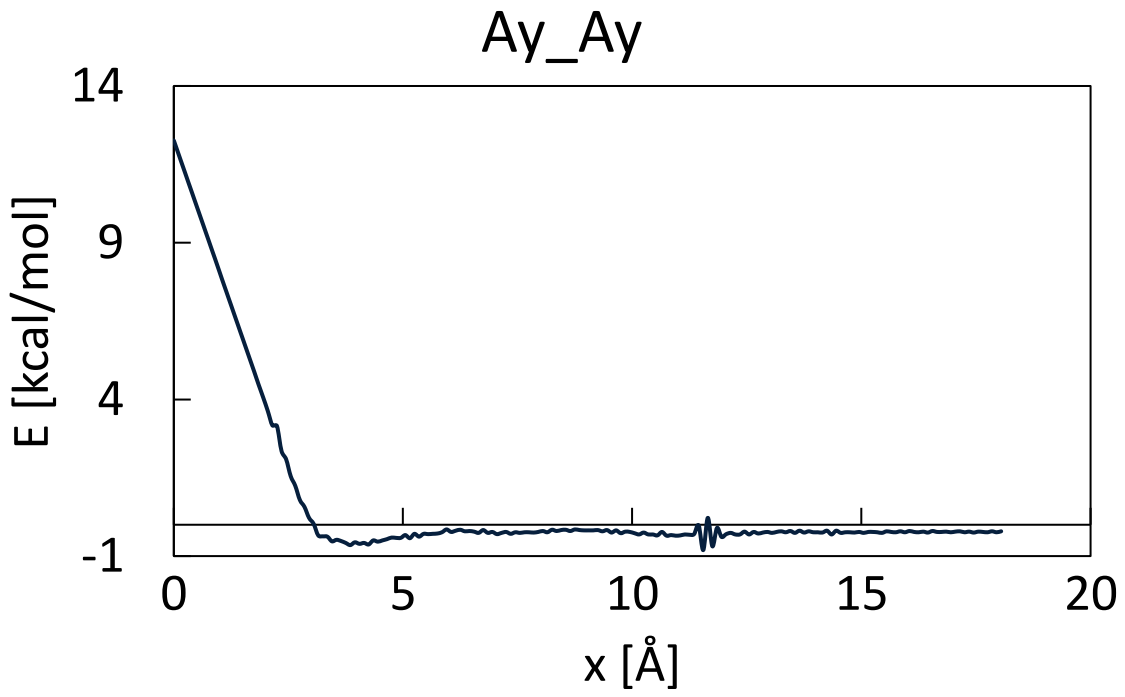
Ay_Ay
14
9
4
-1
E [kcal/mol]
0
5
10
15
20
x [Å]

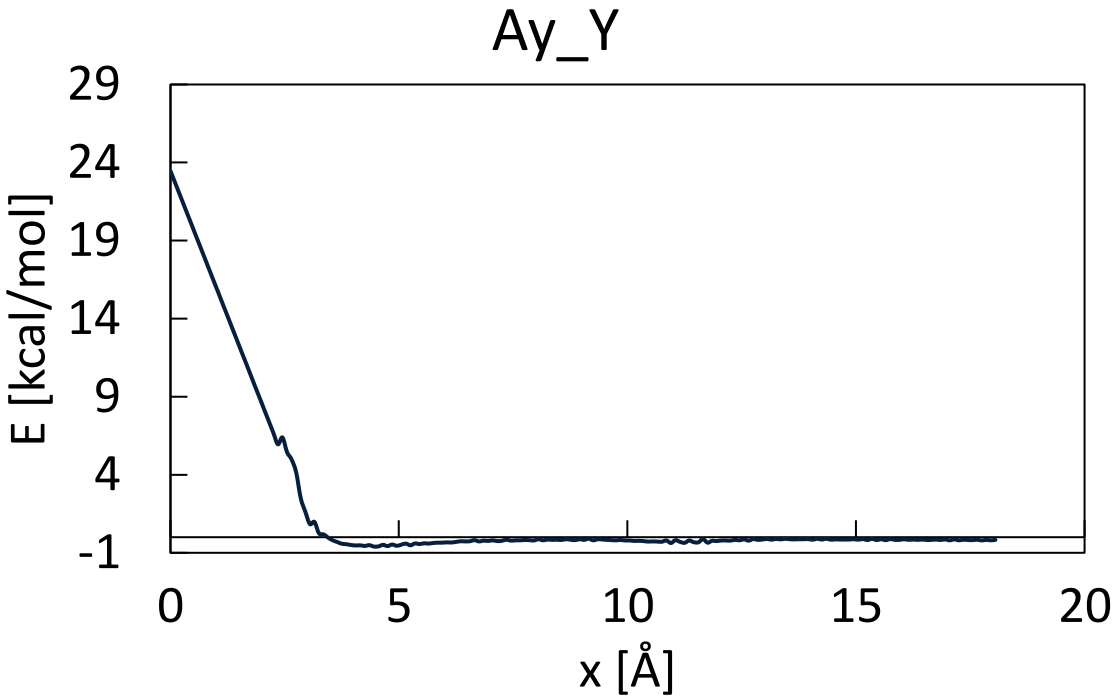
Ay_Y
E [kcal/mol]
29
24
19
14
9
4
-1
0
5
10
15
20
x [Å]

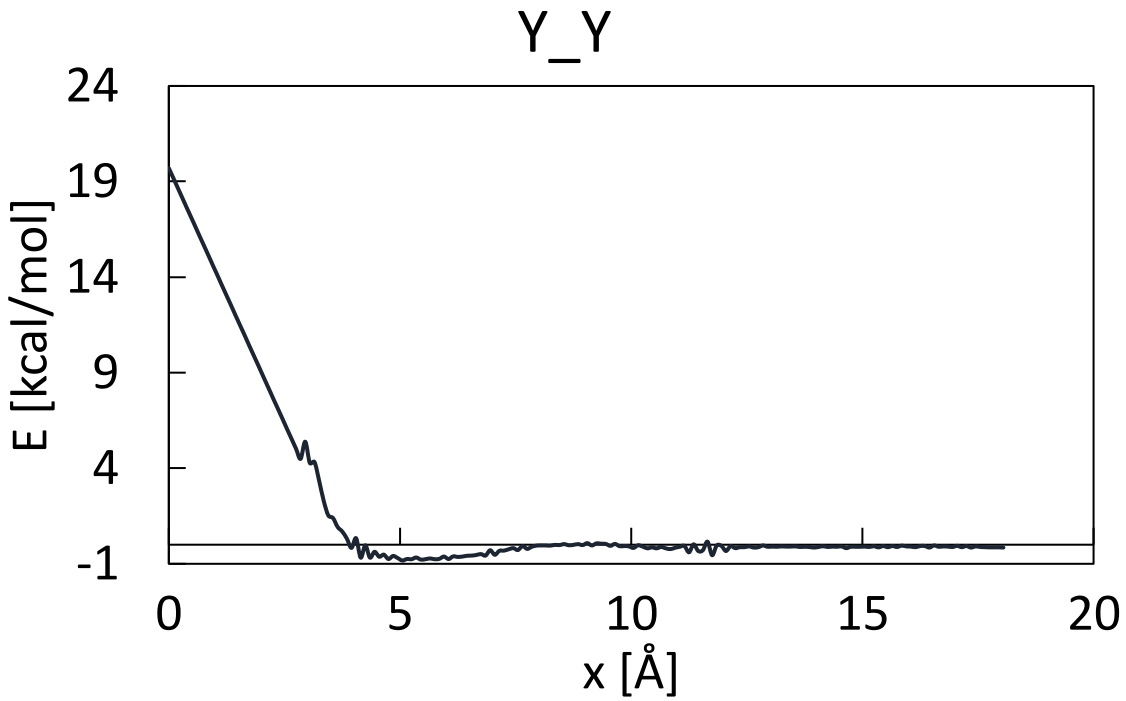
Y_Y
E [kcal/mol]
24
19
14
9
4
-1
0
5
10
15
20
x [Å]

APPENDIX B: IMPLEMENTED SCRIPTS

In this Appendix, all the scripts adopted in procedure P2 and in properties computation starting from P2 output system are reported and commented. LAMMPS files are classified in data files .data, potentials files .ff, and input scripts .in. MATLAB scripts are referred to as .m files.

.data: Data file example for 70% crosslinked system (LAMMPS)

```
#GENERAL INFORMATION

15092 atoms
13 atom types
12892 bonds
9 bond types
10942 angles
35 angle types

#SIMULATION BOX POSITION AND DIMENSIONS

0.0000000000000000e+00 2.1000000000000000e+02 xlo xhi
0.0000000000000000e+00 2.1000000000000000e+02 ylo yhi
0.0000000000000000e+00 2.1000000000000000e+02 zlo zhi

Masses

1 57.0727
2 92.0982
3 42.0813
```

```
4 30.0497

5 43.0688

6 16.0226

7 52.0357

8 58.0807

9 29.0418

10 28.0338

11 42.0609

12 15.0147

13 14.0067


Atoms

#bead_ID   molecule_ID   bead_type   charge[C]   x[Å]   y[Å]
z[Å]

2918      663   2       -0.16       96.56890151    54.1897918
            51.9084238

13642  3101  2       -0.16     56.91667976    68.79810647
4.73022135

13946       3170  10    -0.1654  27.62595337     95.96481963
1.16660421

14818       3367      2      -0.16       27.58485256
5.259186833          5.065285852

14819       3367      2  0.16    23.8209789        5.027667263
2.783143262

14862  3377     2      -0.16    48.15424764     1.820722277
7.718696327

14896  3385     2      -0.16    62.39491976     6.080959026
3.582710882

14897  3385     2       0.16    65.48467941     9.179668352
3.705540601

132       30     4       0       31.77968947     3.607415315
17.78529346

#[…] For all the system beads

14429       3279  7     0       143.8644348     154.7697929
209.8741433
```

```
Bonds
#bond_ID   bond_type   bead1_ID   bead2_ID
1    1    2918    2919
2    2    13642  13643
3    3    13946  13947
4    1    14818  14819
5     1   14862   14863
#[…] For all the system bonds
12892      2   10372        10373

Angles
#angle_ID   angle_type   bead1_ID   bead2_ID   bead3_ID
1    1    2917 2918 2919
2    19   13641     13642     13643
3    7    13947     13946     642
4    7    13947     13946     13583
5    25   642  13946     13583
#[…] For all the system angles
10942     21   14427     14429     14428
```

.ff: Main Force field potentials script (LAMMPS)

```
# EPO-CGff_deposit_forcefield.ff-----------------------------------
-------------------------
# Created by Carlos Saenz - ITAINNOVA for SMARTFAN H2020
# Type of force field: Coarse-grained (CG) force field developed
for epoy resin (EPO)
# -----------------------------------------------------------------
-------------------------
```

```
# BEADS MASSES

mass 1 57.07270
mass 2 92.09818
mass 3 42.08127
mass 4 30.04973
mass 5 43.06885
mass 6 16.02264
mass 7 52.03570
mass 8 58.08067
mass 9 29.04176
mass 10 28.03379
mass 11 42.06088
mass 12 15.01467
mass 13 14.00670

variable forcefield_nonbonded index EPO-CGff_non-bonded_forcefield

# BONDS

bond_style table linear 1000
bond_coeff 1 EPO-CGff_bond_forcefield.ff bondE_G
bond_coeff 2 EPO-CGff_bond_forcefield.ff bondG_B
bond_coeff 3 EPO-CGff_bond_forcefield.ff bondAd_Ae
#[…] For all the bond types
bond_coeff 9 EPO-CGff_bond_forcefield.ff bondE1_Ay2

# ANGLES

angle_style table linear 181
angle_coeff 1 EPO-CGff_angle_forcefield.ff angleE_G_B
```

```
angle_coeff 2 EPO-CGff_angle_forcefield.ff angleG_B_G
angle_coeff 3 EPO-CGff_angle_forcefield.ff angleAy_Y_Ay
#[..] For all the angle types
angle_coeff 35 EPO-CGff_angle_forcefield.ff angleAd2_Ae_Ad2

# NON-BONDED INTERACTIONS
pair_style table linear 1000 ewald
pair_coeff 1 1 ${forcefield_nonbonded}.ff E_E
pair_coeff 1 2 ${forcefield_nonbonded}.ff E_G
pair_coeff 1 3 ${forcefield_nonbonded}.ff E_B
[…] For all the non-bonded interactions types
pair_coeff 13 13 ${forcefield_nonbonded}.ff Ay_Ay

# LONG-RANGE INTERACTIONS SOLVER SETTINGS

kspace_style ewald 1e-4

# NEIGHBOR LISTS BUILDING SETTINGS

neighbor  2.260777 bin
pair_modify    shift no tail yes
special_bonds  lj/coul 0.0 0.0 1.0
```

bond.ff: Bond potentials script (LAMMPS)

```
# EPO-CGff_bond_forcefield.ff-------------------------------------
----------------------
# Created by Carlos Saenz - ITAINNOVA for SMARTFAN H2020
# Coarse-grained (CG) force field developed for EPO
```

```
# ------------------------------------------------------------------
---------------------------------

bondE_G   # type 1
N 172 FP -55.13029 148.24704 EQ 4.395

1    0    34.363 8.3088
2    3.285     7.0693    8.3088
3    3.295     6.9862    8.3088
#[…]  For all type 1 bond lengths
172  10.5 31.6086   -4.5390


bondG_B  # type 2
N 74 FP -530.3260 30.3405 EQ 3.895

1    0       112.3413    29.1071
2    3.635     6.5370    29.1071
3    3.645     6.2459    29.1071
#[…] For all type 2 bond lengths
74   10   486.6019  -82.2216

#[…] For all bond types

bondE1_Ay2   # type 9
N 96 FP -16.8253 87.4299 EQ 2.575

1    0    111.5942  50.5199
2    2.075     6.7655    50.5199
3    2.085     6.2603    50.5199
#[…] For all bond type 9 bond lengths
96   10   125.2464  -16.8253
```

angle.ff: Angle potentials script (LAMMPS)

```
# EPO-CGff_angle_forcefield.ff-------------------------------------
------------------------

# Created by Carlos Saenz - ITAINNOVA for SMARTFAN H2020

# Type of force field: Coarse-grained (CG) force field developed
for EPO

# ----------------------------------------------------------------
---------------------------------


angleE_G_B    # type 1

N 181 FP -0.06402 0.00402


1    0    28.1930   0.1718

2    1    28.0211   0.1718

3    2    27.8493   0.1718

#[…] For all type 1 angles potentials

181  180  3.2726    -0.4140


angleG_B_G    # type 2

N 181 FP -0.084755 -0.01633


1    0    663.8788  27.1067

2    1    637.1929  26.2682

3    2    611.3366  25.4474

#[…] For all type 2 angle potentials

181  180  543.2323  -23.3585


#[…] For all angle types
```

```
angleAd2_Ae_Ad2    # type 35
N 181 FP -0.22341 0.0000

1    0    63.0533   0.5698
2    1    62.4834   0.5698
3    2    61.9136   0.5698
#[…] For all type 35 angle potentials
181  180  76.9416   -4.5698
```

non_bonded.ff: Non-bonded potentials script (LAMMPS)

```
# EPO-CGff_non-bonded_forcefield.ff-----------------------------
----------------------------
# Created by Carlos Saenz - ITAINNOVA for SMARTFAN H2020
# Type of force field: Coarse-grained (CG) force field developed
for EPO
# Rcutoff: 18.05 A
# -------------------------------------------------------------
----------------------------------------



E_E
N    180

1    0.00000001     24.631    7.14
2    0.25 22.84     7.14
3    0.35 22.13     7.14
#[…] For all E_E non-bonded interactions
180  18.05     -0.02     0.14

E_G
```

```
N    180

1    0.00000001     21.3795   5.53
2    0.25 20   5.53
3    0.35 19.45     5.53
#[…] For all E_G non-bonded interactions
180  18.05     0.01 0.11

#[…] For all non-bonded interactions

Y_Y
N    180

1    0.00000001     19.701    5.34
2    0.25           18.37     5.34
3    0.35           17.85     5.34
#[…] For all Y_Y non-bonded interactions
180  18.05     -0.15     0.13
```

deposit.in: Initial deposition script (LAMMPS)

```
# deposit_region_300K.IN-----------------------------------------
-----------------
# this file was generated by Carlos Saenz ITAINNOVA for SMARTFAN
H2020
#--------------------------------------------------------------
----------

units     real                          # It is a predefined set of
units of measure
```

```
atom_style     full            # Each particle is characterized by
mass and partial charge

boundary  p p p         # Periodic boundary conditions in each
direction


# DEPOSITION REGION INFORMATION


region box block 0.0 25.0 0.0 25.0 0.0 25.0

create_box 13 box bond/types 9 angle/types 35 dihedral/types 0
improper/types 0 extra/bond/per/atom 50 extra/angle/per/atom 50
extra/dihedral/per/atom 50 extra/special/per/atom 100


include EPO-CGff_deposit_forcefield.ff  #Force Fieald acquisition



# MOLECULES DEFINITION


molecule dgeba CG-DGEBA.molecule

molecule dicy CG-DICY.molecule

molecule deta CG-DETA.molecule


# INITIAL SEED FOR KSPACE SOLVER

# Deposition of the first particle is needed by LAMMPS to
initialize the simulation

create_atoms 0 random 1 10 box mol dgeba 10 units box


# SIMULATION SETTINGS AND OUTPUT CUSTOMIZATION


timestep  1.0

thermo_style   custom step time etotal pe ke temp press

thermo    10

thermo_modify   norm no lost/bond ignore

atom_modify    sort 10 1000
```

```
# DEPOSITION
# it deposits N molecules, one every 10 steps, with the specified random seed (e.g 237 for DGEBA) in the       # specified nearby of existing particles

fix dgeba all deposit 6 0 10 237 mol dgeba near 3.0 region box
run 20000
unfix dgeba

fix dicy all deposit 2 0 10 138 mol dicy near 3.0 region box
run 10000
unfix dicy

fix deta all deposit 1 0 10 678 mol deta near 3.0 region box
run 10000
unfix deta

#OUTPUT FILES

write_data Epoxy.data nocoeff
```

change.in: Replication and equilibration of the initial sample (LAMMPS)

```
units     real                        # It is a predefined set of units of measure
atom_style     full          # Each particle is characterized by mass and partial charge
boundary  p p p      # Periodic boundary conditions in each direction
```

```
read_data Epoxy.data     # System data file acquisition
replicate 7 7 7                  # Replication of the system for
7 times along x, y and z directions

# FORCE FIELD

include EPO-CGff_deposit_forcefield.ff

# SIMULATION SETTINGS AND OUTPUT CUSTOMIZATION

comm_modify cutoff 18.0  # Inter-processors communication settings
thermo_style custom time step etotal pe ke press temp density
#output on screen
thermo 100     # frequency of the output on screen
thermo_modify norm no

timestep 1.0

#EQUILIBRATION

fix NVEall all nve  # Time integration in micro-canonical ensemble
run 20000
unfix NVEall

fix NVTall all nvt temp 700 700 100
# Time integration in canonical ensemble at 700 K with 100 as
damping factor
run 50000
unfix NVTall

fix NPTall all npt temp 400 400 100 iso 1 1 1000
```

```
# Time integration in isobaric-isothermal ensemble at 400 K with
100 as damping factor and isostatic pressure of 1 atm with 1000 as
damping factor

run 20000

unfix NPTall


# OUTPUT FILES


write_data Epoxy777.data
```

crosslinking.in: Crosslinking algorithm (LAMMPS)

```
# EPO-CGff_cross-linking.in-----------------------------------------
-------------------------

# This file was generated by Carlos Saenz/Francesco Bellussi for
ITAINNOVA H2020 SMARTFAN

# Bonding of atoms thorugh bonds and angles

# NEED EXTRA BONDS, ANGLES, DIHEDRALS AND SPECIAL BONDS OF 20

# Works with CGloop.mod file

# -----------------------------------------------------------------
-------------------------


units     real                        # It is a predefined set of
units of measure

atom_style     full          # Each particle is characterized by
mass and partial charge

boundary  p p p       # Periodic boundary conditions in each
direction

read_data Epoxy777.data extra/bond/per/atom 30 extra/angle/per/atom
30 extra/dihedral/per/atom 30 extra/improper/per/atom 30
extra/special/per/atom 100

# System data acquisition, with extra bonds, angles and dihedrals
for post-crosslinking configuration
```

```
# INPUT VARIABLES


variable degree equal [INSERT]      # define cross-linking degree
(below 1.0)
variable bond0 equal [INSERT]      # define number of initial bonds
in system (total)
variable points equal [INSERT]     # define number of epoxy rings
(type 1 beads) in system


variable ncut equal 6.75
# Defines the radius within reactive beads will look for other
reactants , it has been optimized by performing a sensitivity
analysis on the maximum crosslinking degree achievable


# FORCE FIELD


include EPO-CGff_forcefield.ff    #Force Field acquisition


# SIMULATION SETTINGS AND OUTPUT CUSTOMIZATION


atom_modify    sort 1 1000   # Processors performance settings


timestep  0.5
thermo_style   custom step time etotal pe ke temp press density
#Output on screen
thermo    100  # Frequency of output on screen
thermo_modify  norm no
thermo_modify lost ignore flush yes
comm_modify cutoff 18.0  # Inter-processors communication settings


# INITIAL VELOCITIES


velocity     all create 300 10000 rot yes dist gaussian mom yes
```

```
#Creates an initial velocity profile according #to a normal
distribution


# INITIAL EQUILIBRATION


fix equi all nvt temp 300.0 300.0 100.0

# Time integration in canonical ensemble at 700 K with 100 as
#damping factor


run 5000

unfix equi

reset_timestep 0


# COMPUTE BONDING


compute bonds all property/local btype batom1 batom2  #stores
system bonds


# DUMP OUTPUTS


dump snaps1 all custom 1000 CLsnaps.dump id mol type q x y z

 #provides snaps of the crosslinking process, 1 each 1000 steps


# BONDING


compute sum all reduce sum c_bonds[1]

compute ave all reduce ave c_bonds[1]

variable tbonds equal "c_sum/c_ave"

variable cdegree equal "(v_tbonds-v_bond0)/v_points"
#Calculation of crosslinking degree


fix  degree all ave/time 1 1 1 v_cdegree v_tbonds ave one file
degree.dump
```

```
#Provides CL degree time #evolution
run 1

label loop  #Enters in crosslinking loop
run 1
if "${cdegree} < ${degree}" then "jump CGloop.mod loop"
if "${cdegree} > ${degree}" then "jump SELF break"

label break   #Ends crosslinking loop

# CHARGES UPDATE
#Updates the partial charge of reacted beads from type 8 to type
13

set type 8 charge 0.2427 #E1
set type 9 charge -0.0827 #Ad1
set type 10 charge -0.1654 #Ad2
set type 11 charge -0.0827 #Ae1
set type 12 charge -0.0827 #Ay1
set type 13 charge -0.1654 #Ay2

#OUTPUT FILES

write_data end_state.out nocoeff
print "Curing process has finished correctly"
```

CGloop.mod: Crosslinking loop, part of crosslinking.in (LAMMPS)

```
# CGloop.mod-----------------------------------------------------
# This file is opened from EPO-CGff_cross-linking.in
```

```
# Several bonding steps are produced consecutively --> bonding +
NVT
# ----------------------------------------------------------------


label loop


# BONDING
#It perform one bond per type from type 5 to 9, within ncut radius
and updates the involving beads type, but NOT the angles, then
minimizes the energy of the system
fix bond5 all bond/create 1 1 4 ${ncut} 5 iparam 1 8 jparam 1 9
atype 2
run  1
minimize  0.0 1e-10 10000 10000
unfix bond5


fix bond6 all bond/create 1 1 9 ${ncut} 6 iparam 1 8 jparam 1 10
atype 2
run  1
minimize  0.0 1e-10 10000 10000
unfix bond6


fix bond7 all bond/create 1 1 5 ${ncut} 7 iparam 1 8 jparam 1 11
atype 2
run  1
minimize  0.0 1e-10 10000 10000
unfix bond7


fix bond8 all bond/create 1 1 6 ${ncut} 8 iparam 1 8 jparam 1 12
atype 2
run  1
minimize  0.0 1e-10 10000 10000
unfix bond8
```

```
fix bond9 all bond/create 1 1 12 ${ncut} 9 iparam 1 8 jparam 1 13
atype 2

run  1

minimize  0.0 1e-10 10000 10000

unfix bond9


#EQUILIBRATION

 #After one bond per type within ncut has been performed, system
is equilibrated

fix nvt all nvt temp 300.0 300.0 100.0

#Time integration in canonical ensemble at 300K and 100 as damping
#factor

run 500

unfix nvt


# INTERMEDIATE OUTPUTE FILES


write_data intermediate_state_${cdegree}-degree.out nocoeff


jump EPO-CGff_cross-linking.in loop # Goes back to the main script
```

Angle_Charge_Update.m: Updates angles ID and partial charges values after crosslinking (MATLAB)

```
clear all
close all
clc

Natoms=xlsread('C:Users/Fabio/Desktop/updates1/in.epoxy.xlsx','Fog
lio6','A4'); %Number of atom types
Nangles=xlsread('C:Users/Fabio/Desktop/updates1/in.epoxy.xlsx','Fo
glio6','A8'); %Number of angle types
```

```
system_atoms=xlsread('C:Users/Fabio/Desktop/updates1/in.epoxy.xlsx
','A32:J6399');
system_angles=xlsread('C:Users/Fabio/Desktop/updates1/in.epoxy.xls
x','A8611:E12062');
%ALWAYS UPDATE 'Ax:Ey' field in angles xlsread command !!
LL_at=length(system_atoms(:,1)); %Number of atoms in the system
LL_an=length(system_angles(:,1)); %Number of angles in the system

%% ANGLES UPDATE

angleID=[1:1:Nangles 29 33]'; %vector of angle types
couplings=[1 2 3;2 3 2;6 7 6;4 5 4;8 9 5;8 9 11;8 10 5;8 10 11;8
11 4;8 11 9;...
           8 11 10;2 8 9;2 8 10;2 8 11;8 12 7;8 13 7;2 8 12;2 8
13;8 2 3;13 7 6;...
           12 7 6;12 7 12;12 7 13;13 7 13;8 10 8;8 13 8;4 11 4;4
11 10;9 5 4;10 11 10;...
           4 5 10;9 11 10;10 5 9;4 11 9;10 5 10; 9 11 9; 9 5 9];
%Matrix with rows as "atom1 atom2 atom3"

% IMPORTANT: Angles 9-11-9 and 9-5-9 are considered for simplicity
as respctively 29
% and 33, since potential vs angle curves are similar in the
region near the minimum, while, far from it, potential is high, so
it will immediately assume values near to the minimum during the
simulation!

angles=[angleID,couplings]; %Matrix with each rows as "angletype
atom1 atom2 atom3"
updated_angles=zeros(1,length(system_angles(:,1)))'; %vector of
updated angle_types for each angle in the system
angle_counter=zeros(size(angleID)); %vector of counters of how
many of each angle_types are present in the system
true=[1 1 1];

for ii=1:length(angleID)

    sample=angles(ii,2:end);

    for jj=1:LL_an

       ID=system_angles(jj,3:end);
       types=system_atoms(ID,3)';

       if ((types(2)==sample(2)) && ((types(1)==sample(1) &&
types(3)==sample(3)) || (types(1)==sample(3) &&
types(3)==sample(1))))
           %order of 1st and 3rd beads doesn't matter with the
same central
           %bead, the angle is the same: e.g. 1-2-3 == 3-2-1

           updated_angles(jj)=angles(ii,1);
```

```
            angle_counter(ii)=angle_counter(ii)+1;

        end

    end

end

for uu=1:(length(angle_counter))-2

    if uu==29

        text=sprintf('%d type-%d angles
detected',angle_counter(uu)+angle_counter(end-1),angleID(uu));
        disp(text);

    elseif uu==33

        text=sprintf('%d type-%d angles
detected',angle_counter(uu)+angle_counter(end),angleID(uu));
        disp(text);

    else

    text=sprintf('%d type-%d angles
detected',angle_counter(uu),angleID(uu));
    disp(text);

    end

end

xlswrite('updated_angles.xlsx',updated_angles);

%% CHARGES UPDATE

atomID=(1:1:Natoms)'; %vector of atom types
values=[0.16 -0.16 0 0 0 0 0 0.2427 -0.0827 -0.1654 -0.0827 -
0.0827 -0.1654]';
charges=[atomID values];

updated_charges=zeros(1,length(system_atoms(:,1)))';
atoms_counter=zeros(1,Natoms);

for ii=1:Natoms

    sample=ii;

    for jj=1:LL_at

        type=system_atoms(jj,3);
```

```
        if type==sample

           updated_charges(jj)=charges(ii,2);
           atoms_counter(ii)=atoms_counter(ii)+1;

        end

    end

end

for vv=1:length(atoms_counter)

    text=sprintf('%d type-%d atoms
detected',atoms_counter(vv),atomID(vv));
    disp(text);

end

xlswrite('updated_charges.xlsx',updated_charges);

%% OUTPUT CROSSLINKED DATA FILE

copyfile('in.epoxy.xlsx','out.epoxy.xlsx','f');
xlswrite('out.epoxy.xlsx',updated_charges,'D32:D2847');
xlswrite('out.epoxy.xlsx',updated_angles,'B8611:B12062');
%ALWAYS UPDATE 'Bx:By' field in angles xlswrite command !!
```

equilibration.in: Post-crosslinking equilibration script, for 70% crosslinked system (LAMMPS)

```
units      real                        # It is a predefined set of
units of measure

atom_style     full          # Each particle is characterized by
mass and partial charge

boundary  p p p       # Periodic boundary conditions in each
direction


read_data Epoxy_updated_0.7.data    #System data acquisition

#read_restart  Ep1.300000                    #Restart from restart
files data, instead of .data file, if needed
```

```
#FORCE FIELD

include EPO-CGff_forcefield.ff

#SIMULATIONS SETTINGS AND OUTPUT CUSTOMIZATION

timestep 0.5
thermo_style   custom step time etotal pe ke temp press density  # Output on screen
thermo    100  #Frequency of output on screen
thermo_modify norm no

comm_modify cutoff 25.0  # Inter-processors communication settings

minimize 1.0e-4 1.0e-6 100 1000  #initial energy minimization, by iteratively adjust beads positions



# EQUILIBRATION

fix NVEAll all nve  #Time integration in micro-canonical ensemble
run 10000
unfix NVEAll

fix NVTAll all nvt temp 300.0 300.0 100.0
# Time integration in canonical ensemble at 300K with 100 as #damping factor
run 10000
unfix NVTAll

fix NPT all npt temp 300.0 300.0 100.0 iso 1.0 1.0 1000.0
```

```
# Time integration in isobaric-isothermal ensemble at 300K with
100 as damping factor and isostatic pressure of 1 atm with 1000 as
damping factor


#DUMP OUTPUTS


dump snaps3 all custom 10000 NPT2snaps.lammpstrj id mol type x y z
#provides 1 snap every 10000 steps


#RESTART FILES


restart 10000 Ep1 #Generates one restart file each 10000 steps


run 3000000


#OUTPUT FILES


write_data end_state2.out nocoeff
```

mechanical.equil.in: initial equilibration for tensile deformation of 63% crosslinked system (LAMMPS)

```
units     real                        # It is a predefined set of
units of measure
atom_style     full          # Each particle is characterized by
mass and partial charge
boundary  p p p       # Periodic boundary conditions in each
direction


read_data CG-EPO_0.7.data   #System data acquisition
include EPO-CGff_forcefield.ff  #Force field acquisition
```

```
# SIMULATION SETTINGS AND OUTPUT CUSTOMIZATION


timestep 0.1

thermo_style   custom step time etotal pe ke temp press density
#Output on screen

thermo    1000    #Frequency of output on screen

thermo_modify  norm no


comm_modify cutoff 25.0  # Inter-processors communication settings


#EQUILIBRATION


fix NPT all npt temp 300.0 300.0 100.0 iso 0.0 0.0 1000.0

#Time integration in isiobaric-isothermal #ensemble at 300K with
100 as damping factor, and zero pressure with 1000 as damping
factor

dump snaps3 all custom 10000 NPT2snaps.lammpstrj id mol type x y z
#dump 1 snaps each 10000 steps


restart 100000 Ep1 #Write restart file each 100000 steps


run 100000


#OUTPUT FILES


write_data end_state2.out nocoeff
```

[DIRECTION].mechanical.tensile.in: [DIRECTION] tensile deformation of 63% crosslinked system (LAMMPS)

([DIRECTION] can be xx, yy or zz)

```
units     real                        # It is a predefined set of units of measure
atom_style     full          # Each particle is characterized by mass and partial charge
boundary  p p p      # Periodic boundary conditions in each direction

read_data CG-EPO_0.63_zeroP.data    #System data acquisition
include EPO-CGff_forcefield.ff    #Force field acquisition

# COMPUTES

compute csym all centro/atom 12
compute 2 all stress/atom NULL
compute mytemp all temp
compute 11 all reduce sum c_2[1]
compute 12 all reduce sum c_2[2]
compute 13 all reduce sum c_2[3]
compute 14 all reduce sum c_2[4]
compute 15 all reduce sum c_2[5]
compute 16 all reduce sum c_2[6]

# SIMULATION SETTING AND OUTUT CUSTOMIZATION

neighbor     0.3 bin     #Neighbor lists settings
neigh_modify delay 10

timestep 0.1
thermo_style custom step temp etotal press pxx pyy pzz lx ly lz #Output on screen
thermo 1000   #Frequency of output on screen

#ENERGY EQUILIBRATION
```

```
reset_timestep 0
fix 1 all nve   #time integration in micro-canonical ensemble
fix 2 all temp/rescale 10 300.0 300.0 1.0 0.5
# Reset the temperature of a group of atoms by explicitly
rescaling their velocities every 10 steps, with a temperature
target of 300K, a tolerance window of 1 K and with a rescaling
factor of 0.5
dump 1 all custom 10000 dump.equilibrate.* id type x y z


run 1000
unfix 1
unfix 2


#PRESSURE EQUILIBRATION


fix 1 all npt temp 300.0 300.0 100.0 aniso 0.0 0.0 1000.0 drag 0.3
#Time integration in isobaric-isothermal #ensemble at 300K with
100 as damping factor and non-isostatic zero pressure with 1000 as
damping #factor and 0.3 as drag coefficient
run 1000
unfix 1
undump 1
shell cd ..
shell mkdir deform
shell cd deform


#INITIAL VARIABLES


variable tmp equal "[INSERT]"  #insert lx ly or lz
variable L0 equal ${tmp}  #Stores initial length
print "Initial Length, L0: ${L0}"
variable strain equal "v_srate/1e12"
```

```
#DEFORMATION


reset_timestep 0

fix 1 all deform 1 [INSERT] erate 0.001 units box   #insert x, y
or z

#Deforms the box in x direction with a strain rate of 0.001
[Å/step], every time step.

fix 2 all nvt temp 300.0 300.0 100.0

  # Time integration in canonical ensemble at 300 K and 100 as
damping factor


# OUTPUT VARIABLES


variable strain equal "([INSERT] - v_L0)/v_L0"    #insert lx,ly or
lz

variable p1 equal "v_strain"

variable p2 equal "-pxx*0.101325*0.001"    # stress in x direction
in GPa

variable p3 equal "-pyy*0.101325*0.001"   #stress in y direction
in GPa

variable p4 equal "-pzz*0.101325*0.001"    #stress in z direction
in GPa

variable p5 equal "lx"  #box x dimension

variable p6 equal "ly"  #box y dimension

variable p7 equal "lz"   #box z dimension

variable p8 equal "temp"   #Temperature

variable p9 equal "pe"      #potential energy

variable p10 equal "ke"   #kinetic energy

variable p11 equal "-pxy*0.101325*0.001"   # xy stress in GPa

variable p13 equal "-pyz*0.101325*0.001"   # yz stress in GPa

variable p12 equal "-pxz*0.101325*0.001"   # xz stress in GPa
```

```
variable fm equal "(v_p2+v_p3+v_p4)/3" # Hydrostatic stress

variable fv equal "sqrt((v_p2-v_p3)^2+(v_p3-v_p4)^2+(v_p4-
v_p2)^2+6*(v_p11^2+v_p12^2+v_p13^2)/2)"

 # Von Mises Stress

variable t equal "v_fm/v_fv"

variable fd equal (((v_p2-v_fm)*(v_p3-v_fm)*(v_p4-v_fm))-
v_p11^2*(v_p4-v_fm)-v_p12^2*(v_p3-v_fm)-v_p13^2*(v_p2-
v_fm)+2*v_p11*v_p12*v_p13)    # Deviatoric Von Mises stress



# OUTPUT FILES


dump 2 all custom 10000 dump.defo id type x y z c_csym c_2[1]
c_2[2] c_2[3] c_2[4] c_2[5] c_2[6]

fix def_print all print 1 "${p1} ${p2} ${p3} ${p4} ${p5} ${p6}
${p7} ${p8} ${p9} ${p10} ${p11} ${p12} ${p13} ${fm} ${fv} ${t}
${fd}" file xxdefo.txt screen no

run 10000
```

[DIRECTION].thermal.in: [DIRECTION] thermal load application in 63% crosslinked system (LAMMPS)

([DIRECTION] can be xx, yy or zz)

```
#INIZIALIZATION


units     real                        # It is a predefined set of
units of measure

atom_style     full          # Each particle is characterized by
mass and partial charge

boundary  p p p      # Periodic boundary conditions in each
direction
```

```
read_data CG-EPO_0.63.data   #System data acquisition
include EPO-CGff_forcefield.ff   #Force field acquisition

# SIMULATION SETTINGS AND OUTPUT CUSTOMIZATION

neighbor 0.3 bin
neigh_modify every 1 delay 0 check yes   #neighbor lists building settings

thermo_style custom step etotal temp press vol density  #output on screen
thermo 1000    #frequency of output on screen
timestep 0.1

#THERMALIZATION

velocity all zero linear   #velocity distribution to set to zero system momentum
fix nvt all nvt temp 300.0 300.0 100.0
 #time integration in canonical ensemble at 300K with 100 as damping factor
run 10000
unfix nvt

fix nve all nve #time integration in micro-canonical ensemble
run 10000
unfix nve

#MULLER-PLATHÈ ALGORITHM

fix nve all nve #time integration in micro-canonical ensemble
variable kb equal 1.38e-23 #  Boltzmann constant in J/K
```

```
variable Na equal 6.022e23 # Avogadro’s number in atoms/mol

variable JtoKcal equal 2.39e-4 #conversion factor in Kcal/J

compute KE all ke/atom # Kcal/mol  #compute kinetic energy of each bead

variable Tatom atom c_KE/(${kb}*1.5*${JtoKcal}*${Na})  #calculates each atom T by Kinetic Theory

compute layers all chunk/atom bin/1d [DIRECTION] lower 0.05 units box

#Divides the box in layers along the thermal load direction. [DIRECTION] can be x, y or z

fix Tlayer all ave/chunk 10 100 1000 layers v_Tatom file [DIRECTION]tmp.profile

#Calculates an average temperature of each layer to build a 1D temperature profile. [DIRECTION] can be xx, #yy or zz

fix mullerplathe all thermal/conductivity 100 [DIRECTION] 20

#applies the Muller-Plathè Algorithm in one direction, considering 20 layers and performing kinetic energy #exchange every 100 steps. [DIRECTION] can be x, y or z.

fix e_exchange all ave/time 100 50 5000 f_mullerplathe file xxheat.dump

# compute and averages Muller-Plathè output vector every 5000 steps, and writes heat flux time evolution in output.

run 1000000


unfix nve

unfix Tlayer

unfix mullerplathe

unfix e_exchange
```